SYNTHESIS AND CHARACTERIZATION OF PARTIALLY PHOSPHORYLATED POLY (VINYL ALCOHOL) – ALUMINUM PHOSPHATE (PPVA – $AlPO_4$) NANOCOMPOSITE

ASMALINA BINTI MOHAMED SAAT

FACULTY OF ENGINEERING
UNIVERSITY OF MALAYA
KUALA LUMPUR

2016

SYNTHESIS AND CHARACTERIZATION OF PARTIALLY PHOSPHORYLATED POLY (VINYL ALCOHOL) – ALUMINUM PHOSPHATE (PPVA-$AlPO_4$) NANOCOMPOSITE

ASMALINA BINTI MOHAMED SAAT

THESIS SUBMITTED IN FULFILMENT OF THE REQUIREMENTS FOR THE DEGREE OF DOCTOR OF PHILOSOPHY

FACULTY OF ENGINEERING
UNIVERSITY OF MALAYA
KUALA LUMPUR

2016

UNIVERSITY OF MALAYA

ORIGINAL LITERARY WORK DECLARATION

Name of Candidate: Asmalina Mohamed Saat (I.C/Passport No:)

Registration/Matric No: KHA100020

Name of Degree: Doctor of Philosophy

Title of Project Paper/Research Report/Dissertation/Thesis (~~"t~~his Work"):

Synthesis and Characterization of Partially Phosphorylated Poly (vinyl alcohol)– Aluminum Phosphate (PPVA – $AlPO_4$) Nanocomposite

Field of Study: Polymer

I do solemnly and sincerely declare that:

(1) I am the sole author/writer of this Work;
(2) This Work is original;
(3) Any use of any work in which copyright exists was done by way of fair dealing and for permitted purposes and any excerpt or extract from, or reference to or reproduction of any copyright work has been disclosed expressly and sufficiently and the title of the Work and its authorship have been acknowledged in this Work;
(4) I do not have any actual knowledge nor do I ought reasonably to know that the making of this work constitutes an infringement of any copyright work;
(5) I hereby assign all and every rights in the copyright to this Work to the University of Malaya ("~~U~~M"), who henceforth shall be owner of the copyright in this Work and that any reproduction or use in any form or by any means whatsoever is prohibited without the written consent of UM having been first had and obtained;
(6) I am fully aware that if in the course of making this Work I have infringed any copyright whether intentionally or otherwise, I may be subject to legal action or any other action as may be determined by UM.

Candidate's Signature Date:

Subscribed and solemnly declared before,

Witness's Signature Date:

Name:

Designation:

ACKNOWLEDGEMENT

First of all, thanks and grateful to Allah, The One that blessed me to finish this study. I also would like to express my sincere thanks to those who have helped me to complete this study. My sincere gratitude goes to my research supervisor Assoc. Prof. Dr. Rafie bin Johan for his knowledge, guidance, patience and for the extraordinary amount of personal support, motivation throughout the study. My special thanks to all the Universiti Kuala Lumur MIMET who provide me a study leave and continuous support for me to reach the end lane. Also full of appreciation and thanks to the Mechanical Engineering staff and students of University Malaya and Universiti Kuala Lumpur MIMET that helps me a lot in characterization and documentation part during the research. Not forgetting in loving memory to my late parent Mohamed Saat bin Haji Ramli (02/02/1938-10/10/2014) and Jamaliah binti Ali (13/9/1941-01/03/2002), their prays and remembrance always in my heart. It is a motivation for me to move forward. Lastly, thanks to my dear sons, Muhamad Adam Umar, Muhammad Ali Luthfi and Muhammad Adel Eusoff. Only Allah knows how I am thankful to have you….all.

To them all, thank you very much.

ABSTRACT

Partially phosphorylated polyvinyl alcohol - aluminum phosphate (PPVA-$AlPO_4$) composite were synthesized through continuous stirring and condensation at 80 °C. Interaction of pure polyvinyl alcohol (PVA) with phosphoric acid (PA) produced partially phosphorylated poly vinyl alcohol (PPVA) and the addition of aluminum (Al) source produces a PPVA-$AlPO_4$ composite. Fourier Transform Infrared (FTIR) and Raman spectra of PPVA confirmed the phosphate group in PPVA-$AlPO_4$ composite. The phosphate group had bonded with aluminum at C-O-P- $AlPO_4$, O-P-O- $AlPO_4$ and also OH-Al. The optical properties of these PPVA and PPVA-$AlPO_4$ nanocomposite samples were examined by UV-visible and photoluminescence (*PL*) spectroscopy. *UV* analysis of PPVA shows single peak at 274 nm while in PPVA-$AlPO_4$, the peak was shifted to lower wavenumber of 208 nm. PL spectra of PPVA-$AlPO_4$ shows broad peak at range of 304-371, 450-550 and 560-700 nm. This confirmed that the phosphate group in PPVA created bonding with aluminum. Transgravimetric (TGA) analysis shows that the weight residue of PPVA-$AlPO_4$ composite was higher than PPVA and PVA. X-ray diffraction (*XRD*) pattern of PVA shows a single peak at angle of 20°. However, the peak become broadened as PA added. Meanwhile, the addition of aluminum source produced multiple peaks referring to the multiple phases of $AlPO_4$ in the nanocomposite. Field Emission Scanning Electron Microscopy (FESEM) confirmed the existence of multiple geometrical phases and nanosize of spherical particles. The influence of important synthesis parameters such as, effect of PPVA, effect of aluminum sources, pH and crystallization time are also studied.

ABSTRAK

Komposit polivinil alkohol separa fosfat – aluminum fosfat (PPVA-$AlPO_4$) telah disintesis melalui pengacauan berterusan dan kondensasi pada suhu 80 °C. Polivinil alkohol (PVA) tulin bertindakbalas dengan asid fosforik (PA) untuk menghasilkan polivinil alkohol separa fosfat (PPVA) dan tindakbalasnya dengan sumber aluminum (Al) menghasilkan komposit PPVA-$AlPO_4$. Analisis spektra Inframerah Transformasi *Fourier* (FTIR) dan Raman terhadap PPVA membuktikan kewujudan kumpulan fosfat di dalam komposit PPVA-$AlPO_4$. Kumpulan fosfat ini membentuk ikatan dengan aluminum pada C-O-P-$AlPO_4$, O-P-O- $AlPO_4$ dan OH-Al. Sifat optik polivinil alkohol separa fosfat dikaji menggunakan spektroskopi *uv-visible* (UV-vis) dan *photoluminescence* (PL). Analisis UV menunjukkan PPVA mempunyai satu puncak pada 274 nm manakala puncak PPVA-$AlPO_4$ berubah kepada panjang gelombang yang lebih rendah iaitu 208 nm. PPVA-$AlPO_4$ menghasilkan puncak PL yang melebar pada lingkungan panjang gelombang 304-371, 450-550 and 560-700 nm. Ini mengesahkan kumpulan fosfat dalam PPVA mempunyai ikatan dengan aluminum. Analisis thermogravimetrik (TGA) menunjukkan sisa berat komposit PPVA-$AlPO_4$ adalah lebih banyak dari PPVA dan PVA. Pencirian pembelauan sinar X (XRD) menunjukkan puncak PVA pada 20° melebar setelah asid fosforik ditambah. Manakala penambahan sumber aluminum menghasilkan beberapa puncak menunjukkan kehadiran beberapa fasa $AlPO_4$ komposit nano yang berbeza. Mikroskopi Elektron Imbasan Pancaran Medan (FESEM) menunjukkan kehadiran pelbagai fasa geometri dan zarah sfera yang bersaiz nano. Parameter penting seperti kesan PPVA, kesan sumber aluminum, pH dan masa penghabluran juga dikaji.

TABLE OF CONTENT

LIST OF FIGURES

LIST OF TABLES

LIST OF SYMBOLS AND ABBREVIATIONS

1-D	1 dimensional
2-D	2 dimensional
3-D	3 dimensional
$AlPO_4$	Aluminum Phosphate
DMF	N,N-dimethylformamide
DMSO	Dimethyl sulfoxide
DP	Degree of phosphorylation
DSC	Differential Scanning Calorimetry
DTG	Derivative Thermogravimetric
EDX	Energy Dispersive X-Ray Spectrometer
Eg	Band gap
FA	Fumaric Acid
FESEM	Field Emmission Scanning Electron Microscope
FTIR	Fourier Transform InfraRed
GA	Glutaraldehyde
HAp	Hydroxyl Apatite
H_3PO_2	Tetrabutylammonium hydroxide
H_3PO_4	phosphoric acid
IR	Infra-Red
KOH	Kalium Hydroxide/potassium hydroxide
LAP	Lamellar aluminophosphate
MB	Methylene Blue
MW	Molecular Weight
NH_4OH	Ammonium hydroxide

NH_4NO_3	Ammonium Nitrate
NMR	Neutron Magnetic Resonance
P_2O_5	phosphorus pentoxide
PA	Polyamides (nylons)
PbS	Plumbum Sulphide
PC	Polycarbonate
PE	Polyethylene
PEG	Poly Ethylene Glycole
PHPMMA	polyhydroxylated methylmethacrylate
PNC	Polymer Nano Composite
POCL	phosphorus oxychloride
PP	Polypropylene
PS	Polystyrene
PTFE	Polytetrafluoroethylene
PPVA	Partially phosphorylated poly(vinyl alcohol)
PV	Poly vinyl pyridine
PVA/PVOH	Poly(vinyl alcohol)
PVA-P	poly vinyl alcohol phosphate
PVA-DP	polyvinyl alcohol diphosphate
PVA-TP	polyvinyl alcohol diphosphate
PVPH	Polyvinylphosphonic acid
P4VP	polyvinyl pyporyl
PVC	Polyvinyl chloride
RB	Rhodamine B
SAXS	Small Angle X-Ray Scattering
SDS	Sodium Dodecyl Sulfate

SDTA	Simultaneous Differential Thermal Analysis
SEM	Scanning Electron Microscope
SFS	Sodium Formaldehyde Sulfoxylate
SiO_2	Silica Oxide
SPE	Solid Polymer Electrolyte
TBAOH	Tetrabutylammonium hydroxide
TEA	Triethylamine
TEM	Transmission Electron Microscope
TEOS	Tetraethoxysilane/silicon alcoxide
Tg	Glass Transition Temperature
Tg	Melting Temperature
TGA	Thermogravimetric analysis
UV-Vis	Ultra Violet Visible
XRD	X-Ray Diffraction

LIST OF APPENDICES

Chapter 1

INTRODUCTION

1.1 Background

Nanocomposites are a new class of materials with superior properties as compared to their microcomposite counterparts. They are usually refer to the composites in which at least one phase (the filler phase) possesses ultrafine dimensions (on the order of a few nanometers). The driving force for nanocomposites research is toward the potential application such as in the next generation of the marine industry. Meanwhile, polymer nanocomposites have drawn a great interest recently due to the materials possess high potential achievement properties. The addition of small amount of nanoparticles can significantly improve a variety of properties without sacrificing the lightweight of polymer matrices. Well-dispersed nanoparticles in the polymer matrix may serve as nucleation sites to facilitate the bubble nucleation process. Polymer nanocomposites cover vast array of different polymer matrices and nanoparticles. They are widely used in the automotive, aerospace, marine, construction and electronic industries due to their improved mechanical (e.g., stiffness, strength) and physical properties over pure polymers. Meanwhile, micron-sized particulates and long fibers are most widely used in traditional polymer composites.

Polyvinyl alcohol (PVA) is among the most important polymeric materials in the industry due to it‘s environmentally friendly with low economic cost. As a hydrophilic polymer, PVA is frequently used as a matrix for a variety of inorganic particles. Here, PVA provides a convenient route to prepare composites whereby the inorganic particles are dispersed to a high degree of uniformity and fineness. PVA is a corrosion inhibitor for mild steel in 0.5 M H_2SO_4 with 30% of maximum efficiency (Umoren et al., 2006).

Polymer composite PVA–L–serine coated mild steel give 95% efficiency of 0.6% by weight (Sabirneeza et al., 2011).

The addition of polyacids to water-soluble PVA produces hydrogen bonded complexes. In the case of strong phosphoric acids (PA), the reaction of PVA may produce partial reactions to cyclic phosphate esters (Pritchad, 1970). The remaining replaceable hydrogen of the cyclic phosphate groups is ionized in water and the esterified polymer behaves as a polyelectrolyte with interesting conductive coating properties. Partially phosphorylated poly (vinyl alcohol) (PPVA) acts as co-dopant and stabilizer for PANI nanoparticle. The colloidal PANI/PPVA produced maximum electrical conductivity at 40wt% PPVA ratio with spherical shape and significant re-dispersion stability (Jiang et al., 2014). Earlier, Mohapatra et al. (2006) also reported that PPVA coated magnetite surface form a Fe-O-P bonding. The phosphorylation of PVA with phosphoric acid in producing PPVA has also attracted considerable interest in the applications such as electrolyte/membrane (Chen & Liu, 2011b), metal chelating (Bayer et al., 1983), paper making (Chen et al., 2005), sensor (Prajapati & Gupta, 2009), synthetic bone/tooth (Datta et al., 2012), nanoparticle (Mohapatra et al., 2006; Chen & Liu 2011b) fire retardant materials (Sergio I. Sanchez 2007), conductive coating (Chen & Liu, 2011a) and nanocomposite (Thanganathan et al., 2011; Pramanik et al., 2008). PPVA has a chemical structure with pendant of phosphate and hydroxyl group. It is a type of polymer with inside chemically bound phosphorus, has a broad range of application and also exhibits good flame retardant properties that include both reactive and additive products which can easily be integrated to the materials by physical mixing only (Wang, 2011).

Meanwhile, aluminum phosphate ($AlPO_4$) is used in organic coating as a new approach. $AlPO_4$ is explored in an inhibition of steel corrosion in 0.33M H_3PO_4 and improved about 84% of its efficiency at 0.01 M of $AlPO_4$ (Alaoui et al., 2008). $AlPO_4$ is also

widely explored depending on its structure either in the form of dense or microporous crystalline. $AlPO_4$ nanocomposite is stable at elevated temperature with no polymorphic transformation of berlinite, tridymite and cristobalite compared to conventional $AlPO_4$ ceramic (Sambasivan, 2000). This ceramic has low oxygen diffusivity and good corrosion resistance at elevated temperatures, which may provide oxidation protection to substrates when deposited as a coating.

Palacios et al. (2013) recently reported on the synthesis of $AlPO_4$ at various temperature, crystallization time and pH but still within the acidic region. On the other hand, the synthesis and morphology of $AlPO_4$ in the alkaline region has yet to be explored. Yang & Kau, (2005) reported on the synthesis of $AlPO_4$ nanoparticle in the alkaline region (pH 10, 11 and 12) with various morphology emerged from nanoparticles, nanorod, and nanowire. However, various types of $AlPO_4$ morphology are not only dependent on the pH solution, but also on the use of structural direction agent $(EO)_x$. The common method used to synthesis $AlPO_4$ was a chemical precipitation and hydrothermal method at heat treatment temperature of 150^o (Hu et al., 1995) or 180°C (Liu et al., 2010). It is a challenge to produce PPVA–$AlPO_4$ nanocomposite at much more lower temperature than that.

In the marine industry, all the facilities are exposed to humidity whereby ships and the oil and gas structures suffer considerably by the presence of the corrosion. Hence coating using PPVA–$AlPO_4$ is a new approach in organic coating of marine industry. In this study, we have developed a PPVA–$AlPO_4$ composite that contains the conducting polymer PVA as an anti-corrosive agent in order to substitute the conventional coatings used. The present study is aimed directly to synthesize a PPVA–$AlPO_4$ nanocomposite that can improve the bonding reaction with other materials, preferably in marine application either as a coating material or as a fire retardant material. Both PPVA and $AlPO_4$ are known to have their own separate purpose in the coating, binder and fire

retardant industry. It is a challenge to produce PPVA–$AlPO_4$ nanocomposite that improves the interaction between aluminum and phosphate groups which result, better and improved coating and fire retardant materials. It is imperative to understand the principles and methodologies for characterizing the physical properties of both PPVA and PPVA–$AlPO_4$ nanocomposite.

In these specific applications related to the marine industries, the understanding of the interaction between $AlPO_4$ surface and other substances is of great interest. This interaction relates to the surface structure and properties of $AlPO_4$, such as surface functional groups, surface charge, hydrophilicity and porosity. $AlPO_4$ surface was reported to have P–OH and Al–OH groups. Therefore, the regulation of these surface sites is expected to give rise to many properties, such as acidity and basicity, affinity and reactivity of molecules, and catalytic activity (Mathews, 2010). It is a huge challenge to investigate the interaction of surface and properties of PPVA–$AlPO_4$ nanocomposite. Furthermore, the morphology evolution and structural diversity are other aspects that need to be investigated. The monitoring of crystal growth from a systematic chemical variation of pH reaction, temperature, and crystallization time in order to control the evolution of environment is also an important aspect to explore.

The purpose of this study is to understand the modification mechanism affected by the phosphate ion on polyvinyl alcohol polymer and the interaction of phosphate group to produce aluminum phosphate reinforcement. The modification varies the polymer hydrophilic and hydrophobic structure. The phosphate group bonded is replacing hydroxyl or –OH group in the polyvinyl alcohol structure and produced a polyvinyl phosphate or partially phosphorylated PVA (PPVA). Further process involves the formation of aluminum phosphate nanofiller embedded in the modified polymer by in situ process with a different pH reaction in alkaline region from pH 7 to pH 12. Aluminum will create a bond with phosphate group on the modified polymer. It will

also give better mechanical properties as a result of better nanoparticles distribution. The reaction is expected to give good surface interaction, bonding, and good strength bonding properties of nanocomposite polymer.

Final part of this study is the morphological and characterization process. Morphological and characterization study will be carried out by using FESEM, XRD, FTIR, RAMAN, and thermal analysis using thermogravimetric analysis (TGA) and differential scanning calorimetry (DSC).

1.2 Problem Statement

Both PPVA and $AlPO_4$ are important materials for coating (Chen, He, & Shang, 2003; Chen & Liu, 2011a) and fire retardant materials (Joseph & Tretsiakova-mcnally 2011; Jiang et al. 2013). The structural, chemical and morphology analysis shows that there is great potential of compatibilities between PPVA and $AlPO_4$. A wider range of applications can be explored due to enhanced properties from improvement in the interaction or bonding (Wang & Sherwooda, 2003) between the element of PPVA and $AlPO_4$. The application of newly improved materials can be explored not only in the field of coating and fire retardant, but also in other fields. It is possible to explore its application as heat resistant firefighter protective clothing and fire retardant material (Joseph & Tretsiakova-mcnally 2011) for fiberglass boats. Other than that, in the field that requires corrosion protection, the coating properties with the fire retardant function and improved adhesion (Chung 2003) will be interesting for further exploration.

Complexed partially phosphorylated polyvinyl alcohol (PPVA) produced a nanocomposite by in situ synthesis of $AlPO_4$ nanoparticle. Complexed PVA through its pendant phosphate groups can give better adhesion with $AlPO_4$ and hence improve the thermal stability of the nanocomposites.

Composite methods have been explored to a great degree because of the necessity to engineer a material with specific properties. Designing organic inorganic composites show controllable physical properties such as thermal, electrical, and mechanical behavior by combining the properties of both organic polymers and inorganic compounds (solid inorganic proton conductors).

1.3 Research objectives

This research focuses on the modification of poly (vinyl alcohol) polymer using phosphoric acid and synthesis of aluminum phosphate nanocomposite by in situ technique. Modification of polymer with phosphoric acid is carried by condensation process. Meanwhile, aluminum phosphate is prepared by chemical reduction method by controlling the solution pH in alkaline environment. The resultant nanocomposites are subsequently put through the autoclaving process to analyse the effect of crystallization time on nanocomposite morphology. The objectives of this study are as follows:

i. To synthesize modified polymer and PPVA–$AlPO_4$ nanocomposite by polymer modification and in situ polymerization.

ii. To characterize the thermal, structural, and morphology of modified polymer and PPVA–$AlPO_4$ nanocomposite.

iii. To analyze the effect of aluminum sources and ratio on PPVA–$AlPO_4$ nanocomposite.

iv. To investigate the effect of solution reaction pH and crystallization time on PPVA–$AlPO_4$ nanocomposite morphology.

1.4 Thesis Overview

The major reason behind the intensive activities in this area is to produce improved interaction and bonding of PPVA–$AlPO_4$ nanocomposite that can be applied particularly in the marine field, and not only as fire retardant material or anti-corrosion coating but for more wide field and applications. Other than that, the effect of aluminum source used, temperature, and crystallization time also are evaluated in this study.

Chapter 1 discusses on the background of the study, the problem statement, research objective, and scope of thesis covered in this study.

Chapter 2 elaborates on the literature review of poly vinyl alcohol polymer, modification of PVA with phosphoric acid (PPVA) and $AlPO_4$. The literature review of characterization for PVA, PPVA and $AlPO_4$ were also analyzed focused on thermal (TGA, DSC, SDTA), structural (XRD, FTIR, Raman), optical (UV-Vis, Photoluminescence), and morphological properties (FESEM).

Chapter 3 explains about the materials and methodology used in the modification of PVA with phosphoric acid and synthesis of PPVA–$AlPO_4$ nanocomposite. A summary of characterization equipment used is also discussed in this chapter.

Chapter 4 presents all the resulting data and elaboration of related discussions. This chapter explains about the background of sample preparation, followed by discussion of effect of phosphoric acid on PVA, effect of pH on PPVA–$AlPO_4$ nanocomposite, effect of aluminum sources on PPVA–$AlPO_4$ nanocomposite, effect of aluminum ratio on PPVA–$AlPO_4$ nanocomposite, effect of crystallization time on PPVA-$AlPO_4$ nanocomposite, and finally the synthesis of PPVA–$AlPO_4$ nanocomposite at optimum sample (pH 10).

Chapter 5 concludes all the findings and future recommendations for this study.

References give all the details of references referred in this thesis.

Appendices presents all the front pages of accepted papers published related to this study.

Chapter 2

LITERATURE REVIEW

This chapter describes the properties of polymer in general, and then specifically focuses on poly (vinyl alcohol) (PVA), PVA modification, and partially phosphorylated PVA (PPVA). After the modification of polymer is explained, the synthesis of nanoparticle is also looked into. Other than that, aluminum phosphate composite and nanocomposite are also portrayed by focusing on the synthesis process, the properties, and the characterization methods.

2.1 Polymer

The word *polymer* derives from the classical Greek words; *poly* meaning ―many" and *meres* meaning ―parts." Simply stated, a polymer is a long-chain molecule that is composed of a large number of *repeating units* of identical structure. Classification of polymer materials used as matrices in composite includes thermoset, thermoplastic, elastomer, and rubbers. Thermoplastic can be divided into two types known as non-crystalline and crystalline. Non-crystalline of thermoplastics, which is also known as amorphous, has molecular chain with random arrangement, such as that in polystyrene and polycarbonate. Meanwhile, crystalline has a structure of molecular chain with better arrangement, such as that in polyethylene and polypropylene. On the other hand, thermoplastics are materials that readily flow under stresses at elevated temperatures, so allowing it to fabricate into the required component, besides becoming solid and retaining its shape when cooled to room temperature. These polymers may be repeatedly heated, fabricated, and cooled, and consequently, be scrapped off for recycling, though there is evidence that this will slightly degrade the properties probably

due to a reduction in molecular weight. Some well-known thermoplastics are Polyethylene (PE), Polypropylene (PP), Polyolefin copolymers, Polyvinyl chloride (PVC), Polytetrafluoroethylene (PTFE), Polystyrene (PS), Acrylic materials, Polyamides (nylons) (PA), Polycarbonate (PC), and Polyacetal. The useful properties of polymer thermoplastics material are their low densities, high resistance to chemical attack, thermal and electrical insulation properties, as well as their ease of fabrication into a variety of shapes, either simple or complex. However, the main disadvantages of plastics are low in strength and elastic modulus values in comparison to metals, low softening and thermal degradation temperature, besides possessing comparatively high thermal expansion coefficients. These disadvantages usually improve with filler addition as reinforcement materials in thermoplastics.

2.2 Poly(vinyl alcohol) (PVA)

Poly(vinyl alcohol) is classified as a polyhydroxy polymer and known as PVA or PVOH. It is the largest synthetic water soluble polymer derived from monomer ethanol (vinyl alcohol) with a chemical formula of $CH_2 = CHOH$ (Kirk Othmer, 1983). It has about 4400 carbon atoms per molecule combined with hydrogen atoms and OH group. Vinyl alcohol monomer does not exist in a free state and only can be found in the form of polymer. PVA is synthesized indirectly through polymerization of vinyl acetate, and followed by hydrolysis of poly vinyl acetate to remove the acetate group. The structure of PVA is given in Figure 2.1.

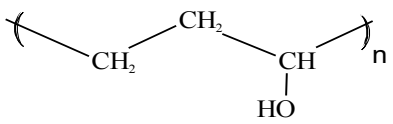

Figure 2.1: Structure of poly (vinyl alcohol)

In 1924, Herrmann and Haehnel added alkali to clear the alcoholic solution of poly vinyl acetate, but unexpectedly, they obtained an ivory-colored PVA (Pritchad, 1970). This is the report on PVA, which was published in 1927, and followed by more publications about PVA (Pritchad, 1970). PVA is well known as a biomaterial and also as an environmental-friendly material. It appears as white to yellowish granular with pH 5-7, specific gravity in the range of 1.25–1.32, and density at 1.19 g/cm^3. PVA resin has excellent chemical and physical properties. It is divided into various kinds depending on the degree of polymerization, hydrolysis, and the presence of hydroxyl group. PVA can be found either as fully hydrolyzed (99-90%) or partially hydrolyzed (70-80%). Moreover, the OH group in PVA contributes to the strong hydrogen bonding for both inter and intra-molecular. Partially hydrolyzed PVA contains an acetate group, which has hydrophobic characters that weaken the hydrogen bond. In fact, glass transition temperature (T_g) and melting temperature (T_m) for fully hydrolyzed PVA are higher than those of partially hydrolyzed PVA. The melting temperature for fully hydrolyzed PVA was recorded in the range of 210 – 230 ºC, while partially hydrolyzed PVA in the range of 150 – 190 ºC. PVA becomes decomposed rapidly above the melting temperature, where the T_g for fully hydrolyzed PVA and partially hydrolyzed PVA are 85 and 58 ºC, respectively. This polymer becomes elastic and flexible when it reaches above or equal to its T_g. Besides, PVA thermally experiences gradual discoloration at 100 ºC, then, continues to darken rapidly at temperature 160 ºC and above. Gradual decomposition of PVA starts at 180 ºC, with partial decomposition at a temperature range of 200 - 250 ºC, and rapid decomposition above 250 ºC.

PVA with high molecular weight contains chain associated with weak Van Der Waals forces, but stronger in dipole-dipole interactions and hydrogen bonding. In addition, partially hydrolyzed PVA easily dissolves in water at room temperature, whereas fully hydrolyzed solubility varies depending on the degree of crystallinity and can easily

dissolve at higher temperature. Moreover, PVA is soluble in solvents, such as water, DMSO, acetalamide, glycols, and DMF. The viscosity of PVA also increases with increased degrees of polymerization and hydrolysis. PVA hydrophilic properties make its permeable for both water and hydrated salt.

Furthermore, PVA has a number of attributes, for instance, good film forming, adhesive, emulsifying, tensile strength, moldability, impact strength, wear resistance, and excellent electrical insulation. It also has plastic properties that are deformable, melts to form liquid when heated, and freezes to a brittle and glassy state when cooled sufficiently. Other than that, it has been used as raw material to produce coating material, adhesive, as well as to produce finishing agent, soil ameliorator, films, and polyvinyl butyral. This polymer is characterized by outstanding properties, such as high conductivity, stability, transparency, and easy processing.

PVA in liquid form produces a highly polar solution with hydrophilic properties. OH group in PVA contributes to the strong hydrogen bonding both intra and inter-molecular, as well as reduces solubility in water. Moreover, solubility of PVA decreases as temperature increases. Once the temperature is increased, PVA crystallinity also increases, thus, lowering solubility and water sensitivity. Nonetheless, water resistance can be improved via crosslinking. Common crosslinking agents for PVA are melamine-formaldehyde, glyoxal, urea formaldehyde, and trimthylolmelamine. PVA can be great for emulsification and function as a protective colloid because it has low surface tension. It is also an excellent adhesive and has been widely used as glue material. PVA has optimum wet adhesion at pH 4.6-4.9 and alkaline condition must be avoided to prevent permanent gelation. Besides, PVA can generate thin film easily with good flexibility, malleability, and tensile strength. It possesses superior oxygen barrier properties under dry condition. Therefore, PVA is seemed attractive as a starting material for protective coating. PVA can provide strong adhesion to metals and similar

smooth surface after certain modification. Adequate adhesion of coating to metal surface can be achieved with heat treatment at certain temperature (not at the decomposing temperature of coating PVA materials or maybe PVA added with heat stabilizing materials). PVA is also a good dielectric material that possesses high dielectric strength and good charge storage capacity. PVA is resistant to oil, grease, and solvent. PVA exerts good film forming, emulsifying, and adhesive properties. The properties of PVA, in fact, can be modified depending upon its polymer conditions, drying, grinding or chemical modifications. The physical and chemical properties of PVA depend on the degree of polymerization and the degree of hydrolysis that affect the presence, as well as the distribution of the hydroxyl group. The composites of PVA with inorganic acids form a simple system that introduces changes to electrical conductivity.

2.3 Partially Phosphorylated PVA (PPVA)

The development of new polymer-inorganic composite materials has garnered much interest over the years due to their unique microstructures, as well as physical and chemical properties, which are markedly different from other materials. The composition of PVA with inorganic acid changes the properties of PVA, such as electrical conductivity, crystallinity, thermal, and fire retardant properties.

Phosphorylation of PVA is a process of modified PVA functional group from OH group to phosphate group. The resultant modified polymer is generated from method variation involving acid concentration, water, temperature, and reaction time. Phosphorylation of PVA is commonly conducted with three different methods that depend on the types of phosphorus sources. Besides, PVA can be phosphorylated by using a number of methods, such as phosphoric acid (H_3PO_4) (Peng et al., 2014), phosphoric acid-urea (Chen & Liu, 2011c), and phosphorus oxychloride (POCL) (Daul et al., 1954). The

most well-known and the popular method used has been phosphoric acid. Other phosphorylation agents used are phosphorus pentoxide (P_2O_5) (Yu & Carlsen, 2008) , H_3PO_2 (Vargas et al., 2000), and H_3PO_3 (Banks et al., 1993). In addition, studies of PVA reaction with phosphate group revealed that phosphoric acid (H_3PO_4) has been the most common chemical choice and easier to form phosphate group in polymer compared to phosphorus pentoxide (P_2O_5) or H_3PO_2 or any other phosphate salt. The addition of polyacids to water-soluble PVA produces hydrogen bonded complexes. In the case of strong phosphoric acids, the reaction of PVA may produce partial reactions to cyclic phosphate esters (Pritchad, 1970). The remaining replaceable hydrogen of the cyclic phosphate groups is ionized in water and the esterified polymer behaves like a polyelectrolyte. The reaction produces mixed ester that contains single, double, and possibly, triple bound phosphorus, which makes the product either water soluble (hydrophilic) or partially soluble (hydrophobic). Only the urea-phosphate method offers single bound phosphorus that generates a complete hydrophilic product. Hydrophobic poly vinyl phosphate is used as an effective ration in exchange of resin. Moreover, reaction of PVA with phosphoric acid produces hydrogen and covalent bonding depending on the amount of phosphoric acid and water. Addition of phosphate group or any acid in polymer will produce plasticization effect that can change the thermal properties of the system. Modified PPVA has plasticization effect that comes from both phosphoric acid and water. Furthermore, there is also effect of physical rubbery after esterification (Somani et al., 2003). The addition of phosphate group can improve hydrophilicity, anionic properties, compatibility, solution stability, and retention of PVA. PPVA increases the amorphous structure of the polymer by decreasing its glass transition temperature (T_g) and melting temperature (T_m) (Suzuki et al., 2000). PPVA complexes possess favorable properties, such as good film forming, ion exchange (Suzuki et al., 1999), cation exchange, conductivity, chemical resistance, metal

complexes (Bayer et al., 1983), as well as flammability (Banks et al., 1993). Table 2.1 summarizes the properties of PVA and PPVA.

Table 2.1 : Properties of PVA and PPVA

Details	PVA	PPVA
Method	Hydrolysis of Poly vinyl acetate	Phosphorylation of PVA Urea-phosphoric acid method Phosphoric acid method
	PVA physical and chemical properties depend on 1) degree of polymerization, 2) hydrolysis, 3) present distribution of hydroxyl group.	properties depends on degree of phosphorylation, types of PVA, ratio of phosphate in PVA, temperature, and reaction time
	Produces polarization polymer	Produces bonded complexes with ionic character
	Partially crystalline	Amorphous phase increases
Glass transition temperature, (T_g)	Fully hydrolyzed = 85 °C Partially hydrolyzed = 58 °C	Depends on degree of phosphorylation 65 °C
Melting temperature	Fully hydrolyzed = 210-230 °C Partially hydrolyzed = 150-190 °C	222 (Prajapati et al., 2010)
Types	Fully hydrolyzed = 210-230 °C Partially hydrolyzed = easily dissolves in water at room temperature (Datta et al., 2012)	Phosphate = water soluble Di-Phosphate = partially insoluble (Zhan et al., 2004) Tri-Phosphate = partially insoluble Soluble in hot water DP 11.3% (Datta et al., 2012)
Properties	Low in cost	Low in cost
	Environmentally friendly	Functions as base for more complex compounds (for film preparation)
	Dielectric material, high dielectric strength	Good performance in solid state application (polymer electrolyte membrane fuel cells)
	Good charge storage capacity	Has ion exchange properties
	Resistant to oil, grease, and solvent	Flammability (characteristic of phosphorus)
	Flexibility, Malleability, Strain strength	Good electrical conductivity
Films appearance	PVA film transparent film	Transparent, yellow to brown film. High concentration of PA wet and oily film (Somani et al., 2003)
	PVA maintains at pH 4.6-4.9 for optimum wet adhesion, and alkaline condition must be avoided to prevent irreversible gelation	Mixture of PVA with phosphoric acid is very acidic; pH less than 1
Flame properties	PVA has organic volatiles that can easily produce flame	High retention of more organic materials in the form of char. Higher flame retardance properties
Surface tension	Surface tension 47.7 Mn/m (Datta et al., 2012)	Surface tension 52.1Mn/m (Datta et al., 2012)
Shear viscosity	Shear viscosity , 4.59±0.12 mPa s (Datta et al., 2012)	Shear viscosity 2.48 ± 0.07 mPa s at 0.5 s−1 (Datta et al., 2012)

2.4 Phosphorylation of PVA with phosphoric acid

The phosphorylation of PVA with phosphoric acid (PA) in producing partial phosphorylated poly(vinyl alcohol) (PPVA) has attracted considerable interest in some applications, such as textile (Daul et al., 1954), coating material/corrosion (Narayanan, 2005), fire-retardant materials (Joseph & Tretsiakova-mcnally, 2011; Wang et al., 2007), electrolyte (Prajapati et al., 2010; Gupta, 2008), membranes (Thanganathan et al., 2011; Ahmad & Sheha, 2013), metal chelating (Bayer et al., 1983; An et al., 1995; An et al., 1996), paper making (Chen et al., 2005), sensors (Somani et al., 2000; Prakash R. Somani et al., 2001), synthetic bones/teeth (Yu & Carlsen, 2008), as well as nanoparticle/nanocomposite (Rajkumar et al., 2010; Pramanik et al., 2008; Mohapatra et al., 2006). The reaction of PVA with PA forms hydrogen bonding by removing the OH group in PVA and replacing it with PO_4^{3-} group. Phosphorylated PVA with PA is written in different terms depending on its functional group and properties, such as phosphorylated PVA (Peng et al., 2014; Hirofusa Shirai et al., 1996; Banks et al., 1993; Inagaki et al., 1973), partially phosphorylated PVA (PPVA) (Datta et al., 2012; Suzuki et al., 2000; An et al., 1996), partially phosphonate PVA (Iribarren & Lemmetyinen, 2009), Poly (vinyl alcohol) phosphate (PVAP) (Yu & Carlsen, 2008; Pramanik et al., 2008; Mohapatra et al., 2006; Zhan et al., 2004), Poly (vinyl alcohol) diphosphate (Zhan et al., 2004), Poly (vinyl alcohol) tri-phosphate (Banks et al., 1993), and Poly vinyl phosphate (Daul et al., 1954). Besides, the reaction of PVA with highly strong phosphoric acid can produce partial reaction to the cyclic phosphate ester (Pritchad, 1970; Peng et al., 2014; Shirai et al., 1996; Banks et al., 1993), and Inagaki et al., (1973) reported a similar term of phosphorylated PVA. Inagaki et al., (1973) reported that phosphorylation occurs through a two-step chain, which involves scissoning and oxidation. Meanwhile, Peng et al., (2014) produced partially phosphorylated PVA that contained phosphorylated PVA and unphosphorylated PVA, as reported earlier by

Banks et al., (1993). Other than that, reviews concerning flame retardance on phosphorus effect in polymer, presented by Joseph and Tretsiakova-mcnally (2011) and Banks et al., (1993), depicted that PVA can be phosphorylated to a limit of PA critical concentration of less than 6M. Concentration of PVA to PA above 6 M leads to dehydration. The degree of phosphorylation also depends on time and reaction temperature. Banks et al., (1993), hence, concluded that in the mixture of phosphoric acid and PVA, phosphoric acid produces dual effect upon PVA, phosphorylation, and dehydration.

Partially phosphorylated PVA (Figure 2.2) is produced with a lower concentration of phosphoric acid (below 5.7 M), whereas dehydration of PPVA with phosphonate group (Figure 2.3) is produced at a higher concentration of phosphoric acid (more than 5.7 M). Moreover, the fraction of phosphorylated PVA increases as PA is added, but not in linear fashion. This is because; it would begin to level off at 1.5 M.

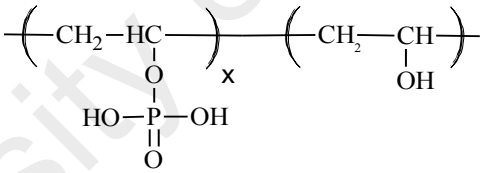

Figure 2.2: Phosphorylated and unphosphorylated PVA (Peng et al., 2014; Datta et al., 2012; Suzuki et al., 2000; Shirai et al., 1996; Banks et al., 1993; An et al., 1995; An et al., 1996)

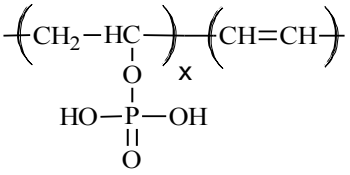

Figure 2.3: Dehydration of PVA+PA produces phosphonate group (Banks et al., 1993)

The phosphonate group reported by Banks et al., (1993) was also observed by Iribarren and Lemmetyinen (2009) when discussing the PVA and PA kinetic study through synthesis reaction of PVA (98.5% hydrolyzed) with low concentration of phosphoric acid. The maximum bonding that can occur in the composition of PVA: PA is 3:1,

where 3 units of PVA can possibly make the maximum bonding for each unit of PA. This reaction is dissolved in 0.9 wt% distilled water to produce polyene; an unsaturated organic compound that contains one or more sequences of alternating double and single carbon-carbon bond. The interaction between these double carbon-carbon bonds is known as conjugation that results in an overall lower energy state of molecules. The reaction schemes are given in Figure 2.4. Thus, it can be concluded that Iribarren and Lemmetyinen (2009) generated partial phosphonate.

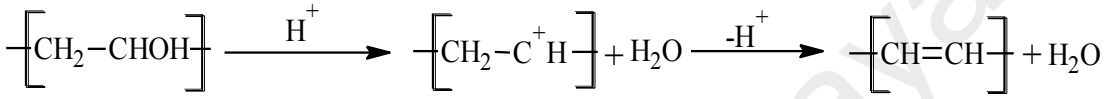

Figure 2.4: Polyvinyl alcohol modified with low phosphoric acid to develop P-O bonding. (Iribarren & Lemmetyinen, 2009)

The reaction of PVA with PA produces unphosphorylated PVA and phosphorylated PVA, which is known as partially phosphorylated PVA. This agrees well with others (Datta et al., 2012; Suzuki et al., 2000; Suzuki et al., 1999; An et al., 1996; An et al., 1995). Datta et al., (2012) reported that PPVA synthesis with 10 g of PVA reacted with 4.5 M PA and refluxed at 85 °C for 3 hours. The synthesized PPVA for biomaterial application can only be dissolved in hot water compared to PVA that can easily dissolve in room temperature water. PPVA as polymer electrolytes prepared via urea-H_3PO_4 method observed an increase in the amorphous part with an increasing degree of phosphorylation (DP) (Suzuki et al., 2000). Meanwhile, Suzuki et al., (2000) analyzed the conductivity of the electrolyte, whereas Suzuki et al., (1999) looked into the crosslinked PPVA with glutaraldehyde (GA). The study showed that the glass transition temperature and the ionic conductivity significantly depended on the degree of phosphorylation. Furthermore, crystallinity was found to decrease with the increasing degree of phosphorylation (DP), which indicated an increase in the amorphous part in the polymer. Other than that, An et al., (1995) also reported on anionic polyelectrolyte of partially phosphorylated PVA, which was synthesized via urea-phosphoric acid

method. Next, Shirai et al., (1996) continued the usage of PPVA to form a complex of PPVA with metal ions. Similar to Banks et al., (1993) and Iribarren and Lemmetyinen (2009), Yu and Carlsen (2008) also produced phosphonate group, but with a different synthesis method. Yu and Carlsen (2008) named the product ‗poly (vinyl alcohol) phosphate', which was used as a polymer backbone for biopolymer applications. Moreover, PVA modified with P_2O_5 and excess of 85% H_3PO_4, created a P-O bond and produced partially phosphonated PVA. However, the phosphate groups had been found to be varied through the control of the stoichiometry of the mixture of reaction and time. Only 26% of the hydroxyl group was converted to phosphate groups that gave polyvinyl phosphate, as indicated by the P analysis. Besides, from Figure 2.5, it can be concluded that Yu and Carlsen (2008) produced partially phosphorylated PVA, which is called poly (vinyl alcohol) phosphate (PVA-P). Other than Yu and Carlsen (2008), several publications also used the same name (polyvinyl alcohol phosphate), such as Zhan et al., (2004), Mohapatra et al., (2006), Pramanik et al., (2008), and Pramanik et al., (2009).

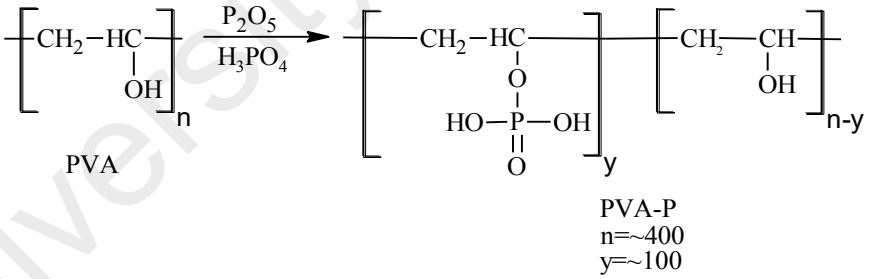

Figure 2.5: Partially phosphonated PVA (PVA-P) (Yu & Carlsen, 2008)

Pramanik (2009) discussed some simple chemistry for biocomposite containing HAp and poly (vinyl alcohol) phosphate. The reaction occurred was between the OH and the phosphate group, which had been heat-treated in autoclave at 120 °C for 3 hours with excess phosphoric acid. The formation of R–O–P or C–O–P bond confirmed the presence of phosphate group. Pramanik et al., (2008) also reported the synthesis of poly (vinyl alcohol) phosphate as nanocomposite with HAp. Hence, it can be concluded that

Pramanik et al., (2008) also produced partially phosphorylated PVA and called it ‗poly (vinyl alcohol) phosphate'. Additionally, Mohapatra et al., (2006) explained the usage of poly (vinyl alcohol) phosphate for surface coating that can produce highly stable aqueous dispersion of magnetite nanoparticles. The method employed to prepare PVA-P was adopted from by Zhan et al., (2004) that suggested to use the term ‗poly (vinyl alcohol) phosphate'. Furthermore, they did not only report the synthesis of PVA-P, but also the synthesis of poly (vinyl alcohol) diphosphate (PVA-DP). Zhan et al., (2004) used 6.6 g of PVA with a small amount of water at 8.5ml and 15 ml of H_3PO_4 added in the flask, and heated to 80 ˚C under constant stirring until PVA was dissolved. The reaction was conducted in a flask equipped with mechanical stirrer, condenser, and thermometer. In the reaction, polyvinyl alcohol phosphate (PVA-P) and polyvinyl alcohol diphosphate (PVA-DP) were produced, as illustrated in Figure 2.6. PVA-P acted as a hydrophilic structure and it was easy to dissolve, while PVA-DP acted as a crosslinking structure and this esterification affected water absorbency. It was also stated that reaction time less than 3 hours produced PVA-P, while reaction time more than 3 hours produced PVA-DP. PVA could not be dissolved completely at a temperature less than 80 °C. In fact, most of the OH groups in PVA molecules were not activated due to hydrogen bond. Moreover, the esterification between PVA and PA only occurred on the surface of the PVA powder. This is because; PVA could not be dissolved completely when the reaction temperature was low and most of the hydroxyls in the PVA molecules action were also low. Therefore, the esterification degree of the product was low. However, all PVA dissolved completely at 90 °C and achieved higher crosslinked densities, where products of PVA-DP and polyvinyl alcohol diphosphate (PVA-TP) were obtained. Furthermore, the increase in crosslinking of di- and tri-phosphate led to the retention of more organic materials in the form of char and portrayed flame retardance properties. Earlier, Banks et al., (1993) reported that

increase in dehydration led to inter-molecular elimination of PA from PPVA. The chain scissoning continued to decrease, and then, followed by the formation of di-phosphate and tri-phosphate crosslinks. Additionally, phosphate and diphosphate reported by Banks et al., (1993) support the findings obtained by Zhan et al., (2004).

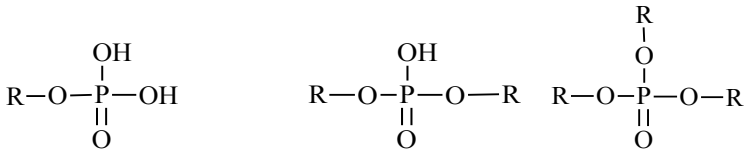

(i) (ii) (iii)

Figure 2.6:(i) phosphate; (ii) di-phosphate, and (iii) tri-phosphate, where R is polymer (Banks et al., 1993; Daul et al., 1954).

From the discussion above, it can be concluded that the reaction of PVA with H_3PO_4 will produce phosphorylation of PVA with two functional groups, which are phosphorylated PVA or known as poly vinyl phosphate, and unphosphorylated PVA (remains as PVA). Phosphorylated PVA with a degree of phosphorylation (75%) is known as poly vinyl phosphate. Polyvinyl phosphate should only contain phosphate group and no hydroxyl group, which has an average molecular weight of 13300 g/mol. Daul et al., (1954) also reported the same structure, but called it poly vinyl phosphate with three different structures of singly bound phosphorus (phosphate), doubly bound phosphorus (di-phosphate), and triply bound phosphorus (tri-phosphate) by using various methods, such as phosphorus oxychloride, phosphorus pentoxide, phosphoric acid, and urea-phosphate. The urea-phosphate method produces complete single bound phosphorus that is water soluble. Meanwhile, other methods may produce either insoluble or partially soluble poly vinyl phosphate. The structure shown in Figure 2.6 (i) illustrates polyvinyl phosphate, (ii) polyvinyl diphosphate, and (iii) poly vinyl triphosphate.

Meanwhile, most phosphorylated PVA with a degree of phosphorylation (5-26%) has been reported as partially phosphorylated poly (vinyl alcohol) or known as poly (vinyl

alcohol) phosphate (Yu & Carlsen, 2008) (26%), (Datta et al., 2012) (12%), (Chen & Liu, 2011b) (a)(5%), and (Chen & Liu, 2011c) (11%)). These poly (vinyl phosphate) and poly (vinyl alcohol) phosphate mainly have the C–O–P bond. Meanwhile, the difference with poly vinyl phosphonic acid is that it has a bond of C–P. Some publications, in fact, suggest that a new method is needed to solve the leakage problem with modification of PVA with H_3PO_4 as it is not covalently bound to polymer matrix (Narayanan, 2005). Before that, Leute (2007) also explained that most modification of PVA and phosphoric acid or any other phosphorus element was not successful due to limitation of knowledge, equipment, and properties of PVA produced at that time. As a result, it failed to spark interest, except for polyvinyl phosphonic acid which is commercially available. Furthermore, the reaction of PVA with phosphoric acid offers a covalent bonding between C–O. C is originated from polymer and O is from phosphoric acid, which is not chemically stable in certain condition. Besides, it is difficult to generate C–P bonding between PVA and phosphoric acid, which is chemically stable and results in poly vinyl phosphonic acid. Moreover, possible applications for those modified polymers are plenty. The combination of a stable carbon backbone and phosphoric acid or ester group could be relevant for many applications. Polyvinyl phosphonic acid is obtained if the reaction between PVA and PA produces C–P bond. Rivas (2004) conducted a research on water soluble polymer materials with the ability to bind metals ions. In his study, polyvinyl phosphonic acid (PVPH) of polychelatogen was analyzed. The structure of poly vinyl phosphonic acid shown in Figure 2.7 contains C–P bond that is difficult to obtain in the simple reaction between PVA and PA.

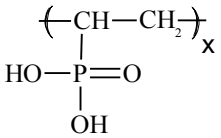

Figure 2.7: Polyvinyl phosphonic acid (PVPH) (Rivas, 2004).

Most bonding refers to C–O–P, where the reaction of PVA with H_3PO_4 produces an interpolymeric reaction of C–O–P covalent bond (Bayer et al., 1983). The starting materials used were PVA, phosphoric acid trialkyl ester (chelating agent), and phosphoric acid chloride. PVA reacts with chloride to form covalent bond, then, cleavage of hydrogen chloride, and process of alkaline hydrolysis to produce partially phosphorylated PVA. On the other hand, the reaction between PVA and phosphorus oxychloride produces three different structures, as shown in Figure 2.8.

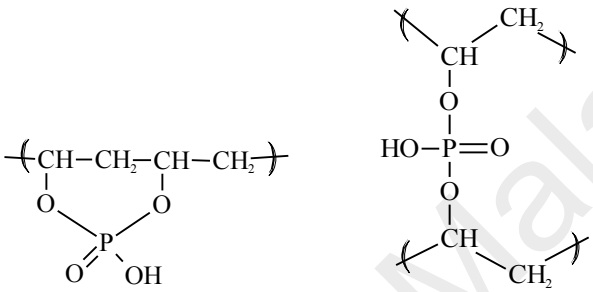

Figure 2.8: Reaction of PVA with phosphoric acid that produces different structures (interpolymeric reaction) (Bayer et al., 1983).

In addition, Lazareva et al., (1999; 2002) discussed about hydrogen bonding and possible structure from phosphorylation of PVA with phosphoric acid. They discussed on the possibility of the practicality and the impracticality of hydrogen-bonded structures that can be formed. They also discussed the mixture of PVA-phosphoric acid-metal produced by hydrogen-bonded complexes with different structures and properties known as liquid crystal (LC) (Lazareva et al., 1999; 2002). Besides, the composition of the PVA and PA used in the system was 4:1 with 10% aqueous PVA (PVA16/1) solution stirred for 30 minutes at a temperature of 20-80 °C to obtain composites containing 15, 25, and 40 wt% of H_3PO_4. Both the practical and impractical reactions of PVA with phosphoric acid are illustrated in Figures 2.9 and 2.10.

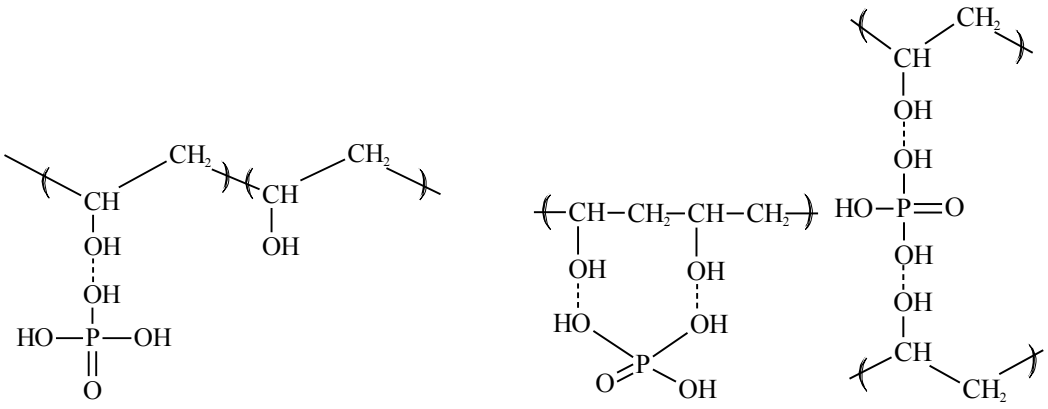

(i) (ii) (iii)

Figure 2.9: Reaction of PVA with phosphoric acid that produces structure with the formation of hydrogen-bonded structures (Lazareva et al., 1999).

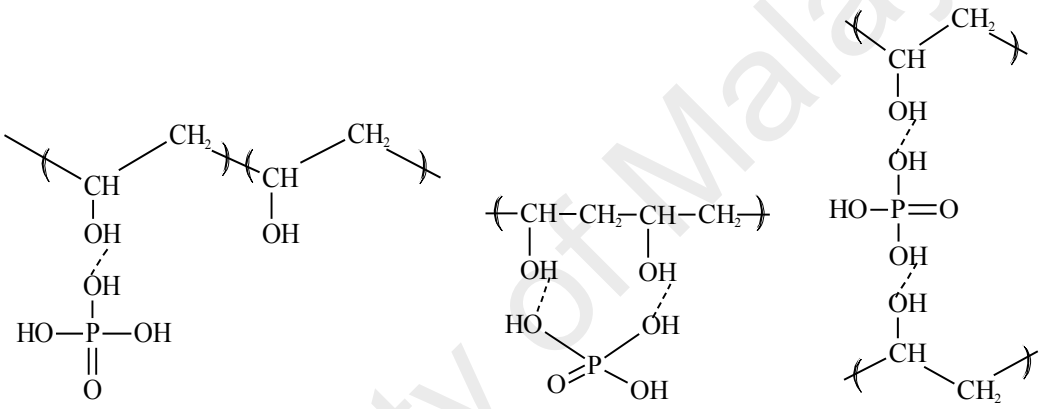

(i) (ii) (iii)

Figure 2.10: Formation of improbable hydrogen-bonded structures (Lazareva et al., 2002).

LC experiences structural change in the presence of external dielectric, magnetic, mechanical, and thermal effects, besides possessing the potential in many technology designs as in robotics, instrument making, and mechanical engineering. Furthermore, Lazareva et al., (1999) discovered a few factors that influence the complexation, such as composition and concentration (PVA-phosphoric acid molar ratio) of the component, solution temperature, method of preparing the composition, the way of complexes formation, shear rate, PVA structure, and also the effect of the structural reorganization.

In fact, composites of polyvinyl alcohol (PVA) with inorganic and poly acids (silicotungstic, phosphoric, polyacrylic, and polymethacrylic) have wide applications,

such as membranes preparation, various coatings, paper sizing formulations, and others. Addition of polyacids or inorganic acids to PVA solutions produces hydrogen-bonded complexes. Besides, most of the bonding display the reaction of PVA and PPVA at C–O–P covalent bonding (Datta et al., 2012) and not hydrogen bonding. Lazareva et al., (1999) reported more details on the hydrogen bonding structure that may occur. Further discussion on these covalent and hydrogen bonding occurrences is discussed in the FTIR section.

Besides, researches on PPVA have drawn interest in metal chelates and composite due to its OH and phosphate functional group. The metal-PPVA complexes may be useful as metal selective absorbents, coating materials, non-inflammable materials, and artificial teeth. Other than that, reported on PVAP as stabilizer to produce poly aniline nanoparticles (Jiang et al., 2014) and magnetite nanoparticle (Mohapatra et al.,2006). Pramanik, (2008) produced poly (vinyl alcohol) phosphate that functioned to improve the interfacial bonding between PVAP and HAp. PVAP with 4.5% of P produced the most stable colloidal particle for synthesis of HA, as shown in Figure 2.11.

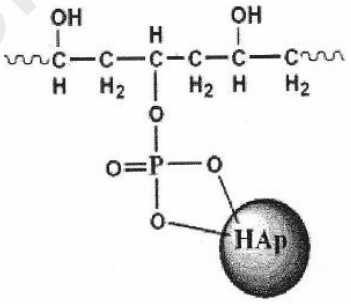

Figure 2.11: Poly vinyl phosphate interfacial bonding with HA particles (Pramanik, 2008)

The hydroxyl groups of PVA also contribute to complexation with nickel ion besides the phosphorus units (Bayer et al., 1983). The metal binding was lower than the neutral media at lower pH values. Metal complexation is favored in neutral and alkaline media based on the dissociation equilibrium between alcohol and alcoholate. In fact, the

introduction of phosphoric group yielded several changes. Furthermore, polychelatogen increased as the pH value increased.

PPVA in solution phase displayed higher surface tension and shear viscosity compared to PVA (Datta et al., 2012). PPVA also increased its semi-crystalline polymer, which indicated stronger intermolecular interaction like hydrogen bond compared to PVA solution (Jin et al., 2007). Properties of PPVA can be modified depending upon its polymer conditions, drying, grinding or chemical modification. Besides, PVA and PPVA have been used as base polymer for metal binding, nanoparticle, and nanocomposite synthesis. Furthermore, the hydroxyl group and the phosphate group in PPVA act as chelating site to interact with metal ions, leading to the formation of a closely packed three-dimensional network structure. In situ, synthesis of nanoparticles in a polymer matrix has the potential to control mean particle size, as envisaged in earlier studies. Nevertheless, the homogeneous dispersion of particles in the polymer matrix would lead to the formation of nanocomposites with improved thermal, barrier, and mechanical properties. Table 2.2 summarizes the literatures related to PPVA.

Table 2.2: Summary of partially phosphorylated PVA starting materials and preparation methods

No.	Starting Materials	Methods	Product	References
1	• PVA powder (10g) • H_3PO_4 (50ml) • Urea • distilled water (50ml)	• Used three-neck round bottom flask equipped with a vigorous mechanical stirrer, a condenser, and a thermometer. • The mixture was heated up to 90 °C under constant stirring until the formation of homogeneous melt mixture. • Refluxed at 90 °C for 3 h, cooled to room temperature, and precipitated in excess ethanol. • The gel product was washed thoroughly to remove unreacted molecules with ethanol until the pH value of washed solution reached 5.0–6.0. • Finally, the product was then freeze-dried.	• Phosphorylated PVA • DP range from 1.75 to 7.69 depends on urea dosage.	(Peng et al., 2014)
2	• PVA (DP 1700) • Hcl (36%-38%) • Ammonium peroxydisulfate	• Method and preparation were referred to Chen and Liu (2011c).	• Partially phosphorylated PVA (PPVA) (stabilizer of Pani)	(Jiang et al., 2014)
3	• polyvinyl alcohol (86-89%)(10g) • 4.5 M orthophosphoric acid solution • methanol (Himedia, India)	• Mixed with vigorous mechanical stirring. • Completely homogenous melt mixture was refluxed at 85 °C for 3 h, cooled to room temperature, and product precipitated in excess of methanol. • The precipitate was repeatedly resolubilized in deionized water, reprecipitated, and washed with methanol to remove unreacted molecules. • The product was then vacuum-dried at 60 °C for 3 days. • DP 11.3% (±0.6, n = 5)	• Partially phosphorylated PVA (PPVA)	(Datta et al., 2012)
4	• PVA (1800), 7% (w/v) PVA, • 1cm^3 of H_3PO_4	• H_3PO_4 ratios used were 0.00, 0.85, 1.7, 3.4, 5.1 M.	• PVA/ H_3PO_4membrane	(Ahmad & Sheha, 2013)
5	• PVA 80,000 g mol^{-1} • H_3PO_4 (99%)	• No detailed explanation on how to prepare PPVA.	• PVA doped H_3PO_4	(Thanganathan et al., 2011)
6	• PVA (6g), • H_3PO_4(6g) • Deionized water (60ml)	• H_3PO_4 mixed with deionized water and the mixture was heated at 85 °C under constant stirring until the solution became clear.	• PVA/ H_3PO_4 gel electrolyte	(Yuan et al., 2011)
7	• PVA (dp 1700) (88% hydrolyzed), • Phosphoric acid (H_3PO_4,	• 50 g of phosphoric acid, 20 g of PVA, and 0.4 g of urea were added to 50 mL of distilled water in a flask and stirred for 24 h at room-temperature. The mixture was heated to 90 °C and	• Partially phosphorylated PVA (PPVA) •	(Chen & Liu, 2011c)

	85%) • Urea ($(NH_2)_2CO$, 99.9%)	stirred thoroughly for about 3 h until the pH value of the mixture was 5-6. • Degree of substitution (DS) of the P-PVA or the phosphorus content of the P-PVA was 5.42wt %.		
8	• PVA(dp=1788±50), Mw=76, 500-80, 800, degree of hydrolysis of 88%. • Phosphoric acid (H_3PO_4, 85%), • Urea ($(NH)_2CO$, 99.9%)	• 94.0 g of phosphoric acid, 20.0 g of PVA, and 2.4 g of urea were added to 100 mL of distilled water in a flask and stirred for 8 h at 50 ºC. • The mixture was heated to 95 ºC and stirred thoroughly for about 6 h, and a yellowish-white colloidal solution was obtained. • Degree of substitution (DS) of the P-PVA was 12.9 mol%.	• Partially phosphorylated PVA (PPVA)	(Chen & Liu, 2011b)
9	• PVA (dp=1788±50), Mw=76, 500-80, 800, degree of hydrolysis of 88%. • Phosphoric acid (H_3PO_4, 85%), • Urea ($(NH)_2CO$, 99.9%)	• Degree of substitution (DS) of the P-PVA was 12.9 mol% and 2.2:1	• Partially phosphorylated PVA (PPVA)	(Chen & Liu, 2011a)
10	• PVA 25000 • H_3PO_4 88-93% • triply distilled water	• PVA: H_3PO_4= 70:30 was prepared by using triply distilled water as solvent via solution casting method. • Preparation of thin film was referred to Prajapati (2009).	• PVA- H_3PO_4 systems (PVA-doped H_3PO_4)	(Prajapati et al., 2010)
11	• PVA (dp 1700-1800) • H_3PO_4 (88-93%) • triply deionized water	• Mixed and stirred for a long time for homogeneous uniform solution. • Pour on mould, dry open air, and vacuum dry at 10^{-3} Torr.		(Prajapati & Gupta, 2009)
12	• PVA • H_3PO_4	• Mixed in autoclave at 120 ºC for 3 h in excess H_3PO_4.	• PVAP (poly vinyl phosphate)	(Pramanik, 2009)
13	• 98.5% hydrolyzed PVA(0.9wt% PVA) • 85% Phosphoric acid • 100 ml water	• PVA:H_3PO_4 (1:1, 1:2, 1: 3) • Stirred at 90 ºC for 30 minutes and left to repose for 2hrs.	• polyvinyl alcohol–phosphoric acid (PVA-PA) films	(Iribarren & Lemmetyinen, 2009)
14	• PVA(6.6g) • H_3PO_4(15ml) • milipore water (8.5ml)	• Mixed in a 3-neck round bottom flask, stir condenser, and thermometer, heated up to 80 ºC until dissolution and refluxed for 1hr. • Cooled and precipitated with methanol to remove unreacted H_3PO_4 (repeat precipitation). • Gel vacuum-dried at 80 ºC overnight.	• Polyvinyl alcohol phosphate (PVAP)	(Pramanik et al., 2008)

		• PVAP dissolved in hot water, added PVAP particle with vigorous stirring at 3000rpm, and kept in vacuum desiccator to remove bubbles. • Method adhered to that suggested by Mohapatra et al., (2006).		
15	• PVA • oligophosphoric acid (P_2O_5) • 85% H_3PO_4	• PVA that reacted to P_2O_5 was added to access H_3PO_4 and run for 2 days in a desiccator over P_2O_5. • Product was purified via dialysis, precipitated with acetone, and dried. • 26% (DP 26%) hydroxyl was converted into phosphate group	• Partially phosphonated polyvinyl alcohol, PVA-P •	(Yu & Carlsen, 2008)
16	• PVA 1750 (containing 1-2 mole% of acetyl group) + H_3PO_4 and Peg as plasticizer.	• PVA 1750 (containing 1-2 mole% of acetyl group) + H_3PO_4 and Peg as plasticizer.	• Polyvinyl alcohol complexed with phosphoric acid • Application as an electrolyte	(Gupta, 2008)
17	• PVA, phosphoric acid	• PVA, phosphoric acid	• PVA treatment with PA generated phosphoester • Application in fire retardant	(Sergio I. Sanchez 2007)
18	• PVA (87% hydrolyzed, MW: 31,000–50,000) • 85 wt.% phosphoric acid (H_3PO_4) • phosphosilicate	• No details concerning the procedure	• PVA molecules partially reacted with phosphoric species in phosphosilicate gel particles • membrane PVA phosphosilicate	(Jin et al., 2007)
19	• PVA 1700 99% • H_3PO_4	• Method used as suggested by (Zhan et al., (2004) • Phosphorus content increased from 3.2-4.8% by increasing the H_3PO_4 concentration from 2M to 5.5M. • DP 3.2-4.8%.	• Polyvinyl alcohol phosphate	(Mohapatra et al., 2006)
20	• PVA 1600 (97.5-99.5% hydrolysis). Polyphosphoric acid (115% phosphoric acid, Aldrich)	• Degree of substitution (DS) 0.5% was calculated from NMR.	• Poly (vinyl alcohol) phosphate • (paper making)	(Chen et al., 2005)
21	• PVA 1700 99% (6.6g), 15ml H_3PO_4, 8.5ml water.	• Reaction was conducted in flask equipped with mechanical stirrer, condenser, and thermometer. • Stirred at 80 °C for 30 minutes and left to repose for 2hrs, and washed with Na_2CO_3 to remove non-reacted H_3PO_4. • Phosphorus content was estimated spectrophotometrically with molybdovanadophosphoric acid method. Phosphorus analysis	• Poly (vinyl alcohol) (PVA-P) • Poly (vinyl alcohol) diphosphate (PVA-DP)	(Zhan et al., 2004)

		was carried out via molybdovanaphosporic acid method. 1.7-12mg of PVA-P was placed in a 100ml beaker. The content of P was 13.6%		
22	• 5 g of PVA 88% hydrolyzed, 5 mL (H_3PO_4) 85% and 50 mL of H_2O.	• 5 g of PVA 88% hydrolyzed, 5 mL of (H_3PO_4) 85%, and 50 mL of H_2O.	• solution of PVA:phosphoric acid	(Castañeda, 2003)
23	• PVA (99-98%, MW31000-50000), • PVA (99%, MW 50000), • PVA (99%, MW89000-98000), • PVA (99%, MW 124000-186000), • phosphoric acids 86%.	• 10 g of PVA was first dissolved in 100 ml of hot water as indicated above, and then, 10 ml of H_3PO_4 was added. • 1 g of PVA was added into flask with 10 ml of water dispersed into water with electromagnetic stirring, and then, dissolved by heating to 90 °C. After cooling, various amounts of H_3PO_4 had been added to give a homogeneous solution.	• H_3PO_4 activated PVA	(Yue et al., 2003)
24	• Poly(vinyl alcohol) (PVA, MW 104, Loba Chemie) • phosphoric acid (H_3PO_4, 1:1) • Distilled water (1 wt.%)	• PVA:H_3PO_4, 1:1 was dissolved in distilled water (1 wt.%)	• PVA+ H_3PO_4 (solid polymer electrolyte, SPE)	(Somani et al., 2003)
25	• 10% aqueous PVA (16/1), • 90% H_3PO_4 • Water.	• Mixture of 100 ml water, PVA, and various H_3PO_4 ratios; 15, 25, and 40 wt%, were stirred for 30 minutes.	• PVA+ H_3PO_4 system	(Lazareva et al., 2002)
26	• PVA (98–99% MW31000-50000) • H_3PO_2, 50 wt.%,	• PVOH: H_3PO_2 concentrations, e.g. OH:P: 0.02, 0.05, 0.075, 0.1, 0.15, 0.25, and 0.5.	• polymer blend PVOH:H_3PO_2:H2O	(Vargas et al., 2001)
27	• PVA, M.W. 10^4, Loba Chemie. • phosphoric acid	• PVA films containing phosphoric acid 1:1 from aqueous solution 1 wt.%.	• Polyvinyl alcohol complexed with phosphoric acid	(Somani et al., 2001)
28	• PVA, M.W. 10^4, Loba Chemie. films containing • phosphoric acid	• PVA films containing phosphoric acid 1:1 from aqueous solution 1 wt.%.	• Polyvinyl alcohol complexed with phosphoric acid	(Somani et al., 2000)
29	• PVA 2000 • N,N-dimethylformamide (DMF) • Dicyanodiamide • 100% orthophosphric acid	• PVA 2000 was completely hydrolyzed by alkaline in methanol. • Dicyanodiamide was purified by recrystallization from water. • DMF, Dicyanodiamide (30 g), urea (45 g), and PVA were dissolved in DMF (150 ml) at 130 °C, and then, DMF (180 ml) containing 17 wt% of 100% orthophosphric acid was slowly	• Partially phosphorylated PVA (PPVA) •	(Suzuki et al., 2000)

		added at 130 °C with stirring. • Degree of phosphorylation (DP) (mol %) 10.9, 14.1, and 18.9%.		
30	• 5 & 10% PVA, 90% Phosphoric acid	• 5 & 10% PVA, 90% Phosphoric acid, 10, 20, 30,40wt% H_3PO_4. PVA: H_3PO_4= 4: 1. 100 ml water	• PVA+H_3PO_4 system	(Lazareva et al., 1999)
31	• PVAMW 2000, • Dicyanodiamide. • Urea • N,N-dimethylformamide (DMF)	• PVA (18 g), dicyanodiamide (30 g), and urea (45 g) were dissolved in DMF (150 ml) at ca. 130 °C with stirring, and then, a mixture of DMF (150 ml) and 100% orthophosphoric acid (30, 15, and 10 ml) was added slowly. After 5 min, the polymers obtained were dissolved in water and dialyzed for 24 h to remove DMF and unreacted phosphoric acid. Potassium hydroxide (1 M) was added up to pH 11, and P-PVAs with dipotassium salts were obtained through reprecipitation into methanol. • Preparation of P-PVA with high DP (method 2) • Dicyanodiamide (10 g) and urea (15 g) were dissolved in DMF (50 ml) at 130 °C with stirring, and then, a mixture of DMF (150 ml) and 100% orthophosphoric acid (10 ml) was added slowly. PVA (6 g) was added at 150 °C and further stirring was continued for 40 min. P-PVA with dipotassium salts was obtained by the same treatment as method 1. • DP 10.9, 14.1, 18.6, 27.8%.	• Partially phosphorylated PVA (PPVA)	(Suzuki et al., 1999)
32	• (PVA, 1±2 mole % of acetyl group). H_3PO_4	• (PVA, 1±2 mole % of acetyl group). PVA and H_3PO_4 were dissolved in deionized triple distilled water and stirred for 4±5hr at 70 °C to make the solution homogeneous. (H+/VA =0.04).	• polymer complex electrolytes of PVA - H_3PO_4	(Singh & Gupta, 1998)
33	• PVA and H_3PO_4.	• (H+/VA =0.04, 0.14, 0.17, 0.33).	• PVA - H_3PO_4 complexes	(Singh & Gupta, 1998)
34	• PVA • dicyandiamide, • urea • orthophosphoric acid	• PVA, dicyandiamide, urea, and orthophosphoric acid in DMF solution. Added orthophosphoric acid to DMF solution of dicyandiamide and urea. The solution was heated at 140 °C, and PVA was then added. The reaction solution was stirred at 140 °C under nitrogen. The resulting solution was dialyzed against distilled water. To this solution, aqueous solution was added and the solution was again dialyzed. The partially	• Partially phosphorylated PVA (PPVA)	(Shirai et al., 1996)

		phosphorylated PVA was obtained through reprecipitation from above solution. DP 3.3-70 mol % was obtained by using the same procedure, but with varied reaction time. DP 15mol% was used for reaction with metals.		
35	• PVA (DP=2000)	• PVA (DP=2000) was completely hydrolysed by alkali in methanol.	• Partially phosphorylated PVA (PPVA) • Degree of phosphorylation 15 mol %	(An et al., 1996)
36	• PVA (DP=2000)	• PVA (DP=2000) was completely hydrolysed by alkali in methanol. • Degree of phosphorylation 3.3 – 35.8 mol %	• Partially phosphorylated PVA (PPVA)	(An et al., 1995)
37	• PVA • H_3PO_4	• PVA 30g. H_3PO_4 concentration ranged from 0.25 to 5.7M. 21.1g H_3PO_4 Reaction in 5 liter flange neck flask equipped with reflux condenser, thermometer, and stirrers. The mixture was stirred and heated to 100 °C using isomantles for periods 100 4.8weight % phosphorus	• Phosphorylated PVA	(Banks et al.,1993)
38	• PVA MW = 1.33 x 10^5, 99% hydrolyzed. • 0.15 M H_3PO_4.	• 0.2M PVA MW = 1.33 x 10^5, 99% hydrolyzed, and 0.15 M H_3PO_4. Transparent film contained PVA: H_3PO_4 (4:1)	• PVA/phosphoric acid solid state electrolyte	(Laventis et al., 1990)
39	• PVA dp1750, 99% hydrolyse. H_3PO_4	• Mol ratio of PVA repeat unit to acid 4: l. The PVA was dissolved in deionized water, and weighted phosphoric acid was added to the above solution, and then, the mixture was transferred to a dry box, where a transparent film was, thus, obtained. Final drying was performed in a vacuum oven at 50 °C for 24 h.	• Polyvinyl alcohol complexed with phosphoric acid	(Gong & Shou-Cai, 1989)
40	• PVA, MW = 1.33 X 10^5 0.11 M phosphoric acid (H_3PO_4)	• One drop of an aqueous solution containing 0.15 mM PVA and H_3PO_4 transparent film (- 100 μm in thickness) contained one H_3PO_4 per four PVA repeating units, (PVA)	• Polyvinyl alcohol/phosphoric acid solid state electrolyte	(Chao & Wrighton, 1987)
41	• Hydrophilic polymer PVA (15000g/mol, • phosphoric acid trialkyl esters, • phosphorus oxychloride,	• No details concerning the procedure were given. Referred to other literature. • 9.58, 9.80, and 15.46% P	• Polymeric complexing agent	(Bayer et al., 1983)

	phosphoric acid ethylester dichloride, • phosphoric acid diethyl ester chloride ethanol			
42	• Fully hydrolysed PVA (less 0.1mol % acetyl content) molecular weight $61.6x10^3$	• No details about the procedure. Referred to other literature. • Phosphate content was 1-13.51wt%	• Phosphorylated Poly(vinyl alcohol)	(Inagaki et al., 1973)
43	• phosphorus oxychloride method • phosphoric acid method • phosphoric acid-urea method	• Reported using phosphorus oxychloride method (14.72% P). 36.4% as singly bound, 39.1% as doubly bound, and 24.5% triply phosphorus bound. 1 phosphate for 3 vinyl group. • Phosphoric acid method (8%P) (partially soluble to water) and • Phosphoric acid-urea method (P content 19.6% and nitrogen content 9.8%)@3 PA in 4VA) (21.5%P @ 1PA in 1VA). • Product ranged from water soluble to water insoluble.	• Poly vinyl phosphate	(Daul et al., 1954)

2.5 Characterization of PVA and PPVA

Characterization of PVA and PPVA focuses on morphology by FESEM, structural and chemical properties by XRD, FTIR, and RAMAN, thermal characteristic by TGA and DSC, and finally, the optical properties by using UV visible and photoluminescence spectroscopy.

2.5.1 Differential Scanning Calorimetry (DSC)/Transgravimetric Analysis (TGA)/Simultaneous Thermal Differential Analysis (STDA) on PVA/PPVA

The glass transition temperature (T_g) for PVA had been at 69 °C (Prajapati et al., 2010) and at 89-90 °C (Somani et al., 2003). However the T_g for PPVA was observed at lower temperature, for instance, 65 °C (Prajapati et al., 2010) and lower than 89 °C (Somani et al., 2003). Meanwhile, DSC traces showed multiple peaks due to endothermic activity of PVA and PPVA (Somani et al., 2003). The first broad endothermic peak below 100 °C mainly referred to the elimination of moisture (Gong & Shou-Cai 1989). Moreover, Alexy et al., (2002) also explained that at 150 – 220 °C, there were elimination of volatile products in PVA. Next, Prajapati et al., (2010) revealed that at endothermic peak of 120 °C, the elimination of moisture changed the structures of PVA and PPVA. However, other researchers stated that the elimination of H-bond water had been at 160 °C (Jiang et al., 2014), 130 – 260 °C (Gong & Shou-Cai, 1989), 200 – 300 °C (Chen & Liu, 2011c), and 250 – 350 °C (Inagaki et al., 1973). Other than that, Somani et al., (2003) and Alexy et al., (2002) asserted that C=C was formed after moisture elimination in PVA. Nonetheless, a different observation was found in PPVA other than formation of C=C of phosphonate group at 168 °C (Yue et al., 2003), where further crosslinking of phosphate, di-phosphate, and tri-phosphate had

been observed (Zhan et al., 2004; Banks et al., 1993; Daul et al., 1954). Somani et al., (2003) explained that the formation of di-phosphate and tri-phosphate started from the breaking of PPVA complex.

At higher temperature, melting temperature (T_m) of PVA was observed at 217 and 224 °C, as well as a range of 180-190 °C (Gong & Shou-Cai, 1989; Prajapati et al., 2010; Somani et al., 2003). Meanwhile, for PPVA, the T_m was observed at a lower temperature than that of PVA at 177 and 222 °C, as well as a lower range of 180 – 190 °C (Gong & Shou-Cai, 1989; Prajapati et al., 2010; Somani et al., 2003). Additionally, Alexy et al., (2002) and Khanna et al., (2005) reported that spontaneous degradation of PVA occurred at temperatures of 260 and 280 °C, respectively. Other than that, Jiang et al., (2014) also observed a breaking of polymer chain in PPVA at 280 °C, while Chen and Liu (2011c) reported a breakage of the main chains of polymers at 450 – 600 °C.

Furthermore, PPVA was reported to decrease in T_m and T_g as compared to pure PVA (Prajapati et al., 2010; Suzuki et al., 2000; Suzuki et al., 1999; An et al., 1995). The decrease occurred in both T_m and T_g because of the plasticizing effect generated by phosphoric acid. Since both water and organic acid are known to produce plasticizing effect on PVA (Alexy et al., 2002), it leads to an increase in the amorphous part that indicates the weakening of dipole-dipole interaction in PVA. Also, it had been reported that phosphorylation restricted the thermal decomposition of PVA backbone and had an effect upon the disorder of PVA crystallinity (Suzuki et al., 1999). However, Somani et al., (2003) conducted phosphorylation of PVA with PA in 1:1 ratio and reported that T_g and T_m of PPVA increased due to hydrogen bonding, as well as ionic complexed formation.

In addition, the DSC curve observed by Somani et al., (2003) produced two peaks. The first peak for PVA was below 100 °C. However, the first peak in PPVA shifted to a higher temperature at 150 °C. Meanwhile, the second peak was observed below 200 °C

and more than 200 °C for PVA and PPVA, respectively. Both peaks had become more intense in PPVA curve. On the other hand, thermal degradation of PVA was found to exhibit three degradation stages. Starting with elimination of water at a lower temperature below 100 °C, then followed by degradation process of PVA with the formation of conjugated double bond, and breaking the main chain (Somani et al., 2003). Most researchers reported that elimination of water occurred at lower temperature below 100 °C, followed by degradation of PPVA that occurred at 200 °C with formation of conjugated double bond, and then, breaking of the PPVA complexes (Somani et al., 2003). However, Alexy et al., (2002) claimed that the first stage of degradation begins as PVA experienced the elimination of water and acetate group, as well as formation of double bonds. Meanwhile, in earlier discussion by Banks et al., (1993), degradation begins with breaking of PPVA complexes after removing water at lower temperature. The breaking of PPVA complexes started with the intra-molecular elimination of phosphoric acid as dehydration (formation of double bond) occurred and continued with a decrease in chain scissoning, as well as formation of crosslinking diphosphate and triphosphate. Besides, Yue et al., (2003) (Figure 2.12) supported the findings obtained by Banks et al., (1993) that PPVA at 168 °C experienced color change, which indicated that the phosphoric acid caused pyrolysis of PVA. H_3PO_4 promoted dehydration, but at a lower temperature. It experienced crosslinking reaction due to phosphoric acid three reaction sites (O=P (OH)).

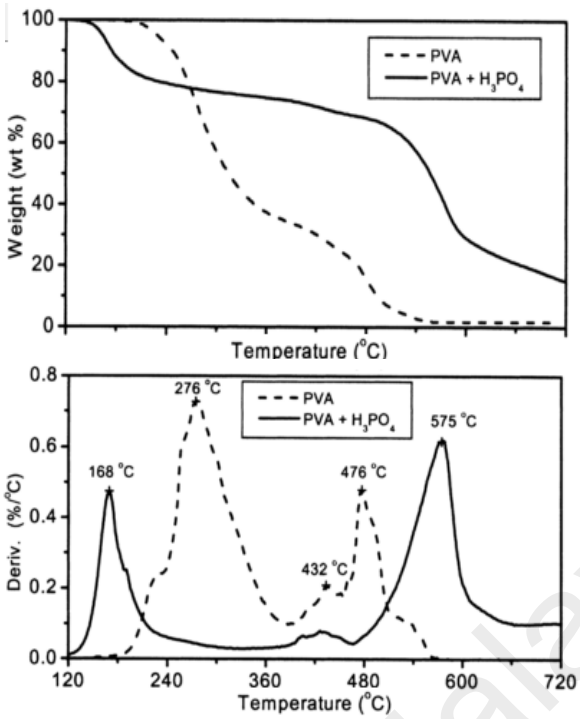

Figure 2.12: TGA analysis of PVA powder, as well as mixture of PVA and H_3PO_4 in air at a heating rate of 10 °C/min (Yue et al., 2003)

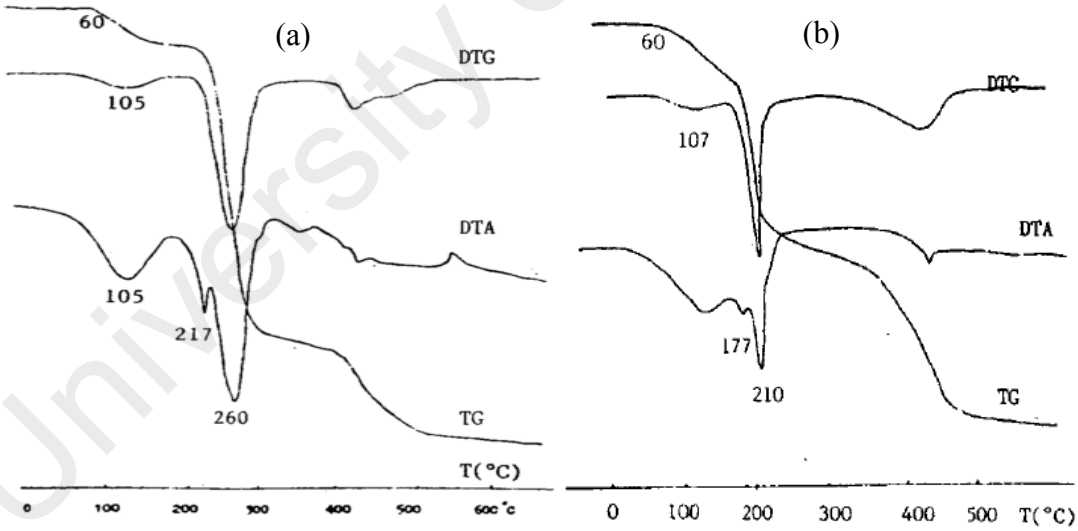

Figure 2.13: TGA and DTA traces for (a) PVA and complexed (b) PVA (4:1) (Gong & Shou-Cai, 1989)

However, Gong and Shou-Cai (1989) discovered a temperature range of 130 to 260 °C for a growing of weight loss by elimination of volatile products (mainly water) (Figure 2.13). In fact, Chen and Liu (2011c) agreed with Gong and Shou-Cai (1989) that the mass losses between 200 and 300 °C reflected the superposition of the release of H-

bond water of P-PVA. Moreover, Inagaki et al., (1973) reported earlier that the reaction of PVA with H_3PO_4 generated a thermal pseudo-stable stage at a temperature range of 250-350 °C. However, this stage had been missing in thermal degradation of PVA due to the H bond of water. Jiang et al., (2014) also reported that elimination of H bond water occurred at 160 °C, then, it continued with the breaking of the main polymer chain at 280 °C. Both Khanna et al., (2005) and Alexy et al., (2002) also supported the finding retrieved by Jiang et al., (2014) that PVA alone started to decompose with spontaneous degradation at about 280 and 260 °C. Next, the second stage of degradation occurred between 270 and 460 °C due to the break-up of PVA backbones, as well as degradation of acetate groups (Alexy et al., 2002). Lastly, the third stage of degradation occurred between 460 and 600 °C, where the PVA decomposed into impurities and other volatile materials. Furthermore, it had been found that PVA could be decomposed completely at 600 °C. Banks et al., (1993), with 4.5% of phosphorus content, discussed that degradation started with intra-molecular elimination of H_3PO_4. Then, at the second stage, chain scission decreased, owing to the formation of di and tri-phosphate, and at the final stage, the residue would begin to decompose at 650 °C and continue beyond 900 °C. PPVA contained high residue with process of oxidation that continued at a higher temperature and stopped at 950 °C. Meanwhile, in PVA, oxidative degradation and stabilization occurred above 700 °C. PPVA complexes that contained phosphate group had the tendency to absorb moisture (Gong and Shou-Cai, 1989). This may refer to the uncrosslinking phosphate that contained OH group. Meanwhile, for partially phosphorylated PVA, the degradation of PVA was catalyzed by the elimination of acetic acid. Acidic compound (acetic acid) may influence the stability of vinyl alcohol unit by protonating OH group (Alexy et al., 2002). Besides, Wan et al., (1999) and Gong and Shou-Cai (1989) reported that the plasticization of PVA was also influenced by water. Furthermore, excess of water may destroy the formation of PVA complexes

and phosphoric acid, as shown by multiple endothermic peaks. Phosphorylation of PVA restricted the thermal decomposition of PVA backbone (An et al., 1996; Suzuki et al., 2000). Moreover, the crystallinity of PVA backbone is disordered by the phosphorylation. Suzuki et al., (1999) asserted that the glass transition temperature and the ionic conductivity were significantly depended on the degree of phosphorylation.

On top of that, TGA analysis of PVA and PPVA, basically, exhibited three stages of degradation that involved water elimination at temperature below 100 °C, where breaking of complexes at temperature beyond melting temperature and breaking of PVA backbone take place (Inagaki et al., 1973). Furthermore, PPVA produced higher weight residue compared to PVA (Inagaki et al., 1973). Thermal degradation of PPVA formed a double bond group at lower temperature to produce phosphate, di-phosphate, and tri-phosphate PVA. PPVA generated phosphoesters during degradation, underwent dehydration with subsequent crosslinking of the polymer, which led to the formation of and intumescent char (Inagaki et al., 1973; Banks et al., 1993). Besides, PPVA showed an increase in the waste residue due to more crosslinking that produced di-phosphate and tri-phosphate, which would later produce more char formation. Less volatile organic materials had been produced and larger proportion of residue remained unoxidized at higher phosphorus content (Inagaki et al., 1973). Table 2.3 summarizes the thermal degradation of both PVA and PPVA.

Table 2.3: Thermal analysis data (DSC, DTG, and TGA) for PVA and PPVA

PVA				PPVA			
DSC/SDTA		TGA		DSC/SDTA		TGA	
Temperature (°C)	Details	Temperature (°C)	Details	Temperature (°C)	Details	Temperature (°C)	Details
69 (70;30) (Prajapati et al., 2010) 89-90(1:1) (Somani et al., 2003)	Glass transition temperature , T_g	<100		65 (Prajapati et al., 2010) > 89-90 (Somani et al., 2003)	Glass transition temperature	<100	
<100 60 (Gong & Shou-Cai, 1989)	Elimination of moisture	100 – 260		<100, 60 (Gong & Shou-Cai, 1989)	Elimination of moisture	100 – 260	
150 to 220 (Alexy et al., 2002)	Elimination of volatiles product in PVA	270-460	Break-up of PVA backbones and degradation of acetate groups (Alexy et al., 2002).	160 (Jiang et al., 2014) 130-260 Gong 200-300 (Chen & Liu, 2011c) 250-350 (Inagaki et al., 1973)	Elimination of H-bond water	260-350 (Inagaki et al., 1973)	thermal pseudo-stable stage related to H-bond water
(Somani et al., 2003) (Alexy et al., 2002)	Formation of C=C			168 (Yue et al., 2003) (Zhan et al., 2004) (Banks et al., 1993) (Daul et al., 1954) (Banks et al., 1993) (Daul et al., 1954) (Somani et al., 2003)	Formation C=C, phosphonate group crosslinking of phosphate, and di-phosphate. Formation of tri-phosphate. Breaking up complex PPVA		
217(Gong & Shou-Cai, 1989) 224 (Prajapati et al., 2010)	Melting temperature, T_m	260-460		177 (Gong & Shou-Cai, 1989) 222 (Prajapati et al., 2010) >180-190 (Somani et	melting point of PPVA		

180-190 (Somani et al., 2003) 260 (Alexy, 2002) 280 (Khanna)	Spontaneous degradation PVA	460-600	Breakage of carbon backbone	al., 2003) 280 (Jiang et al., 2014)	Breaking polymer chain	450–600 (Chen & Liu, 2011c) 650-900 (Banks et al., 1993)	Breakage of the main chains of PVA polymers PVA decomposes into impurities and other volatile materials. The PVA decomposes completely at 600.
		600-1000	0% weight residue			700-950(Banks et al., 1993)	Oxidative reaction occurs above 700. weight 38.33 wt.%

2.5.2 X-Ray diffraction (XRD) analysis on PVA/PPVA

XRD analysis of PVA and PPVA had been reported in a number of publications. Datta et al., (2012) displayed the XRD pattern by using partially hydrolyzed PVA (86-89%) to produce PPVA with 11.3 % degree of phosphorylation. Pure PVA peak was recorded at an angle of 19.8 and shifted to 19.58° with increased intensity. However, the peak at the angle of 22.8° in pure PVA disappeared in PPVA. Another peak at an angle of 41.1° also shifted, but the peak was less intense and broader. Datta et al., (2012), thus, suggested that the increased crystallinity of the semi-crystalline polymer after phosphorylation (peak 19.58°) indicated stronger intermolecular interactions, such as hydrogen bonding in PPVA.

Meanwhile, in another publication, pure PVA was reported to display diffraction peaks at angles 14, 17, and 20° (Prajapati et al., 2010). Moreover, Gupta and Singh (1996) reported that the XRD pattern for pure PVA peak was between 17.5° and 27.5°. Both authors observed broader and less intense peaks as phosphoric acid content increased. Similar finding was observed by Helen et al., (2007), where PVA produced less intense peak at the angle of 20° corresponding to the (101) plane. Instead, the peak at 20°, due to the hydroxyl groups side-chain, was replaced by phosphate group and disappeared in PPVA (Prajapati et al., 2010), as shown in Figure 2.14 (a).

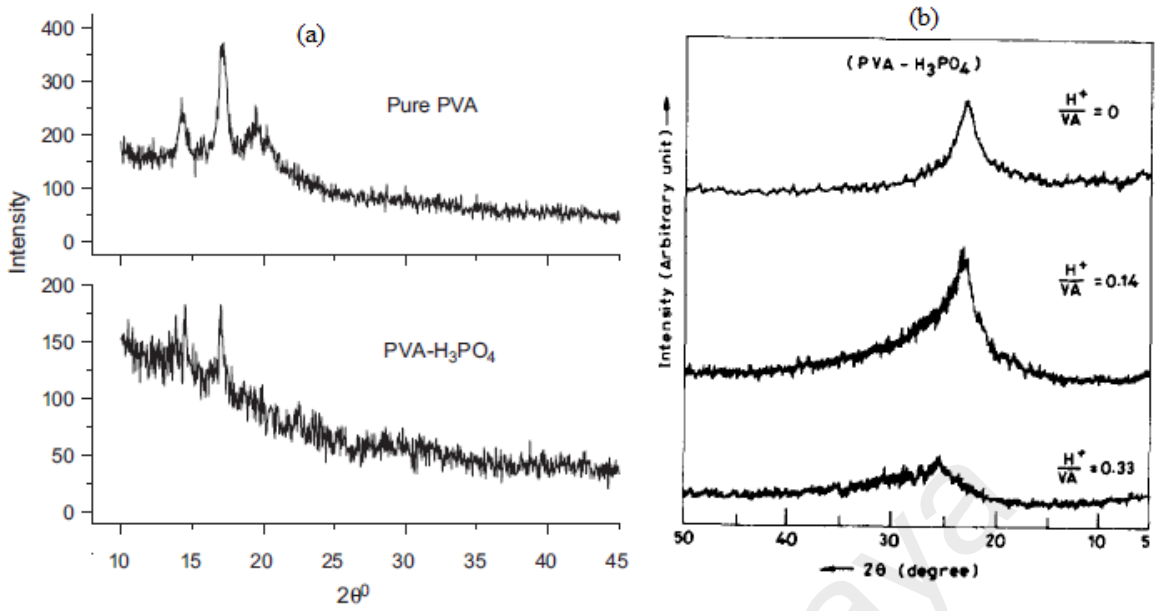

Figure 2.14 : XRD patterns of (a) Pure PVA and PVA- H_3PO_4 (PPVA) (Prajapati et al., 2010) and (b) Pure PVA complexed with H_3PO_4 at different molar ratios (Gupta & Singh, 1996).

Gupta and Singh (1996) also supported the findings after mixing PVA with phosphoric acid in different molar ratios (0, 0.14, and 0.33), as shown in Figure 2.14 (b) that the amorphousness of the polymer increased with the increase in H_3PO_4 concentration. Additionally, Jin et al., (2007) explained that once the number of hydroxyl group in PVA decreases, the crystallinity of the composite also would decrease. Furthermore, amorphocity results from the hydrogen bonding interaction between hydroxyl group in PVA and phosphosilicate, thus offering strong crosslinking or binding. This increases the hydrophobicity of the composite. Earlier, Jin et al., (2007) observed that the pure PVA membrane produced a sharp peak at 22.5° and a broad peak at 47°. The peak at 22.5° corresponded to the (101) plane attributed to the hydroxyl groups in their side-chain. Besides, PVA hydroxyl group was recorded to have reaction with phosphate group in phosphosilicate that behaved as amorphous, which led to low-density and the broad diffraction peak shifted from 22.5 to 24.5°. Phosphoric species in phosphosilicate had been reported to react partially with the hydroxyl group in PVA. Moreover, the diffraction angles differed from those in the XRD patterns of the membranes, whereas

the phosphosilicate gel powder demonstrated binding or crosslinking between the PVA and the phosphosilicate gel particles (Jin et al., 2007). However, Pramanik et al., (2008) observed the XRD pattern for polyvinyl alcohol phosphate at a lower angle of 19.46°. Other than that, Fernandes et al., (2011) observed pure PVA with a strong peak at 19.8°, a mild peak at 22.9°, and a small peak at 40.6°. In addition, irradiated PVA films showed that the crystallinity increased with UV irradiation. Meanwhile, Chen and Liu (2011c) reported that the peak at the angle of 20° was due to crystallization of phosphorylate ester side chain in PPVA, which later produced partly crystalline of mixture PANI/P-PVA. PVA was found to readily dissolve in water, while PPVA had been solubilized only in hot water. This may be due to the increased crystallinity of the semi-crystalline polymer after phosphorylation, which indicated stronger intermolecular interactions in the solid state of polymer. Moreover, the introduction of phosphate groups promoted a number of intermolecular associations; suggesting stronger intermolecular reaction like the hydrogen bonds present in PPVA solutions compared to those in PVA solutions. Table 2.4 summarizes the 2θ values of PVA and PPVA samples.

Table 2.4: Summary of 2θ value for pure PVA, PPVA, and $AlPO_4$

PVA	PPVA
-14, 17(Prajapati et al., 2010) -17.5 (Gupta & Singh, 1996)	-14, 17 are less intense in PPVA(Prajapati et al., 2010) -peak broadened and less intense (Gupta & Singh, 1996)
19.787 (Datta et al., 2012) 19.8(strong), 2011 D.M Fernandes 20 (Prajapati et al., 2010) (Helen et al., 2007)	19.58 – shifted (Datta et al., 2012) 19.46 (Pramanik et al., 2008) -20 disappeared in PPVA (Prajapati et al., 2010) - 20 less intense peak (Helen et al., 2007) -20 due to crystallization phosphate group (Chen & Liu, 2011c)
22.5 (Jin, 2007) 22.849 (Datta et al., 2012) 22.9 (mild) 2011(Fernandes et al., 2011) 27.5 (Gupta & Singh, 1996) 41.066 (Datta et al., 2012) 40.6 (small). 2011 (Fernandes et al., 2011) 47 (Jin et al., 2007) -broad	-24.5° (shifted) low-density and broader diffraction peak (Jin et al., 2007) -22.849 – vanished (Datta et al., 2012) -peak broadened and less intense (Gupta & Singh, 1996) 40.97-shifted (Datta et al., 2012) - broadened and disappeared (Jin et al., 2007)

2.5.3 Fourier Transform Infrared (FTIR) analysis on PVA/PPVA

FTIR analyses of PVA and PPVA were reported in a number of publications. FTIR is important and it is a simple way to prove the occurrence of phosphate bond on the PVA. The spectrum of fully hydrolysed PVA mainly showed the O–H, C–H, C=O, C=C, CH_2, C–O–H, and skeleton bands at the fingerprint region (3600-3400 cm^{-1}) (Somani et al., 2003), range of 3163-2853 cm^{-1} (Somani et al., 2003; Jin et al., 2007), range of 1724 – 1729 cm^{-1} (Somani et al., 2003; Jin et al., 2007), range of 1658-1600 cm^{-1} (Inagaki et al., 1973; Somani et al., 2003), range of 1465 – 1377 cm^{-1} (Mohapatra et al., 2006; Iribarren & Lemmetyinen, 2009), 1090 cm^{-1} (Iribarren & Lemmetyinen, 2009), and range of 920-800 cm^{-1} (Somani et al., 2003), respectively. Besides, most authors agreed that peak in the range of 3600-3400 cm^{-1} referred to O–H group, either in fully hydrolyzed PVA or partially hydrolyzed PVA. Next, the second peak occurred after O–H group as C–H group mainly comes from PVA polymer backbones. The observed C=O peak in partially hydrolyzed PVA had more acetate group compared to that in fully hydrolyzed PVA. The stretching vibrations of carbonyl and/or carboxyl groups in the minor acetate groups (–CO(O)CH) in the PVA contributed to the existence of this peak (Yue et al., 2003). In addition, there were intra-inter molecular hydrogen bonds between the acetate groups in the PVA and adjacent OH group at 1635 cm^{-1} (Jabbar et al., 2010; Bhajantri et al., 2006). However, the same peak describes the existence of bending mode to absorb water molecules (Jin et al., 2007). Meanwhile, at the same range, C=C occurred due to the crystallization peak (Somani et al., 2003). The next peak that commonly occurred was CH_2, which also originated from PVA. The C–O–H peak that comprised of OH group was affected in the modification process. The peak at fingerprint region (<900cm^{-1}) is known as skeleton band. Phosphorylation of PVA contributed to various changes, such as the occurrence of new peak, broadening of peak, vanishing of peak, as well as shifting and changing in peak intensity. FTIR peak for PPVA, which inherited the

original peak from PVA, such as OH (3000-3750 cm^{-1}), CH, and C=C (1651 – 1622 cm^{-1}); also showcased appearance of new bonds like POH, P=O, C–O–P, mixture of C–O–P and P–O, P–O, and O–P–O at ranges of 2335, 1370 – 1150, 1082 – 1000, 1000 – 950, 950 – 880, and 620 – 550 cm^{-1}, respectively. The OH peak that became broader at the range of 3000-3750 cm^{-1} led to lower broaden stretching frequencies, which indicated strong interaction between O–H (PVA) and phosphoric acid to produce P–OH (Iribarren & Lemmetyinen, 2009; Inagaki et al., 1973; Jin et al., 2007). The broadening peak of OH group proved that phosphate group was replaced by the OH group in the polymer. O-H vibrations were bonded with phosphate at a range of 3400-3600 cm^{-1}. Meanwhile, the non-bonded –OH stretching band appeared at a range of 3600-3650 cm^{-1} (Somani et al., 2003). Besides, the peak of C=C had been observed to arise slightly with small H_3PO_4. However, with addition of more H_3PO_4, the intensity would have been enhanced due to the hydrogen bond association (Iribarren & Lemmetyinen, 2009). Additionally, overlapping bending vibration of CH_2 with P=O stretching of phosphate group ester occurred at a range of 1370-1150 cm^{-1} (Mohapatra et al., 2006). Besides, Banks et al., (1993), Inagaki et al., (1973), and Iribarren and Lemmetyinen (2009) reported that the C–OH peak disappeared, whereas the C–O–P peak appeared upon the addition of H_3PO_4. The disappearance of C–OH peak is attributed to the chemical modifications of PVA. When phosphoric acid is added, the broad peak of vO–H and the intense peak of C–O(H)) at 1090 cm^{-1} disappeared due to PVA and phosphoric acid interaction, where C–O(P) bond formed at 1082 cm^{-1}. Earlier, Banks et al., (1993) also found the replacement of C–O–H bond with C–O–P bond at 1096 cm^{-1}. Meanwhile, Mohapatra et al., (2006), Jin et al., (2007), and Iribarren and Lemmetyinen (2009) observed the overlapping of *v*P–O(C) and *v*HPO_4^{2-} vibration groups, which produced an intense peak. The C–O–P groups of covalent bond became weaker at higher concentration of PA due to the formation of hydrogen bonds (*v*HPO_4^{2-}). In addition, Iribarren and Lemmetyinen

(2009) stated that C–O(P) disappeared and a new peak arose; corresponding to ɣP–OH of free phosphoric acid at 982.55 cm^{-1}. Additionally, the intense peak at 980 cm^{-1} appeared due to the overlapping of vP–O(C) and $vHPO_4^{2-}$ vibration groups (Iribarren & Lemmetyinen, 2009). Mohapatra et al., (2006) further reported that the vibration of very low diphosphate $vHPO_4^{2-}$ occurred at 880 and 993 cm^{-1}. The summary of FTIR data is presented in Table 2.5.

Table 2.5: Summary of FTIR data for PVA and PPVA.

PVA		**PPVA**	
Band assignments	**Wavenumber (cm^{-1})**	**Band assignments**	**Wavenumber (cm^{-1})**
OH	3400-3600(Somani et al., 2003)	OH	Broaden and shifted 3400-3100(Iribarren et al., 2009) 3350(Inagaki et al., 1973) 3000-3750(Jin et al., 2007)
C–H	3163, 2914, and 2853 (Somani et al., 2003) -3285(Jin et al., 2007)		
CH_2 vibration	2940, 2900 (stretching) (Iribarren et al., 2009) -2939, 2910(Jin et al., 2007)		
		PO-H	2335(Iribarren et al., 2009)
C=O	1724 (Jin et al., 2007) 1720 (Inagaki et al., 1973) 1465 (Mohapatra et al., 2006)		
CH_2	1420, 1377(wagging) and 1246 (wagging) (Somani et al., 2003) 1423 (bending) (Iribarren et al., 2009)		
		P=O &CH_2	1370-1150 (Mohapatra et al., 2006)
		P=O	1250 (Inagaki et al., 1973)
C-O-H	1090 (Iribarren et al., 2009)	C-O-P	1082 (Iribarren et al., 2009)
		C-O-P	1000 (Inagaki et al., 1973) 1000-1020(Jin et al., 2007)
		P–OH	1000-950(Banks et al., 1993) 1060 (Mohapatra et al., 2006)
skeletal peaks (Sk)	920 - 800 (Somani et al., 2003)	C-O-P & P–O	980 (Iribarren et al., 2009)
		P–O	993 & 880 (Mohapatra et al., 2006) 960-980 (Jin et al., 2007) 982.55 (Iribarren et al., 2009)
		cis C=C	740 (Inagaki et al., 1973)
		O-P-O	620.23, 584.97 to 570.60 (Inagaki et al., 1973)
		PO_4^{3-}	550 (Neuder et al., 2003a)

2.5.4 Raman spectroscopy analysis on PVA/PPVA

There is limited number of publications regarding Raman spectrum of PVA and none about PPVA. Raman amplifies on scattering of light, whereas FTIR is based on absorption of light by the vibrating molecules. Raman normally offers indication of covalent character, but FTIR, in contrast, provides ionic character. Since PPVA is mainly comprised of ionic character with hydrogen bonding, therefore, this is the main reason for nil publication on Raman spectrum concerning PPVA. However, Raman spectra of phosphate or phosphoric acid are discussed in relation to phosphate group in PPVA.

Nevertheless, Raman spectra of PVA has been recently reported by Rajeswari et al., (2013), where bands at 2914, 1341, 1147, and 850 cm^{-1} were assigned to O–H bending and C–H stretching, C–H bending, C–O stretching, and C–C stretching, respectively. Besides, Prosanov and Matvienko (2010) looked into Raman and FTIR spectra of pure PVA and also additional information on thermally-treated PVA. However, dehydration of PVA had been found to lose it polarization of O–H group, but replaced with C–C and C=C bonds that have weak Raman shift. They also stated that information on syndiotactic and isotactic sequences in PVA can be obtained (Prosanov & Matvienko 2010). Meanwhile, Tripathi et al., (2013) reported the annealed PVA at 25 and 65 °C, with comparison of doped PVA and pure PVA. The strong spectra at 2750 – 3500 cm^{-1} disappeared due to fluorescent of Rhodamine B in PVA matrix. Raman shift within 1545 – 760 cm^{-1} also showed changes, which concluded that the fundamental PVA peak vanished or modified upon doping or annealing. In addition, Selvasekarapandian et al., (2010), in similar observation, reported pure and doped PVA, but with different doping materials, for instance, NH_4NO_3. In pure PVA, broad Raman shift appeared at a range of 2750-3500 cm^{-1}. C-H peak at 2914 cm^{-1} shifted when doped with NH_4NO_3 due to interaction of anion with molecular species. Ester oxygen C(O)–O–C at 1147 cm^{-1} was

also obviously affected by the doped materials and confirmed the complexation between polymer and NH_4NO_3 (Selvasekarapandian et al., 2010). Besides, Raman peaks at 1445 and 1366 cm^{-1} with mixture of C-H bending and O-H bending vibrations referred to crystallinity peak that showed broadening, which indicated that the amorphous phase was present due to doping effect (Selvasekarapandian et al., 2010). Meanwhile, C–C stretching vibration at 850 and 908cm^{-1} changed with increased concentration of NH_4NO_3 corresponding to less polarization (O-H) due to the formation of ionic bonding (Selvasekarapandian et al., 2010). Furthermore, Shadak Alee et al., (2013) conducted an analysis of PVA mixed with observed new peak that occurred at 245 cm^{-1} after irridiation. Other than that, Raman shift for phosphate group produced OH water bands at 3596, 3435, and 3220 cm^{-1}. Szumera (2015) also observed PO_2 of the non-bridging O_2 atoms bonded to phosphorus atoms (O-P-O) at 1270 cm^{-1}. Meanwhile, Szumera (2015) and De Jager and Prinsloo (2001) observed the vibration of phosphate units vs(PO_2) within the range of 1180 – 1100 cm^{-1}. Symmetric breathing (A1) of P $(OH)_4$ occurred at 914 cm^{-1} (Jager, 2001) and P-O-P backbone vibrations occurred at 705, 670 cm^{-1}. Earlier, Venkateswaran (1936) reported on PO_4 radicals, HPO_4, and H_2PO_4 ions. The summary of literature for both PVA and phosphate groups is given in Table 2.6.

Table 2.6: Summary of Raman shift for PVA and phosphate group

PVA		Phosphate group	
Wavenumber (cm^{-1})	**Band assignments**	**Wavenumber (cm^{-1})**	**Band assignments**
3016	Valence C–H vibration in CH=C group (Prosanov & Matvienko, 2010)	3596, 3435, 3220	OH water band (Venkateswaran, 1936)
2917, 2914	C-H stretching (Tripathi et al., 2012)		
2925-2914	C-H stretching (Hema et al., 2010)		
2913	v C-H of CH_2 (Shadak Alee et al., 2013)		
2900	C-H stretching (Prosanov, 2011)		
2914	O–H bending and C–H stretching (Rajeswari et al., 2013)		
1730	C = O band (Hema et al., 2010)		
1600	C = C (Prosanov, 2011)		
1490	C-H in CH_2 (Tripathi et al., 2012; Prosanov, 2011)		
1446-1419, 1372-1341	C–H(b), O–H(b) (Hema et al., 2010)		
1445, 1438, 1366	CH and OH bending vibration (Tripathi et al., 2012)		
1428, 1343	CH_2 and OH (Shadak Alee et al., 2013)		
1341	C–H bending (Rajeswari et al., 2013)	1270	$v_{as}(PO_2)$ of the non-bridging O_2 atoms bonded to phosphorus atoms (O-P-O) (Szumera, 2015)
1094 and 1330	O–H deformation and C–O valence bond vibrations of secondary alcohols in PVA (Prosanov & Matvienko, 2010)		
1150-1147	C–C(s), C–O(s) (Hema et al., 2010)		
1147	Ester oxygen C(O)-O-C (Tripathi et al., 2012; Rajeswari et al., 2013; Hema et al., 2010)		
1121	C-OH valence asymmetric ring vibration (Shadak Alee et al., 2013)	1180 (strong)	the vibrations of phosphate units $vs(PO_2)$ (Szumera, 2015)

1111	C-OH vibration (Tripathi et al., 2012) (Prosanov & Matvienko, 2010)
1110	C-OH stretching (Tripathi et al., 2012)
1088	OH (Prosanov, 2011)
1070, 1080	deformation C–H bonds vibrations(Prosanov & Matvienko, 2010)
960–1000	C-C stretching vibration (Shadak Alee et al., 2013)
921, 818	C-C stretching vibration (Tripathi et al., 2012)
912, 908, 850	C-C stretching vibration (Hema et al., 2010)
908cm−1 and 850cm−1	C-C stretching vibration (Rajeswari et al., 2013)
850	CH=CH– polymer chain fragments. ((Prosanov & Matvienko, 2010)
700–760	OH(Shadak Alee et al., 2013)
646	C-O, CH out of plane (Shadak Alee et al., 2013)
479	

1149	PO_2 (De Jager & Prinsloo, 2001)
1100	pyrophosphate groups and assigned to (P - O) groups (Szumera, 2015)
1085, 980(st), 515, 363	PO_4 radicals (Venkateswaran, 1936)
1080, 975(st), 889(w), 363	HPO_4 ion (Venkateswaran, 1936)
1085, 885(st), 515,363	H_2PO_4 ion (Venkateswaran, 1936)
914	Symmetric breathing (A1) of $P(OH)_4$ De Jager & Prinsloo, 2001)
705, 670	P-O-P backbone vibrations

2.5.5 UV visible spectroscopy analysis on PVA/PPVA

The chemical group that strongly influences the molecular absorption characteristics is called chromophore. Chromophores, which can be detected by UV/Vis spectrophotometers, are always involved in multiple bonds, such as C=C, C=O or C≡N, and may be conjugated with other groups to form complex chromophores. Species with a non-metal atom double bonded to oxygen absorb in the ultraviolet region, and there are several inorganic double-bond chromophores that show characteristic absorption peaks. In some instances, measurement of inorganic materials may demand a secondary process, such as complexation with a color-forming reagent or oxidation. Besides, variations of the PA concentration result in a color change in the complexes from transparent to brown (Somani et al., 2003). Pure PVA have been reported to display absorption at 195.5, 193.3, and 197.6 nm at different dilute solutions; 4.0g/dl, 3.0 g/dl, and 1.0g/dl, respectively (Ram & Mandal 2004). The first peak that experienced blue shift indicated predominantly a quantum confined size effect over the salvatochromic effect in planar PVA polymer molecules, which are refined progressively in the dilute solutions on magnetic stirring. Next, the second weak band was observed at 224 and 222 nm at 3.0 g/dl and 1.0g/dl, respectively. Nonetheless, the prominent band at 195.5 or 193.3 nm referred to the s-PVA conformer, while those at the longer wavelengths to a- or i-PVA conformers, which offer not so extensive interchain bridging.

PPVA with various concentrations of phosphoric acid and annealed at 70 °C for 20 h produced an absorption peak at 350 nm (Iribarren & Lemmetyinen, 2009). The peak intensity increased and became more visible with an increase in PA concentration. Earlier, Maruyama et al., (1985) presented similar discussion on PVA film after heat treatment, where the peak was shifted to higher wavelength and increase of intensities was reported. Meanwhile, Li et al., (2003), in an almost similar case, observed that interaction of PVA and PWA that contained phosphate groups showed two intense

characteristic absorption peaks of phosphotungstic acid at 199 and 270 nm for PWA/PVA composite membranes. Besides, Somani et al., (2001) discussed the UV-visible spectra of PVA/H_3PO_4/CV system, but weak absorption peaks were observed for the PVA/H_3PO_4 complexes. Meanwhile, in the system of PVA/H_3PO_4 and methylene blue, the absorption band was observed at 425 nm due to the presence of PVA/H_3PO_4 (Somani et al., 2003). Earlier, An et al., (1996) explained that the UV-visible spectra of Cu II–PPVA system recorded at 20–300 nm and 550–800 nm showed the presence of two absorption bands at 253 and 780 nm for pH level of 2.5–3. The system became blue shifted when the pH level increased to 7, in which the absorption peak was shifted to a lower wavelength of 218 nm.

Furthermore, the optical band gap is defined as the difference between the bottom of the conduction band and the top of the valence band, and basically, represents the optical transition. First, the absorption coefficient α needs to be determined in order to calculate the optical band gap of the films with the following formula:

$$\alpha(\nu) = 2.303\frac{A}{d} \qquad (2.1)$$

where *A* is the absorbance and *d* is the film thickness. In fact, Davis and Mott (1970) reported that electronic transition occurred near the absorption edge and could be determined by plotting $(\alpha h\nu)^2$ as a function of photon energy (hν). The absorption coefficient α is rewritten as:

$$\alpha(\nu) = \beta\frac{(h\nu - Eg)^2}{h\nu} \qquad (2.2)$$

where β is a constant, $h\nu$ is the photon energy, and Eg is the optical band gap. In this study, the values of $(\alpha h\nu)^2$ was plotted as a function of photon energy (hν), and the Eg values were extracted to determine the direct transitions by extrapolating $(\alpha h\nu)^2 = 0$. Table 2.7 summarizes the uv-vis data for PVA/PPVA samples.

Table 2.7: Summary of UV visible for PVA and phosphate group

PVA		PPVA@Phosphate group	
Wavenumber (nm)	**Details**	**Wavenumber (nm)**	**Details**
204, 277 and 324 (Li et al., 2003)	Pure PVA	425nm (Somani et al., 2003)	PVA/H_3PO_4 system
		350nm (Iribarren et al., 2009)	Annealed PPVA at 70°C for 24h
		199.3 and 270.1 nm (Li et al., 2003)	PWA/PVA system
		exhibited very weak absorption (Somani, 2001)	PVA/H3PO4
		253, 780 (An, 1996)	Cu-PPVA system at pH 2.5-3
		218	Cu-PPVA system at pH 7

2.5.6 Photoluminescence (PL) analysis on PVA/PPVA

Kushwaha et al., (2012) reported that the PL spectra of CdSe/PVA excitation wavelength at 380 nm obtained a single peak at 510 nm. The intensity of peak increased with the increase of PVA content, but decreased in CdSe size. Other than that, Fernandes et al., (2011) reported that PL spectra with excitation wavelength at 365 nm obtained a broad band between 400-600 nm; corresponding to the $\pi^* \rightarrow n$ electronic transition of the OH groups, which characterized the three distinct polymer configurations in aqueous solution, which were, isotactic, syndiotactic, and atactic. The PL peak shifted to lower wavelength due to oxygen vacancies and impurities. Moreover, Fernandes et al., (2011) conducted deconvoluted of 95/05 PVA/ZnO PL spectrum by using five Gaussians: 400, 415, 439, and 465 nm due to the PVA structure and 506 nm due to the ZnO nanoparticles. Furthermore, Ram and Mandal (2004) observed four distinct bands at 399.8, 415, 437, and 465 nm due to resonance excitation with vibration of O-H stretching, vibration at excitation wavelength of 350 or 400 nm. Besides, the water content in PVA changed the coplanar structure of the polymer backbone through covalent bond modifications or H-bonding, which also intensified PL. In a diluted solution, the PL had red shifted at 432, 435 or 449 nm or vanishing in a further diluted

solution. In a diluted solution of PVA, the interaction between H-bonding of H_2O and PVA lowers the vibration level, as well as the electronic transition energy. The stereoregularity of the OH groups along the backbone chain generates three distinct polymer configurations; isotactic, syndiotactic, and atactic (Ram & Mandal, 2004). In addition, diluted solution produces an intermolecular interaction of PVA with H_2O and modifies the three vibrational components similar to the a-PVA value. Syndiotactic PVA (s-PVA) is mechanically stronger in structure compared to the other two PVA configurations (atactic PVA (a-PVA) and isotactic (i-PVA).

The PL spectrum for partially phosphorylated PVA does not exist in the literature. However, the relevant work is related to phosphoric acid. In fact, a recent publication by Nourmohammadi et al., (2012) about PL emission of nanoporous anodic aluminum oxide films prepared in phosphoric acid at 394 nm close to UV region due to widening of the electronic sub-band of the oxygen vacancies. Somani et al., (2003) also observed the overlapping peaks PVA/H_3PO_4 where the PVA peak appeared at 425 nm. Chen et al., (2002) concluded that the PL peak observed had been related to the presence of P–O–Zr lumophores in tetrapodal framework due to the post-treatment with phosphoric acid and also related to the defects of oxygen vacancies in the mesoporous zirconia itself. On top of that, a blue shift from 206 to 217 nm was observed after treatment with phosphoric acid. Other PL peaks were observed at 390 and 440 nm due to the intrinsic defect luminescence induced by the presence of P–O–Zr lumophores and the other defects, such as the presence of oxygen vacancies. Table 2.8 summarizes the PL data of PVA and phosphate group.

Table 2.8: Summary of photoluminescence review for PVA and phosphate group

PVA		Phosphate group	
Excitation wavelength (nm)	**Description**	**Excitation wavelength (nm)**	**Description**
365 (Fernandes et al., 2011)	broad peak between 400-600, deconvulate 400, 415, 439, and 465		217 (Chen et al., 2002)
380 (Kushwaha et al., 2012)	510		392 (Nourmohammadi et al., 2012)
350 (Ram & Mandal 2004)	400, 415, 437 and 465		390 and 440 (Chen et al., 2002)
			425 (Somani et al., 2003)

2.6 Aluminum phosphate

Aluminum phosphate ($AlPO_4$) is a compound that contains aluminum (Al), phosphate (P), and oxygen (O). $AlPO_4$ appears as a white crystalline powder with an average molecular weight of 121.95 g/mol, specific gravity of 2.566 g/cm^3, refractive index of 1.54, and melting temperature at 1800 °C. It generally consists of bonding [O -]P(= O)([O^-]. [Al^{3+}] is not soluble in water, but has slight solubility in acid, such as Hcl and HNO_3. $AlPO_4$ has specific and unique properties, such as hydrophilicity, porosity, surface change, and surface functional groups that contain P-OH group and Al-OH groups. $AlPO_4$ is also known by other names, such as aluminum acid phosphate, aluminum monophosphate, monoaluminum phosphate, and aluminum phosphate (1:1); depending on the supplier, as well as the ratio of aluminum and phosphate element in the compound. The ratio of aluminum over phosphate is equal to three or less is a binder, while more than three is called as acid aluminum phosphate. Al rich $AlPO_4$ with a ratio of Al/P between 5:1 and 1:1 produces homogeneous amorphous aluminum phosphate with a surface area of 100 to 300m^2/g, pore diameter less than 1m, and pore volume higher than 0.1cm^3/g (Rosseto et al., 2006).

Moreover, $AlPO_4$ can be classified depending on its structure. The diversity in Al: P ratio produces various structures of $AlPO_4$; either in dense and crystalline micro porous series framework. Crystalline micro porous framework and zeolite (molecular sieve) share the same chemical composition of $AlPO_4$ and have framework structures with microporous cavities that are made up of alternating AlO_4 and PO_4 tetrahedra. Basically, it is a dense $AlPO_4$ with many micropores. The typical reaction is AlOH reacts with phosphoric acid to produce dense $AlPO_4$, whereas for other aluminium sources, such as $AlNO_3$ or alkoxide under pH control with the presence of organic amines, produce a porous of $AlPO_4$. The organic molecule acts as templates to direct growth of porous framework. Crystalline micro porous framework can exist in a 1 dimensional (1-D)

chain structure, 2 dimensional (2-D) lamellar layered structure, and 3 dimensional (3-D) open micro porous framework. The 2-D layered structure of lamellar aluminophosphate (LAP) shows various sheet structures, stacking sequence, and stoichiometries (Jiang et al., 2013). LAP consists of macro anionic sheet developed by alternation of Al element at the center of polyhydra (AlO_4, AlO_5, AlO_6) and P at the center of P $(O_b)_n$ $(O_t)_4$ – n tetrahedral where, t is terminal and n varies from 1 to 4. In the LAP synthesis, structure-directing agents, such as protonated organic amine or complex cations, is important for the development of interlayer region. Besides, LAP has weak van der Waals force between its layers, thus producing a strong interaction between adjacent aluminophosphate nanolayer. In general, the properties of 2-D lamellar structure in polymer or known a nanocomposite is classified as immiscible, intercalated or exfoliated. In fact, the lamellar structure has great potential to delaminate within polymer, besides possessing characteristics of catalytic activity, large surface area and aspect ratio, as well as high modulus, thermal, and chemical stability. Furthermore, introduction of 2-D lamellar onto polymer can improve thermal properties, flame retardance, and mechanical properties.

Aluminophosphate molecular sieves $AlPO_4$ – n, which was first reported in 1982, focused on its potential as catalyst, adsorption, and host guest assembly chemistry. The n acronym was referred to the number that denotes the structure type. Moreover, $AlPO_4$-n is a common solid acid catalyst, which could catalyze dehydrogenation of polymers and promote the charring of polymers. Some of the most common 3-D microporous molecular sieve $AlPO_4$-n are $AlPO_4$-5 (Yang et al., 2014), $AlPO_4$-8, $AlPO_4$-11 (Hu et al., 1995), $AlPO_4$-18 (Bhagwat et al., 2003), and $AlPO_4$-42 (Hu et al., 1995), which exhibited zeolites properties that are similar to quartz silica. In this family, $AlPO_4$-5 (IZA structure code: AFI) has been the most extensively studied. An AFI crystal has a hexagonal structure with space group of P6cc. Its framework consists of 1-D 12-ring

channels (inner diameter: 0.73 nm) that are packed in parallel to the c-axis. AFI single crystals are electrically insulating and optically transparent from ultraviolet to infrared and thermally stable up to 900 °C. These excellent physical properties, plus their unique opened pore structures, offer an excellent template to fabricate host–guest nanostructured composites that have many potential applications in non-linear optics devices. Similar to 2-D, synthesis of molecular sieve $AlPO_4$ also needs a structure-directing agent or template to synthesis the crystalline porous structure. Tetrabutylammonium hydroxide (TBAOH) is usually used as template for synthesis of AFI crystalline porous aluminophosphate VPI-5 and ($AlPO_4$-n) (Jiang et al., 2006). Earlier, Jiang et al., (2005) used TPA as template for synthesizing large-sized and optically clear $AlPO_4$-5 single crystals. Meanwhile, dense $AlPO_4$ generally lacks a porous structure that has chiral tetrahedral configurations. It exits in various polymorph structures, such as amorphous, berlinite, trydimite, and cristobalite, which can be designed by controlling the amount of water in $AlPO_4$ system, pH change, and heat treatment. The dehydration process is important for improving and strengthening the structure of $AlPO_4$ (Palacios et al., 2013).

$AlPO_4$ may exist as a natural mineral or synthetic bound that normally has ratios of Al:P as 1:3 and 3:1. It can also exist either in the anhydrous or hydrated form. Hydrate $AlPO_4$ has a general formulation as $AlPO_4.xH_2O$ with x as the number of water attached to it. Commercially, aluminum phosphate gel in hydrated form is $AlPO_4.1.5H_2O$. Hydrate $AlPO_4$, variscite in orthorhombic $AlPO_4{\cdot}2H_2O$ structure and metavariscite in monoclinic $AlPO_4{\cdot}2H_2O$ structure was obtained at pH ≤ 6 and at low temperature below 200°C (Druppel et al., 2007). Moreover, $AlPO_4$ complex $[(AlOPO_3H)(H_2)_5]^+$ in a solution form may act as neutral, acidic or basic. The polymorph of variscite, $AlPO_4{\cdot}2H_2O$ depends on the phosphoric acid concentration. Dehydration of variscite will convert to berlinite that exhibits structures of tridymite and cristobalite. $AlPO_4$

minerals refer to berlinite ($AlPO_4$), hydrate $AlPO_4$ ($AlPO_4.xH_2O$), orthorhombic varriscite, monoclinic metavariscite ($AlPO_4.H_2O$), agelite ($Al_2PO_4(OH)_3$), trolleite [$Al_4(PO_4)_3(OH)_3$], and wavellite [$Al_3(PO_4)_2(OH)_3 \cdot 5H_2O$]. Meanwhile, others are varied depending on the ratio of Al:P:O (Druppel et al., 2007). In addition, monohydrogen phosphate and dihydrogen phosphate lose water to produce a condensed phosphate (inorganic polymer) at low consolidation temperature with good mechanical resistance. Besides, the polymorph structure of $AlPO_4$ can occur as aluminum phosphate monohydrate $AlPO_4 \cdot H_2O$-H_4 (Boonchom et al., 2008).

Aluminum phosphate ($AlPO_4$) is used in industry as a high temperature dehydrating agent. In addition, $AlPO_4$ also serves as a fluxing agent in ceramics, catalyst in organic synthesis, binders in refractories, fillers in polymer, pigment in paint, and metal coatings. $AlPO_4$ has a dense high strength ceramic with very good properties in high temperature applications. In a dense microstructure, durable and thermally stable aluminum phosphate provides non-porous films that protect metallic surfaces against abrasion, corrosion, and oxidation over a range of temperature and harsh environment. A wide range of temperature makes it an excellent material for application; where bonding or sealing is required. Amorphous Al-rich $AlPO_4$ is more thermally stable than Al-poor composition that crystallizes at a lower temperature. Aluminum ions in the mixed phosphates, nevertheless, play an important role in avoiding the sintering of solids, which is mainly responsible for lowering surface area. In addition, the increasing amount of aluminum ions in the amorphous solid leads to a higher number of acid-base sites that improves the catalytic performance. Moreover, $AlPO_4$ pigment as a nano-structured amorphous aluminum phosphate with closed pores was successfully obtained (Rosseto et al., 2006). $AlPO_4$ nanoparticles are strongly compatible with latex particles by the mechanism of capillary adhesion in the dispersion drying followed by ion-cluster mediated electrostatic adhesion (in the dry film). This compatibility is so high that

bicontinuous networks are formed in many cases and strongly compatible with other particulate solids, which are commonly used as paint fillers, such as various silicates, carbonates, and oxides, found in formulating water-based dispersion. This contributes to the cohesion and the strength of the paint dry film. $AlPO_4$ has also been used as building blocks for new materials endowed with interesting or unusual properties. They can be formed into gels with high proton conductivity, as well as hybrid films with polypyrrol and polyaniline that host organic dyes. Other than that, interpenetrating networks are formed by blending aluminum polyphosphate with thermoplastic latexes and producing films with improved adhesion to many substrates.

The challenges found in the $AlPO_4$ synthesis are the difficulties in developing a systematic crystal growth and in controlling the morphology. The morphology relates to the interaction of surface structure and properties of $AlPO_4$. $AlPO_4$ has a functional group of P-OH, and Al-OH groups that vary the surface change, hydrophilicity, and porosity, besides influencing the properties of $AlPO_4$, such as acidity, basicity, affinity, and reactivity.

2.7 Aluminum phosphate nanocomposite

2.7.1 Composite

Composite is defined as a material with two or more distinct constituents or phases (Callister, 2000). However, there are other criteria that must be satisfied before the material can become a composite. The criteria are;

- Both constituents must present in reasonable proportions
- When the constituent phases have different properties, the composite must have noticeably different properties from the constituent.
- A man-made composite is usually produced by intimately mixing and combining the constituents by various means.

Composite is composed of two (or more) chemically distinct phases on a microscopic scale separated by a distinct interface. The constituent that is continuous and often present in greater amount in the composite is termed as matrix. The normal view is that, it is the properties of the matrix that are improved by incorporating another constituent to form a composite. The second constituent is termed as reinforcing phase or reinforcement. The reinforcement work enhances or reinforces the mechanical properties of the matrix. Reinforcement is usually harder, stronger, and stiffer than the matrix, although there are some exceptions. Composite can be classified into three main categories depending on the matrix. There are metal matrix composite, ceramic matrix composite, and polymer matrix composite. Nonetheless, this study concentrates more on polymer matrix composite, which is highly developed and has a promising future.

The methods to produce composites have been explored to a great degree because of the necessity to engineer a material with specific properties. They are achieved by selecting suitable materials with the best desired attributes and combining them into one composite material. The development of new polymer-inorganic composite materials

with polyacid can find wide applications. Polyvinyl alcohol (PVA) is one of the most important polymeric materials for its many applications in industry, relative to low cost and environmental friendly aspects. Besides, the addition of polyacids to PVA soluble produces hydrogen bonded complexes that offer a suitable surface for synthesis of aluminum phosphate.

2.7.2 Nanocomposite

Polymer nanocomposite consists of distinct organic polymer and inorganic regions that self-organize naturally into composite ―building blocks" with a dimension on the order of nanometer, or billionth of meter. When put together, these basic units form a bulk material.

The importance of polymer and composite has been widely realized and their production began as early as the 1900s. Nanotechnology has opened a new realm of polymer world and has further accelerated the progress in polymer nanocomposite. Polymer nanocomposite was developed in the late 1980s in both commercial research organizations and academic laboratories. Polymer nanocomposites combine two concepts; composites and nanometer-size materials. It is the blend of nanometer-sized fillers with either a thermoset or thermoplastic polymer. Polymer nanocomposites have different properties compared to conventional materials. It alters the properties to improve tensile strength, modulus, heat distortion temperature, barrier properties, UV resistance, and conductivity. Improvements in tensile strength, modulus, and heat distortion temperature lead to widespread speculation that polymer nanocomposites would replace conventionally-filled materials on a large scale.

Moreover, thermoplastics filled with nanometer-size materials has different properties compared to thermoplastics filled with conventional materials. Some properties of nanocomposites, such as increased tensile strength, may be achieved by using higher

conventional filler loading at the expense of increased weight and decreased gloss. Other properties of nanocomposites, such as clarity or improved barrier properties, cannot be duplicated by filled resins at any loading. Most commercial interests in nanocomposites have focused on thermoplastics. Thermoplastics can be divided into two groups, which are less expensive commodity resins, as well as more expensive and higher performance engineering resins.

One of the goals in nanocomposites is to allow substitution of more expensive engineering resins with less expensive commodity resin nanocomposite. Substituting a nanocomposite commodity resin with equivalent performance to a more expensive engineering resin should yield overall cost savings. Two types of polymer nanocomposites are:

- Thermoplastic nanocomposites: These materials are divided into two major categories, i.e., commodity resins and engineering resins. The potential of polymer nanocomposite commodity resin is covered for each resin. Engineering resin nanocomposites are restricted to resins that have been developed.
- Thermoset nanocomposites: These materials have received less commercial interest in their development than thermoplastic nanocomposites. However, these materials may be easier to bring into production. Furthermore, thermoset nanocomposites can offer some significant advantages over conventional thermosets.

The use of organic and inorganic fillers is a common practice in the plastics industry in order to improve the mechanical properties of thermoplastic materials, such as heat distortion temperature, hardness, toughness, stiffness, and mold shrinkage or to decrease other properties, such as gas permeability. The filler effect on the composite properties strongly depends on its shape, size, aggregation state, surface characteristics, and degree of dispersion. In general, the mechanical properties of a composite material with micron-sized fillers are inferior to the properties of a composite with nano-sized fillers.

Physical properties, such as surface smoothness and barrier properties, cannot be achieved effectively by using conventional and micron-sized fillers.

2.7.3 Nano and bulk composites of Aluminum phosphate

Nano and bulk composites of $AlPO_4$ have been reported in several publications, such as Kalbasi and Izadi (2013), Jiang et al., (2013), Devamani (2012), Lee et al., (2013), Wang (2011), Mekky and Nicholson (2007), Gutiérrez-Mora et al., (2006), and Xu et al., (2006). Other than that, Chung (2003) compiled a review of $AlPO_4$ composite and coating. $AlPO_4$ was also reported as a successful coating material on LiCoO by Lee et al., (2013), Oh et al., (2008), and Lee et al., (2004). Meanwhile, Gutiérrez-Mora et al., (2006) and Chen et al., (2003) discussed about $AlPO_4$ as a ceramic coating. $AlPO_4$ was also reported in various types of coating, such as carbon coating film (Monteiro et al., 1999), intumescent coating (Wang, 2011), oxide coating (Devamani, 2012), and metal coating (Palacios et al., 2013).

In both composite and coating of $AlPO_4$, the use of Aluminum nitrate has been given focus as an aluminum source. Aluminum nitrate, as a starting material, was previously reported by Lee et al., (2013), Gutiérrez-Mora et al., (2006), Yang and Kau (2005), Lee et al., (2004), and Kandori et al., (1998).

2.8 Synthesis of $AlPO_4$ nanocomposite

The two key factors in producing polymer nanocomposite are nanoparticles size and their shape. The most applicable methods in producing polymer nanocomposite at present are ex-situ and in-situ synthesis methods.

In the in-situ technique, nanoparticles are generated inside the polymer matrix via decomposition of metal precursors. First, monomer is polymerized in the solution

containing metal ions chemical species. Then, the nanoparticles are obtained by reducing particles ions through chemically, thermally or photolysis methods.

Meanwhile, in the ex-situ technique, nanoparticles that are produced by chemical methods are distributed into polymer or monomer solutions. Other types of techniques have been studied in order to obtain the optimal properties of nanoparticles in polymer matrix, such as by vapor deposition cryochemical synthesis. In fact, numerous works have been implemented worldwide, which have led to a large number of publications about the topic. Using nanotechnology, the future of polymer nanocomposites is to produce engineered nanomaterials that can be potentially used for a variety of diverse applications, such as optical devices, filter color, sensors, polizares, magnetic data storage nano-system, and others. In this study, the researcher attempted to produce in situ $AlPO_4$ nanoparticles embedded in modified polymer.

The common technique of synthesizing $AlPO_4$ is either co-precipitation or hydrothermal method, which is followed by filtering, washing, and drying before further heat treatment process (Wang, 2011). The pH of solution is important in the chemical co-precipitation method where it needs to have cation and anion to react and increase the nucleation, as well as crystal growth. It is also a method of neutralization an acidic solution of Al^{3+} and hydrogen phosphate ions. After pH determination, the product is precipitate, filtered, washed, and dried before calcine process. In the synthesis of $AlPO_4$, the pH modifier used are KOH and NH_4OH (Palacios et al., 2013). Co-precipitation is a typical method for synthesis of micro and nanoparticles through three mechanisms of inclusion, occlusion, and adsorption. Inclusion occurs when impurities occupy the crystal structure lattice. Occlusion, meanwhile, is impurities that are physically trapped inside the crystal structure as it grows and adsorbed to the surface of the precipitate.

Hydrothermal method is widely used to synthesis $AlPO_4$. It is a method to synthesis crystal in hot water under high pressure and depends on the solubility of the samples.

Hydrothermal synthesis has the presence of excess water, which increases nucleation and reduces crystallization time. In contrast to hydrothermal method, solvothermal is a possible method to control the amount of water that has an effect on the crystal size.

Furthermore, Ma et al., (2008) discussed a method of conventional heating and microwave heating that affected the crystallization process. They also discussed the amount of water in the crystallization of molecular sieves and concluded that water promotes both nucleation and crystal growth. Ma et al., (2008) further concluded that heating method affected the crystallization process. Meanwhile, the process of hydrolysis and condensation are elaborated as a basic reaction of the formation and transformation of solution active species. The pH of solution, which contributed to the amount of H^+ and OH^- also induced hydrolysis and condensation reactions. Water, additionally, promoted the kinetic synthesis by promoting the H^+ and OH^- production and transportation. Both water and pH produced faster crystallization time. Hence, water and polar element are important in the synthesis of molecular sieves as they accelerate the hydrolysis and condensation processes, thus affecting the crystallization process. Additionally, Ma et al., (2008) used $NH_4H_2PO_4$ (no crystal water) as the starting material for phosphate source, pseudobohemite (AlOOH, 78.6 wt % $A_{l2}O_3$, dried at 110 °C for 24 h in dry air as aluminum sources and NH_4F (no crystal water)). The quantities of water was controlled with ratio 1 and had been proven to have great effect on crystallization kinetics. Ma et al., (2008) and Kawamura et al., (2007) have similarity in discussing $AlPO_4$ synthesis in relation to pH solution. Kawamura et al., (2007) found that by controlling the pH and the temperature, the number of H_2O molecules that correlated with the morphologies of the $AlPO_4.xH_2O$ particles can be controlled.

Changing the pH precipitation, in fact, produced a complex precipitate mixture with amorphous hydrated structure. Different phosphate and aluminum sources formed

multiple equilibria reactions. Complex ion $[Al(H_2O)_6]^{3+}$ had been found to exist for pH lower than 3. However, at pH more than 3, sample experienced successive deprotonation $[Al(H_2O)]_5(OH)^{2+}$ and a myriad of successive hydrocomplex salts. Minimum solubility occurred at pH around 7 with the precipitation of hydrous $Al(OH)_3$. Finally, in a more basic solution, this solid re-dissolved due to the formation of tetrahedral aluminate ion $[Al(OH)_4]^-$**.** In addition, ion protonation/deprotonation also led to the formation of multiple phosphate species. The ratios of phosphate groups to hydroxyl or aluminum atoms can vary widely. Ions within the precipitate exhibited different solvation degrees around the cores, including condensed O-X-O bridges that promoted the formation of polynuclear complexes. Moreover, in the case of aluminum polyphosphate, this could lead to a large number of complex species. The formation might be affected by ions variability and concentration, stoichiometry, temperature during reaction process, and especially, the precipitation pH.

Furthermore, the synthesis of $AlPO_4$ depends on aluminum source, phosphate source, ratio of aluminum to phosphate, and method of synthesis. In the earlier period, $AlPO_4$ was synthesized by using aluminum oxide as aluminum source. This had been well-established and this kind of synthesis usually refers to the Al_2O_3–P_2O_5–H_2O system. $AlPO_4$ is obtained with P/Al ratio of 1. All dehydrated phosphates are situated between ortho- and meta-phases in the Al_2O_3–P_2O_5 binary phase diagram. According to the three component system of Al_2O_3–P_2O_5–H_2O, metaphosphate is obtained from the monobasic phosphate $(Al(H_2PO_4)_3)$ with increasing temperature when the atomic P/Al ratio is 3. Besides, the recent aluminum source used is aluminum nitrate that produces various geometrical structures, such as nanocrystal (Gutiérrez-Mora et al., 2006), nano spherical, and nanoplate for coating (Oh et al., 2008), nanoparticle, nanowire, and nanoropes (Yang & Kau, 2005), nanoparticle (Devamani, 2012; Mekky & Nicholson, 2007), and nanocoating (Lee et al., 2013). Other aluminum source used recently is

aluminum oxide that produces nanoporous (Rives et al., 2013). Phosphate sources are also important in the synthesis of aluminum phosphate. Campelo et al., (2003) have reported on the synthesis of $AlPO_4$ catalysts by using aluminum chloride and three different types of phosphate sources H_3PO_4 (85%), $(NH_4)H_2PO_4$, and $(NH_4)_2HPO_4$. Another phosphate source that has also been widely used is P_2O_5, but mainly in the synthesis of molecular sieve (Yang et al., 2014; Jiang et al., 2006). However, in the synthesis of nanosize $AlPO_4$, two phosphate sources that have been recently used are $(NH_4)_2HPO_4$ (Lee et al., 2013) and H_3PO_4 (Palacios et al., 2013).

Moreover, nano and bulk composites that consist of $AlPO_4$ have been discussed earlier by Kalbasi and Izadi (2013), Jiang et al., (2013), Wang (2011), and Mekky and Nicholson (2007). Kalbasi and Izadi (2013) produced an $AlPO_4$ composite with PVP, while Jiang et al., (2013) used LAP with PU, and Wang (2011) mixed between mineral $AlPO_4$ known as taranakite with PVA, whereas Mekky and Nicholson (2007) used EG with $AlNO_3$ to produce $AlPO_4$. Table 2.9 summarizes the synthesis of $AlPO_4$ with varies geometrical structures.

Table 2.9: Summary of $AlPO_4$ synthesis with various geometrical structures

Aluminum sources	Phosphate sources	Ratio/ method	Product	Remark	References
Molecular sieve (3D)					
Al_2O_3	P_2O_5	Al_2O_3 + deionized water stirring for 0.5 h at RT + H_3PO_4. After stirring for 0.5 h, 0.24 mL of TEA, and stirred for 0.5 h. + HF. stirred for 2 h. Autoclaved in microwave at 180°C for 3 minutes at different microwave power. Ratio $1.0Al_2O_3$:1.0 P_2O_5:0.7 TEA:(1.5) HF:225 H_2O	$AlPO_4$-5	triethylamine (TEA).	(Yang et al., 2014)
Al tri-isopropoxide ($Al.P_2O_5$)/Al hydroxide (AlOH)	H_3PO_4	Hydrothermal synthesis of $AlPO_4$-5. 1. AlOH source (H_3PO_4+distilled water+Aloh+TEA+final pH 5.5 +autoclaved at 185 °C,24h+filter wash with distilled water+dry at 80 °C for 10h+calcined at 550 °C for 5.5h). 2.AlP_2O_5 source (H_3PO_4+distilled water + ALP_2O_5 + TEA + autoclaved at 185 °C for 13h. Same procedure was done, but pH was adjusted to 5.5-6.5 by using H_3PO_4@mixture Hcl/H_2O.	$AlPO_4$-5	Organic template triethylamine (TEA).	(Kalbasi & Izadi, 2013)
pseudoboehmite alumina (73.6 wt % Al_2O_3)	H_3PO_4, 85 wt % in water	The gel was homogenized by mixing, transferred into an autoclave for a hydrothermal treatment at 175 °C for 4 h. Product was vacuum-filtered and oven-dried (120 °C) before calcination in flowing air (50 mL/min) using a heating profile of 5 °C/min from room temperature to 550 °C and a dwell time of 3 h.	zeolite-type AlPO4-5	The structure-directing agent triethylamine (TEA 99%)	(Rives, 2013)
pseudoboehmite (78.6 wt % Al_2O_3, dried in air at 110°C for 24h).	$NH_4H_2PO_4$ (no crystal water),	pseudoboehmite + $NH_4H_2PO_4$ + NH_4F (no crystal water).quantities of water (H_2O/Al) =1, molar ratio) . Conventional and microwave heating.			(Ma et al., 2008)
$Al(NO_3)_3.9H_2O$	ammonium phosphate $(NH_4)_2HPO_4$	Polymerization complex method. Citric acid + ethylene glycol+aluminum nitrate + ammonium phosphate dibasic. Heated at 130 °C for 3 hours for polymerization and gelation.	Molecular sieve		(Mekky & Nicholson, 2007)
Al_2O_3	P_2O_5	Hydrothermal synthesis. Autoclaved aging at 180 °C, quenched autoclave in cold water, separated product by decanting, dried overnight at 80 °C Al_2O_3:P_2O_5:xTBAOH:500H_2O. HF to adjust pH values.	$AlPO_4$-5	TBAOH template.	(Jiang et al., 2006)
Pseudomehimite	H_3PO_4	$Al_2O_3$65.25% + H_3PO_4+TPA (+ethanol)+distilled water +HF. Ratio of Al/P is equal to 1	Large $AlPO_4$-5 crystal.,	Template TPA	(Guo et al., 2005)

Pseudoboehemite	H_3PO_4	Stirred and obtained gel. Autoclaved at 160 °C in 6 days. Dried in oven at 110 °C for 12h. Calcined at 550 °C for 24h	$AlPO_4$-18	Template N-di-isopropyl ethylamine	(Bhagwat et al., 2003)
Layered aluminumphosphate (2D)					
$AlCl_3 \cdot 6H_2O$ (aluminum chloride hexahydrate)	H_3PO_4	$AlCl_3 \cdot 6H_2O$+ H_3PO_4, Tetramethylammonium hydroxide (TMAH).DDA, DMF, ethanol, and Polyurethane 4190.	Layered structure $AlPO_4$		(Jiang et al., 2013)
Aluminum isopropoxide	phosphoric acid	Hydrothermal methods. Aluminum isopropoxide and H_3PO_4 (2:3) were added to butane, stirred until homogeneous, and butylamine was added. The gel was heated to 150°C, and then transferred into Teflon-lined autoclave for 24 hrs. Filtrated and washed with distilled water and dried in air at 80°C.	Layered structure $AlPO_4$		(Wang, 2011)
$Al(NO_3)_3 .9H_2O$	KH_2PO_4	Co precipitation methods. $Al(NO_3)_3 .9H_2O$ in deionized and decarbonated (heat the water to 100 °C for 2 hours to release the CO_2 in the water) water was added dropwise to a solution of KOH (0.24 mol for Al/P molar ratio 1:2 or 0.18 mol for Al/P molar ratio 2:3) and KH_2PO_4 (0.24 mol for 1:2 or 0.18 mol for 2:4) in deionized water (180 mL) with vigorous stirring. The pH was about 4 ~ 5. Aged at room temperature stir 24 hours, washed with deionized and decarbonated water, dried it in air at room temperature.	Layered structure $AlPO_4$-taranakite		(Wang, 2011)
Aluminium isopropoxide	H_3PO_4	Aluminium isopropoxide + H_3PO_4 + distilled water (stirred at room temperature separately) +benzylamine.Stirr 2h, transferred to autoclave for hydrothermal reaction at 180 °C for 4 days. Cooled in room, filtered, washed with distilled water, and dried at ambient temperature.	Layered structure $AlPO_4$		(Liu et al., 2010)
Aluminum phosphate dense					
Al_2O_3	H_3PO_4	Al_2O_3+ H_3PO_4+Deionized water+TPA. Formed gel at room temperature for 1h, Transferred to autoclave lining with Teflon for 150 °C, 25h static condition, Filtered white powder, washed with deionized water, and dried at 70 °C overnight.		TPA	(Boonchom et al., 2008)
$Al(OH)_3$ @ $AlSO_4$	phosphorus pentoxide	Catalyts (Al/P ratio between 5:1 and 1:1). Al sources aluminum hydroxides and potassium aluminum sulfate. Thin film used sol-gel technique with phosphorus pentoxide and hydrated aluminum nitrate, dissolved in ethanol or other	$AlPO_4$ as catalyst, pigment, vaccine adjuvant, thin	Review of non-crystalline (aluminum (poly)phosphate	(Rosseto et al., 2006)

		liquids. Pigment used lower ratios of P/Al with a nano-structured amorphous $AlPO_4$.	films,	materials	
aluminum hydroxide	phosphoric acid	Dissolving aluminum hydroxide in phosphoric acid, with a P/Al molar ratio of 23	$AlPO_4$ as Binder	Review of acid $AlPO_4$	(Chung, 2003)
$AlCl_3$	H_3PO_4 (85%), $(NH_4)H_2PO_4$ and $(NH_4)_2HPO_4$.	Gel precipitation method. $Alcl_3$+H_3PO_4@$(NH_4)H_2PO_4$ @ $(NH_4)_2HPO_4$)+ NH_4OH + continued stirring. Added NH_4OH to obtain pH7, dried at room temperature, filtered, wash with deionized water, and 2 propanol, dried at 120 °C for 24h, then calcined at 500, 650, 800, and 1000 for 3 hours.	$AlPO_4$ as catalyst		(Campelo et al., 2003)
Aluminum phosphate nanoparticles/nanocomposite					
$Al(NO_3)_3.9H_2O$	ammonium phosphate $(NH_4)_2HPO_4$	$Al(NO_3)_3.9H_2O$ + $(NH_4)_2HPO_4$ dissolved in distilled water. Obtained white nanoparticle suspension.	$AlPO_4$ nanoscale Coating		(Lee et al., 2013)
$Al(OH)_3$	H_3PO_4	Al $(OH)_3$ was dissolved in H_3PO_4. Al/P molar ratio of 1: 3. Added deionized water. A NH_4OH solution for pH change, continued magnetic stirring. The pH values of 3, 4.8, and 6.	Aluminum phosphate nanolayer		(Palacios et al., 2013)
$AlSO_4$	$NaPO_4$	Co-precipitation method. $AlSO_4$ in distilled water (0.1M)+ $NaPO_4$(0.1M). Mix reagent, stir, precipitate, filter, washed, dried, and ground	$AlPO_4$ nanoparticles		(Devamani, 2012)
$Al(NO_3)_3.9H_2O$	ammonium phosphate $(NH_4)_2HPO_4$	Dissolved in distilled water with constant stirring.	metal-phosphate-nanoparticle solution		(Oh et al,. 2008)
Al_2O_3	Excess H_3PO_4	Al_2O_3+excess H_3PO_4 +H_2O (1:1) (1:2) sealed in gold capsule carried hydrothermal with horizontal arranged. Al:P 1:3 and 3:1.			(Druppel et al., 2007)
$Al(NO_3)_3.9H_2O$	H_3PO_4	Mixed in autoclave, heated to 175 °C for 2 days. Washed with ethanol/methanol.	$AlPO_4$ nanocrystal,	nanoparticle, nanowire,nanorope	(Yang & Kau, 2005)
$Al(NO_3)_2.9H_20$	$(NH_4)_2HPO_4$)	Mixed, stirred, filtered, and dried. Heated in furnace at 700 °C for 5h(annealing)	$AlPO_4$ nanoscale Coating	Coating on $LiCoO_4$	(Lee et al., 2004)
AlOH	H_3PO_4	Al:P (1.0-1.5:3). Dissolved and stirred slightly at elevated temperature. Dried in air.	$AlPO_4$ ceramic Coating		(Chen et al., 2003)

2.9 Characterization of Aluminum Phosphate ($AlPO_4$)

Characterization of $AlPO_4$ was performed like that done for PVA and PPVA. The characterization of $AlPO_4$ had been focused on TGA, DSC, XRD, FESEM, FTIR, RAMAN, UV-visible, and PL.

2.9.1 Differential Scanning Calorimetry (DSC)/Trangravimetric Analysis (TGA)/Simultaneous Thermal Differential Analysis (STDA) on Aluminum Phosphate

Thermal properties of $AlPO_4$ were reported in a number of publications. The latest publication was made by Kalbasi and Izadi (2013), who conducted TGA of $AlPO_4$ and composite with PVP under nitrogen gas. They reported that the water evaporation in $AlPO_4$-5 pores structure began at a lower temperature of 61 °C. Other than that, Mekky and Nicholson (2007) also mentioned that temperature below 100 °C involved elimination of moisture. However, Bhagwat et al., (2003) and Boonchom and Kongtaweelert (2010) proposed higher temperature of water desorption (25-198 °C), elimination of crystal water (<150 °C), and water elimination with co-ordination of the metal atom (>150 °C). Meanwhile, Boonchom and Kongtaweelert (2010); Boonchom et al., (2008), and Chen et al., (2003) discussed that elimination of water or dehydration generated endothermic effect and transformation of $AlPO_4 \cdot H_2O$-H_4 to $AlPO_4 + H_2O$ at 120 °C, as well as $AlH_3(PO_4)_2.3H_2O$ to $AlH_2(PO_4)_3 + AlH_3(PO_4)_2.H_2O$ at 105 °C, respectively.

At a higher temperature of 220 °C, Chen et al., (2003) reported that $AlH_2(PO_4)_3$ transformed to $AlH_2P_3O_{10}.2H_2O$ and $AlPO_4$ (trigonal system). They also mentioned that at 200 °C, $AlH_2(PO_4)_3$ had been in its most effective bonding (Chen et al., 2003), while Druppel et al., (2007) reported that 200 °C was the thermal stability limit of variscite,

which transformed to more stable phases, such as berlinite, augelite, trolleite, and Al-metaphosphate [$Al(PO_3)_3$].

In different cases of composite, both Mekky and Nicholson (2007) and Kalbasi and Izadi (2013) observed the elimination of light organic (270 °C) and the degradation of polymer PVP in PVA-$AlPO_4$ composite began at 210 °C and continued to 346 °C. Chen et al., (2003) further highlighted that at a temperature range of 400-1000 °C, a variation of $AlPO_4$ crystal system occurred at 400 °C. Besides, no dehydration existed, but the phase of transformation took place for $AlPO_4$. A small crystallization peak was observed at 480 °C, which corresponded to the transition of amorphous $AlPO_4$ to $AlPO_4$ (tridymite) since there was no corresponding weight loss (Kawamura et al., 2007). In addition, Mekky and Nicholson (2007) similarly stated that the crystallization of $AlPO_4$ was completed at 680 °C, together with decomposition of all organic materials (polymer). Mekky and Nicholson (2007) also found that $AlPO_4$ was crystallized to $AlPO_3$ at temperature 850 °C. Phase transformation and crystallization of amorphous $AlPO_4$ to crystalline α-cristobalite $AlPO_4$ occurred at 867-879 °C (Campelo et al., 2003) and tridymite at 780 °C (Kandori et al., 1996).

On the other hand, thermal properties of composite $AlPO_4$ were also reported in a number of publications. The composite was produced by various $AlPO_4$ geometrical structures, aluminum phosphate layers, molecular sieves, and amorphous phases. Kalbasi and Izadi (2013) reported on the composite of PVP with $AlPO_4$, which produced higher thermal stability in comparison to PVP, whereas Jiang et al., (2013) reported on the synthesis of nanocomposite that consisted of PU with aluminum phosphate layer. Good interfacial interaction and dispersion of exfoliation between LAP layer and PU chain increased Tg. In this case, TGA was determined in air with several weight losses (10%, 50%, and 90%). Early degradation of polymer (10%) catalyzed by LAP (solid acid catalyst) produced less stable than that of PU. LAP promoted

dehydrogenation of polymer at low temperature and catalyzes the char formation. The main loss began from 250 °C, attributed to the loss of DDA molecules with the aluminophosphate residue yielded at 47.4 wt % in the DDA-LAP system. At half degradation (50%), the nanocomposite weight loss increased gradually at a temperature range of 373.4 to 380.9 °C as DDA-LAP content arose. Finally, at last stage of degradation (90%), decomposition of nanocomposite occurred at a higher temperature (584 °C) compared to pure PU (500 °C). The nanocomposites exhibited enhanced endurance against thermal oxidation at high temperature due to the charring of polymers. The weight residue of nanocomposite (8.7-15.6 wt%), which was found higher than PU (4.9wt%), indicated that nanocomposite consisted of both char from the polymer matrix and the DDA-LAP residue.

Another composite of $AlPO_4$ was produced from the mixture of $AlPO_4$ mineral known as taranakite with a structure of PVA layer. This research was the most similar to the proposed system, which used the same polymer source (PVA). Wang (2011) described that taranakite is a hydrated alkali iron aluminum phosphate mineral with chemical formula $(K,Na)_3(Al,Fe^{3+})5(PO_4)_2\ (HPO_4)_6 \cdot 18H_2O$. It forms from the reaction of clay minerals or aluminous rocks with solutions enriched in phosphate derived from bat or bird guano or less commonly from bones or other organic matter. Figure 2.15 shows that PVA mixed with aluminum phosphate taranakite produced two DTG peaks. The first peak was mainly due to loss of water (100 °C), while the second peak (150 °C) was due to sluggish phase transformation. DTG peak was observed at higher temperature of 300 and 450 °C for nanocomposite of PVA/taranakite. This can be expected due to the formation of hydrogen bonding between PO_4^{3-} ions in the taranakite layers and –OH groups of PVA. PVA in this system experienced decomposition by two steps, where the first step is dehydration and elimination of remaining acetate group, while the second step is hydrogen bond formation of OH and phosphate group. PVA was reported to have

no weight residue, whereas addition of taranakite to the system increased the weight residue up to 10% with 10% of taranakite composition. Table 2.10 summarizes the TGA and the weight residue of PVA, as well as PVA-taranakite composite.

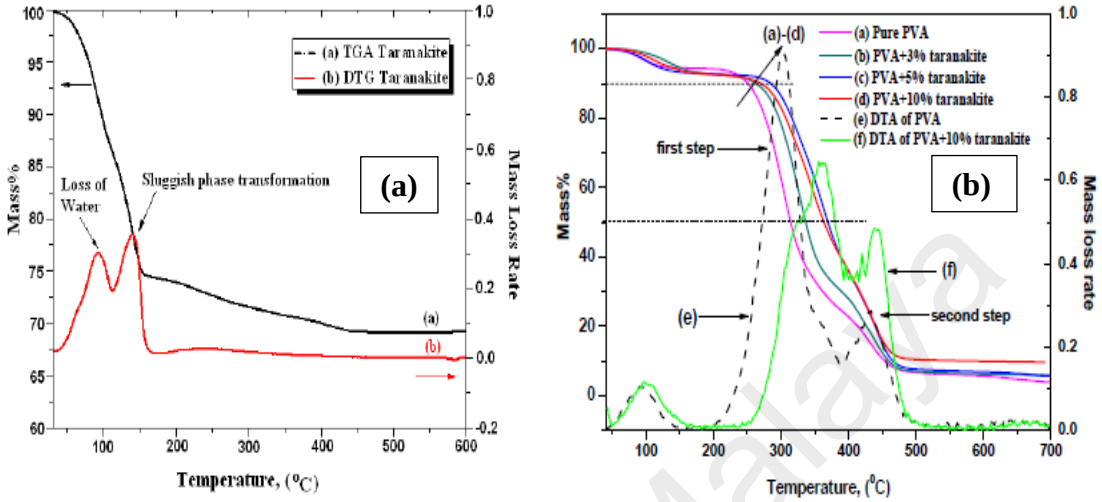

Figure 2.15: TGA and DTA of (a) $AlPO_4$ (Taranakite) and (b) composite PVA-Taranakite (Wang 2011)

Table 2.10: Summary of TGA and weight residue of PVA and composite PVA-taranakite (Wang, 2011)

Formulation	$T_{0.1}$	$T_{0.5}$	Experimental Char (%)	Expected Char (%)
PVA	257 ± 3	313 ± 3	4.0 ± 0.2	NA
PVA+3%taranakite	264 ± 2	337 ± 1	6.3 ± 0.3	6.0
PVA+5%taranakite	285 ± 2	367 ± 2	6.9 ± 0.1	7.3
PVA+10%taranakite	288 ± 3	378 ± 3	9.7 ± 0.2	10.0

$AlPO_4$ composite was also produced from $AlNO_3$ as aluminum source and mixed with EG via complex polymerization method (Mekky & Nicholson 2007). The DTA presented four exothermic and one endothermic peaks. The sample exhibited a rapid weight decrease by ≈100 °C due to residual water content. The first weight loss was about 60% due to dehydration and evaporation of volatile organic components and water. The weight gradually decreased to 270 °C due to the elimination of light organic constituents from polymer. The first mass loss using EG included the pyrolysis of EG

and citric acid, resulting in the breaking of bond and removal of free organics from metal-ion sources. This can be detected via the change in slope of TGA plot at 150 and 180 °C. The second weight loss with approximately 20% contained exothermic peaks at 360 and 550 °C due to the burnt residual carbon. Besides, polymer decomposition can occur in two steps; degradation of the polymeric structure that is pyrolysis, and oxidation of the residual carbon. Moreover, an exothermic peak was observed at 680 °C due to removal of the polymerized molecules, where decomposition of all organic materials contained in the precursor took place via combustion and complete crystallization of $AlPO_4$ also occurred. Another exothermic peak that appeared at 825 °C was attributed to the crystallization or phase change of $AlPO_4$ to $AlPO_3$.

Furthermore, Bhagwat et al., (2003) reported on the thermal properties of AEI sample that showed five degradation stages. Weight loss of 19.8% was due to removal of water from the inside pores of aluminum phosphate at a range of 25 – 198 °C, which also observed a broad endothermic peak. The next stage occurred within 199 – 373 °C with endothermic peak corresponding to the loss of physisorbed amine that derived from the template. Also, being observed had been the three steps weight losses between the temperature ranges of 268 – 373 °C, 374 – 461 °C, and 462 – 636 °C due to the decomposition of the protonated amine, and followed by the combustion of coke between the high temperature regions.

In other cases, Boonchom et al., (2008) conducted a study on thermal properties upon the existing $AlPO_4$ from Fluka, where Boonchom and Kongtaweelert (2010) synthesized the $AlPO_4$. H_2O-H_4 from Al_2O_3, H_3PO_4, and tripopylamine (TPA) functioned as templates. Meanwhile, Druppel et al., (2007) discussed similar finding for $AlPO_4.2H_2O$ in the Al_2O_3-P_2O_5-H_2O system at temperature below 200 °C, where several Al-phosphates hydrated with the general composition of $AlPO_4 \cdot xH_2O$ ($1 \leq x \leq 3$). Al-phosphates hydrate, which is known as variscite and metavariscite, was obtained

in solution with pH ≤ 6. Aluminum was found stable in Al-phosphate solution complex $[Al(OPO_3H)(H_2O)_5]^+$ at pH 6 or less where this solution may act as neutral, acidic or basic. Moreover, Druppel et al., (2007) found that water content of the hydrates decreased with increasing temperature at lower temperature range (113 – 133 °C) in atmospheric pressure. Furthermore, both Boonchom and Kongtaweelert (2010) and Boonchom et al., (2008) agreed that water elimination at 200 °C and below can be considered as crystallization water. However, Boonchom and Kongtaweelert (2010) clearly explained that elimination of water below 150 °C originated from crystal water, whereas water elimination at 200 °C and above indicated co-ordination of water with metal atom. DTA and DTG traces showed endothermic peaks at 120 and 124 °C (Boonchom & Kongtaweelert, 2010), and 120 °C (Boonchom et al., 2008) due to the dehydration reaction. Druppel et al., (2007) also discussed the same dehydration of hydrate Al-phosphates at a temperature range of 113 – 133 °C.

$AlPO_4.H_2O \rightarrow AlPO_4+H_2O$ (Boonchom & Kongtaweelert, 2010)

$AlPO_4 \cdot H_2O\text{-}H_4 \rightarrow AlPO_4+H_2O$ (Boonchom et al., 2008)

variscite = berlinite + $2H_2O$ (Druppel et al., 2007)

Druppel et al., (2007) reported that the stable phases existed for berlinite, augelite, trolleite, and Al-metaphosphate [Al $(PO_3)_3$] at temperature above 200 °C. TGA of $AlPO_4$ showed a steep curve with weight loss of 12.58% at a range of 77 – 300 °C in relation to the elimination of water for $AlPO_4.H_2O$ (Boonchom & Kongtaweelert, 2010). However, earlier observation in $AlPO_4 \cdot H_2O\text{-}H_4$ produced mass loss in the range of 14.58 – 16.48% (Boonchom et al., 2008). Additionally, elimination of water in DTA and DTG curves was observed by endothermic peaks at 124 and 120 °C, respectively. Boonchom and Kongtaweelert (2010) also observed a DTA exothermic peak at 591 °C, which ascribed a transition from amorphous to crystalline phase of $AlPO_4$. In the TGA

curve, there was no weight loss and the retained mass had been 87.42% (Boonchom & Kongtaweelert, 2010) and 85% (Boonchom et al., 2008). On the other hand, Campelo et al., (2003) reported the TG curve by two stages until 377 °C. 15% of weight loss occurred in the temperature range from 20 – 227 °C due to desorption of water and 2-propanol. Other peaks were also observed at 142 and 135 °C in DTG and DTA. The decomposition and removal of occluded organics occurred at higher temperature of 217 and 210 °C, as noted from DTG and DTA, respectively. TG at a range of 227 – 377 °C showed weight residue of 22% due to removal of occluded ammonium chloride. This can also be observed at 320 and 315 °C in DTG and DTA curves. In the temperature range of 377 – 1200 °C, a slight weight loss was observed mainly due to the surface hydroxyls-hydroxyl condensation. The peaks observed within the temperatures of 867, 873, and 879 °C had been due to phase transformation of amorphous $AlPO_4$ to a crystalline α-cristobalite $AlPO_4$. Moreover, Jiang et al., (2006) discussed the effect of crystallization temperature and time for $AlPO_4$. Nucleation occurred on the surface at a temperature of 170 °C, while the crystal size increased at 180 °C. The crystal was transparent with a smooth surface at 15h. However, the size of the crystal was smaller and the surface was not smooth at 182 °C. In fact, a small trydimite phase occurred at the 20^{th} hour with occurrence of speckles on the surface and continued at longer time of 36h, where perfect hexagonal was obtained. Nonetheless, the size of the crystal was smaller and the surface was very rough at 190 °C. With additional longer heating time, crystal erosion occurred and generated a large amount of tridymite-like phase. Table 2.11 summarizes $AlPO_4$ thermal analysis.

Table 2.11: Summary of $AlPO_4$ thermal analysis

DSC/SDTA		TGA	
T (°C)	Details	T (°C) and Weight residue (%)	Details
61 °C (Kalbasi & Izadi, 2013)	Evaporation of water for alpo4-5 that was present in the pores structure	25-198 (Bhagwat et al., 2003)	Desorption of water
<100 100 (Mekky & Nicholson, 2007)	Elimination of moisture	67–103 (Wan et al., 1999)	-the maximal loss for the first peak was in the range -due to loss of water, which had filled the channels in the structure during the synthesis.
25-198 (Bhagwat et al., 2003)	Desorption of water		
DTA 100–150 (Kandori et al., 1998)	Endothermic peak	0-200 (Kandori et al., 1998)	-steep weight loss took place up to 200 °C. -the release of adsorbed and/or coordinated water
105(Chen et al., 2003)	Dehydration $AlH_3(PO_4)_2.3H_2O$ transform to $AlH_2(PO_4)_3$ and $AlH3(PO_4)_2.H_2O$		
120 (Boonchom et al., 2008)	endothermic effect $AlPO_4 \cdot H_2O$-H_4----→$AlPO_4$+H_2O		
DTG 142 DTA 135(Campelo et al., 2003)	Endothermic due to desorption of physically adsorbed water and 2-propano	- 20-227 (15%)(Campelo et al., 2003)	- two stages profiled up to 377‘C -desorption of physically adsorbed water and 2-propanol.
<150 (Boonchom & Kongtaweelert, 2010) <200°C (Boonchom et al., 2008)	Elimination of crystal water	77-300 (12.58 % (Boonchom & Kongtaweelert, 2010)	Elimination of water for $AlPO_4.H_2O$. (0.98 mol H_2O) by mass,
>150 (Boonchom & Kongtaweelert, 2010)	Water eliminated with co-ordination of the metal atom.	200 (Wan et al., 1999)	The second peak
150 (Druppel et al., 2007)	Variscite, metavariscite, and several hydrates with general compositions $AlPO_4 \cdot xH_2O$ ($1 \leq x \leq 3$) existed	198-373 (Bhagwat et al., 2003)	Desorption of physisorbed amine

>200 (Druppel et al., 2007)	The thermal stability limit of variscite, stable phases were berlinite, augelite, trolleite, and Al-metaphosphate [$Al(PO_3)_3$]		
DTG 217 DTA 210 (Campelo et al., 2003)	DTA endothermic	25-377 (Campelo et al., 2003)	Decomposition and removal of occluded organics.
218(Kandori et al., 1998)	Exothermic peak described the combustion of IPA included in the particles.		
200(Chen et al., 2003)	$AlH_2(PO_4)_3$ (most effective bonding)		
220(Chen et al., 2003)	$AlH_2(PO_4)_3$ transform to $AlH_2P_3O_{10}.2H_2O$ and $AlPO_4$(trigonal system)		
270(Mekky & Nicholson, 2007)	Elimination of light organic		
DTG 320 DTA 315 (Campelo et al., 2003)	Due to the removal of occluded ammonium chloride	227-377 (22%) .(Campelo et al., 2003)	Due to the removal of occluded ammonium chloride
400(Chen et al., 2003)	No dehydration, occur phase transformation	420–480 (Wan et al., 1999)	The third peak in the range was attributed to the loss of triethylamine.
480 (Kawamura et al., 2007)	The transition from amorphous $AlPO_4$ to $AlPO_4$ (tridimite)	480(Kawamura et al., 2007)	No corresponding weight loss. Crystallization peak
680(Mekky & Nicholson, 2007)	Decomposition of all organic (polymer) and crystallization of $AlPO_4$ were completed	373-461 (Bhagwat et al., 2003)	Decomposition of the protonated amine
708 (Kandori et al., 1996)	Exothermic crystallization of amorphous samples to tridymite	200-1000 (Kandori et al., 1996)	Monotonous weight loss
850(Mekky & Nicholson, 2007)	Crystallization of $AlPO_3$. Phase changed from $AlPO_4$ to $AlPO_3$	461-763 (Bhagwat et al., 2003)	Coke combustion Total weight loss 19.8%
867, 873, 879 (Campelo et al., 2003)	Phase transformation of amorphous AlPO4 to a crystalline α-cristobalite AlPO4.	377-1200(Campelo et al., 2003)	Slight weight loss mainly due to the condensation of surface hydroxyls - hydroxyl condensation
377 and 1200	A slight weight loss was observed, mainly due to the condensation of surface hydroxyls, together with an exothermic DTA peak.	400-1000 (Chen et al., 2003)	Variation of crystal system

2.9.2 X-Ray diffraction (XRD) analysis on $AlPO_4$

Synthesis of $AlPO_4$ can produce a molecular sieve geometrical structure (Yang et al., 2014; Kalbasi & Izadi, 2013; Jiang et al., 2006; Bhagwat et al., 2003) for $AlPO_4$-5, $AlPO_4$-11, and $AlPO_4$-18, respectively. Yang et al., (2014) showed the XRD patterns for all $AlPO_4$ samples were recorded at angles 7, 13.5, 15, 19, 21, 23, 26, 29, 30.5, 34, 35, and 37.5°. However, the crystallization was incomplete at 160 °C. Meanwhile, the crystallization time only influenced the aspect ratio and uniformity of particles. Prismatic crystal was observed at temperatures of 170 and 180 °C, but reduced at higher temperature of 190 °C as the nucleation and the growth accelerated at higher temperature. They also concluded that excessive temperature was not beneficial to the perfect single crystal of $AlPO_4$-5. Besides, Kalbasi and Izadi (2013) presented XRD patterns for pure $AlPO_4$-5, $AlPO_4$-11, berlinite, and composite P4VP/ $AlPO_4$-5. The lattice planes were also recorded at (100), (110), (200), (210), (002), (211), (220), (311), (400), (222), (410), (402), and (213). They synthesized $AlPO_4$-5 by using aluminum hydroxide at low angle of $2\theta = 7.32$ ° (100) and by product berlinite at $2\theta = 26.5$ °. Meanwhile, the synthesis of $AlPO_4$-5 using AlP_2O_5 showed 67% of crystallinity corresponding to $AlPO_4$-11 and no $AlPO_4$-5 phase. AlP_2O_5, was easily hydrolysed and produced reactive aluminum that reacted quickly with H_3PO_4, whereas in using AlOH, berlinite phase was easily obtained. Both $AlPO_4$-11 and $AlPO_4$-5 phases were observed in XRD pattern after addition of H_3PO_4. H_3PO_4, as pH modifier, changed the molarity of phosphate in gel composition, decreased the interaction of aluminum with phosphoric acid, and influenced Al complexes. Consequently, pure $AlPO_4$-5 could not be synthesized. However, by using HCl as pH modifier, pure phase of $AlPO_4$-5 with (100), (110), (200), (210), (002), and (220) lattice planes had been obtained. Furthermore, TEA as a template was easily protonated by mixture of HCl/H_2O. Hence, Kalbasi and Izadi (2013) concluded that AlP_2O_5 is the optimized Al source for synthesizing $AlPO_4$-5

at shorter time (13h). Acid used in pH adjustment protonated the TEA, and lead to diversify in the resulting structure. $AlPO_4$-5 was mixed with PVP and calcine showed no effect on its crystalline structure. The pH also strongly influenced crystallinity and purity of $AlPO_4$-5 (Kalbasi & Izadi 2013).

On the other hand, Jiang et al., (2006) conducted a hydrothermal synthesis of optical clear large $AlPO_4$-5 crystals and presented a list of peaks for $AlPO_4$ with AFI structure and tridymite-like phase. XRD patterns of AFI treated at 180 °C for 30 hours showed lattice planes of (100), (110), (200), (210), (002), (102), (220), (311), (400), (410), and (213). Likewise, heat-treated samples at 190 °C for 30 hours exhibited lattice planes at (112), (-404), (310), (-406), (-315), and (020), which contained mixed phase of AFI and tridymite. Trydimite increased with the increase of temperature and prolonged crystallization time. Bhagwat et al., (2003) reported the XRD pattern for $AlPO_4$-18 as a monoclinic crystal system. The unit cell parameters were: a = 18.477 Å, b = 12.598 Å, c = 13.554 Å, β = 95.129 °, and V =3142.38 (Å3), where the crystal system showed a space group C2/c.

In different cases, the synthesis of $AlPO_4$ produced a layered geometrical structure (Jiang et al., 2013; Liu et al., 2010; Wang, 2011). Jiang et al., (2013) found the layered structure of $AlPO_4$ and recorded three peaks in the low-angle region that corresponded to (001), (002), and (003) lattice planes. The high intensity of (001) peak suggested the highly ordered organization of DDA-LAP nanolayers. Besides, large basal spacing (30.8 Å) was noted at (001) due to long-chain DDA molecule in the interlayer. Meanwhile, the DDA-LAP composite produced an XRD pattern that slowly vanished for (001) and completely vanished for (002) and (003) peaks with an increase in the PU content. A weak and broad peak at angle 2.03 ° appeared with small addition of PU as the nanolayer had the tendency to agglomerate in polymer and retard the penetration of polymer chain into the interlayer. Peak (001) was shifted to the left, corresponding to

the increase in basal spacing that suggested the polymer chain penetrated into the interlayer and expanded the interlayer. The long-range ordering in the inorganic phase was completely destroyed and DDA-LAP nanolayers were completely exfoliated in the PU matrix. Moreover, DDA had enlarged gallery between the nanolayers and improved interfacial between LAP nanolayer and PU matrix. However, the distribution of DDALAP nanolayers was destroyed by the polymer chains. Liu et al., (2010) observed that the layered structure of $AlPO_4$/Benzylamine exhibited a strong peak at 4.54° and weak peaks at 9.2°, and 13.8°, corresponding to (100), (200), (300), lattice planes respectively. Strong peak discovered at the angle of 4.54° had a hexagonal unit cell with 19.463 Å or 1.95 nm cell parameter. Synthesis of layered aluminum phosphate (ALP) produced a similar XRD pattern with Taranakite (PDF 29-981) and exhibited strong XRD peak at 5.85° (Wang 2011). Meanwhile, by using the hydrothermal pattern, the strong peak at 5.85° was missing. Composite of taranakite with PVA produced weak peak and left shifted at 4.9° due to higher content of taranakite. In addition, Wang (2011) differentiated the layered materials composite structure between three different types of dispersions and XRD pattern, as shown in Figures 2.16 and 2.17. The layer failed to intercalate into galleries due to the immiscibility of phase that separated the composite. The intercalated composite produced a well-ordered multilayer structure of alternating polymeric and inorganic layer. Meanwhile, in the exfoliated system, it depicted a uniform dispersion and maximum polymer-layer material interaction, which commonly delaminated the XRD pattern to become a single broad peak.

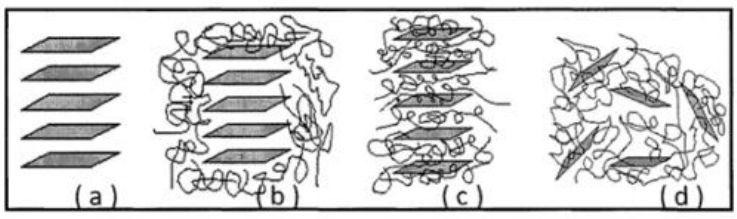

Figure 2.16: Polymer/layered materials composite structure and the three different dispersions (a) original layered compound; (b) immiscible system (microcomposite) (c) intercalated nanocomposite (d) exfoliated (Wang, 2011).

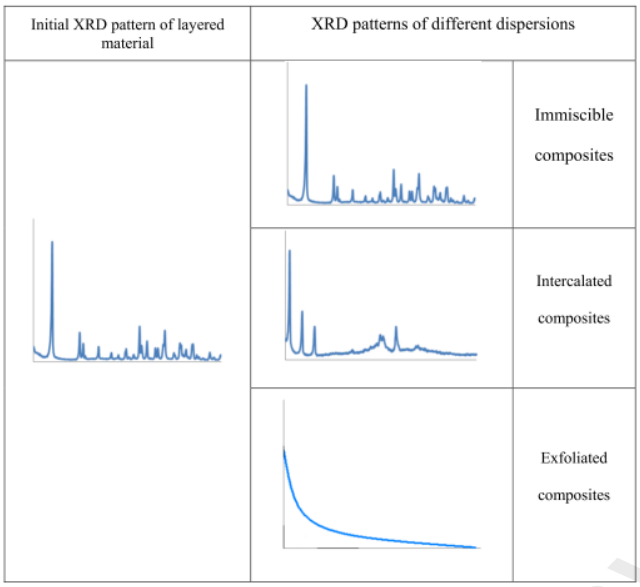

Figure 2.17: XRD patterns of initial layered materials and the three different dispersions (Wang, 2011).

Kawamura et al., (2007) reported that XRD analysis at 125 and 150 °C produced $AlPO_4.2H_2O$ (variscite) and $AlPO_4$ (tridymite), respectively. The structure was primarily amorphous after 1 h at 1100 °C with a presence of small amount of crystalline phase corresponding to the presence of nanocrystals in the matrix (Gutiérrez-Mora et al., 2006). The tridymite peak arose from the formation of $AlPO_4$ nanocrystals. There were no significant changes in the XRD patterns with further increase in temperature and annealing time. However, there were clear signs of the presence of cristobalite form of $AlPO_4$ plus α-Al_2O_3 at 1400–1600 °C for extended periods. Campelo et al., (2003), who did calcination at 500 and 650 °C, exhibited only a very broad band in the angle range of 15° to 30°, a characteristic of the amorphous $AlPO_4$. Further calcination at 800 °C developed a crystalline $AlPO_4$ and became fully crystalline at 1200 °C. $AlPO_4$ crystalline corresponded to the orthorhombic symmetry of α-cristobalite $AlPO_4$ at angles 21.8° (4.075 Å), 28.2° (3.159 Å), 30.8° (2.869 Å), and 35.8° (2.503 Å). The small peak at angle 20.6 (4.313 Å) was incompatible with the orthorhombic symmetry of α-cristobalite, but may be related to the presence of structural defects. The mixture of tridymite and R-cristobalite is enriched in the R-cristobalite phase as thermal treatment

temperature increasing with pseudohexagonal tridymite was identified by its characteristic reflections at angles 20.4° (4.348 Å), 21° (4.110 Å), and 23.2° (3.830 Å). Furthermore, Chen et al., (2003) discussed the synthesis of $AlPO_4$ as ceramic coating and the optimum ratio of aluminum with phosphate. $AlH_3(PO_4)_2.3H_2O$ was found as the dominant phase of all reaction products with different Al/P ratios. However, there are characteristic peaks of H_3PO_4 due to excess of H_3PO_4 at the Al/P ratios of 1:3, 1.1:3 and 1.2:3. Meanwhile, at higher aluminum content in Al/P ratio 1.4:3, there are excess of Al $(OH)_3$. Moreover, the optimal Al/P ratio in aluminum phosphate was in a range of 1.3:3 to 1.4:3. Table 2.12 presents the chemical composition of the binder with Al/P ratio at different temperatures.

Table 2.12: Chemical composition of the binder with Al/P ratio of 1.4:3 at different temperatures (Chen et al., 2003).

Temperature (°C)	Dominant phase	Secondary phase
60	$AlH_3(PO_4)_2 \cdot 3H_2O$	
105	$AlH_3(PO_4)_2 \cdot H_2O$ (monoclinic system)	$Al(H_2PO_4)_3$ (hexagonal system)
200	$Al(H_2PO_4)_3$ (hexagonal system)	
220	$AlPO_4$ (trigonal system)	$AlH_2P_3O_{10}$ $2H_2O$
250	$AlPO_4$ (trigonal system)	$AlH_2P_3O_{10}$ $2H_2O$
300	$AlPO_4$ (trigonal system)	$AlH_2P_3O_{10}$ $2H_2O$
400	$Al(PO_3)_3$ (hexagonal system)	$AlH_2P_3O_{10}$ $2.5H_2O$
500	$Al_2P_6O_{18}$	$Al(PO_3)_3$ (cubic)
600	$Al_2P_6O_{18}$	$Al(PO_3)_3$ (cubic)
700	$Al_2P_6O_{18}$	$Al(PO_3)_3$ (cubic)
800	$Al(PO_3)_3$ (cubic)	$AlPO_4$ (trigonal system)
900	$Al(PO_3)_3$ (cubic)	$AlPO_4$ (rhombic system)
1000	$Al(PO_3)_3$ (cubic)	$AlPO_4$ (rhombic system)

Burrell et al., (1999) also observed a broad band centered at the angle of 29.48°, corresponding to 3.04 Å. This is the most intense diffraction lines of variscite, $AlPO_4.2H_2O$ and can be concluded that adjuvant A consisted of very small platelets of a

poorly ordered precursor of variscite. In addition, Kandori et al., (1996) reported that all freshly prepared $AlPO_4$ was amorphous after treated at 1000 °C for 2 h in air, where the XRD pattern produced four sharp peaks at angles 20.3°, 21.5°, 23.0°, and 35.5°. These peaks corresponded to $AlPO_4$ (tridymite). Meanwhile, Beppu et al., (1996) observed precipitated with amorphous broad diffraction band around 28° and weak broad band at 10 – 15°. XRD analyses of bulk and nanocomposite that consisted of $AlPO_4$ were discussed earlier by Kalbasi and Izadi (2013), Jiang et al., (2013), Wang (2011), and Mekky and Nicholson (2007). Kalbasi and Izadi (2013) produced a composite of $AlPO_4$ with PVP, meanwhile Jiang et al., (2013) used LAP with PU, Wang (2011) mixed the $AlPO_4$ mineral known as taranakite with PVA, and Mekky and Nicholson (2007) used EG with $AlNO_3$.

The synthesis of $AlPO_4$ produced a combination of particle and layer (Palacios et al., 2013). Sample was prepared with P/Al ratio between 1.3 and 2.4 in acidic environment (pH 3, 4.8, and 6). They observed effect of ageing time and pH on crystallinity, size, and morphology of $AlPO_4$. Sample prepared in shorter ageing time showed a broad XRD pattern between 20 – 35°; corresponding to amorphous phase, while the sample prepared at pH 4.8 aged at 8 hours to produce francoanellite (F) and aluminum orthophosphate ($AlPO_4$) phases. Francoanellite is a mineral based on an acid mixed aluminum potassium phosphate with idealized composition $H_6K_3Al_5(PO_4)_8.12H_2O$. However, at lower pH 3, predominant phase, which is metaphosphate with XRD pattern, corresponds to taranakite and monoammonium phosphate ($NH_4H_2PO_4$) phases. Meanwhile, the XRD pattern shows broad peak at pH 6 due to the amorphous phase. Additionally, the treated sample at 900 °C contained orthophosphate phase ($AlPO_4$) and metaphosphate phase ($Al(PO_3)_3$) in all cases.

Other than that, Devamani (2012) synthesized nanoparticle of $AlPO_4$ from a mixture of aluminium sulphate and sodium phosphate by chemical precipitation method. The XRD

patterns showed many peaks at angles 19.16, 20.48, 21.58, 22.86, 25.68, 28.17, 29.11, 32.25, 33.99, 38.21, and 48.92°. The average size of the particle was 55.75 nm, as calculated by using the Scherrer formula. Furthermore, Yang and Kau (2005) synthesized the $AlPO_4$ nanocrystal with different morphology, nanoparticle, nanowire, and nano rope. The XRD pattern showed a berlinite phase that at pH 10, whereas berlinite with cristobalite phase at pH 11 and 12. Boonchom and Kongtaweelert (2010) observed XRD patterns with broad peaks that contributed to a very low degree of crystallinity for $AlPO_4$ (15 – 35°) and $AlPO_4.H_2O$(20 – 35°). This indicated a poor crystallization or amorphous phase, as well as nanoparticles of these materials. $AlPO_4$ was transformed from amorphous to a crystalline phase at 500 °C. Earlier, Boonchom et al., (2008) observed peaks of $AlPO_4{\cdot}H_2O$-H_4 and $AlPO_4$ by comparing data in PDF #821454 and PDF #511674, respectively. Both structures were in monoclinic system with space group C2/c (Z=8) for $AlPO_4{\cdot}H_2O$-H_4 and Pc (Z=2) for $AlPO_4$. Meanwhile, the crystallite size for (–111), (112), (–113), and (–221) peaks were calculated at 67±25 nm for $AlPO_4{\cdot}H_2O$-H_4. In $AlPO_4$, the average crystallite size was 55±19 nm, resulting from (–406), (–213), (114), and (–619) peaks. XRD data also support other methods of characterization as calcination of $AlPO_4{\cdot}H_2O$-H_4 produces $AlPO_4$. Table 2.13 summarizes the XRD results for $AlPO_4$.

Table 2.13: Summary of XRD results for $AlPO_4$

2θ/ unit cell/Crystal structure	Indication	References
Molecular sieve (3D)		
7, 13.5, 15, 19, 21, 23, 26, 29, 30.5, 34, 35 and 37.5.	XRD pattern for all sample $AlPO_4$-5.	(Yang et al., 2014)
(100), (110), (200), (210), (002), (211), (220), (311), (400), (222), (410), (402) and (213).	The XRD pattern for pure $AlPO_4$-5	(Kalbasi & Izadi, 2013)
weak 2θ at 7.32° (100) and by product berlinite (strong 2θ peak 26.5°)	$AlPO_4$-5 synthesis used aluminum hydroxide produced pure $AlPO_4$-5 and by product berlinite.	(Kalbasi & Izadi, 2013)
$AlPO_4$ -11	Synthesized $AlPO_4$-5 using AlP_2O_5 showed 67% of crystallinity corresponding to $AlPO_4$ -11 and no $AlPO_4$-5 phase	(Kalbasi & Izadi, 2013)
broad X-ray peaks appeared at 300 °C	Product was amorphous to 300 °C. Crystallized to metaphosphates formation of ortho- and meta-phosphate ($AlPO_4$ and $Al(PO_4)_3$). Crystallization started at ≈500 °C and a developed crystalline structure was detained at 900 °C.	(Mekky & Nicholson, 2007)
(100)(110)(200)(210)(002)(102)(220)(311)(400)(410)(213)	AFI at 180 °C 15h	(Jiang et al., 2006)
(112)(-404)(310)(-406)(-315)(020)	Tridymite at 190 °C 30h Trydimite increased with increase in temperature and prolonged crystallization time.	(Jiang et al., 2006)
Unit cell parameters a = 18.477 Å, b = 12.598 Å, c = 13.554 Å, β = 95.129° and V =3142.38 (Å3). The crystal system showed a space group C2/c.	$AlPO_4$-18 pattern with a monoclinic crystal system.	(Bhagwat et al., 2003)
Layered aluminumphosphate (2D)		
low-angle region (001), (002) and (003)	diffractions of the $AlPO_4$ layered structure	(Jiang et al., 2013)
strong 5.85°.	Taranakite (PDF 29-981)	(Wang, 2011)
weak left shifted peak at 4.9°	Composite of taranakite with PVA.	(Wang, 2011)
Strong at 4.54°(100), and weak peaks at 9.2°(200), and 13.8°(300)	Layered structure of $AlPO_4$/Benzylamine. The strongest peak at 4.54° was calculated to have the hexagonal unit cell with 19.463 Å or 1.95 nm cell.	(Liu et al., 2010)
Aluminum phosphate dense		
$AlPO_4$(15-35°) and $AlPO_4.H_2O$(20-35°)	XRD patterns with broad peak that contributed to very low degree of crystallinity	(Boonchom & Kongtaweelert, 2010)
$AlPO_4 \cdot H_2O$-H_4. (–111), (112),(–113), and (–221), $AlPO_4$,(–406), (–213), (114), and (–619).	$AlPO_4 \cdot H_2O$-H_4 monoclinic (space group C2/c (Z=8)(a=7.13(5), b=7.10(6), c=12.80(2)-PDF #82145. ($AlPO_4$) monoclinic (space group Pc (Z=2)) for$AlPO_4$.(a=37.02(9), b=5.00(7), c=25.97)-PDF #511674. $AlPO_4$, average crystallite size was 55±19 nm. $AlPO_4 \cdot H_2O$-H_4 average	(Boonchom et al., 2008)

	size of 67±25 nm.	
$AlPO_4.2H_2O$ (variscite) and $AlPO_4$ (tridymite)	XRD analysis at 125 °C and 150 °C produced $AlPO_4.2H_2O$ (variscite) and $AlPO_4$ (tridymite), respectively.	(Kawamura et al., 2007)
Amorphous $AlPO_4$, tridymite , α-Al_2O_3 ()	Amorphous (primary). $AlPO_4$ nanocrystals - tridymite (1 h at 1100 °C). $AlPO_4$ and α-Al_2O_3 (1400–1600 °C)	(Gutiérrez-Mora et al., 2006)
Broad band in the 2θ range from 15° to 30° (500 and 650 °C). $AlPO_4$ crystalline (1200 °C) have α-cristobalite $AlPO_4$ with 2θ at 21.8° (4.075 Å), 28.2° (3.159 Å), 30.8° (2.869 Å) and 35.8° (2.503 Å). Pseudohexagonal tridymite 2θ at 20.4° (4.348 Å), 21° (4.110 Å) and 23.2° (3.830 Å).	Broad band in the 2θ range from 15 to 30° (500 and 650 °C), a characteristic of the amorphous $AlPO_4$. Crystalline $AlPO_4$ (800 °C). Fully crystalline (1200 °C)-the orthorhombic symmetry. The small peak 2θ at 20.6° (4.313 Å)-the presence of structural defects. Heat treatment was increased and a mixture of tridymite and R-cristobalite was found in enriched R-cristobalite.	(Campelo et al., 2003)
broad band 2θ at 29.48°	Corresponding to 3.04 Å was the most intense diffraction lines of variscite, $AlPO_4.2H_2O$.	(Burrell et al., 1999)
Amorphous (fresh prepared) 2θ peak lists of 20.3, 21.5, 23.0, and 35.5° (1000 °C for 2 h in air). $AlPO_4$ (tridymite).	$AlPO_4$ (tridymite).	(Kandori et al., 1996)
Amorphous broad band 28 ±6° Weak broad band at 10-15°.	$AlPO_4$	(Beppu et al., 1996)
Aluminum phosphate nanoparticles/nanocomposite		
A broad XRD pattern between 20-35° corresponding to amorphous phases.	A broad XRD pattern between 20-35° corresponding to amorphous phases.	(Palacios et al., 2013)
2θ peak lists of 19.16, 20.48, 21.58, 22.86, 25.68, 28.17, 29.11, 32.25, 33.99, 38.21 and 48.92°.	The average grain size of the particles was found to be 55.75 nm.	(Devamani, 2012)
pH 10 (berlinite phase), pH 11 and 12 (berlinite with cristobalite phase)	nanoparticle, nanowire, nanorope	(Yang & Kau, 2005)

2.9.3 Field Emission Scanning Electron Microscopy (FESEM) analysis on $AlPO_4$

Yang et al., (2014) studied the reaction time, the reaction temperature, and the reaction power on the synthesis of $AlPO_4$-5 through hydrothermal and solvothermal methods. They reported that crystallization time influenced the aspect ratio and the uniformity of crystal. Besides, prismatic crystal with good uniformity was obtained at shorter crystallization time (0.5 h). Increasing of crystallization time, in fact, produced prismatic crystal with different aspect ratios and non-uniformity distribution, such as one hour crystallization time produced a mixture of dominant hexagonal crystallites and prismatic crystal. For additional hour, prismatic and hexagonal crystallites were found to grow with occurrence of amorphous phase. Therefore, the prismatic crystal became bigger and the amorphous phase became larger; contributing to non-uniformity at longer time. Yang et al., (2014) also reported that temperature helped the nucleation of $AlPO_4$ at a lower temperature of 160 °C as incomplete crystallization was observed. Prismatic crystal was obtained, but at 170 and 180 °C. Nonetheless, the homogeneity of crystallinity was better at 180 °C. Prismatic crystal was reduced at higher temperature of 190 °C. Moreover, high temperature increased the nucleation, accelerated the growth and morphology change from hexagonal plate to hexagonal rod, but excessive temperature was not conducive to perfect crystal. Other than that, the effect of HF on the $AlPO_4$ was also discussed. Irregular sphere was produced without HF. Meanwhile, a spherical crystal was obtained at lower HF. Polycrystallines and globular crystal were produced at increasing concentration of HF that was formed from crossing prismatic crystals. Prismatic crystals were dispersed at 0.05ml HF, but at concentration higher than that, no change occurred in prismatic crystal.

On the other hand, Kalbasi and Izadi (2013) also discussed about $AlPO_4$-5, but in the form of poly (4-vinylpyridine)/$AlPO_4$-5 nanocomposite, which showed no change in

$AlPO_4$-5 morphology. Polymerization of P4VP on the surface of $AlPO_4$ occurred in the $AlPO_4$ pores. Jiang et al., (2013), however, discussed about $AlPO_4$ composite of DDA-LAP layer with PU. $AlPO_4$ layer (LAP) was distributed homogeneously on the polymer at a lower percentage of PU. The TEM image shows that LAP nanolayers had been successfully exfoliated in the PU matrix. Pure PU was highly transparent, where the transparency of nanocomposites decreased as the DDA-LAP content increased. The TEM image also shows that the LAP nanolayers had both good dispersion and exfoliation of morphology on PU. In addition, Liu et al., (2010) also observed the nanolayer structure of $AlPO_4$/ Benzylamine from sliced shape (Figure 2.18). The TEM image shows space between two adjacent layers approximately 2 nm, which is in good agreement with XRD peak for d100 spacing value of 1.95 nm.

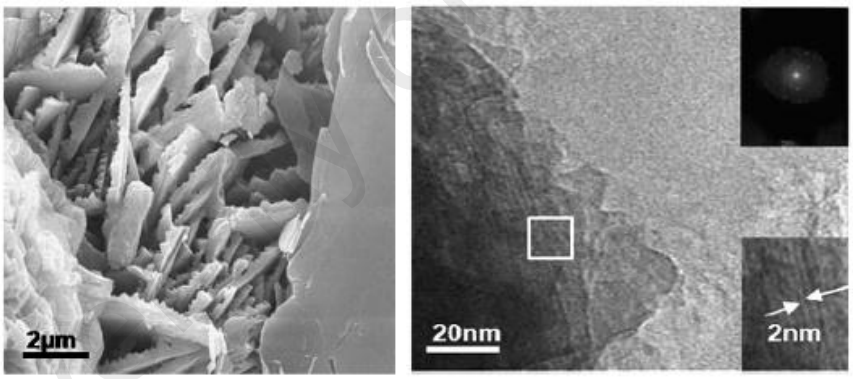

Figure 2.18:(a) SEM image of synthesized $AlPO_4$/ Benzylamine:scale bar 2μm; (b) TEM image of as synthesized $AlPO_4$/ Benzylamine: scale bar 2 nm (Liu et al., 2010)

Kimura (2005) similarly discovered the lamellar structure of $AlPO_4$, but in a bigger size, as shown in Figure 2.19. The morphological image shows the mesostructured AlPO-based materials as lamellar mesostructured AlPOs show plate-like morphologies; reflecting the layered nature.

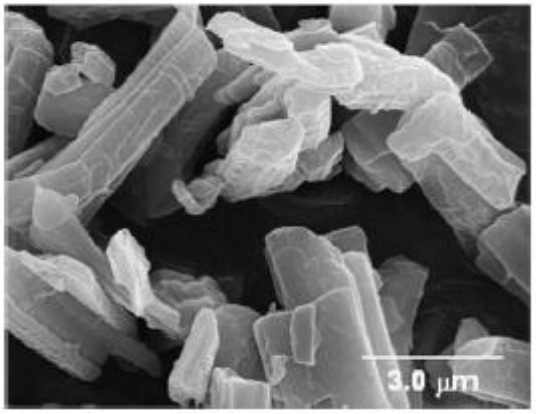

Figure 2.19: SEM image of the lamellar mesostructure $AlPO_4$ with a plate-like morphology (Kimura, 2005).

Palacios et al., (2013) discussed the synthesis of $AlPO_4$ nanoparticles for different cases. They discussed the pH effect on the particle size, as shown in Figure 2.20. Agglomeration with heterogeneous size distribution (100 – 200 nm) with pseudo hexagonal and taranakite structures had been observed at pH 3 with 2 minutes of ageing time. Meanwhile, $AlPO_4$ precipitated at a short ageing time at pH 4.8 and 6 yielded smaller 100 nm with globular morphology. Increase in particle size further occurred with the increase in ageing time for samples prepared at pH 3. However, the increase in pH until pH 6 decreased the particle size (100 nm and below), regardless of the precipitation ageing time. Additional information was obtained from TEM and concluded that the growth of $AlPO_4$ was based on aggregation process. The entire particles experienced the aggregation process and the pH influenced the final shapes of the resultant aggregate.

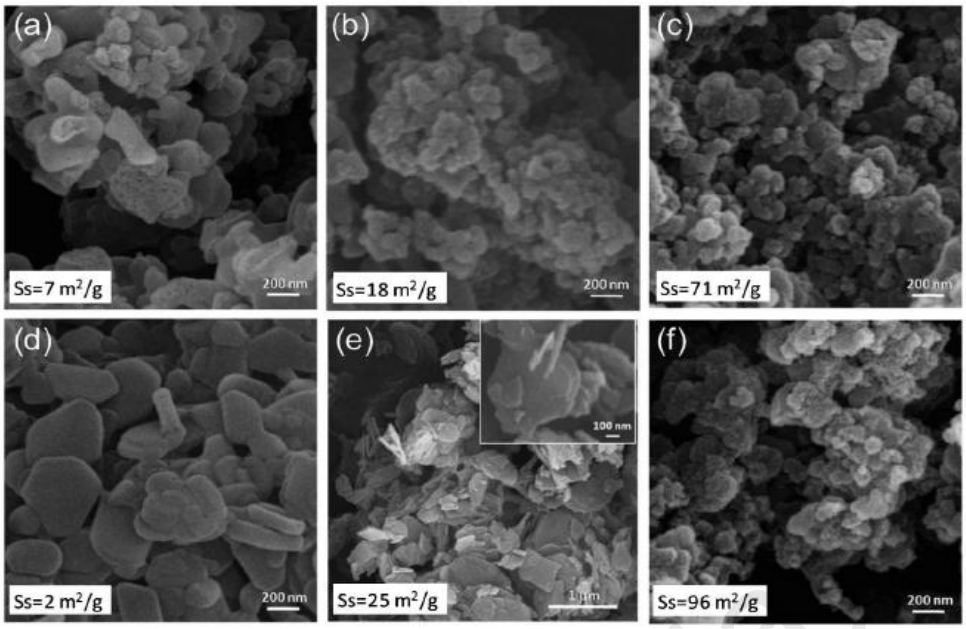

Figure 2.20:SEM micrographs of the as-synthesized aluminum phosphate; (a) pH 3, 2 min; (b) pH 4.8, 2 min; (c) pH 6, 2min; (d) pH 3, 480min; (e) pH 4.8, 480min; (f) pH 6, 480 min. (Palacios et al., 2013)

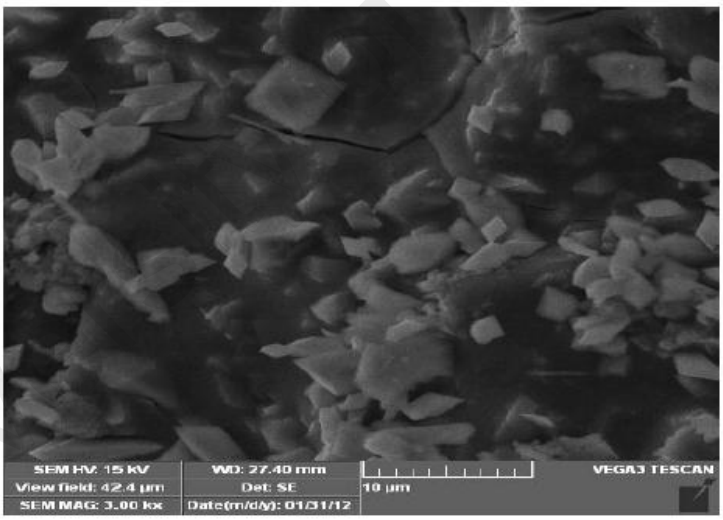

Figure 2.21: SEM image of tetrahedral aluminum phosphate at 3.00kx (Devamani, 2012).

Devamani (2012) also reported on the synthesis of $AlPO_4$ nanoparticle, but with tetrahedral morphology (Figure 2.21). They used chemical precipitation method with aluminum sulphate and sodium phosphate. Meanwhile, Boonchom and Kongtaweelert (2010) observed $AlPO_4$ particles with spherical shape and a range of sizes from 80 – 200 nm. They also observed $AlPO_4.H_2O$ particles with 30 – 100 nm for $AlPO_4$ with

merging aggregates, as shown in Figure 2.22. Thermal dehydration of $AlPO_4$ produced nanoparticles with smaller size compared to $AlPO_4.H_2O$. Other than that, Mekky and Nicholson (2007) observed nano-sized particles after calcined at 700 and 900 °C, as shown in Figure 2.23. SEM images show the grain size less than 1 micro and composed of cluster of smaller particles with round edges. Those clusters were formed because of the high reactivity associated with the nano-sized element in powder form. With support of TEM, the particle size of calcined sample at 300 °C showed an average particle size of less than 10 nm.

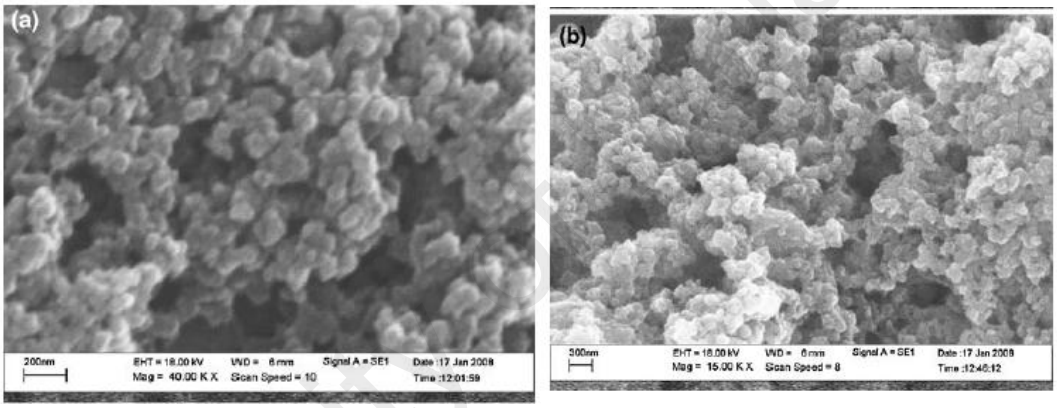

Figure 2.22: SEM micrographs of (a) $AlPO_4.H_2O$ and dehydration product (b) $AlPO_4$ (Boonchom & Kongtaweelert, 2010)

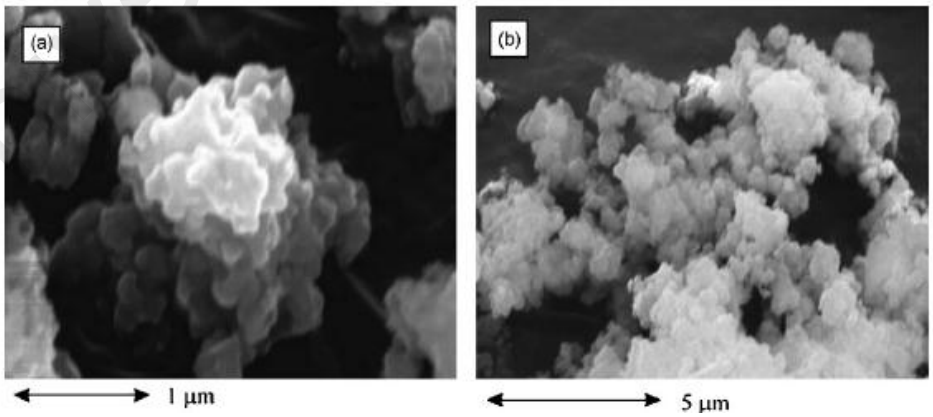

Figure 2.23: SEM of sample calcined at (a) 700 °C and (b) 900 °C (Mekky & Nicholson, 2007)

Furthermore, Gutiérrez-Mora et al., (2006) showed that the SEM images of $AlPO_4$ contained isolated internal porosity. Spherical pores were distributed throughout the samples. Meanwhile, the TEM photomicrograph of as-fabricated $AlPO_4$ sample showed the presence of $AlPO_4$ nanocrystals in an amorphous aluminum phosphate matrix. These nanocrystals were typically about 20 nm in diameter. Other than that, Yang and Kau (2005) discussed that the SEM image of pH 10 sample produced a large number of aggregated nanoparticles with diameter size that ranged from 25 – 35 nm. Two sets of categories were included, one set contained smaller nanoparticles ($d<35nm$) and the other was comprised of larger particles ($d>50nm$) with non-spherical shapes. The smaller nanoparticle size was confirmed by TEM with diameter 20 – 30 nm and the outline of the octagonal shape of non-spherical particles at about 85 nm. A directional aggregation of nanoparticles into chain-shape after four days of reaction was observed at pH 11. The morphology appeared to be interwoven in spaghetti format nanowires with 30 nm diameter. Meanwhile, at pH 12, the SEM image showed a multi-strand nanowire with diameter (nano ropes) 150 – 250 nm with ball like ends. In the preparation of $AlPO_4$ without surfactant template F127, the SEM image showed a number of irregular polygonal crystal more than 1 μm and tetragonal rods were obtained. However, no evidences of nanoparticles were found, which concluded that the formation and the evolution of morphology for $AlPO_4$ depended solely on pH and also the surfactant template F127.

In different cases, Oh et al., (2008) explored $AlPO_4$-metal as a coating material for $LiCoO_2$. $AlPO_4$ nanoparticle was applied as nanoscale coating that was expected to improve thermal stability, as well as better electrochemical performance compared to the bare and surface-modified $LiCoO_2$. $AlPO_4$ nanoparticles phases (amorphous, tridymite, or cristobalite) were coated by spin coating and annealed at 400 °C. Amorphous and cristobalite nanoparticles were in spherical shape with sizes of 20 – 50

nm, while the tridymite nanoparticles were plate-shaped with ~200 nm in diameter. The amorphous nanoparticle $AlPO_4$ (Al-P-O coating) the coated the $LiCoO_2$ with a thin film blocked the degradation of Li^+ diffusivities, thus providing the cycle-life performance.

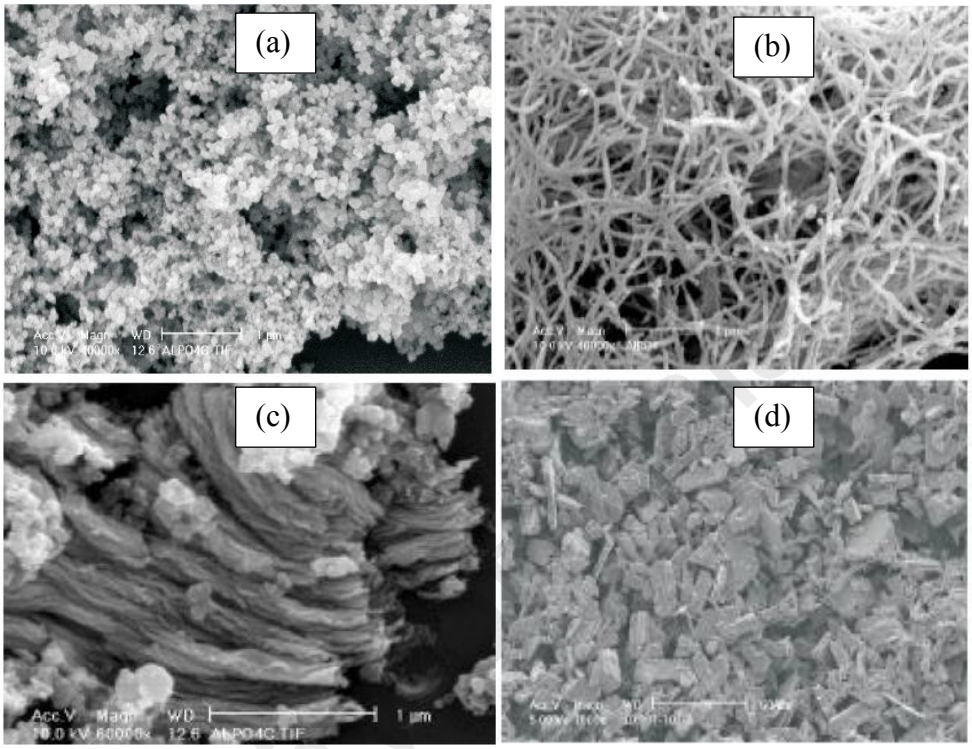

Figure 2.24: SEM image for product synthesis from a four day reaction (a)AP10; (b) AP11; (c) AP12; (d) NAP (Yang & Kau, 2005).

Kawamura et al., (2007) synthesized $AlPO_4$ without Al-EDTA chelated in autoclave produced chemical composition of $AlPO_4.1.1\text{-}1.3H_2O$ at pH 2. The sample did not exhibit any homogeneous morphology, but for pH 7, the sample appeared in the form of amorphous. The precipitation produced heterogeneous particles or no particles at all. Meanwhile, the morphology of $AlPO_4$ that had been synthesized by using EDTA and H_2O_2 produced different sizes and morphologies. Spherical particles comprising of small crystals were formed at pH 2 at 125 °C, whereas rod-like hexagonal crystal-like particles were formed at 150 °C with an approximate size of 50 mm. The hexagonal rod was transformed to hexagonal plate at a higher temperature. The morphology of $AlPO_4$ synthesis via EDTA, but without H_2O_2, produced hexagonal morphology for pH 2 – 4

and needle-like morphology for pH 6 – 8. Table 2.14 shows the details of composition and morphology of $AlPO_4$ under hydrothermal condition.

Table 2.14: Compositions and morphologies of $AlPO_4$ formed under hydrothermal condition (Kawamura et al., 2007) .

Conditions	pH	T(°C)	$[H_2O_2]_T$	Time (h)	Composition XRD and ICP	Number of hydrate water x (T_g - DTA)	SEM
No EDTA[a]	2	150	0.7	18	$AlPO_4$ + $AlPO_4.2H_2O$		
	7	150	0.7	18	Amorphous		
	2	200	0	0.16	$AlPO_4.xH_2O$	1.1 – 1.3	
	7	200	0	0.16	Amorphous		
EDTA	2	125	0.7	26	$AlPO_4.2H_2O$	1.93	Spherical
		150	0.7	64	$AlPO_4$	0.33	Hexagonal rod
		200	0.7	2.1	$AlPO_4$	0.047	Hexagonal plate
	4-8	100-225	0.7	0.3-122	Amorphous ($AlPO_4.xH_2O$)	1.04 – 1.90	Spherical
Al-EDTA	2-4	250-265	0	18	$AlPO_4$		Hexagonal
	6-8	220-225	0	18	$AlPO_4.2H_2O$		Needle

[a]Precipitation experiments at 150 °C were carried out by using a high pressure glass tube and those at 200 °C were carried out by using a stainless-steel autoclave.

2.9.4 Fourier Transform Infrared (FTIR) analysis on $AlPO_4$

FTIR analyses for $AlPO_4$, $AlPO_4$ nanoparticles, and $AlPO_4$ nanocomposite have been reported in a number of publications. Devamani (2012) and Mathews Jose (2010) presented both FTIR peaks for bulk $AlPO_4$ and $AlPO_4$ nanoparticles. Besides, Yang and Kau (2005) also presented $AlPO_4$ nanoparticle FTIR peak with the effect of EO and pH. Meanwhile, Wang (2011) and Jiang et al., (2006) presented FTIR peak for layered mineral $AlPO_4$ (taranakite) and molecular framework, respectively. Furthermore, both Boonchom and Kongtaweelert (2010) and Boonchom et al., (2008) discussed about $AlPO_4.H_2O.H_4$ and $AlPO_4$. Additionally, Kandori et al., (1998) looked into $AlPO_4$ doped with metal Fe^{3+}. FTIR analysis can provide understanding of the interaction between the surface of $A1PO_4$ and other substances. The interactions are related to the

surface structure and the properties of $AlPO_4$, such as surface functional groups, surface charge, hydrophilicity, and porosity.

In general, the surface of $AlPO_4$ consists of P-OH and Al-OH groups that exhibit two different bonds; a weaker Al-O and a stronger P-O. Either bulk or nanoparticles of $AlPO_4$ possess the basic structure element with two types of tetrahedral unit known as $(AlO_4)^{5-}$ and $(PO_4)^{3-}$. FTIR peaks in the range of 3793 – 3700 cm^{-1} were discussed by Kandori et al., (1996) and Jiang et al., (2006) as having a functional group on the surface between Al–OH. Kandori et al., (1996) also reported that functional group of P-OH occurred at 3680 cm^{-1}. However, in many publications, 3600 – 3000 cm^{-1} had been the region related to water vibration from free O-H strength alcohol (Yang & Kau, 2005), water bending vibrations in $AlPO_4.H_2O.H_4$ (Boonchom et al., 2008; Boonchom & Kongtaweelert, 2010), H_2O stretching bands in ($AlPO_4.2H_2O$) (Pînzaru & Onac, 2009), and O-H stretching in nano crystalline $AlPO_4$ (strong peak) (Devamani, 2012). Wang (2011) also suggested that taranakite adsorbed water molecules due to broad FTIR band of water hydroxyl groups at 3372 cm^{-1}. Moreover, the functional group related to C-H stretching occurred at 2950 – 2850 cm^{-1} (Wang, 2011; Yang & Kau, 2005). Jiang (2006) further concluded that the overtones appeared due to the combinations of Al–O–P vibrations from the $AlPO_4$-5 framework at a lower wavenumber (2600 – 2000 cm^{-1}). Besides, the bond related to water molecules had been observed at a range of 1700-1600 cm^{-1} (Boonchom & Kongtaweelert, 2010), water stretching vibrations in $AlPO_4.H_2O.H_4$ (1660 – 1600 cm^{-1}) (Boonchom et al., 2008), and water molecule in nano crystalline $AlPO_4$ (strong and sharp peak) (1666.38 cm^{-1}) (Devamani, 2012). On the other hand, Yang and Kau (2005) observed CH_2- scissoring at a range of 1450 – 1380 cm^{-1}. However, Devamani (2012) proposed CH_2 in nano crystalline $AlPO_4$ at 1402.15 cm^{-1}. Wang (2011), meanwhile, observed other anions, such as nitrate and carbonate at 1385 cm^{-1} and 1365 cm^{-1}, respectively. Yang and Kau

(2005) presented that saturated aliphatic C-O-C asymmetric stretching occurred at a range of 1260 – 1240 cm^{-1}, whereas Wang (2011) discussed that P=O occurred at a range of 1200 – 1100 cm^{-1}. This finding was in contrast with most other researchers that within the range of 1250 – 1022 cm^{-1}, there occurred a stretching mode of P-O with aluminum element in either bulk $AlPO_4$ (Devamani, 2012), nanocrystalline $AlPO_4$ (Devamani, 2012), (berlinite) $AlPO_4$, variscite ($AlPO_4.2H_2O$) (Pînzaru & Onac, 2009), and $AlPO_4.H_2O.H_4$ (Boonchom et al., 2008). Another important peak in FTIR was to show the existence of aluminum. Pînzaru and Onac (2009) reported that Al-O in berlinite occurred at 750, 705, 698, and 648 cm^{-1}. Meanwhile, Devamani (2012) reported that nano aluminum was observed at 661.54 and 611.39 cm^{-1}. Other publications, in addition, discussed the existence of PO_4^{3-} bond in the $AlPO_4$ within the range of 605-411 cm^{-1}. Besides, Rokita et al., (2000) reported FTIR peak for low temperature $AlPO_4$ berlinite, phosphocristobalite, and phosphotridymite. Furthermore, Mathews Jose (2010) discussed the other aspect that crystal symmetry was degraded in nano size. The degradation resulted in shifting of FTIR peak. The blue shifted occurred within the range of 5 – 30 cm^{-1}. Moreover, in vibrational spectroscopy, the spectral features were affected not only by structural symmetry, but also by the character of chemical bonds. Boonchom and Kongtaweelert (2010) also compared the FTIR peak of $AlPO_4.H_2O.H_4$ and $AlPO_4$ with a conclusion that bands in 1600 – 1700 and 3000 – 3500 cm^{-1} were related to water bending and stretching vibration. Meanwhile, Boonchom et al., (2008) summarized that vibrational units for $AlPO_4.H_2O.H_4$ were contributed by PO^{3-}, O-H, and Al-O, while for $AlPO_4$, it had been PO^{3-} and Al-O. Jiang et al., (2006) also reported that peaks within the range of 2600 – 3400 cm^{-1} had been due to the template TBA^+ cations and the peak at 3245 cm^{-1} was related to the N–H vibration mode of tributylammonium, formed by the decomposition of TBA^+. Kandori et al., (1998) further reported that $AlPO_4$ doped Fe^{3+} produced FTIR peak at 3671 cm^{-1} had

been assigned to the stretching mode of OH groups coordinated to Fe^{3+} ions and/or strongly adsorbed onto the particles. Phosphate ions, rather than Al^{3+} and Fe^{3+} ions, were found to be preferentially exposed on the particle surface produced with Fe^{3+} ions. The exposed phosphate ions made the particle surface electrostatically negative and it became a great protective film. The details of FTIR peaks are summarized in Table 2.15.

Table 2.15: Summary of FTIR analysis $AlPO_4$

Wavenumbers (cm^{-1})	Functional group	References
3793 and 3733	surface Al–OH	(Kandori et al., 1998)
3680	surface P–OH	(Kandori et al., 1998)
3671	stretching mode of OH groups of H_2O molecules to Fe^{3+} ions	(Kandori et al., 1998)
3700 – 3400	O–H vibrations of crystal water that exits in the framework $AlPO_4$-5	(Jiang et al., 2006)
3550 – 3500	Free O-H strength alcohol	(Yang & Kau, 2005)
3500 – 3050	O-H strength from H_2O	(Yang & Kau, 2005)
3477, 3369, 3121 (3000–3500)	water bending vibrations in $AlPO_4.H_2O.H_4$	(Boonchom et al., 2008)
3588, 3110, and 2945	H_2O stretching bands in ($AlPO_4.2H_2O$)	(Pînzaru & Onac, 2009)
3418, 3205 (3500 – 3000)	water stretching vibrations	(Boonchom & Kongtaweelert, 2010)
3404.13cm	O-H stretching in nano crystalline $AlPO_4$ (strong peak)	(Devamani, 2012)
3372	O-H stretching in Taranakite (Mineral $AlPO_4$)	(Wang, 2011)
3063, 1643	O-H strength H_2O	(Wang, 2011)
2913 and 2856	are assigned as the C-H stretching bands of alkyl chain	(Wang, 2011)
2950-2920, 2870 – 2850	Terminal $–CH_3$ asymmetric stretching	(Yang & Kau, 2005)
2600-2000	the overtones and their combinations of Al–O–P vibrations from the $AlPO_4$-5 framework	(Jiang et al., 2006)
2410 (weak, broad) and	stretching vibrations of the PO- H^+ bond	(Mathews Jose, 2010)
2102 (weak narrow)	free H^+ ions	(Mathews Jose, 2010)
1717 and 1638 cm-	in-plane H-O-H bending vibrations of two different types of water molecules	(Mathews Jose, 2010)
1700 – 1600	water bending	(Boonchom & Kongtaweelert, 2010)
1695 and 1622	In-plane H-O-H bending vibrations of water molecules.	(Mathews Jose, 2010)
1666.38	water molecule in nano crystalline $AlPO_4$(strong and sharp peak)	(Devamani, 2012)
1660 – 1600	water stretching vibrations in $AlPO_4.H_2O.H_4$	(Boonchom et al., 2008)
1450 – 1380	$-CH_2-$ scissoring	(Yang & Kau, 2005)
1402.15	CH_2 in nano crystalline $AlPO_4$	(Devamani, 2012)
1260 – 1240	Saturated aliphatic C-O-C asymmetric stretching.	(Yang & Kau, 2005)
1250	asymmetric stretching P-O in pure bulk $AlPO_4$	(Devamani, 2012)
1263, 1171, 1130, 1114	PO_4 stretching modes in berlinite ($AlPO_4$)	(Pînzaru & Onac, 2009)
1200-1100	P=O	(Wang, 2011)

1153, 1089,1067 (ν_3)	antisymmetric stretching mode PO_4^{3-} in $AlPO_4.H_2O.H_4$	(Boonchom et al., 2008)
1131(ν_3)	antisymmetric stretching mode PO^{3-} in $AlPO_4$	(Boonchom et al., 2008)
1122.49	symmetric stretching mode of $[PO_4]^{3-}$ in nano crystalline $AlPO_4$	(Devamani & M. 2012)
1100	symmetric stretching P-O in pure bulk $AlPO_4$	(Devamani & M. 2012)
1160, 1075, 1050, and 938	PO_4 stretching modes in variscite ($AlPO_4.2H_2O$)	(Pînzaru & Onac, 2009)
1022(ν_1)	symmetric stretching mode PO_4^{3-} in $AlPO_4.H_2O.H_4$	(Boonchom et al., 2008)
750, 705, 698, and 648	Al–O modes on berlinite ($AlPO_4$)	(Pînzaru & Onac, 2009)
694 and 526	Water liberations in $AlPO_4.H_2O.H_4$	(Boonchom et al., 2008)
695	asymmetric bending P-O in pure bulk $AlPO_4$	(Devamani, 2012)
661.54 and 611.39	nano aluminium in nano crystalline $AlPO_4$	(Devamani, 2012)
605, 511, 480, 451, 379	berlinite ($AlPO_4$) with PO4 bending modes	(Pînzaru & Onac, 2009)
515, 450, and 420	PO_4 bending modes in variscite ($AlPO_4.2H_2O$)	(Pînzaru & Onac, 2009)
501,485,435 and 418	bending vibrations PO	(Mathews Jose, 2010)
491 (ν_4)	symmetric bending mode PO^{3-} in $AlPO_4$	(Boonchom et al., 2008)
480	symmetric bending P-O in pure bulk $AlPO_4$	(Devamani, 2012)
466.74	symmetric bending in nano crystalline $AlPO_4$	(Devamani, 2012)
451(ν_2)	symmetric bending mode of PO_4^{3-} in $AlPO_4.H_2O.H_4$	(Boonchom et al., 2008)
497, 458, 422 (ν_4) 411(ν_2)	symmetric bending mode PO_4^{3-} in $AlPO_4.H_2O.H_4$	(Boonchom et al., 2008)
1117, 748, 706, 484, 380, 278	Berlinite	(Rokita et al., 2000)
1231, 1126, 735, 714, 623, 565, 500, 465, 384, 233	Phosphocristobalite	(Rokita et al., 2000)
1134, 727, 488, 226	Phosphotridymite	(Rokita et al., 2000)

2.9.5 Raman spectroscopy analysis on $AlPO_4$

Raman shift of $AlPO_4$ is almost similar with FTIR peak analysis. However, some missing vibration peaks were noted due to weak vibration energy. Boonchom et al., (2008), who conducted a Raman analysis on $AlPO_4.H_2O$-H_4 and $AlPO_4$, observed water band, but it disappeared at 1642, 3447, and 3111 cm^{-1} in $AlPO_4$. Meanwhile, Liu et al., (2010) observed peaks at 1586 and 1606 cm^{-1} referring to C-C stretching vibration of benzene ring, which indicated the existence of benzylamine layer in the layered $AlPO_4$/Benzylamine. Raman shift in the range of 1234 – 1017 cm^{-1} was related to vibrations of $(PO_4)^{3-}$ (Pînzaru & Onac, 2009; Rokita et al., 2000; Campelo et al., 2003; Boonchom et al., 2008). However, Pînzaru and Onac (2009) added that Raman fingerprints had been observed for berlinite $AlPO_4$ at 1111 and 1104 cm^{-1} wavenumbers. Meanwhile, Rokita et al., (2000) and Pînzaru and Onac (2009) observed aluminium sub-lattice vibrations due to the Al-O stretch at lower Raman shift in the range of 750-570 cm^{-1}. Vibrations of PO_4^{3-} group further occurred within the range of 595-388 cm^{-1} (Liu et al., 2010; Pînzaru & Onac, 2009; Rokita et al., 2000). Liu et al., (2010) also explained that phosphate group, due to vibrations of PO_4^{3-} at 480 and 1130 cm^{-1}, indicated the existence of the $AlPO_4$ layer in $AlPO_4$/Benzylamine and $AlPO_4$/NCG, respectively. Moreover, Pînzaru and Onac (2009), who conducted Raman analysis on natural Berlinite, reported that all bands were connected to the internal $[PO_4]_3^2$ tetrahedron vibrations. Additionally, Campelo et al., (2003) and Gregora and Magneron (2003) reported on the α and β phases of $AlPO_4$. Campelo (2003) observed that at higher temperature, more than 800 °C, Raman shift revealed five intense peaks at 1125, 484, 384, 280, and 194 cm^{-1}, which indicated crystalline $AlPO_4$ in α-cristobalite form. Besides, Rokita et al., (2000) presented Raman spectra of low-temperature polymorphic forms of $AlPO_4$ (berlinite, phosphocristobalite, and phosphotridymite). The summary of Raman shift is presented in Table 2.16.

Table 2.16: Summary review of $AlPO_4$ Raman shift

RAMAN shift (cm^{-1})	Description	References
3447 and 3111	Water band in $AlPO_4$•H_2O-H_4	(Boonchom et al., 2008)
1586 and 1606	C–C ring stretching	(Liu et al., 2010)
1230	Medium weak peak E (LO + TO) PO_4^{3-} stretch	(Cîntă Pînzaru & Onac, 2009)
1234 (berlinite), 1221 (phosphocristobalite), 1134 (phosphotridymite)	0.2 vibrations of $(PO_4)^{3-}$ Internal $(PO_4)_3^2$ tetrahedron vibrations	(Rokita et al., 2000)
1117 (berlinite), 1124 (phosphocristobalite), 1246 (phosphotridymite)	A_1 vibrations of $(PO_4)^{3-}$ Internal $(PO_4)_3^2$ tetrahedron vibrations	(Rokita et al., 2000)
1133(tridymite), 1125(α-cristobalite)	$AlPO_4$ phase	(Campelo et al., 2003)
1111 &1074(antisymmetric stretching mode, v3), 1017(symmetric stretching mode, v1)	PO_3^{-4} in $AlPO_4$•H_2O-H_4	(Boonchom et al., 2008)
1111 and 1104	berlinite Raman fingerprint PO_4^{3-} stretch	(Cîntă Pînzaru & Onac, 2009)
721 & 571(berlinite),719(phosphotridymite)	Pseudolattice Al vibration (aluminium sub-lattice vibrations)	(Rokita et al., 2000)
719 & 623(phosphocristobalite),		
725, 650	Very weak peak of Al-O stretch	(Cîntă Pînzaru & Onac, 2009)
740 – 570	aluminium sublattice vibrations	(Rokita et al., 2000)
500 – 595	v1$(PO_4)^{3-}$ stretching mode	(Cîntă Pînzaru & Onac, 2009)
530 – 360	Internal $(PO_4)_3^2$ tetrahedron vibrations	(Rokita et al., 2000)
500 – 335	the v4 and v2 of $(PO_4)^{3-}$ bending region	(Cîntă Pînzaru & Onac, 2009)
480	E vibrations of PO_4^{3-} group, in the $AlPO_4$ layer.	(Liu et al., 2010)
467 (berlinite), ,488 (phosphocristobalite), 467 (phosphotridymite)	0.2 vibrations of $(PO_4)^{3-}$ Internal $(PO_4)_3^2$ tetrahedron vibrations	(Rokita et al., 2000)
462, 221	α-berlinite $(PO_4)^{3-}$	(Cîntă Pînzaru & Onac, 2009)
388 (berlinite), 390(phosphocristobalite), 397(phosphotridymite)	E vibrations of PO_4^{3-} group Internal $(PO_4)_3^2$ tetrahedron vibrations	(Rokita et al., 2000)
<300 (285)	overtone or a result of sub-lattice aluminium defects in berlinite	(Rokita et al., 2000)
284(berlinite),284(phosphocristobalite), 282(phosphotidymite)	Librations (lattice vibration)	(Rokita et al., 2000)
1125, 1124, 488, 484, 390, 384, 284, 280, 194	α-cristobalite phase	(Campelo et al., 2003)
1112, 1104, 728, 461, 439, 336, 221and 162.	The α phase identified in the spectra at temperature below 587 °C. Strong A1 221, 461, and 1112 cm^{-1}, weaker A1 162, 336, 439, 728, and 1104 cm^{-1}.	(Gregora & Magneron, 2003)
1112, 1104, 461, 439 and 221.	the β phase identified in the spectra at temperatures more than 587 °C	(Gregora & Magneron, 2003)

2.9.6 UV visible spectroscopy analysis on $AlPO_4$

Uv vis spectra of $AlPO_4$ was reported by Trukhin et al., (2013) and Devamani (2012) with almost similar bandgaps of 5.75 eV and 5.41 eV, respectively. Trukhin et al., (2013) explained that the self-trap excitation (STE) in $AlPO_4$ was contributed from the oxygen-oxygen bond creation and PO_4 molecular ion. Absorption band at 210 nm was observed in several orthophosphate crystals that had been ascribed to the PO_4 complex. The UV Vis band for pure $AlPO_4$ showed two intense peaks at 4.3 and 5.75 eV in contribution of PO_4 complex.

Meanwhile, Xu et al., (2006) presented that $AlPO_4$ in a solution form, was encapsulated with Rhodhamine B and produced main absorption peak at 551 and shoulder peak at 520 nm. The dominant peak at 551nm was contributed from p–p* transitions along the longest dimension of the conjugate system. Meanwhile, the blue shoulder around 520 nm was attributed to a dimer. The $AlPO_4$ film encapsulated with Rhodhamine B exhibited a red shift with strong fluorescence intensities at 578 nm. The observation proved successful encapsulation of monomers by Rhodamine dimers.

Earlier, Ganschow et al., (2001) observed almost similar cases, as reported by Xu et al., (2006). However, Ganschow et al., (2001) explained that strong shoulder at 527 nm originated from increased transition of the vibrational ground state to and excited vibrational state of a monomer. Absorption of Rhodamine BE50 in aqueous solution was also observed at 557/582 nm and when encapsulated in $AlPO_4$-5, they appeared at 550/608 nm. The summary of UV-visible data for $AlPO_4$ is presented in Table 2.17.

Table 2.17: Summary review of $AlPO_4$ UV-visible

Wavelength (nm)/ Band gap (eV)	Description	References
550/608 nm	Rhodamine BE50 when encapsulated in $AlPO_4$-5	(Ganschow et al., 2001)
557/582 nm;	absorption/fluorescence maxima Rhodamine BE50 in aqueous solution	(Ganschow et al., 2001)
578	$AlPO_4$-5 film encapsulate with Rhodamine B	(Xu et al., 2006)
551	$AlPO_4$-5 aqueous solution encapsulate with Rhodamine B	(Xu et al., 2006)
527	Shoulder transitions from the vibrational ground state to an excited vibrational state of monomer	(Ganschow et al., 2001)
520	Rhodamine B dimer	(Xu et al., 2006)
450	related to oxygen–oxygen bond creation	(Trukhin et al., 2013)
210 (5.75)	Orthophosphate related to the PO_4 molecular complex. UV luminescence is a property of orthophosphates	(Trukhin et al., 2013)
5.41	Optical band gap for nano $ALPO_4$	(Devamani & M. 2012)

2.9.7 Photoluminescence (PL) analysis on $AlPO_4$

Photoluminescence studies of $AlPO_4$ were reported in a few publications such as Trukhin et al., (2013), Xu et al., (2006), and Yang et al., (2007). Trukhin et al., (2013) reported that PL emission at 210 nm was related to the PO_4 molecular complex. Yang et al., (2007) found that at 533, 582, 649, and 688 nm wavelengths, strong PL in the AlP/SiO_2 nanocomposites arose from the hydrogen-related species. Xu et al., (2006), in addition, observed approximately similar emission spectra at 578 nm from PL emission of Rhodamine B-loaded $AlPO_4$-5 films that produced strong fluorescence intensities. Meanwhile, absorption spectra at 550 nm of $AlPO_4$-5 polar framework with Rhodamine B had been similar to an aqueous solution of Rhodamine B, which concluded the occurrence of dipole–dipole interactions. Table 2.18 summarizes the PL review of $AlPO_4$.

Table 2.18: Summary review of $AlPO_4$ Photoluminescence.

Wavelength (nm)	Description	References
578	Emission spectra of PL Rhodamine B-loaded $AlPO_4$-5 films had strong fluorescence intensities	(Xu et al., 2006)
533, 582, 649 and 688	A strong photoluminescence was observed from the AlP/SiO_2 nanocomposites. Emissions may arise from the hydrogen-related species,	(Yang et al., 2007)
210 (5.75ev)	Orthophosphate related to the PO_4 molecular complex. UV luminescence is a property of orthophosphates, related to oxygen–oxygen bond creation	(Trukhin et al., 2013)

Chapter 3

METHODOLOGY

This chapter describes the materials used and detailed stage of synthesis procedure. Characterization equipment are also being elaborated thoroughly.

3.1 Materials and equipment

Starting materials used in the polymer modification were partially hydrolyzed polyvinyl alcohol with 87.5 – 88% hydrolyzed and phosphoric acid with 85% concentration obtained from R&M chemicals. Two different sources of Aluminum are used for the synthesis of $AlPO_4$ nanocomposite that is Aluminum Nitrate ($Al(NO_3)_3.9H_2O$) and Aluminum hydroxide ($Al(OH)_3$). Potassium hydroxide (KOH) was used for pH variation. Meanwhile, methanol and deionized water were used for the filtering and washing the final products. All the details of materials and chemicals used were tabulated in Table 3.1

Table 3.1: Details of materials chemicals used in the synthesis of PPVA - $AlPO_4$ nanocomposite

Chemical	**Brand**	**Formula**	**MW(g/mol)**	**Density(g/ml)**
Polyvinyl alcohol	R&M chemicals	C_2H_4O	44	bulk density of 0.4–0.6
Phosphoric acid (85%=14.7M)	R&M chemicals	H_3PO_4	98	1.685
Aluminum Nitrate	R&M chemicals	$Al(NO_3)_3.9H_2O$	375.13	
Aluminum hydroxide	R&M chemicals	$Al(OH)_3$		
Potassium hydroxide/Kalium hidroksida 10%w/v	R&M chemicals	KOH		
Methanol	R&M chemicals			

Table 3.2 summarizes all the equipment and apparatus glassware used in the synthesis of PPVA- $AlPO_4$ nanocomposite. The reflux equipment setups is illustrated in Figure 3.1

Table 3.2: Details of apparatus and equipment used the synthesis of PPVA - $AlPO_4$ nanocomposite

Apparatus and Equipment	**BRAND**	**Details**
Round bottom three neck flask	Pyrex	Glassware
Condenser	Pyrex	Glassware
Conical flask	Bomex	Glassware
Thermometer		
Heating mantle		
Magnetic stirrer	Stable Temp, Cole Parmer	Stir and heat
Magnetic bar		31x6mm, PTFE coated, cylindrical
Balance Machine		
Casting plate	Custom made	
pH meter	TR-TI9000 WalkLAB Microprocessor pH meter TI9000	
Closed oven		
Portable autoclave	Custom made	
DSC	Perkin-Elmer DSC-7	
TGA/SDTA	Mettler Toledo TGA/SDTA851	
XRD	Panalytical Empyrean Diffractometer	
FESEM	JEM-2100F Field Emission Electron Microscope	
FTIR	Perkin Elmer System 2000 Fourier Transform Infrared (FTIR)	
RAMAN	Horiba Scientific Xplora Raman spectrometer	
UV Visible	Cary 50 Uv-Visible spectrophotometer.	
Photoluminescene	Perkin Elmer LS 55 luminescense spectroscopy, Photoluminescence spectrophotometer (PL)	

3.2 Synthesis of PPVA-$AlPO_4$ nanocomposite

In this research, the synthesis of PPVA-$AlPO_4$ was performed in two stages that is the first stage is modification of PVA polymer and the second stage is in-situ or co-precipitation of $AlPO_4$ nanoparticles.

3.2.1 Preparation of modified polymer

The first step to produce polymer nanocomposite involved in preparation of modification polymer poly vinyl alcohol (PVA) surface. Method used for modification of PVA with phosphoric acid (H_3PO_4) was adapted and modified from Zhan et al. (2004) and Chen & Liu (2011c). The polymer is modified by replacing the –OH bonding in PVA with phosphate group from phosphoric acid. A set of fabrication system was prepared consists of the three necks round bottom flask, thermometer, heating mantel, stirrer set and reflux. 6.6g of PVA was mixed with deionized water and H_3PO_4 in the three neck round bottom flasks as shown in Figure 3.1. The mixture was dissolved by heating at 90 °C for 30 min and reflux for 1 hour with a stirring rate of 120 rpm. Then, the dissolved sample was left to cool in stirring mode. Later, the resulting products were poured on the casting plate and left dried at room temperature for three days. The films were then sent for various characterizations. Equation (3.1) expressed the mole ratio (R) of PA over PVA. Partially phosphorylated PVA (PPVA) was prepared with various ratios and label as summarizes in Table 3.3.

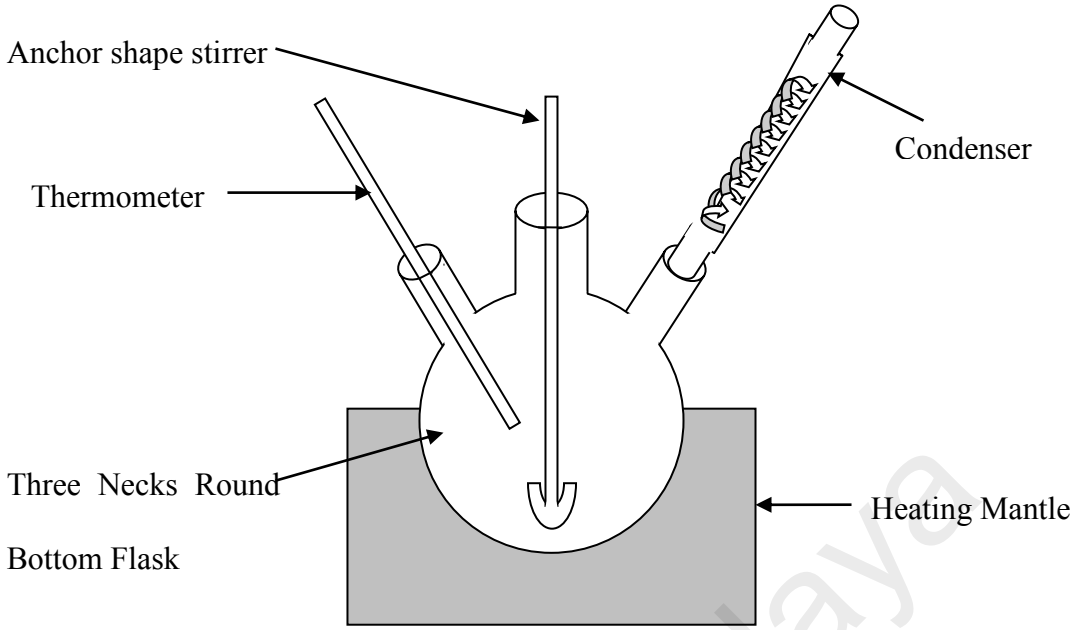

Figure 3.1: Schematic diagram of reflux (condensation) equipment

$$R = \frac{\text{mol PA}}{\text{mol PVA}} \qquad (3.1)$$

Table 3.3: Modification of polyvinyl alcohol by phosphoric acid

Tag	PVA (mole)	H_3PO_4 (mole)	H_3PO_4 (Molar)	R(X=mol PA/mol PVA)
Pure PVA	0.1500	0.0000	0.00	0.0000
0.1	0.1500	0.0172	0.59	0.1150
0.2	0.1500	0.0345	1.18	0.2299
0.3	0.1500	0.0517	1.76	0.3449
0.4	0.1500	0.0690	2.35	0.4599
0.5	0.1500	0.0862	2.94	0.5748
1.1	0.1500	0.1724	5.88	1.1497
1.7	0.1500	0.2587	8.82	1.7245

3.2.2 Preparation of polymer nanocomposite

The second step is involved the synthesis of PPVA-$AlPO_4$ nanocomposite. The resultant PPVA was added with aluminum sources and samples were maintained with continuous stirring for 1 hour at temperature of 90 °C. Table 3.4 summarized the formulation of nanocomposite. The pH of PPVA-$AlPO_4$ nanocomposite synthesis using aluminum nitrate as the aluminum source was varied from pH 7 – 12 and heat treated in autoclave at 120 °C for various crystallization times, 2, 12 and 24 hours. Table 3.5 summarized all PPVA-$AlPO_4$ nanocomposite samples prepared at various pH and crystallization time. Figure 3.2 shows the flowchart of complete procedure for synthesis and characterization of PPVA-$AlPO_4$ nanocomposites. The synthesis process can be divided into three parts, polymer modification, nancomposite preparation and characterization process has been explained earlier.

Table 3.4: Formulation for synthesis of aluminum phosphate nanocomposite

Ratio of Al:P	**PPVA**	**Mole P in PPVA**	**Al $(NO_3)_3.9H_2O$**	
			Sample	**mole Al**
1.0:3	0.2	0.01091	AP 1.0	0.00364
1.1:3	0.2	0.01091	AP 1.1	0.00401
1.2:3	0.2	0.01091	AP 1.2	0.00437
1.3:3	0.2	0.01091	AP 1.3	0.00472
1.4:3	0.2	0.01091	AP 1.4	0.00508
1.5:3	0.2	0.01091	AP 1.5	0.00575

Table 3.5: Formulation for synthesis of PPVA-$AlPO_4$ nanocomposite at various pH and crystallization time.

Samples	Crystallization time (hour)	Ratio of Al:P	Heat treatment	Reaction pH
NAP7-A	As prepared	1.3:3	No heat treatment	7
NAP8-A		1.3:3	No heat treatment	8
NAP9-A		1.3:3	No heat treatment	9
NAP10-A		1.3:3	No heat treatment	10
NAP11-A		1.3:3	No heat treatment	11
NAP12-A		1.3:3	No heat treatment	12
NAP13-A		1.3:3	No heat treatment	13
NAP7-B	120° C, 2hours	1.3:3	120 °C, 2 hours	7
NAP8-B		1.3:3	120 °C, 2 hours	8
NAP9-B		1.3:3	120 °C, 2 hours	9
NAP10-B		1.3:3	120 °C, 2 hours	10
NAP11-B		1.3:3	120 °C, 2 hours	11
NAP12-B		1.3:3	120 °C, 2 hours	12
NAP7-C	120° C, 12hours	1.3:3	120 °C, 12 hours	7
NAP8-C		1.3:3	120 °C, 12 hours	8
NAP9-C		1.3:3	120 °C, 12 hours	9
NAP10-C		1.3:3	120 °C, 12 hours	10
NAP11-C		1.3:3	120 °C, 12 hours	11
NAP12-C		1.3:3	120 °C, 12 hours	12
NAP7-D	120° C, 24hours	1.3:3	120 °C, 24 hours	7
NAP8-D		1.3:3	120 °C, 24 hours	8
NAP9-D		1.3:3	120 °C, 24 hours	9
NAP10-D		1.3:3	120 °C, 24 hours	10
NAP11-D		1.3:3	120 °C, 24 hours	11
NAP12-D		1.3:3	120 °C, 24 hours	12

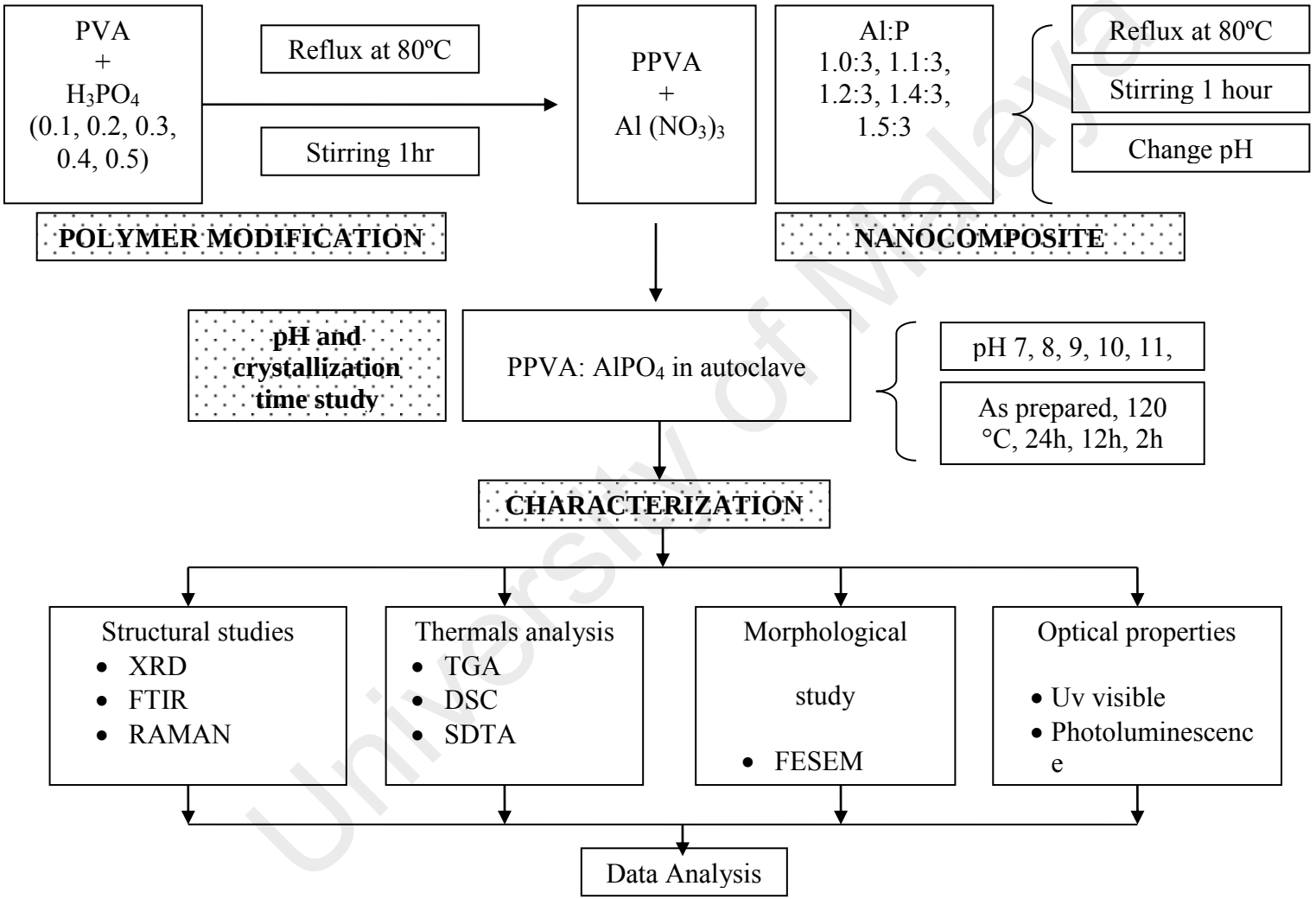

Figure 3.2: Flowchart of synthesis and characterization of PPVA-$AlPO_4$ nanocomposites.

3.3 Characterization of material properties

Thermal properties such as melting temperature and degradation of both PPVA and PPVA-$AlPO_4$ nanocomposite were analyzed using Differential Scanning Calorimetry (DSC) and Transgravimetric Analysis (TGA). Structural properties of both PPVA and PPVA-$AlPO_4$ nanocomposite was characterized using X-ray Diffraction (XRD), Fourier Transform Infrared (FTIR) and RAMAN spectroscopy. Optical properties was conducted using UV Visible and Photoluminescence spectroscopic. Finally the morphological studies of PPVA-$AlPO_4$ nanocomposite were observed using Field Emission Scanning Electron Microscopy (FESEM).

3.3.1 Thermal Studies

3.3.1.1 Differential Scanning Calorimetry (DSC)/ Transgravimetric Analysis (TGA)/ Simultaneous Differential Thermal Analysis (SDTA)

Thermal analysis studies were analyzed by using two equipment that is TGA and DSC as shown in Figure 3.3. TGA was used to study the thermal degradation of PPVA and PPVA-$AlPO_4$ nanocomposite. Meanwhile, DSC was used for characterization of PPVA film for determine the glass transition temperature (T_g) and melting temperature (T_m). Thermal analysis of PVA, PPVA and PPVA-$AlPO_4$ has been conducted in air atmosphere for both TGA and DSC using Mettler Toledo TGA/SDTA851 and A Perkin-Elmer DSC-7, respectively. TGA with heating rate of 10 °C/min and heated from 25 to 1000 °C. For DSC experiments, about 10 – 20 mg of the sample was encapsulated in an aluminum volatile sample pan that has a tightly fitting lid. The lid was pierced with a small hole through which the water vapor escapes. The samples are heated from 20 °C to 350 °C at a heating rate of 10 °C/min.

Figure 3.3: (a) Perkin-Elmer DSC-7 and (b) Mettler Toledo TGA/SDTA851

Data obtained from DSC is in the form of temperature (°C) and power (mW). The information of the endothermic/exothermic reaction and phase transformation can be obtained from this technique. Simultaneous differential thermal analysis (SDTA) provides the similar information as DSC. Only the SDTA data measured in the temperature for comparison of samples with reference meanwhile DSC data measures the energy required to keep both reference and sample at the same temperature. The TGA produced raw data in the form of temperature (°C) and mass (mg). Data analysis needs to be conducted for calculation of the amount of weight loss or weight residue in the percentage.

3.3.2 Structural Studies

3.3.2.1 X-Ray Diffraction (XRD)

Figure 3.4: Panalytical Empyrean X-Ray Diffractometer

The structural properties of PPVA and PPVA-$AlPO_4$ samples were analyzed by using Panalytical Empyrean Diffractometer with Cu Kα radiation (λ = 1.54060A) as shown in Figure 3.4. The angle was 2θ measured starting from 2º and end at 80º. XRD is a nondestructive technique that provides information about crystallinity, crystal structure, lattice parameters, phase identity, phase purity and percentage of phase composition. Samples are prepared in powder form, grind and packed tightly in the sample holder to ensure the high intensity of XRD peaks. Loose powder may produce poor intensities of

XRD peak. The sample is placed at sample holder and subjected to X-Ray light sources. The interaction of sample products with the incident rays produces a diffracted ray with satisfying condition of Bragg‘s Law. The law is related to the wavelength of electromagnetic to the diffraction angle and the lattice spacing in a crystalline sample. All atoms in the samples are arranged differently and it produced a various diffraction pattern. X ray diffraction produces an elastic scattering, the outgoing X-rays have the same energy and wavelength as the incoming X-rays, but at different direction. The raw data recorded from XRD provide a general information of 2θ angles, peak intensity, peak shapes and width. The diffraction peaks, then converted to d-spacing using the Debye-Scherer formula and compared to the d-spacing of standard reference patterns. For the known expected materials, confirmation can be made by search and match using the JCPDS database that compile about 100,000 patterns of XRD. However, for new materials, a process of index the pattern with information of unit cell, lattice parameter and symmetry is necessary.

3.3.2.2 Fourier Transform Infra-Red (FTIR)

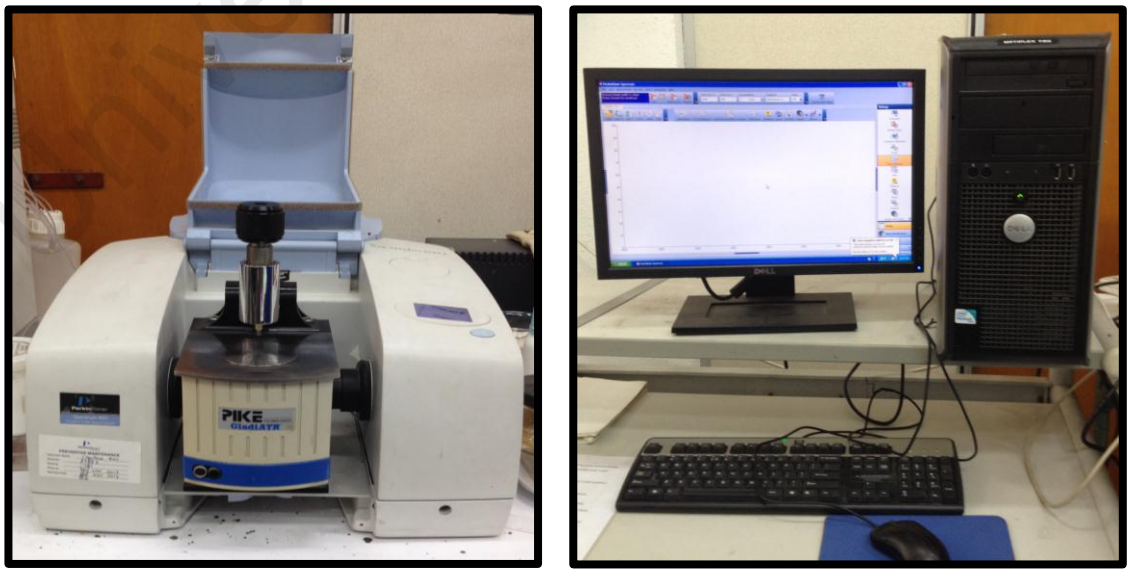

Figure 3.5: Perkin Elmer System 2000 Fourier Transform Infrared Spectrometer

Chemical properties and structures of powder and film were analyzed using FTIR spectroscopy as shown in Figure 3.5. The room temperature FTIR spectra were recorded in the range of 4000 to 400 cm^{-1} with four scans on a Perkin Elmer System 2000 Fourier Transform Infrared (FTIR) with the resolution of $4cm^{-1}$. All samples were used directly but for different type of sample (film, powder and solution) needs to use different types of holders and tip. FTIR data was obtained in the form of wavenumber (cm^{-1}) and intensity in value of transmittane (%T) or in absorbance. FTIR is a nondestructive method that has an infrared radiation that passed through a sample with some of the radiation absorbed by the sample and some of it was transmitted. The resultant signal produces a spectrum that represents the molecular absorption and transmission. Each sample has their own identity of molecular absorption or known as molecular fingerprint of the sample. FTIR can be used to identify unknown materials, determine the amount of component in a mixture and the quality of a sample.

3.3.2.3 RAMAN Spectroscopy

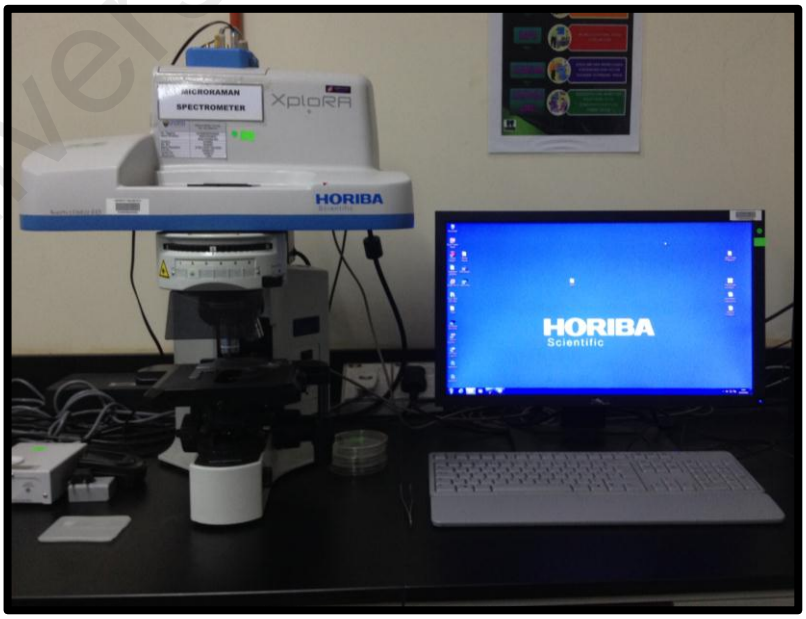

Figure 3.6: Horiba Scientific Xplora MicroRaman Spectrometer

Raman spectroscopy is a nondestructive chemical analysis technique that based on the interaction of light with the chemical bond that exist in a material. It provides information about chemical structure, crystallinity, molecular interaction, phase and polymorph. Sample of specimen conducted with Raman Spectrometer was shot with high intensity of laser source. The molecules that interact with laser will experience vibration, phonon and excitation resulting the laser energy being shifted up and down. The shift gives information about the vibrational behavior of molecules and Raman spectroscopy usually focused on the fingerprint region. The molecules will scatter the light into different wavelength which depends on the chemical structure. If the scattered light has the same wavelength with the laser source (Rayleigh scattering) it does not provide useful information for chemical structure. Rayleigh scattering also known as elastic scattered radiation, which is all will be filtered out. Only a small amount of light typically 0.0000001% will scattered at different wavelengths (inelastic scattering) and provide useful information on chemical structure known as Raman scattering. Basically, the Raman scattering is a very weak signal as compare to Rayleigh scattered which very intense. Raman need to be used with other accessory to enhanced its signal. Raman spectrum provides information of intensity on the y axis, wavenumber (cm^{-1}) on x axis and pattern of peaks. Each peak corresponds to a specific molecular bond vibration or individual bonds such as C-C, C=C, N-O, C-H and groups of bond, such as benzene ring, polymer chain vibration and lattice modes. Raman can be used in many different forms of samples either in solid, powder, liquid, gel, slurries or gases as in its pure chemicals, mixture or solution. Organic and inorganic samples also suitable for raman analysis, but metals and its alloy are not recommended.

3.3.3 Morphological Studies

3.3.3.1 Field Emission Scanning Electron Microscope (FESEM)

Analysis of the size and morphological of PPVA-$AlPO_4$ nanocomposite samples were studied with a Field Emission Scanning Electron Microscope (FESEM) Jeol JEM-2100F after gold coating. Elemental analysis was carried out with energy dispersion X-ray (EDX), analytical system attached to the scanning electron microscope (Jeol JEM-2100F). Figure 3.7 shows the FESEM equipment used in this research.

Figure 3.7: JEM-2100F Field Emission Scanning Electron Microscope

Magnification of 50k and 100k times were taken for selective specimen. The FESEM is used to visualize fractions of object, topographic details on the surface or entire samples such as the geometrical structure and approximate size of PPVA-$AlPO_4$ nanocomposite can be observed and calculated. This technique can observe the geometrical shapes and size as small as 1 nm. The information obtained in a digital image that can be saved and process later. The light source produced an accelerated electron in high electrical field

gradient and vacuum. Primary electron are focused and deflected by electronic lenses that produce narrow beam and bombard to the samples. Secondary electron emits from the samples produced angle and velocity produces an electronic signal that related to the surface structure of the samples. The signal is amplified and transformed to scan digital image.

3.3.4 Optical Studies

3.3.4.1 UV-visible spectroscopy

Figure 3.8: Cary 50 Uv-Visible spectrophotometer

Absorption spectra of PPVA and PPVA-$AlPO_4$ nanocomposite samples were recorded using a Cary 50 Uv-Visible spectrophotometer (Figure 3.8). The wavenumber used is 200 – 900 nm at 60 nm/min scan speed and conducted in a 3 mm quartz cell. UV-Vis spectroscopy is used to do the quantitative and qualitative measurement of organic materials. The solvent used for the determination of UV-Vis is water for water soluble component or ethanol for organic soluble compounds.

UV-vis spectroscopy based on the absorption of molecules that contained π- electrons or nonbonding electrons (n-electron). This electron can absorb energy from ultraviolet and excite to higher anti bonding molecular orbital (π^*). The more easily excited the electron, the longer the wavelength of light can be absorb. UV Vis data was obtained in the form of wavelength (nm) and intensity in absorbtion or % of transmittance (%T). The graph of absorption versus wavelength and optical band gap can be calculated from the UV Vis analysis that describe the chemical bonding and the energy state of the molecules.

3.3.4.2 Photoluminescence (PL) Spectroscopy

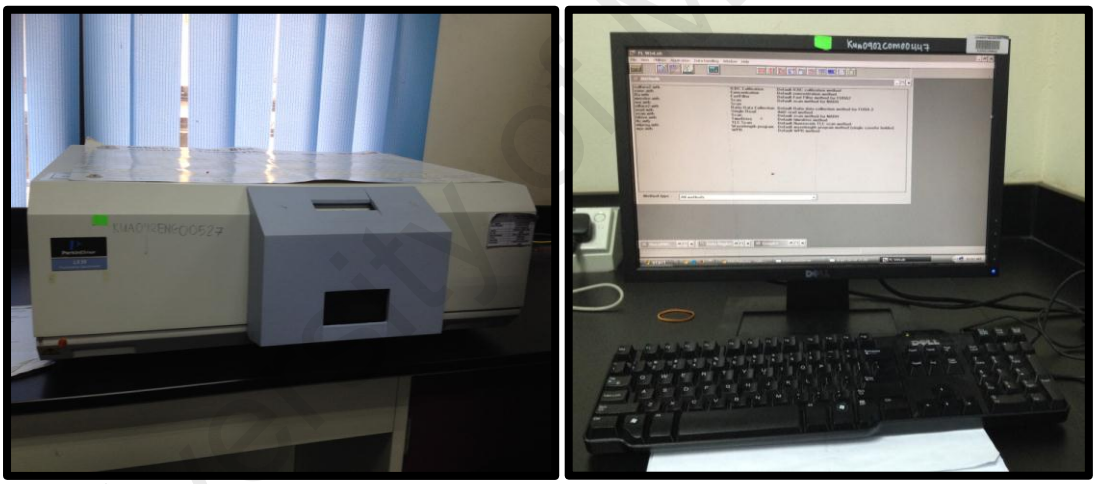

Figure 3.9: Perkin Elmer LS 55 luminescence spectroscopy, (PL).

Optical studies using photoluminescence spectrophotometer (PL) for the partially phosphorylated PVA solution and PPVA-$AlPO_4$ nanocomposite were conducted using Perkin Elmer LS 55 luminescence spectroscopy (Figure 3.9). A fresh solution is used to avoid the effects of aging and other structural changes in interaction with water molecules. Emission spectrum is recorded from 200-900 nm at excitation peaks of 272, 300, 350, 400 and 500nm as observed in UV Vis spectroscopy. The absorption spectra are between 200 to 900 nm of solutions and conducted in a 3 mm quartz cell. PL

spectroscopy is a nondestructive method, with a photo excitation process after sample absorbed a light that focused on it. The photo excitation results a release of energy when the material jump to a higher electronic state, then the photons relax and return to a lower energy level. Photoluminescence is the emission of light or luminescence occurs through the process. PL data obtained in the form of wavelength (nm) and intensity (a.u). PL usually been conducted with known value of UV-visible absorbance as a value for excitation wavelength. Another option is by just running the pre-scan using PL software the Perkin Elmer Winlab, it will give the estimated value for maximum excitation and emission peak for the sample.

Chapter 4

RESULTS AND DISCUSSION

This chapter describes a thorough analysis of as-synthesized materials. It is divided into two parts with the first part dealt with the modification of polyvinyl alcohol with phosphoric acid while the second part dealt with polymer nanocomposite with aluminum phosphate.

4.1 Overview

Firstly, polyvinyl alcohol (PVA) with hydroxyl (OH) branch was modified with various concentrations of phosphoric acid (H_3PO_4). Then, the modified polymer was added with aluminum sources for the composite development. Modification of PVA with phosphoric acid was conducted in the ratio of 0.1 to 1.7245. Partially phosphorylated PVA (PPVA) with a small concentration of H_3PO_4 produced a colourless film. The film was gradually became yellowish, brown and dark brown at higher concentration of H_3PO_4. Table 4.1 summarizes the observation results. The colour observation was also discussed by Mohapatra et al. (2006) that the polymer film appeared to be brownish for phosphorus beyond the concentration range of 2 to 5.5 M. They also discussed about no significant increase of phosphate in the polymer to perform a crosslink. Nevertheless, the phosphate tend to accelerate the dehydration and form conjugate double bond in the polymer. This finding was also supported by Banks et al. (1993) that reaction with PVA will produced phosphorylation at lower concentration of phosphoric acid. However, at high concentration of phosphoric acid (1.5M), phosphorylation is slowly stop and dehydration process is started.

Table 4.1: Visual observation of partially phosphorylated PVA (PPVA) films for various ratio of PVA and phosphoric acid

Tag	H_3PO_4 (M)	Ratio PA:PVA	Observation
Pure PVA	0.00	0.0000	Colourless film
0.1	0.59	0.1150	Colourless film
0.2	1.18	0.2299	Colourless film
0.3	1.76	0.3449	Colourless soft film
0.4	2.35	0.4599	Yellowish moist soft film
0.5	2.94	0.5748	Light brown wet soft film
1.1	5.88	1.1497	Light brown gel/film
1.7	8.82	1.7245	Dark brown gel/film

Secondly, partially phosphorylated–aluminum phosphate (PPVA-$AlPO_4$) nanocomposites were synthesized via chemical and hydrothermal methods through the reaction of PPVA and aluminum nitrate ($Al(NO_3)_3$. $9H_2O$) at various pH values with Al/P atomic ratios of 1:3, 1.1:3, 1.2:3, 1.3:3, 1.4:3, and 1.5:3. The mixtures were mixed in a sealed portable Teflon-lined stainless steel autoclave and heated at 120 °C for 2, 12 and 24 hours crystallization time. The white precipitate was obtained and then filtered and washed with methanol/deionized water, repeatedly. Finally, the end product was dried at 50 °C and stored as powders or suspended in methanol/ethanol for further study.

The mixture of PPVA with Aluminum Nitrate produced a colorless liquid at highly acidic environment (pH < 1). As pH level increases, the liquid change to white color solution. However at pH 13, the white solution change to colorless solution again due to all the reactants were completely dissolved and the reactions could not be initiated. Table 4.2 summarizes the visual observations of all samples. The decrease of pH is due to the formation of additional double hydroxide bridges during exposure with water in autoclave (Burrell et al. 1999).

Table 4.2: Visual observation of as prepared and heat treated samples at 120 °C for various pH values and crystallization time.

Samples		pH <1 (Initial)	KOH Volume (ml)	pH (Intermediate)	Appearance	Final pH (After heat treatment)
As prepared	NAP7-A	Colourless solution	126.50	7.13	White solution	-
	NAP8-A	Colourless solution	129	8.16	White solution	-
	NAP9-A	Colourless solution	131.20	9.22	White solution	-
	NAP10-A	Colourless solution	132.90	10.17	White solution	-
	NAP11-A	Colourless solution	135	11.18	White solution	-
	NAP12-A	Colourless solution	139.90	12	White solution	-
	NAP13-A	Colourless solution	>150	13	Colourless solution	-
120 °C, 2 hours	NAP7-B	Colourless solution	125.10	7.11	White solution	6.37
	NAP8-B	Colourless solution	128.0	8.14	White solution	7.63
	NAP9-B	Colourless solution	130.10	9.14	White solution	8.57
	NAP10-B	Colourless solution	132	10.25	White solution	9.79
	NAP11-B	Colourless solution	134	11.14	White solution	10.86
	NAP12-B	Colourless solution	141	12.07	White solution	12.12
120 °C, 12 hours	NAP7-C	Colourless solution	127.80	7.43	White solution	6.32
	NAP8-C	Colourless solution	130	8.26	White solution	7.47
	NAP9-C	Colourless solution	132.2	9.35	White solution	8.57
	NAP10-C	Colourless solution	133.9	10.35	White solution	9.46
	NAP11-C	Colourless solution	135.4	11.15	White solution	10.13
	NAP12-C	Colourless solution	140	12.10	White solution	11.44
120 °C, 24 hours	NAP7-D	Colourless solution	127.30	7.11	White solution	5.93
	NAP8-D	Colourless solution	129.90	8.16	White solution	7.51
	NAP9-D	Colourless solution	131.80	9.18	White solution	8.50
	NAP10-D	Colourless solution	134.0	10.40	White solution	9.54
	NAP11-D	Colourless solution	135.6	11.18	White solution	10.41
	NAP12-D	Colourless solution	140.0	12.08	White solution	11.26

4.2 Effect of phosphoric acid on PVA

4.2.1 Thermal Analysis (DSC, SDTA, TGA)

Figure 4.1 (a) shows the DSC patterns for PVA and PPVA with different mole ratios (0.1, 0.2, 0.3, 0.4 and 0.5). The DSC pattern for PVA exhibited multiple endothermic peaks in the temperature range of 30 - 250°C. Both PVA film and powder possessed similar values of glass transition temperature (T_g) at 54 °C and melting temperature (T_m) at 195 °C. Meanwhile, glass transition temperatures (T_g) for all PPVA samples are not clearly visible. The first endothermic peak of PVA became broad at temperature lower than 100°C as phosphoric acid concentration increases due to contribution from the water phase. However, for PPVA sample with mole ratio of 0.5, higher concentration of phosphoric acid produced a broad endothermic peak in the temperature range of 96 – 116 °C. The peak then divided into two peaks due to the dehydration and phase separation process as a result of excessive phosphoric acid in the complexes.

Gong & Shou-Cai (1989) and Vargas et al. (1998) also observed the endothermic peak in PPVA at lower temperature of below 100 °C due to the PPVA film‘s nature as a moisture absorbent. These results support the finding of Zhan et al. (2004) and Banks et al. (1993) that poly vinyl phosphate with hydrophilic properties is obtained through the mixture of PVA and phosphoric acid. Polyvinyl di-phosphate and tri-phosphate which inherits the hydrophobic properties can be obtained at higher temperature. DSC traces for PVA and PPVA films show multiple endothermic peaks given that they contained multiple phases (Zurbriggen, 2001) such as water, acetate group, acid group and polymer. The multiple peaks were also due to the melting of original PVA crystal and a series of melting process of new crystal formation, recrystallization, melting the recrystallization and perfected crystal (Bhajantri et al. 2006). Broadening of

endothermic peak can be assigned to coexist of the PPVA complexes, uncomplexed PVA and unreacted phosphoric acid. This is almost similar in the complexation of PVA with NH_4SCN (Agrawal & Awadhia, 2004). It is proposed that the tendency of PPVA films to absorb moisture and coexist compound will influence the broadening and fluctuating of endothermic peak.

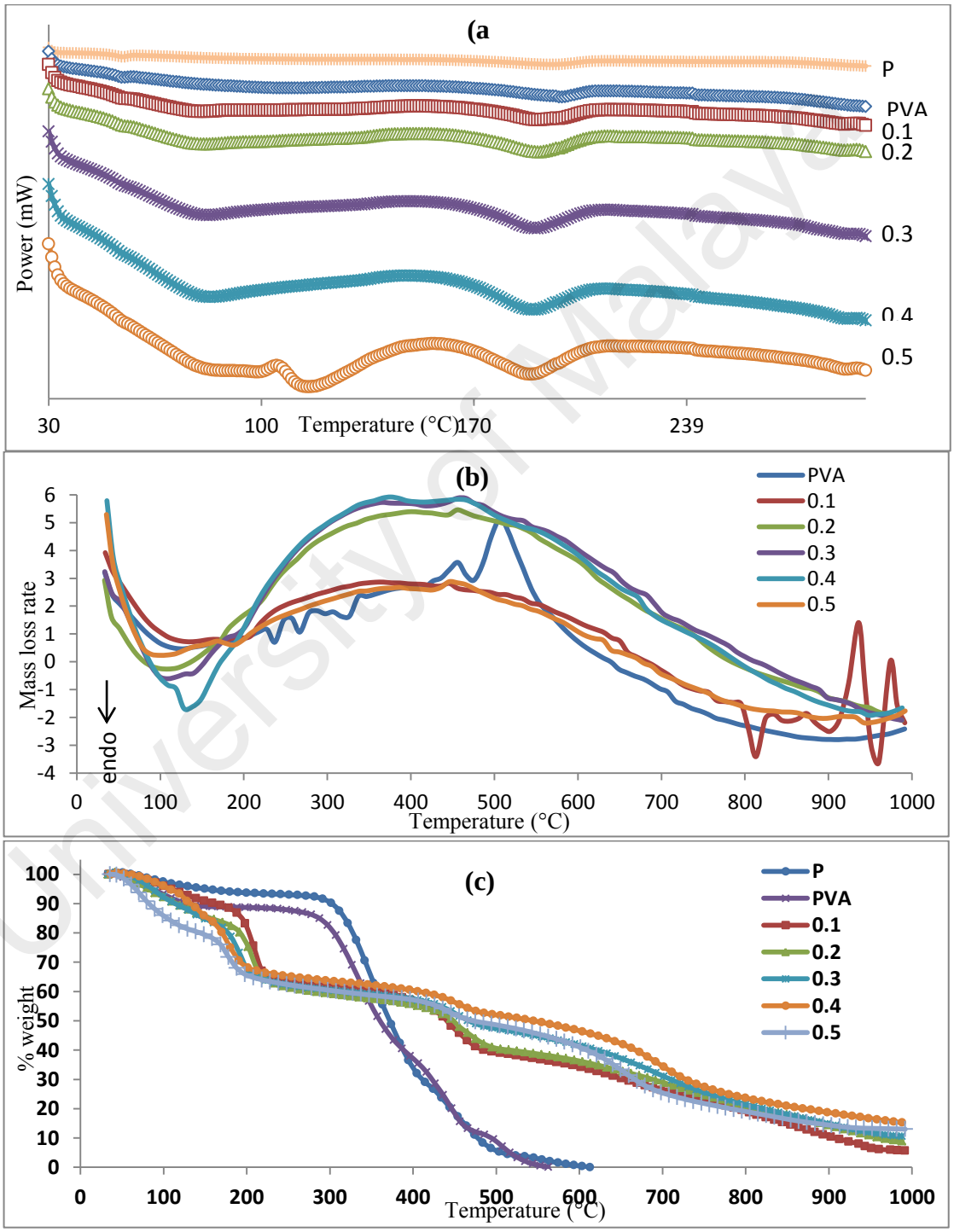

Figure 4.1: Thermal analysis patterns (a) DSC; (b) SDTA and (c) TGA of PVA powder (P), PVA and PPVA films with different mole ratios (0.1, 0.2, 0.3, 0.4 and 0.5)

DSC pattern also shows melting temperature (T_m) at second endothermic peak for all PVA and PPVA samples. PVA possessed T_m at 195 °C and decreased to 189 °C, as phosphoric acid was added, as shown in PPVA sample with mole ratio of 0.1. The decrease in melting temperature of the PPVA sample was expected due to the phosphoric acid which lowered melting temperature at 42.35 °C (Brock, 2005). Other than that, PVA also has the plasticization effect upon the reaction either with water or acid that decreases its melting temperature (Gong & Shou-Cai, 1989). In partially hydrolyzed PVA, its acetate groups act as spacers and restrict the level of hydrogen bonding. PVA backbone became disordered by phosphorylation of phosphoric ester group that prevent crystallization by crosslinking reaction (An et al., 1995). Thus, it lowers the melting temperatures. Results show that T_m, decreased with increasing plasticizer content. The reduction of T_m in PPVA is due to phosphoric acid which increases the motion of charge transport through polymer backbone via dipole-dipole interaction between PVA and phosphoric acid. Plasticizer molecules were penetrated into the polymer matrix and establish polar attractive forces between them and the chain segments. These attractive forces reduce the cohesive forces between the polymer chains and increase the segmental mobility, thereby reducing the T_m. A drop in T_m value of PPVA reveals the disruption of crystalline to amorphous phases (Prajapati et al., 2010). Furthermore, the acetate groups in PVA also experienced an intra/inter molecular hydrogen bonding with the adjacent OH group that contribute to the lower melting temperature of PPVA (Bhajantri et al., 2006; Jabbar et al., 2010).

However in PPVA sample of mole ratio 0.2, the melting temperature slightly increased to 191 °C due to hydrogen bonding and ionic complex formation (Somani et al., 2003). In our observation, the increase of T_m is also due to the covalent bonding of C-O-P which occurred from the maximum reaction between PVA and phosphoric acid. For PPVA samples with mole ratio of 0.3 to 0.5, the decreasing and fluctuating trend of

melting temperature is due to water and phosphoric acid crosslinking and dehydration dual effect on PVA. This may be due to the high amount of water and also the crosslinking and dehydration processes that varies the amount of crystalline and amorphous phases in the complexes. Phosphoric acid will create crosslinking at lower concentration, while the acid element will create dehydration at higher concentration. The remaining acetate group with PVA will also be hydrolyzed by phosphoric acid to produce a higher degree of hydrolyzed PVA which results into more crystalline phase and increase the melting temperature (sample with mole ratio of 0.2). The decrease of melting temperature is due to more hydrogen bonding with water and phosphoric acid compared to covalent bonding with phosphorus element. With an excessive amount of phosphoric acid, the reaction of PVA with phosphoric acid will produce plasticization effect and increase the amorphous phase (Prajapati et al., 2010; An et al., 1996; Suzuki et al., 2000). Excess of water and phosphoric acid content may destroy the complexation of PPVA and influence the thermal behavior. Effect of water content and crystallinity can be seen in the first endothermic peak of DSC pattern (Figure 4.1 (a)).

Control of water content in the system will produce crosslinking between PVA and phosphoric acid at its three reaction sites (O=P(OH)) (Yue et al., 2003). The existence of physically bound or free water has a strong plasticizing effect which decreases the polymer crystallinity by improving the PVA chain mobility. The reaction of water with PVA will produce inter/intra hydrogen bonding and also form new hydrogen bonding which limit the potential of interaction between PVA and phosphoric acid. By controlling the liquid amount at constant value, increasing concentration of phosphoric acid will reduce the water content in the complexes. This will increase the possibilities of reaction between PVA and phosphoric acid. Table 4.2 shows the relationship between glass transition temperatures, endothermic peak, melting temperature and degree of crystallinity of all samples.

Figures 4.1 (b) and (c) show the SDTA and TGA patterns for all samples. SDTA patterns exhibit a broad endothermic peak at temperature range of 0 – 200 °C and small exothermic peak at temperature ranges of 440 – 460 °C and 620 – 650 °C.

The broad endothermic peak is mainly due to the removal of water, that formed the conjugated double bond, crosslinking and melting temperature of PPVA (Somani et al., 2003). During thermal process, the dissociated water and phosphate group re-associated with the losses of water molecules and phosphate. This supported the formation of phosphate at the initial stage, continued with formation of diphosphate and triphosphate at higher temperature. However, at higher temperature (440 – 460 °C), PPVA samples were observed with small exothermic peaks due to the breakage of complexes formation and spontaneous degradation of PVA (Somani et al., 2003).

The TGA curves of all samples are shown in Figure 4.1 (c). The initial weight loss is observed below 100 °C, due to the evaporation of moisture. The first stage of degradation occurs between 130 – 270 °C, where the PVA begins to decompose by elimination of water and acetate groups as well as crosslinking and formation of double bond (Alexy et al., 2002). The partially hydrolyzed PVA released acetic acid at a lower temperature and decomposed at a higher temperature (330 °C) (Holland & Hay, 2002). The second stage of degradation occurs between 270 – 460 °C due to the break-up of PVA backbones as well as degradation of acetate groups (Alexy et al., 2002). This finding was also observed by other researchers in which PVA spontaneous degradation started at 280 °C (Khanna et al., 2005; Jiang et al., 2014) and 260 °C (Alexy et al., 2002), respectively. This stage is usually used in evaluating the thermal stability of the PVA polymer due to its spontaneous degradation. The third stage of degradation occurs between 460 – 600 °C, where PVA is decomposed into impurities and other volatile materials. PVA is completely decomposed at 600 °C. Major degradation of PVA occurs during the second stage which constitutes 63% of weight loss. In contrast, major

degradation of complexed PPVA occurs during the first stage with 36% of weight loss. Hydrogen bonding of the phosphate ions and polymer molecules during degradation stage most likely contributed to the improvement of thermal stability.

Thermal degradation of PPVA produces a condensed phase mechanism which involves dehydration, crosslinking and char formation (Joseph & Tretsiakova-mcnally, 2011). Figure 4.1 (c) shows that the PPVA samples have higher weight residue compared to PVA powder (P) and PVA film (PVA). The first stage of degradation of complexed PPVA films begins at temperature below 100 °C due to water evaporation. The second stage of degradation occurs between the temperature range of 120 – 190 °C due to the elimination of water and volatile products, as well as formation of di-phosphate (Zhan et al., 2004) and tri-phosphate (Banks et al., 1993) and break-up of complexed PPVA (Somani et al., 2003). The second stage of degradation occurs between 190 – 460 °C due to the spontaneous degradation of PPVA and break-up of PVA backbones. Spontaneous degradation of PVA at 280 °C (Khanna et al., 2005; Jiang et al., 2014) and 260 °C (Alexy et al., 2002) were reported in earlier publications and is consistent with our present finding. The decomposition of PVA begins at 460 – 700 °C while the residue oxidation occurs between 700 – 950 °C. Char formation occurs during the final stage of degradation and the unoxidized residue remains at temperatures above 950 °C (Inagaki et al., 1973).

Spontaneous degradation of complexed PPVA films occur at 190 °C upon the addition of PA and the temperature continues to decrease to 170 °C for the sample with mole ratio of 0.5. Pyrolysis occurs at 168 °C due to phosphoric acid whereas crosslinking between the phosphate groups and PVA occurs below 168 °C (Yue et al., 2003). The complete degradation of complexed PPVA occurs at 950 °C compared to pure PVA at 600 °C.

PVA reacts with phosphoric acid to form partially phosphorylated PVA known as polyvinyl alcohol phosphate (PVA-P) below 90 °C and tends to produce polyvinyl diphosphate (PVA-DP) at temperature above 90 °C (Zhan et al., 2004). PVA-P is hydrophilic, whereas PVA-DP is hydrophobic. PVA-P can be produced at less than 3 hours reaction time, whereas PVA-DP requires more than 4 hours reaction time. PVA cannot be dissolved completely at temperature lower than 90 °C. Consequently, the OH groups in PVA are not activated due to hydrogen bonding which leads to esterification of phosphoric acid to PVA at the surface of the PVA powder. PVA-P is mainly produced in sample with mole ratio of 0.3 in which a greater weight loss can be observed due to water elimination and crosslinking of PVA-P to PVA-DP. The formation of PVA-P (hydrophilic) and PVA-DP (crosslink/hydrophobic) is influenced by the water content, reaction temperature and time. The phosphate group that reacts with PVA in the autoclave, yielded favorable properties at reaction temperature of 120°C compared to 70 – 90 °C (Pramanik, 2009). However, conjugated double bonds are formed when the PVA is heated above 120 °C after the polymer experiences rapid chain-stripping elimination of water. The weight residue is increased in complexed PPVA. However the addition of phosphoric acid reduces weight residue in the first stage of PPVA degradation. The degradation process of complexed PVA is represented in Figure 4.2.

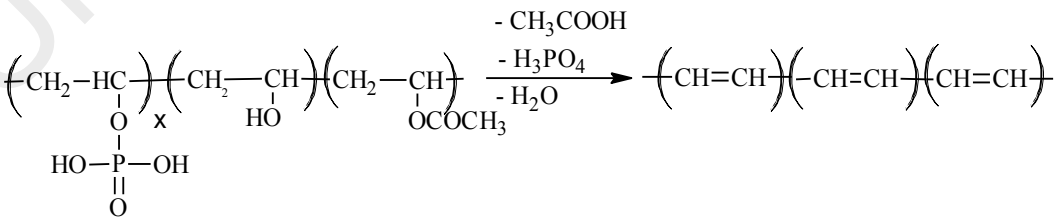

Figure 4.2: The degradation process of partially phosphorylated PVA

It can be seen that there is 14% of weight residue due to water elimination and break-up of complexes for the PVA film upon the addition of 25 ml of water. Even though the

amount of water decreases with an increase of phosphoric acid concentration, the total solution (mixture of phosphoric acid and deionized water) remained as 25 ml which was seen in the case for sample of mole ratio 0.1. However, the weight residue for sample of mole ratio 0.2 increases as the amount of water added decreases due to the formation of complexed PPVA which absorbs more moisture. Maximum bonding between phosphoric acid and PVA occurs for sample of mole ratio 0.3. The maximum weight residue occurs during the first stage of degradation due to break-up of complexed PPVA. The PVA experiences dehydration from high concentrations of phosphoric acid for sample of mole ratio 0.4, whereby less water is absorbed. The plasticization effects of phosphoric acid on PVA tend to level off and phase separation occurs at higher concentration of phosphoric acid which was added into sample of mole ratio 0.5 (Jang, 2003). It is also observed that the sample is sticky, wet and oily.

Table 4.3: Glass transition temperature (T_g), endothermic peak, melting temperature (T_m), degree of crystallinity of PVA films (F0) and PPVA films with different mole ratios (0.1, 0.2, 0.3, 0.4 and 0.5)

	Samples											
Thermal properties	**PVA**		**0.1**		**0.2**		**0.3**		**0.4**		**0.5**	
DSC	T (°C)		T (°C)		T (°C)		T (°C)		T (°C)		T (°C)	
Tg,	54		-		-		-		-		-	
1st peak	-		77 (broad peak)		84 (broad endothermic peak)		85 (broad peak)		86 (broad peak)		96 and 116 (broad with 2 peak)	
2nd peak, Tm	195 (endo)		189		191 (endo)		187		182		188	
SDTA	T (°C)		T (°C)		T (°C)		T (°C)		T (°C)		T (°C)	
1	30-200 (broad endothermic peak)		30-200 (broad endothermic peak)		30-200 (broad endothermic peak)		30-200 (broad endothermic peak)		30-200 (broad endothermic peak)		30-200 (broad endothermic peak)	
2	250		-		-		-		-		-	
3	500		450		450		450		450		450	
4			670		670		670		670		670	
TGA	T (°C)	Weight residue (%)	T (°C)	Weight residue (%)	T (°C)	Weight residue (%)	T (°C)	Weight residue (%)	T (°C)	Weight residue (%)	T (°C)	Weight residue (%)
Water elimination	<100	8	<75	2	<80	6	<80	4	<80	2	<50	4
1st stage	100 – 260	6	75-190	12	80-190	18	80-185	32	80-180	24	50-170	24
2nd stage	260-460	74	190-460	38	190-460	32	185-460	23	180-460	20	170-450	20
3rd stage	460-600	12	460-950	40	460-950	40	460-950	40	460-950	39	460-950	39
Final Weight residue	600-1000	0	950-1000	8	950-1000	8	950-1000	11	950-1000	15	950-1000	13

4.2.1 X-Ray Diffraction (XRD) analysis

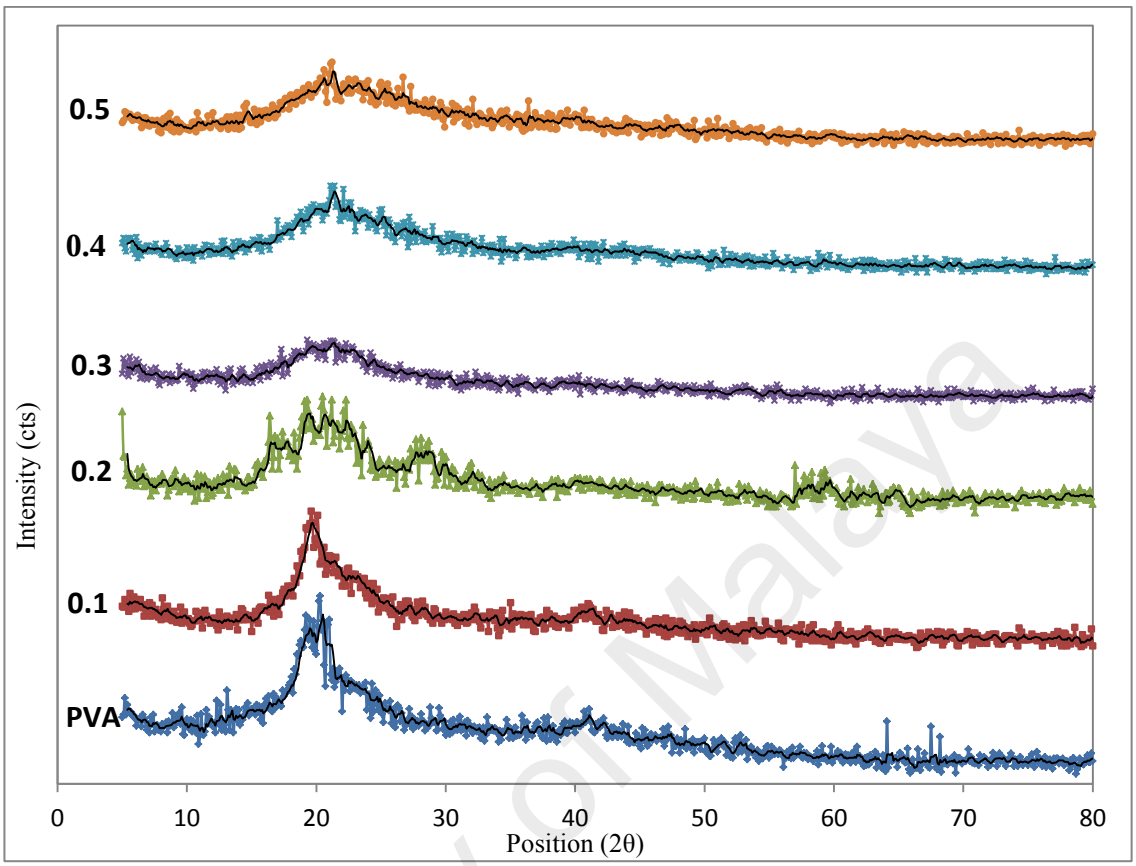

Figure 4.3: XRD patterns for PVA and PPVA samples with different mole ratios (0.1, 0.2, 0.3, 0.4 and 0.5)

Figure 4.3 shows the XRD patterns for both PVA and PPVA samples with different mole ratio of phosphoric acid 0.1, 0.2, 0.3, 0.4 and 0.5. XRD pattern for PVA shows peaks at angle of 19.80, 40.7, 64 and 67°. Similar peaks are observed for PPVA samples at angle of 19.2 – 20.30°. However, the peaks broadened and shifted to higher angle of 2θ as more phosphoric acid is added. Despite that, peaks at angle of 40.7, 64 and 67° slowly vanished as phosphoric acid concentration increases. No pure phosphoric acid (pdf number 01-076-1720) has been found indicating a complete dissociation of phosphoric acid in the polymer matrix. Peaks at angle of 19.80° and 40.7° contained majorly amorphous phase, whereas at angle of 64° and 67°, showed crystalline characteristics. This observation proves that PVA and PPVA samples possess

crystalline and amorphous phases. The amorphous phase produces a short range of atomic order which results into broad scattering peaks. This is in comparison to the crystalline phase, which has a highly in order and long range of atomic arrangement that produced an intense XRD peak.

XRD studies reveal that the samples are nano-sized which give a broadened XRD pattern. The diffraction peak at angle of $2\theta=20°$ shows broadening effect as the phosphoric acid is added due to the reduction of crystallite size. PVA film has a dominant diffraction peak at angle of $2\theta=19.80°$. However the PPVA peak is shifted to angle of 20.30°, and decreases in intensity and broadened after addition of phosphoric acid.

This observation shows more amorphous phase in the complexes after the addition of phosphoric acid. The crystallite size for PVA and PPVA samples are calculated using Debye-Scherrer's formula:

$$L=0.9\lambda/\beta\cos\theta. \qquad (4.1)$$

Where, λ is X-ray wavelength (1.54056Å),

β is the full width half maximum value of diffraction peak,

θ is the degree of the diffraction peak corresponding to the plane.

Samples with mole ratio of 0.3, has the lowest intensity and broadness compared to all PPVA samples. This has happened due to maximum interaction between PVA and phosphoric acid. It also proves that this sample exhibited more crystalline phase. This finding corresponds with the thermal properties. Table 4.4 summarizes the XRD results.

Table 4.4: Summary of XRD analysis and crystallite size

Samples	Mole ratio H_3PO_4/PVA, (R)	Degree of crystallinity, X_c (%)	Angle 2θ	Intensity	Crystallite size, D (nm)
PVA	0	29.51	21	62	2.308163
0.1	0.1150	38.46	21	51	2.019643
0.2	0.2299	39.83	24	43	1.082768
0.3	0.3449	43.87	18	23	1.237277
0.4	0.4599	42.78	24	31.5	1.082768
0.5	0.5748	8.72	25	27.5	0.856439

4.2.2 Fourier Transform Infrared (FTIR) spectroscopy analysis

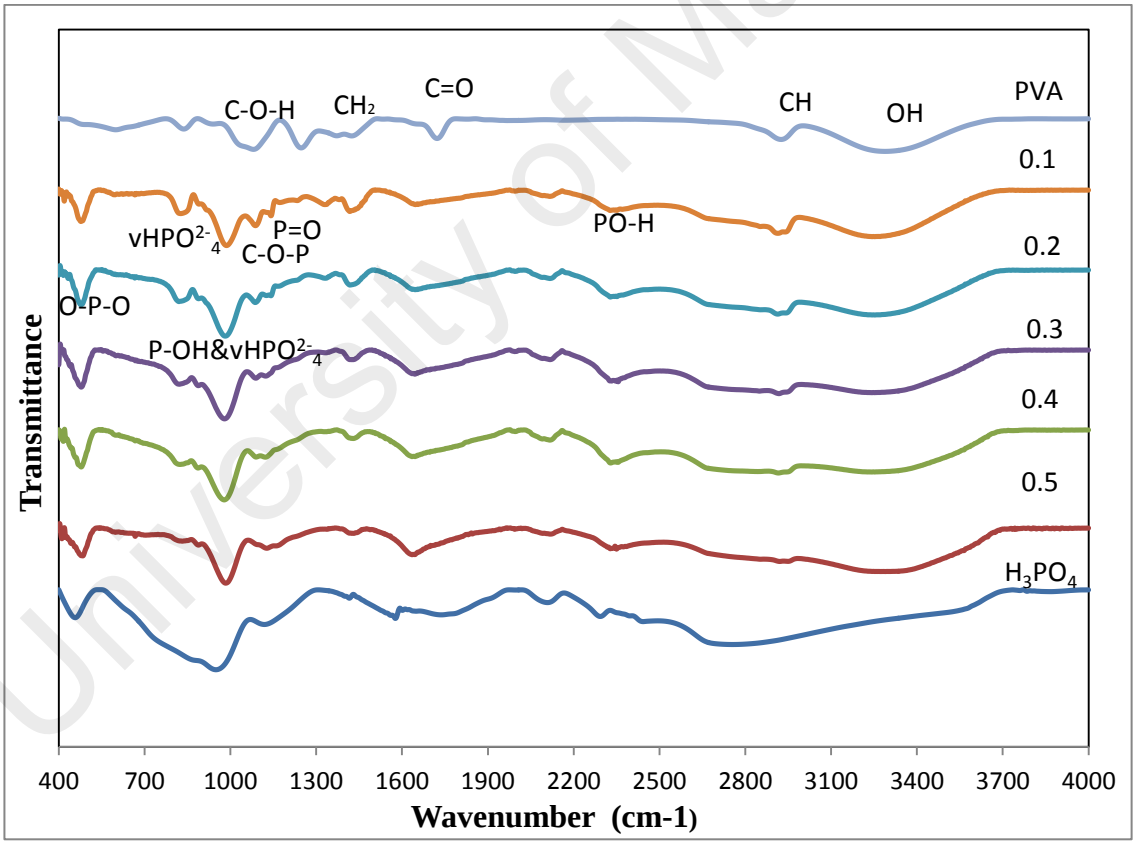

Figure 4.4: FTIR spectra of PVA and PPVA samples with different mole ratios (0.1, 0.2, 0.3, 0.4 and 0.5)

Figure 4.4 shows the FTIR spectra for pure PVA and PPVA samples with a different mole ratio of phosphoric acid (0.1, 0.2, 0.3, 0.4 and 0.5). The spectrum for pure PVA

shows bands of νO-H (3288 cm^{-1}), C-H (2925 cm^{-1}), C=O (1722 cm^{-1}), CH_2 (1423 and 1247 cm^{-1}), C-O-H (1080 cm^{-1}) (Iribarren & Lemmetyinen, 2009; Banks et al., 1993) and skeleton (836 and 599 cm^{-1}) (Somani et al., 2003) at the fingerprint region. The peak at 1722 cm^{-1} corresponds to the C=O stretching mode of the ester groups and occurs mostly in partially hydrolyzed PVA (Jin et al., 2007). The stretching vibrations of carbonyl and/or carboxyl groups in the minor acetate groups (–CO(O)CH) in PVA contribute to the existence of this peak (Yue et al., 2003). In addition, there are inter-intra molecular hydrogen bonds between the acetate groups in PVA and adjacent OH group (Bhajantri et al., 2006; Jabbar et al., 2010).

Introduction of phosphoric acid to PVA observed a shifting, broadening, vanishing and occurrence of peaks. The band corresponding to the free carbonyl stretching at 1722 cm^{-1} is vanished by the introduction of H_3PO_4 which suggests the coordination between the carbonyl carbon and PO_4^{3-} anion. Since PO_4^{3-} is a negative ion which seeks an electron deficient atom (C^+ O^-), it makes an interaction with carbonyl carbon of the polymer chain. PVA also experience dehydration at higher concentration of H_3PO_4 which results into the appearance of an isolated and conjugated C=C bond. Moreover, this formation is accelerated in the vicinity of C=O group. However, in oxygen condition, double carbon bonds are unstable and undergo further oxidation followed by polymer destruction. This is a reason why the correspondent band is not observed in PPVA IR spectra (Prosanov & Matvienko, 2010). Meanwhile peaks for OH, P=O and C-O-P bands disappeared at higher concentration of phosphoric acid in PPVA. Even though the intensity of OH peak is decreased abruptly upon the addition of phosphoric acid, this intensity then increases due to the absorption of moisture by the film. The OH peak then became broad, which indicates the interaction between PVA and phosphoric acid due to their phase separation and dehydration at higher acid concentration. Variations in the P=O peak at 1329 – 1331 cm^{-1} for PVA and PPVA samples with mole

ratio of 0.1 and 0.2 are due to hydrogen bonding, P=O peak completely disappeared in PPVA samples with mole ratio of 0.3 – 0.5. The C-OH peak disappears whereas the C-O peak appears (Banks et al., 1993; Inagaki et al., 1973; Iribarren & Lemmetyinen, 2009) upon the addition of phosphoric acid. The disappearance of C-OH peak is attributed to the chemical modifications of PVA by phosphoric acid. The C-O-P peak shifts to higher wavenumber and attenuates due to hydrogen bonding. The overlapping of *v*P-O(C) and *v*HPO_4^{2-} vibration groups (Mohapatra et al., 2006; Jin et al., 2007) produced an intense peak. The C-O-P groups become weaker at higher concentration of phosphoric acid due to the formation of hydrogen bonds (*v*HPO_4^{2-}). The peaks which are intrinsic to C-H, PO-H, C=C, C-O-P bands are overlapped with P-O, P-O and O-P-O peaks and more apparent with an increase in phosphoric acid concentration. The C-H peak is shifted to a higher wavenumber for sample with mole ratio of 0.3. However this peak is shifted to a lower wavenumber for sample of mole ratio 0.4. Peaks at 1634 and 1273 cm^{-1} wavenumbers are not shifted and correspond to the bending mode of water molecules (Jin et al., 2007) as well as PVA dehydration at higher concentration of phosphoric acid (Iribarren & Lemmetyinen, 2009). The highest wavenumber recorded for the shifting in PO-H peak is 2355 cm^{-1} (Sample 0.3), whereas the lowest wavenumber recorded is 2338 cm^{-1} (Sample 0.4). It can be observed that there is an increase in peak intensity for the P-OH band (Iribarren et al. 2009) and the overlapping of C-O-P and P-O, P-O and O-P-O bands at higher concentration of phosphoric acid, which is attributed to the higher number of free phosphoric acid molecules in the films. These peaks are shifted to higher wavenumbers. The peaks at 986 – 978 cm^{-1} belong to the P-O groups which originated from $(H_2PO_4)^-$ and vHPO_4^{2-} (Mohapatra et al., 2006; Iribarren & Lemmetyinen, 2009; Jin et al., 2007). The emergence of P-O peak can be observed at 825 cm^{-1} for sample with mole ratio 0.2 whereas the vHPO_4^{2-} peak is shifted to a lower wavenumber as the phosphoric acid concentration increases. However, the O-

P-O peak of PPVA samples at 477 cm^{-1} is shifted to a higher wavenumber with an increase of phosphoric acid concentration. The deformation of O–P–O peak as well as vibration modes in PO_4^{3-} are clearly observed (Neuder et al., 2003b). The maximum bonding number for phosphoric acid to PVA occurred at a mole ratio of R = 0.33 as shown in Figure 4.4 (a). This means that the three functional groups of PVA can react with one unit of phosphoric acid. All protons are lost during the formation of C-O-P bonds at this mole ratio. However, it is expected that there will be free, unreactive PVA group for mole ratio R<0.33, due to insufficient free phosphoric acid molecules. On the other hand, there will be additional free phosphoric acid functional group for R>0.33, given that none of the free PVA functional group undergo any reaction. In this case, the free phosphoric acid molecules will react with available OH groups to form hydrogen bond which weakens and breaks the C-O-P bond. Moreover, an increase in HPO_4^{2-} also weakens the C-O-P bond. The bonds are stabilized by losing proton H^+ and forming C=C bond which leads to dehydration as observed in sample of mole ratio 0.4. In this case, the C-O-P band is shifted to a higher wavenumber (1122 cm^{-1}) with an increase in intensity and a decrease of peak width. However, the C=C band for this sample is shifted to a lower wavenumber with a decrease in intensity and an increase of peak width due to dehydration. Meanwhile crosslinking of phosphorylation occurs in samples of mole ratio of 0.1 – 0.3. The nonlinear trend of PVA increase with phosphoric acid molecules is attributed to the acetate groups in the PVA as well as plasticization effect of water on PVA (Alexy et al. 2002). However, this increase tends to level off when mole ratio is R>0.33 or if the molar concentration of phosphoric acid is 1.76 M (Banks et al., 1993). Figure 4.5 (a) shows the possible reaction between PVA and phosphoric acid in order to produce partially phosphorylated PVA (PPVA), which consists of phosphorylated and unphosphorylated OH units as well as acetate groups with intermolecular bonding with adjacent OH as illustrated in Figure 4.5 (b). This agrees

well with the FTIR spectra in Figure 4.4, in which partially phosphorylated PVA (Figure 4.5 (b)) is produced for mole ratio of R<0.33 whereas dehydration of PVA (Figure 4.5 (c)) produced the phosphonate groups for mole ratio of R> 0.33 (Banks et al., 1993). The dehydration of gel component increases while the partially phosphorylated component decreases with increasing concentration of phosphoric acid due to the attenuation of C-O-P bond. Figure 4.5 (d) shows the C=O bond of partially hydrolyzed PVA, whereby bonding occurs with the OH groups in water (Alexy et al., 2002). The acetate group only appears in the pure PVA sample, while the acetate groups have inter-intra molecular bond with available hydrogen in the PPVA samples.

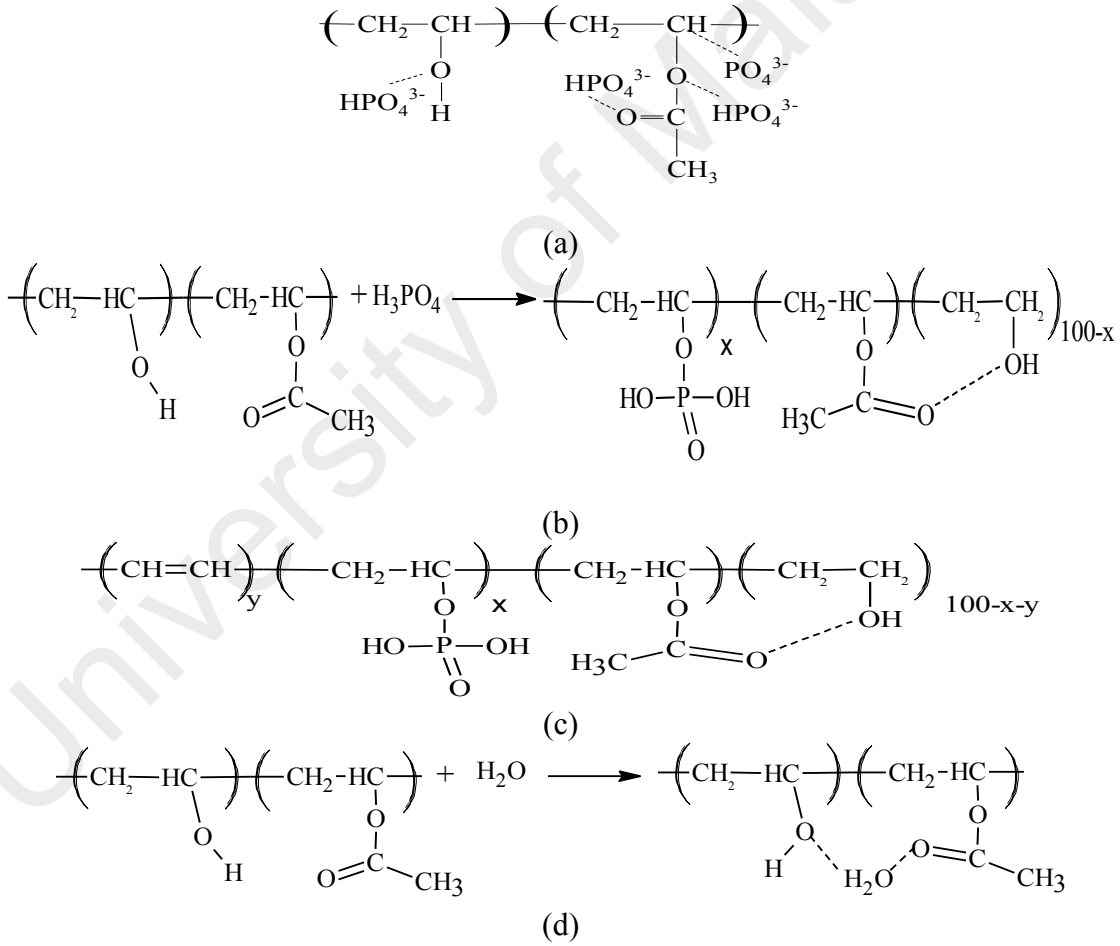

Figure 4.5: Schematic of complexes PPVA reactions: (a) Possible reaction between PVA and phosphoric acid; (b) PPVA consists of phosphorylated and unphosphorylated OH units; (c) Dehydration produces the phosphonate groups and (d) The C=O bond of partially hydrolyzed PVA

In the PPVA synthesis, maximum bonding of the phosphoric acid to PVA occurred in the mole ratio of 1:3 or 0.33. All phosphoric acid proton H^+ is expected to contribute in the formation of C-O-P bond (Iribarren & Lemmetyinen, 2009). If the mole ratio R is greater than 0.33, phosphoric acid molecules will form bonding with available OH group from hydrogen bonds associated with phosphoric acid molecules. This weakens the C-O-P bond until it breaks and produces carbocation. The carbocation stabilizes by losing proton H^+ of polymer structure and produces C=C bond. The formation of hydrogen bond is observed from the P=O peak shifting. It can be concluded that at lower phosphoric acid concentration, reaction with PVA will produce phosphorylation while at higher concentration of phosphoric acid, it competes with dehydration. We also found that the degree of phosphorylation increased as the phosphoric acid concentration increased but it began to level off at phosphoric acid concentration above 1.5 M (Banks et al. 1993). Meanwhile, the PPVA samples appeared to be brownish at phosphoric acid concentration of 2 to 5.5 M. Further concentration of phosphoric acid gave no significance to the sample due to the tendency of polymers to dehydrate and form conjugated double bonds (Mohapatra et al., 2006). Table 4.5 summarizes the FTIR results for all samples.

Table 4.5: Interpretation of FTIR spectra for PVA and PPVA samples with mole ratio (0.1, 0.2, 0.3, 0.4, 0.5)

	Band assignment and wavenumber (cm^{-1})													
Sample	OH	C-H	PO-H	PO-H	C=C	C=O	CH_2	P=O	C-O-P	C-O-H	C-O-P, P-O	P-O	Sk	O-P-O
PVA	3288	2925				1722	1423, 1247		1080				836, 599	
0.1	3243	2913	2327	2116	1645		1417	1329	1087		986	825		477
0.2	3252	2913	2328	2117	1645		1417	1331	1086		981	819		477
0.3	3242	2917	2355	2117	1645		1422		1088		979	821		478
0.4	3242	2915	2338	2116	1634		1424		1122		978	823		478
0.5	3241	2914	2339	2116	1633		1425		1123		977	823		478
Intensity (%)	I	D	D	D	D		I	I	I		D	D		D
Peak Position	L	L	H	U	U		H	H	H		L	L		U
Peak Size	S	S	B	B	B		S	S	S		B	B		B

Sk = Skeletal, Intensity, I = Increase, D = Decrease, Peak position, L= Shift to lower wavelength, H=Shift to higher wavelength, U= Unshifted, Peak size, B = Increase, S = Decrease, U = Unchanged

4.2.3 Raman Spectroscopy Analysis

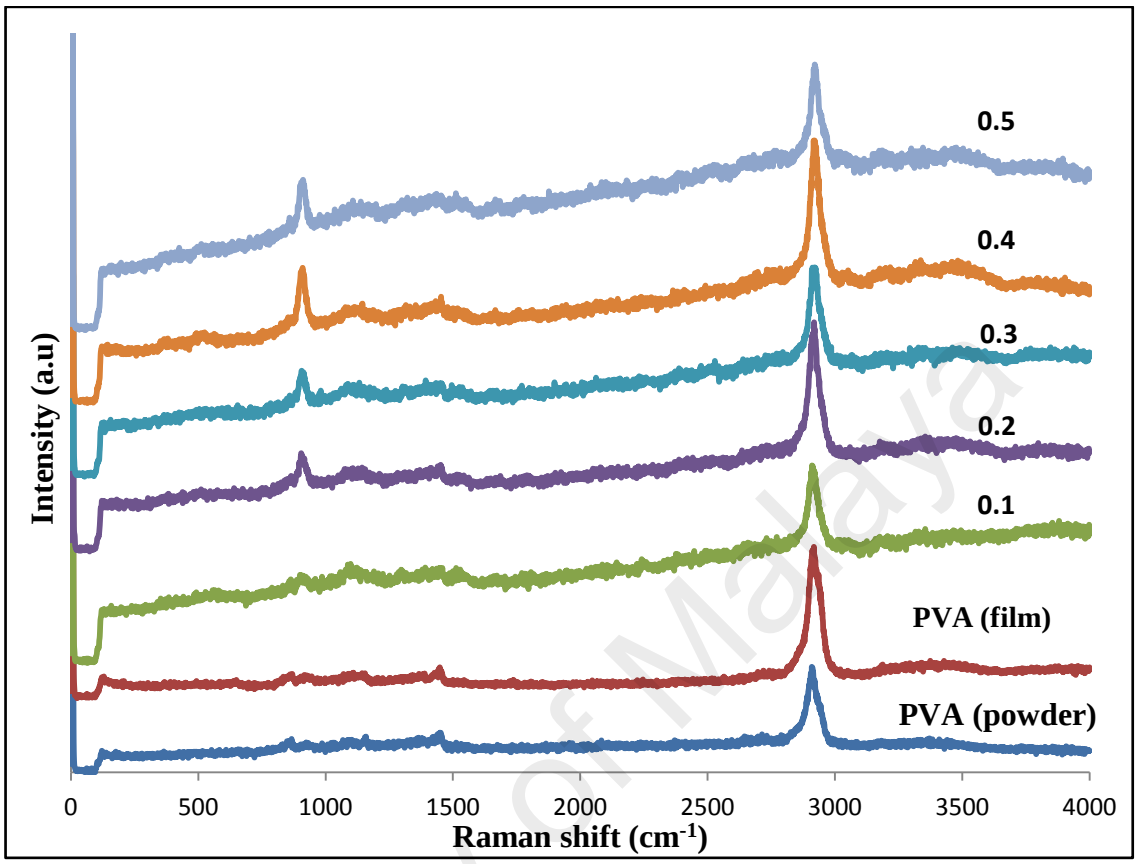

Figure 4.6: Raman spectra of PVA and PPVA samples with different mole ratio (0.1, 0.2, 0.3, 0.4 and 0.5)

Figure 4.6 represents the Raman spectra of pure PVA and PPVA samples with different molar ratios of phosphoric acid (0.1, 0.2, 0.3, 0.4 and 0.5) in the region of 0 - 4000 cm^{-1}. The changes in the Raman spectra of all samples following the addition of phosphoric acid have been tabulated in Table 4.6. Raman band corresponding to pure PVA show weak bands at 850, 1150 and 1450 cm^{-1}, an intense band at 2900 cm^{-1} and a weak broad band at the 3100 – 3600 cm^{-1} range. Peak at 850 cm^{-1} corresponded to the C–C stretching band, as was also observed by others (Rajeswari et al., 2013; Tripathi et al., 2013; Hema et al., 2010). The weak band observed at 1150 cm^{-1} corresponded to the ester of oxygen C–O or C–O–H. Meanwhile weak band at 1450 cm^{-1} corresponded to C–H vibration in CH_2 and O–H bending vibration. The most intense band in Raman shift is observed at 2900 cm^{-1} for PVA referring to C–H stretching (Prosanov, 2011)

and also O–H stretching (Rajeswari et al., 2013). A weak but broad peak is observed at range of 3100 – 3600 cm^{-1} due to the O–H band. PPVA samples produced similar weak with broad bands in the range of 3100 - 3600 cm^{-1} but with increasing intense signals as phosphoric acid concentration increases (Venkateswaran, 1936). The intense in the increasing Raman shift at 2900 cm^{-1} is referring to the OH group and showed minor shifting to higher wavenumber. The broadening occurred at higher wavenumber while shifting at lower wavenumber may be due to the interaction of anion with polymer to form a complexation. Broad bands which were observed at 1150 and 1450 cm^{-1} after increasing the concentration of phosphoric acid are within the range of 1300 – 1600 cm^{-1} and 1000 – 1200 cm^{-1}. The broadening at 1450 cm^{-1} resulted from the formation of contact ion pair (H^+... PO_4^{2-}) and ion aggregates. This confirmed the change in crystallinity which was attributed from the mixture of C–H and O–H bending vibrations. The broadening band in Raman spectra is an indication of amorphous nature in the PPVA polymer complexes (Hema et al., 2010). This observation of amorphous nature is consistent with the XRD results (Figure 4.3). The band at 1150 cm^{-1} corresponding to C–O ester is clearly affected by the introduction of H_3PO_4 into the PVA matrix. The band intensity is decreased with increasing concentration of phosphoric acid. This can be associated with the change in the local conformation of polymer complexation. The intensity variation is due to the interaction of unhydrate PO_4^{3-} with ester carbons and also due to the interaction of H^+ with ester oxygen C(O)–O–C. The broadening of 1150 cm^{-1} band at 1000 – 1200 cm^{-1} wavenumber range is assigned to PO_2 vibrations. Szumera (2015) also supported this finding with observation of a band at 1180 cm^{-1} corresponding to the P-O vibration in PO_2. Tripathi et al. (2013), Shadak Alee et al. (2013) and Prosanov (2011) observed a C–O–H band upon addition of phosphoric acid. C–O–H vibration had interaction with P-O (Szumera, 2015) and produced a C–O–P band and mixture of P–O band. This observation is in line with the

FTIR spectra (Figure 4.5) depicting the occurrence of C–O–P band within the area other than P–O band. The addition of phosphoric acid to PVA also produces an increase in intensity and shifting of C–C band at 850 – 900 cm^{-1} due to P $(OH)_2$ vibration from hydrated HPO_4^{2-}. A frequency shift also occurs due to the formation of contact from C–C in PVA with ion pair (H^+... PO_4^{2-}) and ion aggregates. The significant changes in the C–C vibrational band can be associated with the formation of ionic bond with less polarization. The increase in ionic bonding is the result of charge localization in the polymer. The charge localization is a clear indication of strong interaction between PVA and phosphoric acid. P-OH band is not shifted to lower wavenumbers upon deuteration and therefore assigned to be $P(OH)_2$ vibrations (De Jager & Prinsloo, 2001). Dilution of sample will increase the P–OH band intensity until it becomes the strongest band in the Raman spectra, which is influenced by OH. This is a clear indication of a strong hydrogen bonding. The P–OH vibration is very sensitive to the inductive effects of substituent groups attached to the phosphorus atom and to the molecular interaction (Amorim da Costa & Amado, 2001). Peaks at 850 and 1450 cm^{-1} are completely disappeared in increasing phosphoric acid concentration and replacing with peak broadening within the range of 1000–1200 cm^{-1} and 1300–1600 cm^{-1}, respectively. This suggests that the corresponding bonds have been distorted so that no more micro-Raman active molecules will appear. Similar broadening effect of PVA due to NH_4NO_3 is observed by Hema et al. (2010). New broad bands that appeared at the range of 300–600 cm^{-1} corresponded to bridging phosphate oxygen (P-O-P) backbone vibrations and it may also from either PO_4 radicals, HPO_4 ions or H_2PO_4 ions (Venkateswaran, 1936). With increasing concentration of phosphoric acid, the increase in intensity, shifting, broadening and vanishing occurrence of peaks seen, confirms the structural modification in PVA matrix.

Table 4.6: Interpretation of Raman spectra for PVA and PPVA samples with different mole ratios (0.1, 0.2, 0.3, 0.4 and 0.5)

PVA		**PPVA**					
		0.1	**0.2**	**0.3**	**0.4**	**0.5**	**Band assignments**
wavenumber (cm^{-1})	**Band assignments**	**wavenumber (cm^{-1})**					
3100 – 3600(w, b)	OH	3100 – 3600	3100 – 3600	3100 – 3600	3100 – 3600	3100 – 3600(	Weak and broaden OH
2900	C-H and OH	2900	2900	2900	2900	2900	Increase intensity (reaction between C-H and OH with PO)
1450	C – H vibration in CH_2 and O – H bending vibration	1300-1600	1300-1600	1300-1600	1300-1600	1300-1600	Broad $P(OH)_2$
1150	C – O - H	1000-1200	1000-1200	1000-1200	1000-1200	1000-1200	Broad C – O – P and P – O in PO_4^{3-}
850	C-C stretching vibration	899	900	901	900	901	P-OH in HPO_4^{2-}
		300-600	300-600	300-600	300-600	300-600	Broad O – P – O

4.2.4 UV – Visible spectroscopy analysis

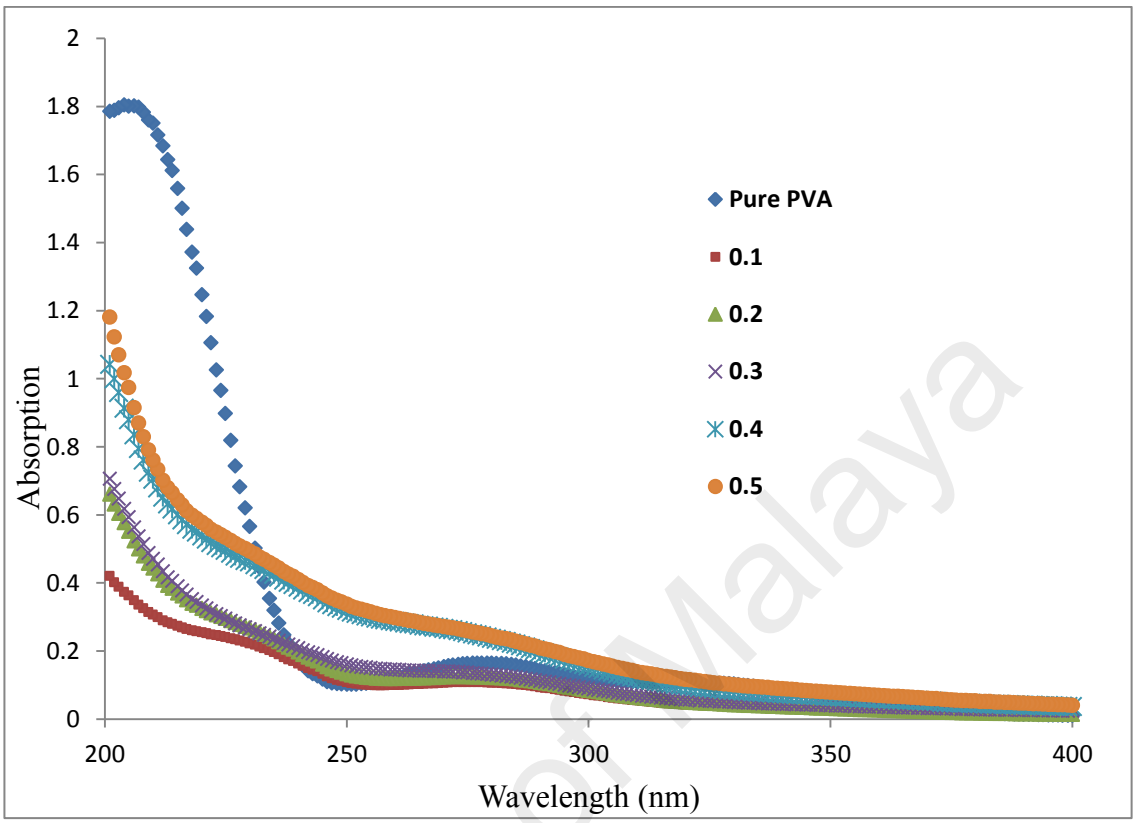

Figure 4.7: Absorption spectra of pure PVA and PPVA films with different mole ratios (0.1, 0.2, 0.3, 0.4 and 0.5)

Figure 4.7 shows the absorption spectra for pure PVA and PPVA films at different mole ratio of phosphoric acid. Pure PVA possessed absorption bands appeared at 204, 277 and 324 nm. A single absorption band appeared at 274 nm due to interaction of PVA with phosphate components (Li et al., 2003). This absorption band is shifted towards lower wavelength (274 to 270 nm) as the mole ratio of phosphoric acid increases. The blue shifts indicate the formation of inter-intra molecular hydrogen bonding between phosphoric acid ions with the adjacent OH groups. The bond reflects the variation of the energy band gap due to the variation of crystallinity within the polymer matrix (Rao, 1967). The intensity of this absorption band also increases with the increase of mole ratio. The more intense the absorption band, indicates the more absorption states or defect energy band that existed in the complexes. The absorption peak becomes less

visible at the highest mole ratio (0.5) since the film became oily and wet due to the plasticization effect as phosphoric acid concentration increases (Somani et al., 2003). This finding is in concurrence with Mitra et al. (2011) where there is no absorption peak for the mixture of PVA, PEG, phosphoric acid and gold nanoparticles at high concentration of phosphoric acid. The optical band gap is defined as the difference between the conduction and valence bands, which explains the optical transition phenomena. In order to determine the optical band gap of the films, the absorption coefficient, (α), is determined using the formula below;

$$\alpha(\nu) = 2.303\frac{A}{d} \tag{4.2}$$

where A is the absorbance and d is the film thickness. Davis & Mott (1970) reported that the electronic transition which occurred near the absorption edge can be determined by plotting $(\alpha h\nu)^2$ as a function of photon energy (hν) as expressed in the equilibrium below:

$$\alpha(\nu) = \beta\frac{(h\nu - Eg)^2}{h\nu} \tag{4.3}$$

where β is a constant, hν is the photon energy and E_g is the optical band gap. From this plots of $(\alpha h\nu)^2$ as a function of photon energy (hν) (also known as Tauc's Plot), the values of E_g are obtained by extrapolating $(\alpha h\nu)^2 = 0$ for the direct transition. Figure 4.8 shows the Tauc's plot for all samples.

Table 4.7 summarizes the optical results. It is evident from the table that the value of E_g increases with increasing mole ratio. The increase of phosphoric acid concentration is responsible for the reduction of defects in the films. These defects produced the overlapped localized states in the optical band gap. Hence, less overlaps of localized states dsprovides evidence for increasing energy band gap, when phosphoric acid content is increased in the polymer matrix. In other words, the increase of optical band gap reflects the decrease in the degree of disorder in the films.

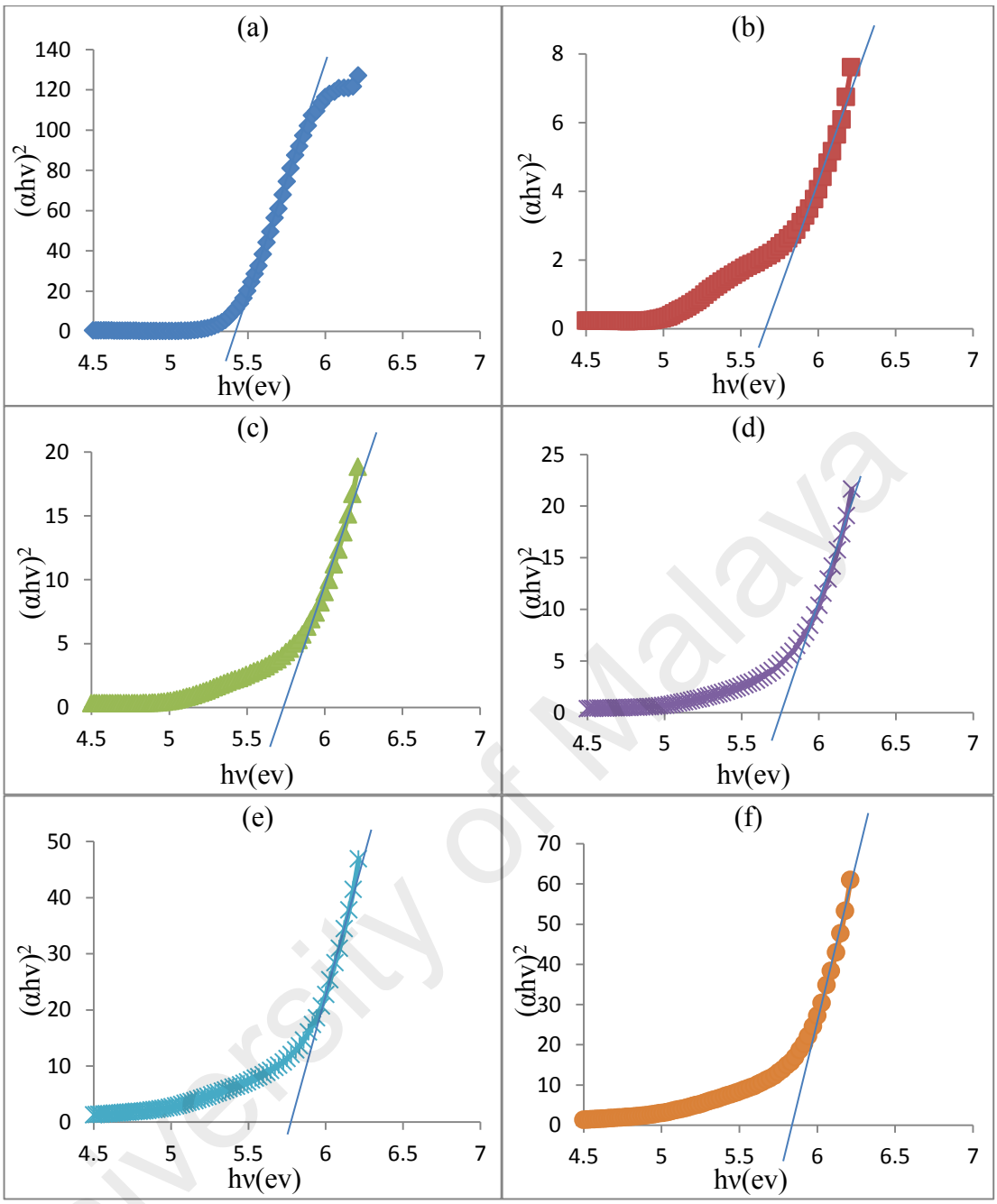

Figure 4.8: Tauc's plots for (a) pure PVA and PPVA films with different mole ratio (b) 0.1; (c) 0.2; (d) 0.3; (e) 0.4 and (f) 0.5

Table 4.7: Optical parameters for pure PVA and PPVA films with different mole ratios (0.1, 0.2, 0.3, 0.4 and 0.5)

Sample (mole ratio)	Absorption peak (nm)	Optical band gap, E_g (ev)
Pure PVA	277	5.45
0.1	275	5.67
0.2	273	5.75
0.3	272	5.77
0.4	271	5.79
0.5	270	5.83

4.2.5 Photoluminescence (PL) spectroscopy analysis

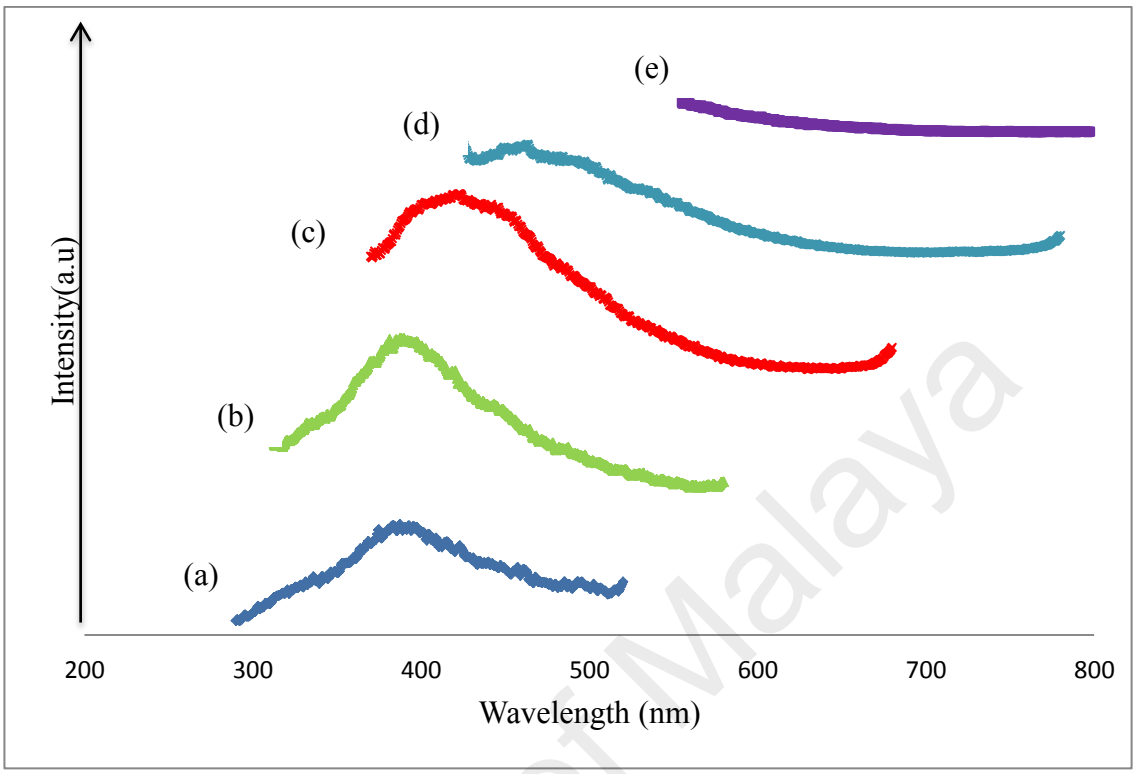

Figure 4.9: PL spectra of PPVA samples with 0.3 mole ratio at different excitation wavelengths: (a) 272; (b) 300; (c) 350; (d) 400; (e) 500 nm

Figure 4.9 shows the PL spectra for PPVA samples with mole ratio of 0.3 (maximum bonding of phosphoric acid with PVA) at five different excitation wavelengths (272, 300, 350, 400 and 500 nm). The peak emissions are broad and red shifted as the excitation wavelengths increased. The broad band emissions appeared around the green-yellow regions for all excitation wavelengths except for 500 nm, where no emission peak is observed. The broad emmission bands correspond to the $\pi^* \rightarrow$ n electronic transition of the OH group characteristics of the three distinct polymer configurations in aqueos solution, that is isotactic (i), syndiotactic (s) and atactic (a). Interaction with H_2O and phosphoric acid modifies bridging in s-PPVA so it changes to a-PPVA structure at higher concentration. Lack of sensitive bridging renders i-PPVA to be more sensitive to H-bonding with H_2O molecules. In general, the result is useful for understanding (i)

modified structure, (ii) optical and other properties and (iii) to design PPVA polymer for new possible applications.

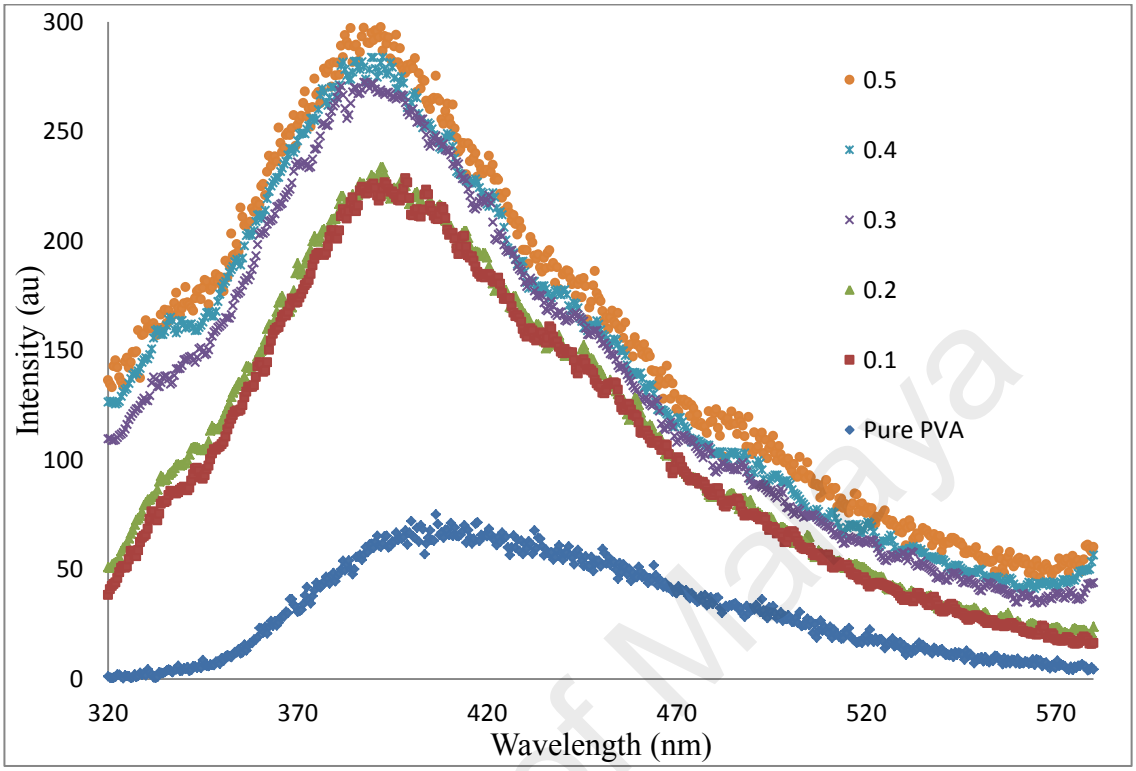

Figure 4.10: PL spectra of pure PVA and PPVA samples with different mole ratios (0.1, 0.2, 0.3, 0.4 and 0.5) at excitation wavelength of 300 nm

Figure 4.10 shows the PL spectra of pure PVA and PPVA samples with different mole ratios at excitation wavelength of 300 nm. The emission bands position are shifted towards the lower wavelength (412 to 389 nm) as mole ratio increases. The intensity of the emission band also increases with the increase of the mole ratio. This proves that the phosphate element has interaction with PVA in the PPVA complexes. A strong PL thus appeared at 389–398 nm region which occurred from a stretching of OH vibration ν_1 (overtone) isotactic from a specific i-PVA/PPVA configuration.

Figures 4.11 and 4.12 show the PL spectra of pure PVA and PPVA samples with different mole ratio at excitation wavelength of 350 and 400 nm. The 350 nm excitation resonates the excited electronic state at broad range of 418–421 nm and 441–446 nm in syndiotactic and atactic PVA/PPVA (Table 4.8). The emission peaks are shifted to a longer wavelength (redshifts) from 418 and 440 nm in pure PVA and to 420 and 446 nm

in PPVA sample with highest mole ratio. O-X-O phosphors in PPVA samples can produce defects in the luminescent emission from its intrinsic which is related to the defect of oxygen vacancies in the complexes at 440 nm (Chen et al., 2002). As a result, emission peak occurred in multiple overlapping peaks as the intensity increases. This probably comes from various kinds of absorption state defects existing in PPVA samples. These results were observed by Somani et al. (2003) but with the existence of PVA/H_3PO_4 peak at 425 nm. In changing the excitation wavelength of 400 nm as shown in Figure 4.12, the broad emission band occurs at range of 462–468 nm and 481–489 nm. From the observation, PPVA complexes contained mainly isotactic PVA/PPVA together with atactic and syndiotactic of PVA/PPVA. The s-PVA/PPVA gives a strong structure, which is difficult to dissolve in pure water. Free OH groups reacted with phosphoric acid in a more stable equilibrium structure. Only a fewer number of free OH groups produced PPVA. Figure 4.13, shows the schematic of possible PPVA molecular structures in polymer form of isotactic, syndiotactic and atactic form. Table 4.13 summarizes the details.

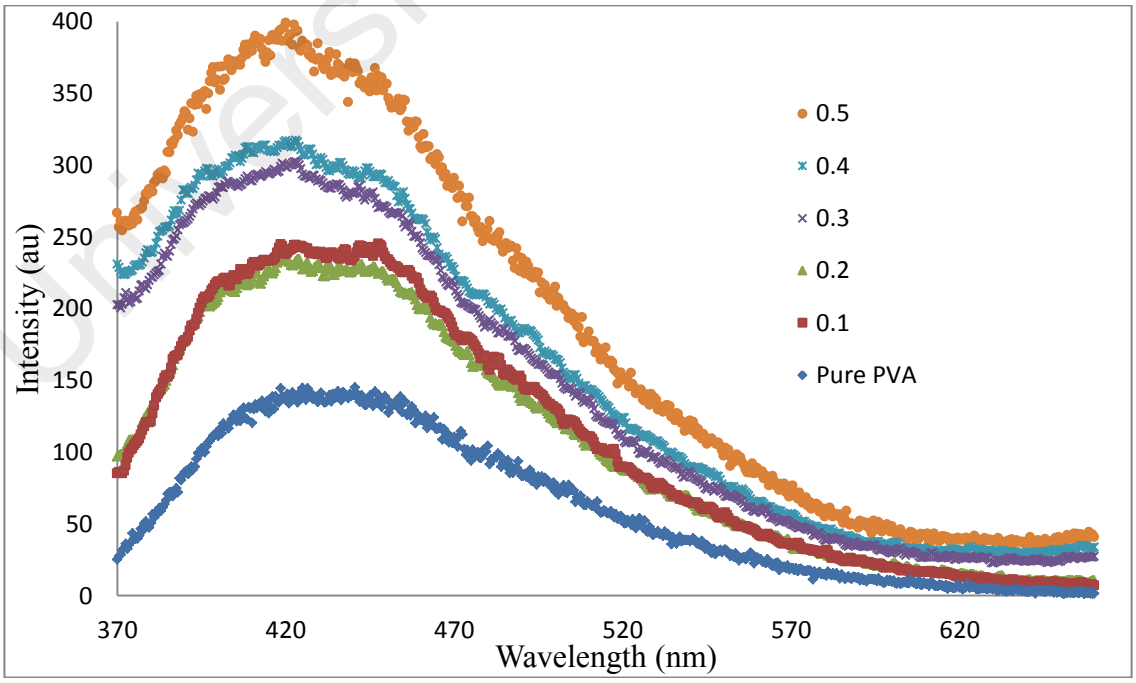

Figure 4.11: PL spectra of pure PVA and PPVA samples with different mole ratios (0.1, 0.2, 0.3, 0.4 and 0.5) at excitation wavelength of 350 nm

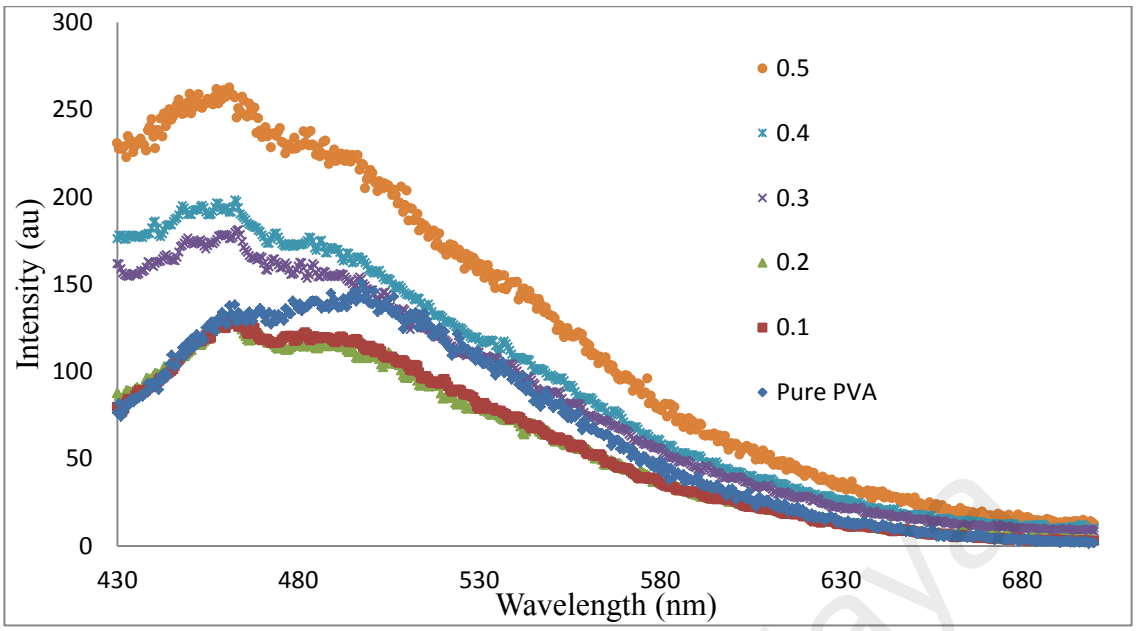

Figure 4.12: PL spectra of pure PVA and PPVA samples with different mole ratios (0.1, 0.2, 0.3, 0.4 and 0.5) at excitation wavelength of 400 nm

Table 4.8: Photoluminescence data in various excitation wavelengths for all samples

Excitation wavelength λ_{exc} (nm)	**Samples (mole ratio)**	**Band position (nm)**		**Intensity**	**Assignments**	
300	Pure PVA	412		70	s-PVA	
	0.1	398		225	i-PPVA	
	0.2	396		230	i-PPVA	
	0.3	391		270	i-PPVA	
	0.4	389		285	i-PPVA	
	0.5	389		295	i-PPVA	
350	Pure PVA	418	440	148,148	s-PVA	a-PVA
	0.1	418	441	245,248	s-PPVA	a-PPVA
	0.2	421	444	235,225	s-PPVA	a-PPVA
	0.3	429	442	305,280	s-PPVA	a-PPVA
	0.4	421	443	315,300	s-PPVA	a-PPVA
	0.5	420	446	400,360	s-PPVA	a-PPVA
400	Pure PVA	462	500	135,150	i-PVA	
	0.1	462	489	125,115	i-PPVA	
	0.2	460	485	125,115	i-PPVA	
	0.3	468	481	180,160	i-PPVA	
	0.4	462	482	199,175	i-PPVA	
	0.5	461	481	265,235	i-PPVA	

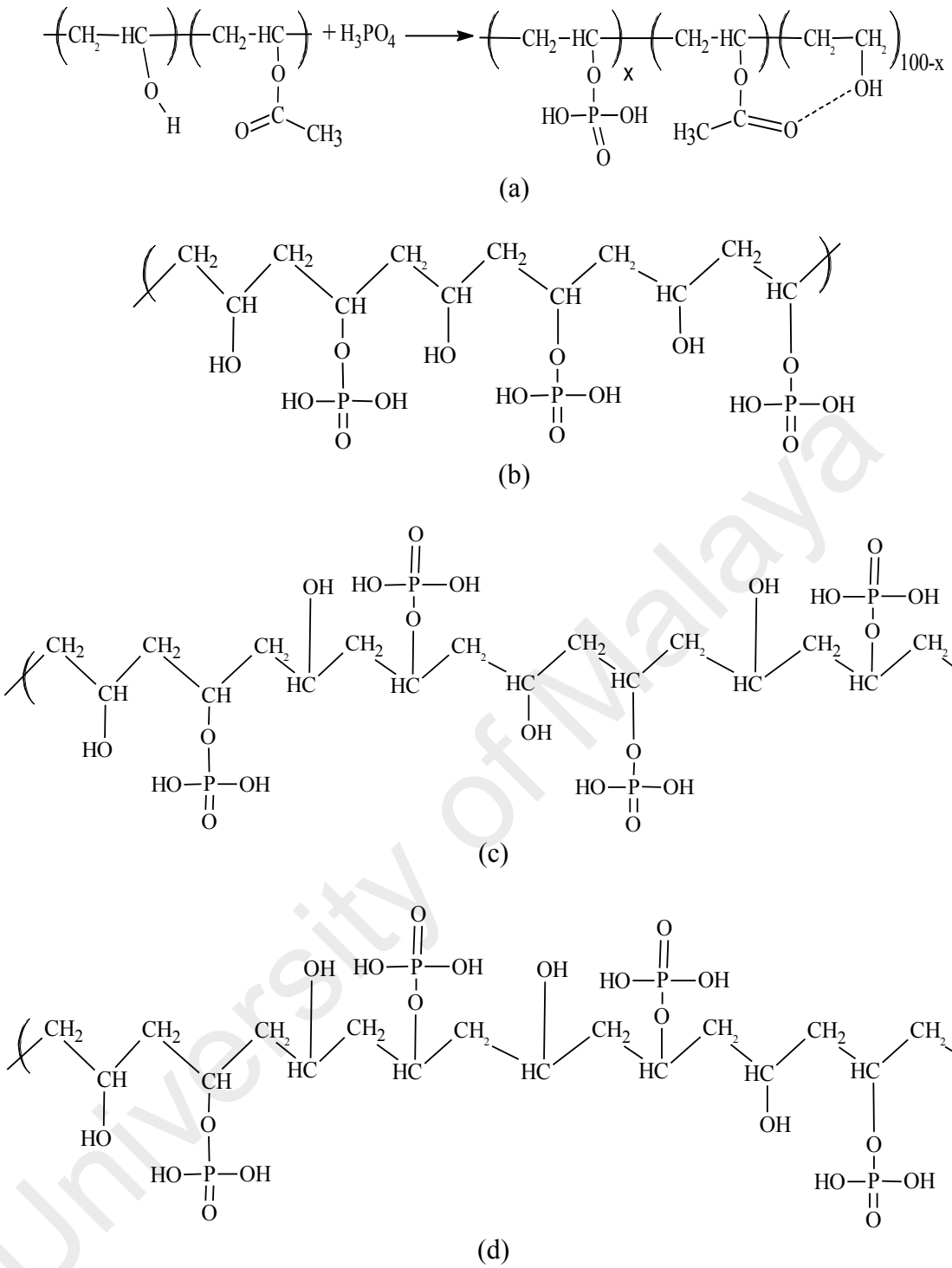

Figure 4.13: Schematic of PPVA molecular structures (a) Monomer of PPVA; (b) Isotactic of PPVA (i-PPVA); (c) Syndiotactic of PPVA (s- PPVA) and (d) Atactic of PPVA (a-PPVA)

The excitation process involved with schematic energy diagrams are shown in Figures 4.14 - 4.16. The 300 nm excitation resonates the excited electronic state at 412 nm in s-PVA (Table 4.8). The remaining bands in PL of 389–398 nm which are the most intense

band of the spectra in Figure 4.10, ascribes to i-PPVA. Meanwhile, the 350 and 400 nm excitation wavelength gave a respective PPVA structure as presented in Table 4.8.

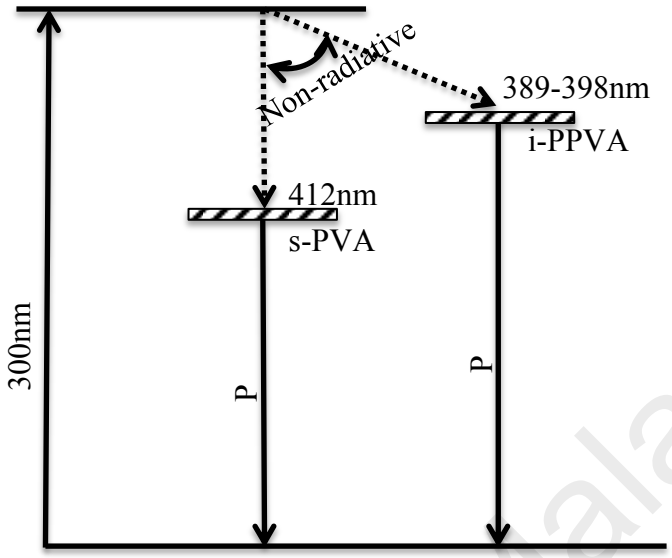

Figure 4.14: Schematic energy level diagram showing the PL emission and non-radiative processes operative simultaneously in resonance excitation 300 nm in s-PVA and i-PPVA polymer molecules

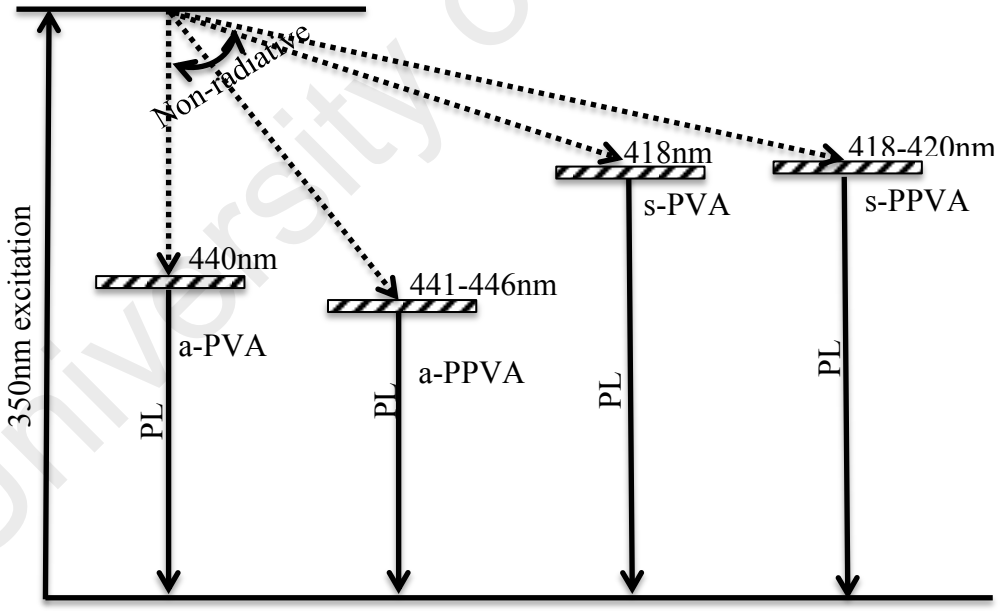

Figure 4.15: Schematic energy level diagram showing the PL emission and non-radiative processes operative simultaneously in resonance excitation 350 nm in a-PVA and s-PPVA polymer molecules

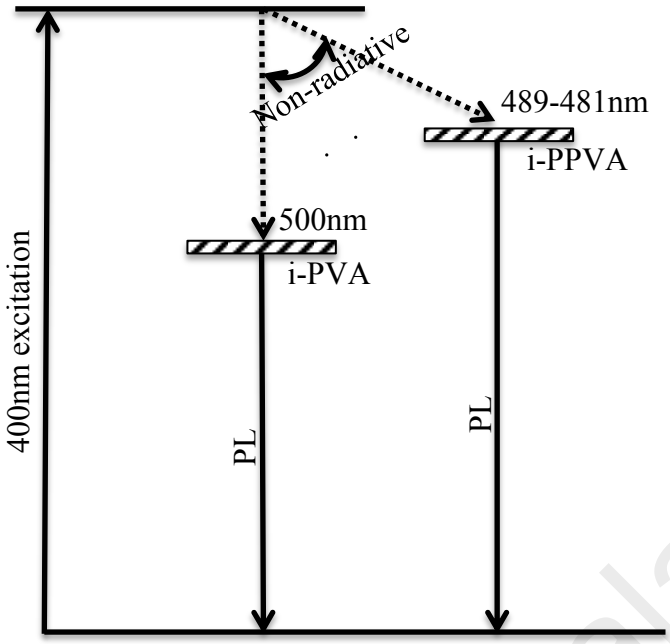

Figure 4.16: Schematic energy level diagram showing the PL emission and non-radiative processes operative simultaneously in resonance excitation 400 nm in i-PVA and i-PPVA polymer molecules

4.3 Effect of Aluminum sources on PPVA-$AlPO_4$ nanocomposites

4.3.1 X-ray diffraction (XRD) analysis

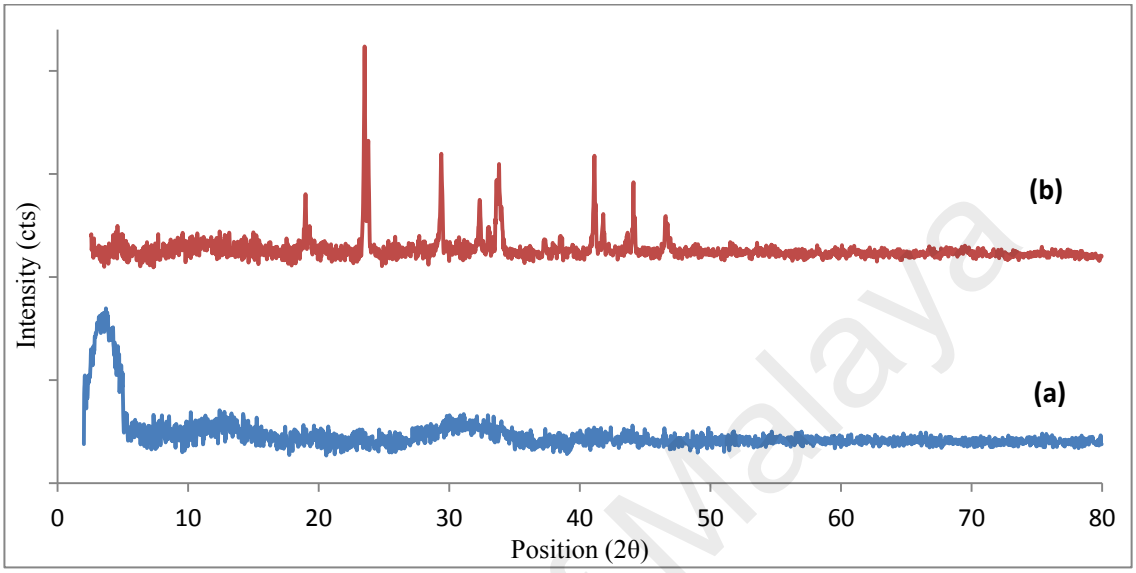

Figure 4.17: XRD patterns for as-synthesized PPVA-$AlPO_4$ nanocomposite with different aluminum sources, (a) Aluminum hydroxide and (b) Aluminum nitrate

Figure 4.17 shows the XRD patterns for as-synthesized PPVA-$AlPO_4$ nanocomposite samples using an aluminum nitrate (NAP-AN) and aluminum hydroxide (NAP-AH) at pH 10. The NAP-AN sample produced a combination of immiscible nano-sized layer and particle in the composite. The degree of crystallinity for sample produced with aluminum hydroxide is lower compared to aluminum nitrate sources. Both samples possessed an amorphous phase at lower angle. Nevertheless, NAP-AH sample shows three broad peaks at lower angle of 2θ = 2-6, 6-18 and 24-36°. Peak at angle of 20-30° is referring to $AlPO_4.H_2O$ which exist in NAP-AH sample (Boonchom & Kongtaweelert, 2010). Synthesis of $AlPO_4$ using aluminum hydroxide sources have a longer reaction time due to the difficulty to form the reactive aluminum which can quickly react with H_3PO_4 during the initial preparation. Aluminum hydroxide source easily produced the berlinite phase and $AlPO_4$-5 as byproduct during the synthesis (Kalbasi & Izadi, 2013). Meanwhile synthesis of $AlPO_4$ using $Al(NO_3)_3$ as a source

produces a mixture of exfoliated nanolayer and nano particle in the crystalline phase without any further heat treatment.

4.3.1 Thermal Analysis (TGA/SDTA)

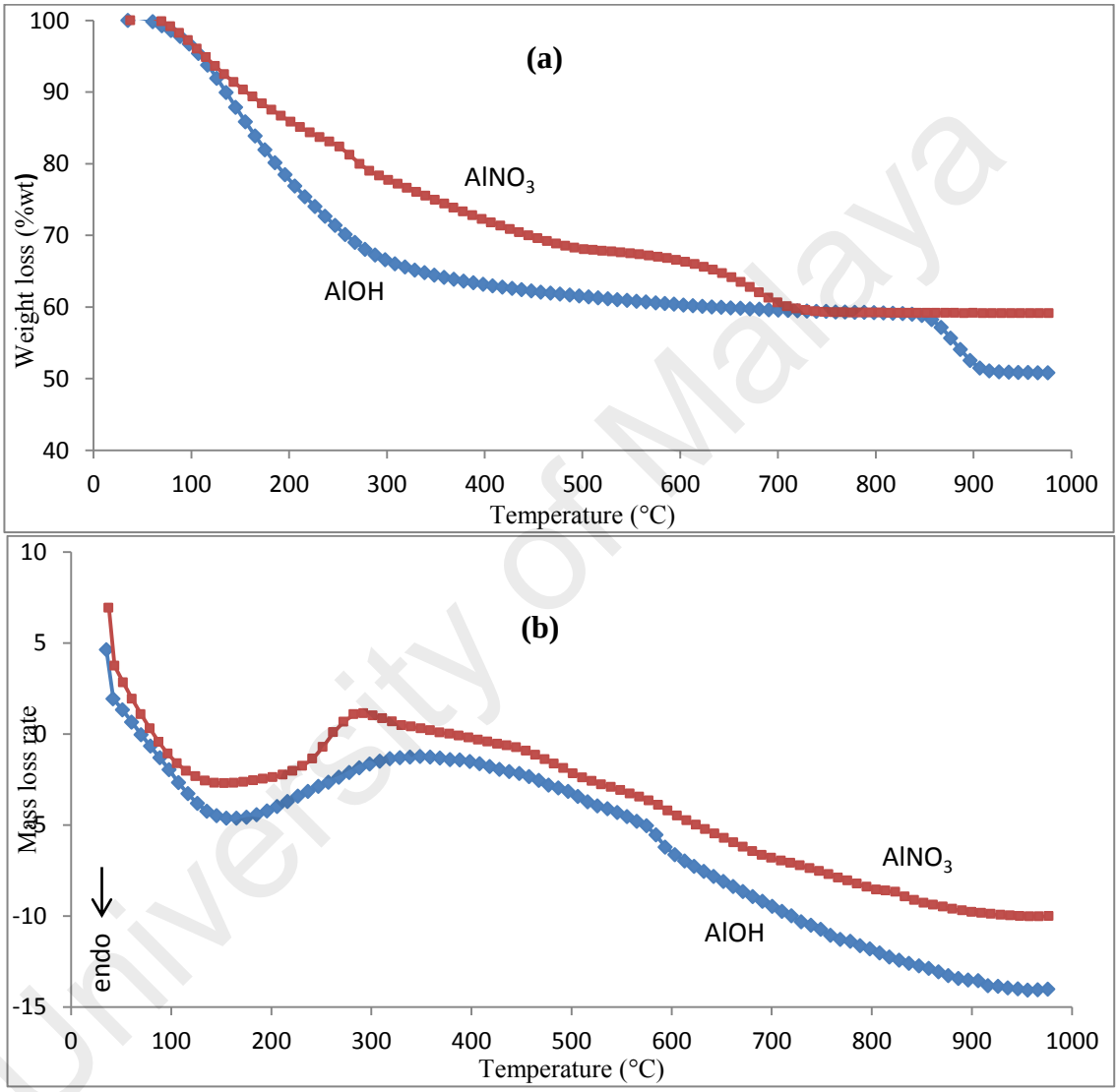

Figure 4.18: Thermal analysis for as synthesized PPVA-$AlPO_4$ nanocomposites with different aluminum sources, Aluminum nitrate and Aluminum hydroxide for (a) TGA and (b) SDTA

Figure 4.18 shows the TGA and SDTA traces for PPVA-$AlPO_4$ nanocomposites using different types of aluminum sources namely, aluminum nitrate (NAP-AN) sample and aluminum hydroxide (NAP-AH) sample. The first endothermic SDTA curve started at lower than 100°C due to the evaporation of water in PPVA-$AlPO_4$ nanocomposite.

Water evaporation for NAP-AN and NAP-AH samples occurred within the range of 30-250°C and 30-300°C, respectively. The second stage of degradation for NAP-AH sample occurred at the range of 300-850°C. A broad endothermic peak coupled with a small endothermic peak is observed at 580°C. A small endothermic peak is also observed at 910°C. The final degradation occurred at 850-1000°C with a total weight residue about 51 wt%. The NAP-AN sample showed four steps of degradation stage, while NAP-AH sample showed only three steps of degradation stage. The final degradation for NAP-AH sample occurred at a much higher temperature due to the oxidation process of higher amount of oxide to form char. Meanwhile, the final degradation stopped at a lower temperature of 700°C for NAP-AN sample due to higher crosslinking of phosphate in the system. This finding agrees well with the total amount of residue obtained for NAP-AN sample that is about 59 wt% which is higher than the NAP-AH sample of 51 wt%. NAP-AN sample produced more weight residue compared to NAP-AH sample due to more crosslinking productions of diphosphate, triphosphate and reaction with aluminum nitrate. These results produced more char formation which remains unoxidized in the residue.

4.4 Effect of Aluminum ratio on PPVA-$AlPO_4$ nanocomposites

4.4.1 X-ray diffraction (XRD) analysis

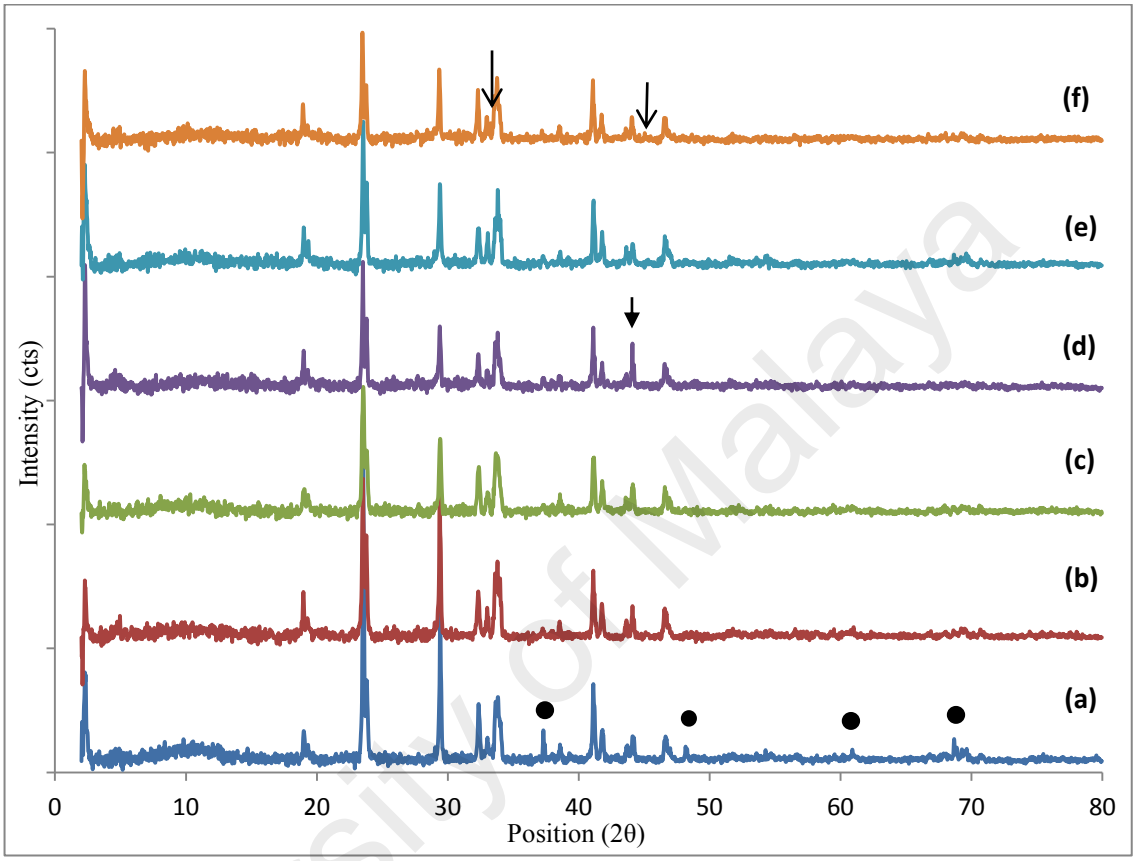

Figure 4.19: XRD patterns for PPVA-$AlPO_4$ nanocomposites with various ratios of aluminum (a) 1.0; (b) 1.1; (c) 1.2; (d) 1.3; (e) 1.4 and (f) 1.5

Figure 4.19 shows the as-synthesized PPVA-$AlPO_4$ nanocomposite with various ratios of aluminum (1.0, 1.1, 1.2, 1.3, 1.4 and 1.5) to three components of phosphate. Peaks related to phosphoric acid appeared at angles of 37.2°, 48.2°, 60.9° and 68.9° and can be clearly seen in the sample with aluminum ratio of 1.0:3 (Figure 4.19). The peak intensity decreases as the aluminum content increases and totally vanished in the sample with an aluminum ratio of 1.5:3 (Figure 4.19 (f)). $AlPO_4$ produce a series of peaks at the angle of 19.0°, double peak (23.5° (s), 23.8° (ms)), 29.4° (ms), 32.3° (m), triple peak (33.0°, 33.6°, 33.8°)(ms), double peak 41.1° (ms), 41.8°(m), 43.6°(m), 44.1°(m) and

46.5°(w). Sample with aluminum ratio of 1.0:3 possessed all the listed peaks with additional weak peaks at angles 48.2° and 69.6° due to excessive phosphoric acid. However, the peak intensity is decreased as aluminum ratio increased and slowly vanished. Peak at the angle of 59.0° appeared with a very weak signal as aluminum ratio increases. The peaks are missing in the sample with aluminum ratios of 1.4 and 1.5. Meanwhile, the maximum peak intensity is observed at angle of 44.1° in the sample with aluminum ratio 1.3. This suggests that the maximum bonding between aluminum and phosphoric acid occurred in this sample. Peak at angle of 23.5° shows maximum intensity. Meanwhile, the peaks observed at angles of 19.0°, 33.6°, 33.8° and 46.6° showed increasing intensity as aluminum increased. This can be concluded that the dominant element in this peak is aluminum. There are excessive aluminum in the composite for the sample with aluminum ratio of 1.5 as shown by the peak at angle of 32.98°. Similar observation by Chen et al. (2003) concluded that the ratio of Al/P within the range of 1.3:3 or 0.4333 will produced the optimal bonding for reaction of aluminum with the phosphate group. This supported our finding for optimum ratio of aluminum that is 1.3:3. For application of coating on steel, excessive H_3PO_4 will react with ferrous element and produce H_2 that further increase the porosity of ceramic coating and effect the wear resistance of the ceramic coating (Chen et al., 2003). The Al/P ratio with value above 1.4:3, produces more phases of Al $(H_2PO_4)_3$ which act as an effective bonding. The phase of $Al(OH)_3$ decreased the binding strength between the ceramic particle and aluminum phosphate binder (Chen et al., 2003).

4.5 Effect of pH on PPVA-$AlPO_4$ nanocomposites

4.5.1 Thermal Analysis (TGA/SDTA)

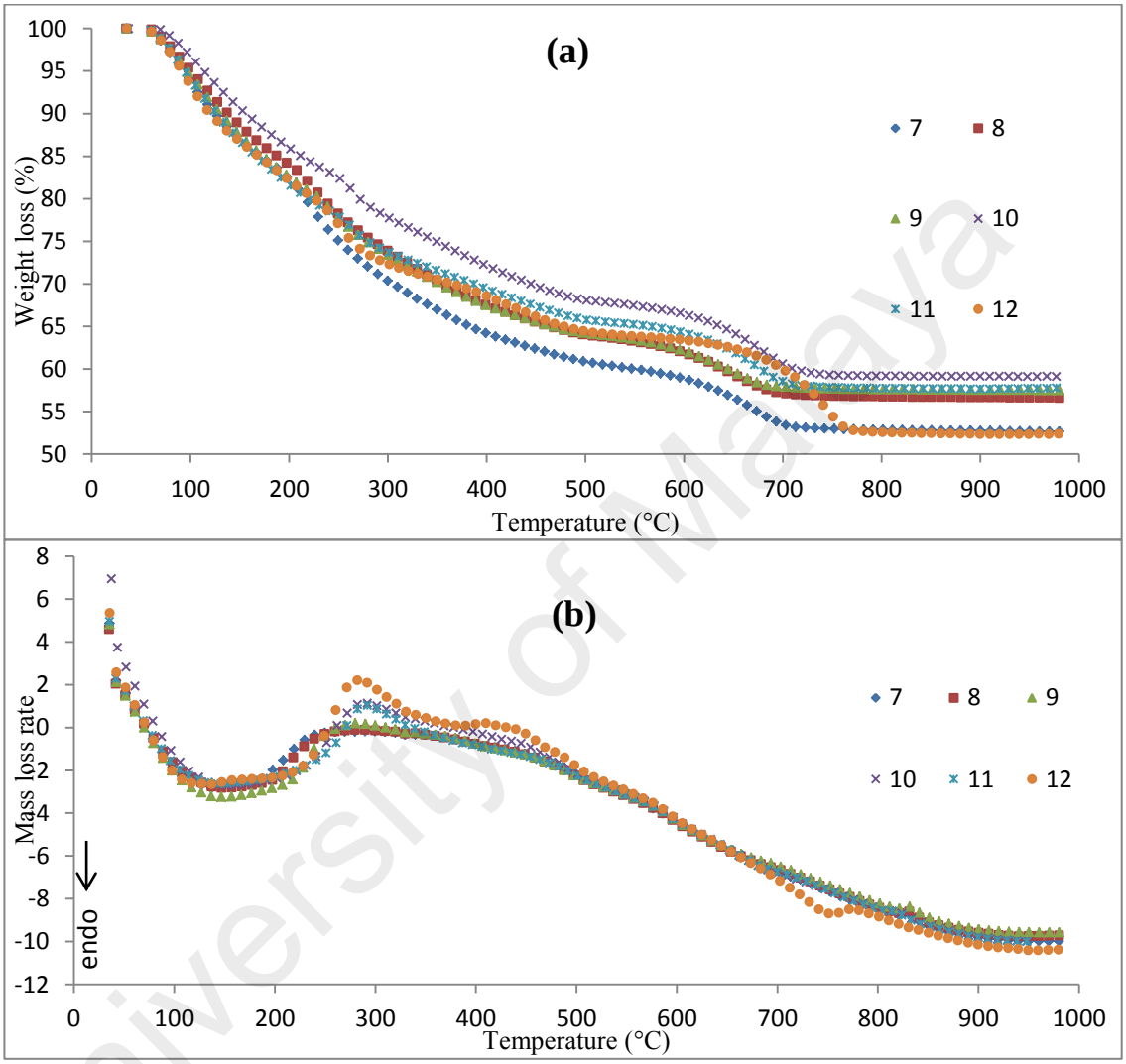

Figure 4.20: Thermal analysis patterns for (a) TGA and (b) SDTA PPVA-$AlPO_4$ nanocomposites samples at different pH (7, 8, 9, 10, 11 and 12)

Figure 4.20 shows the thermal analysis patterns for PPVA-$AlPO_4$ nanocomposite with different pH values (7–12). The SDTA traces show that all samples exhibited a broad endothermic peak within the temperature range of 30–250 °C. Meanwhile, the initial TGA peak in the range of 0 – 120 °C involved the elimination of water and moisture related to the crystal water whereas, in the temperature range of 120 – 260 °C it involved elimination of coordinated water in the $AlPO_4$. Sample with pH 10 showed

that elimination of water coordinated with the metal atom at higher temperature of 280 °C. This suggested that the maximum interaction between PPVA and aluminum occurred in this pH value. This sample had also been observed with minimum amount of water which was eliminated from the composite. Dehydration that also occurred within this range produced an endothermic effect and a possibility of phase transformation. The second stage of weight loss occurred in the temperature range of 260 – 480 °C and varied for each pH. Spontaneous degradation of PPVA and elimination of light organics occurred at this stage. Samples with pH 10, 11 and 12 showed exothermic peaks at 280 °C as observed in SDTA. However samples with pH 7, 8 and 9 showed a broaden peak at lower temperature of approximately 250 °C. The third degradation stage occurred within the temperature range of 450 – 700 °C for samples with pH 7, 8 and 9 and at temperature range of 480 – 720 °C for samples with pH 10, 11 and also at temperature range of 480 – 760 °C for sample with pH 12. A broadened with less intense endothermic peak is also observed at temperature range of 400 – 460 °C due to the breakage of carbon backbone as PPVA was being degraded. The peak becomes more intense for the pH 12 sample. No dehydration existed at the temperature range of 400 – 1000 °C but phase transformation had occurred as shown in SDTA. Table 4.14 shows the variation of $AlPO_4$ crystal system in the temperature range of 400 – 460 °C (Chen et al. 2003) and also at temperatures of 680, 670 and 770 °C. The final weight loss occurred from temperature range of 700 to 1000 °C as a total decomposition of PPVA-$AlPO_4$ nanocomposite with weight residues of about 53, 56, 57, 59, 58 and 52 wt% for samples with pH 7, 8, 9, 10, 11 and 12, respectively. Sample with pH 10 produced the maximum total weight residue which suggested that maximum interaction occurred between PPVA and $AlPO_4$. Sample with pH 12 showed an exothermic peak at 770 °C due to phase transformation and completion of a $AlPO_4$ crystallization (Mekky & Nicholson, 2007). Meanwhile at temperature of 708 °C, crystallization of amorphous

samples transformed to tridymite (Kandori et al., 1996). Weight residue increased as pH of the sample increased to 10, and decreased in similar amounts as per samples of pH 7 and 12. Maximum reaction between PPVA and $AlPO_4$ occurred in pH 10 which resulted to a maximum char formation. Burrell et al. (2001) reported that the Al-OH and Al-PO_4 bonding is reflected and proportionated by the pH of precipitation. This is in good agreement with our finding that maximum bonding of Al-PO_4 had occurred at pH 10 with the highest weight residue (59%) and less Al-OH. This can be seen in the lowest value of water (21%) during the first stage of degradation for sample with pH 10. Table 4.9 summarizes all the TGA and SDTA data.

Table 4.9: Thermal properties of SDTA and TGA for PPVA-$AlPO_4$ nanocomposite for various pH 7 – 12

Thermal properties	**pH 7**		**pH 8**		**pH 9**		**pH 10**		**pH 11**		**pH 12**	
SDTA	T (°C)		T (°C)		T (°C)		T (°C)		T (°C)		T (°C)	
1	30-250 (broad endothermic peak)		30-250 (broad endothermic peak)		30-250 (broad endothermic peak)		30-250 (broad endothermic peak)		30-250 (broad endothermic peak)		30-250 (broad endothermic peak)	
2	250 weak broad (endo)		250 weak broad (endo)		250 weak broad (endo)		285 intense (endo)		285 intense (endo)		280 intense (endo)	
3	Broad less intense exothermic peak at 400-460		Broad less intense exothermic peak at 400-460		Broad less intense exothermic peak at 400-460		Broad less intense exothermic peak at 400-460 (455)		Broad less intense exothermic peak at 400-460		410 small exothermic peak	
4	680		670		670		680		680		770 (exo)	
TGA	T (°C)	Weight residue (%)	T (°C)	Weight residue (%)	T (°C)	Weight residue (%)	T (°C)	Weight residue (%)	T (°C)	Weight residue (%)	T (°C)	Weight residue (%)
1st stage	0-260	28	0-260	37	0-260	38	0-280	21	0-260	25	0-260	27
2nd stage	260-450	11	260-450	10	260-450	11	280-480	9	260-480	8	260-480	9
3rd stage	450-700	8	450-700	9	450-700	8	480-720	11	480-720	9	480-760	12
Final Weight residue	700-1000	53	700-1000	56	700-1000	57	720-1000	59	720-1000	58	760-1000	52

4.5.2 X-Ray Diffraction (XRD) analysis

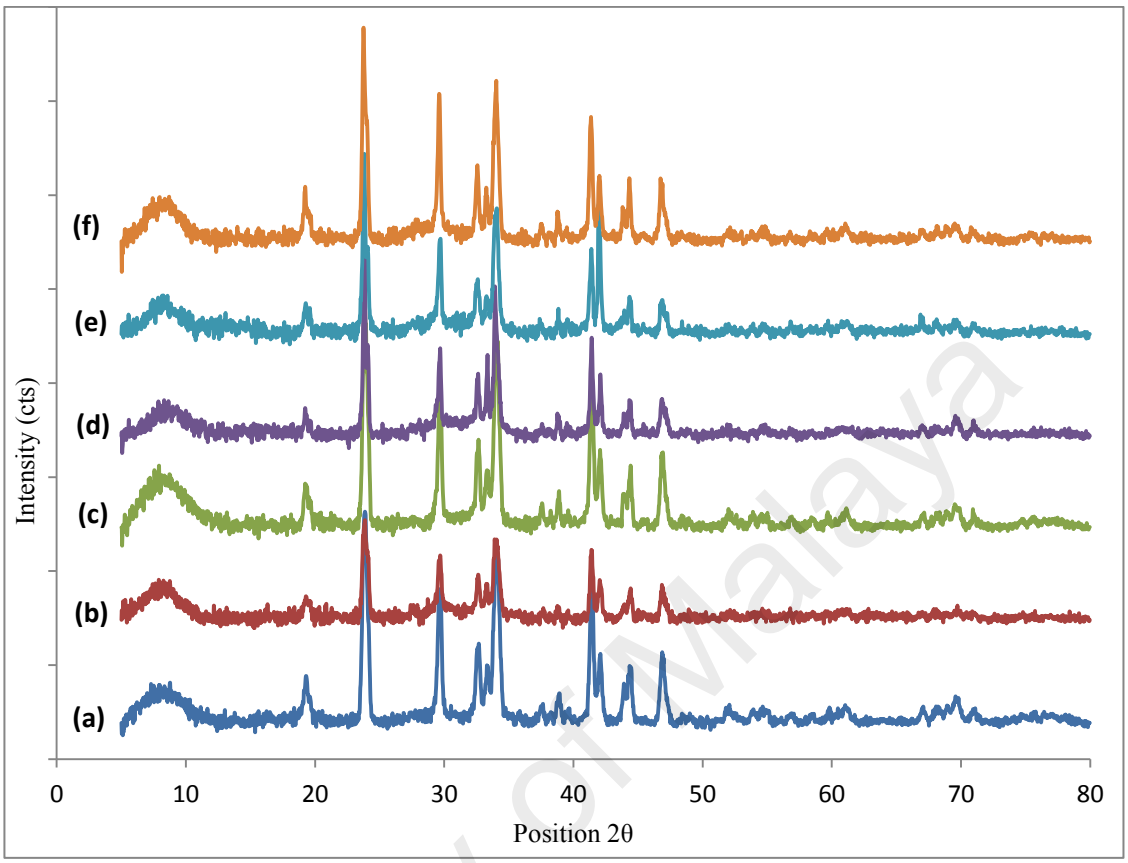

Figure 4.21: XRD patterns for PPVA-$AlPO_4$ nanocomposite samples at different pH values (a) pH 7; (b) pH 8; (c) pH 9; (d) pH 10; (e) pH 11 and (f) pH 12

Figure 4.21 shows the XRD patterns for PPVA-$AlPO_4$ nanocomposite samples with various pH values (7 – 12). All samples show that the XRD patterns consist of a mixture of immiscible layers and spherical particles. All peaks are shifted to lower angles for samples with pH 7 to pH 9. However the peaks are shifted to higher angles for samples with pH 10 to pH 12. Meanwhile, the peak intensity decreases with the increasing of pH values from 7 to 9. However, the intensity is slightly increased from pH 9 to 10 but decreases from pH 10 to 12. Sample with pH 12 shows a broaden peak and almost vanished. The phosphate crystallinity is increased by increasing the acidity for synthesizing of $AlPO_4$ nanoparticles in the acidic region (Palacios et al., 2013). However the XRD patterns show that all samples are in a good crystallinity condition in the alkaline region. Additionally, it is observed that two ranges of microstructure

development of aggregation and agglomeration of small particles occurred in the alkaline region from pH 7 to 9 and pH 10 to 12. This observation suggested that at lower alkaline region (pH 7 to 9), the microstructure is developed from the reaction of minor presence of OH^-. Nevertheless, H^+ still influenced the microstructural development and nucleation of PPVA-$AlPO_4$ nanocomposite. However, at pH 10 to 12, the nucleation and aggregation were affected by the OH^- ion that was excessively present. A stable particle size of PPVA-$AlPO_4$ nanocomposite was obtained for samples with lower OH^- at pH 10.

Figure 4.22 shows the particle size of all samples which were calculated using Scherer equation. Samples at pH 7, 8 and 10 have an average small particle size distribution. Increasing pH values favored the crystallite size but the crystallinity and amorphous phases are maintained. The growth of phosphate particles is based on the aggregation of globular primary nanoparticles where pH in the solution is determined by the ions in solution and has an effect upon the composition and crystallite size (Palacios et al., 2013). The component of H^+ and OH^- ions are dependent on the pH of the solution where in strong alkaline environment, OH^- becomes the dominant ion. Variation of pH induces hydrolysis and condensation that increases the kinetic of synthesis and also promotes the production and transport of H^+ and OH^-. The induction time of the crystallization curve is longer if less water or H^+ and OH^- component is present. Therefore, pH is important in controlling the rate of crystallization, thus controlling the particle or crystallite size distribution. Excess amount of OH^- ions reduces the yield of precipitate and the best condition for larger yields include high levels of P and Al (Beppu et al., 1996). This is in good agreement with results obtained for sample with pH 10.

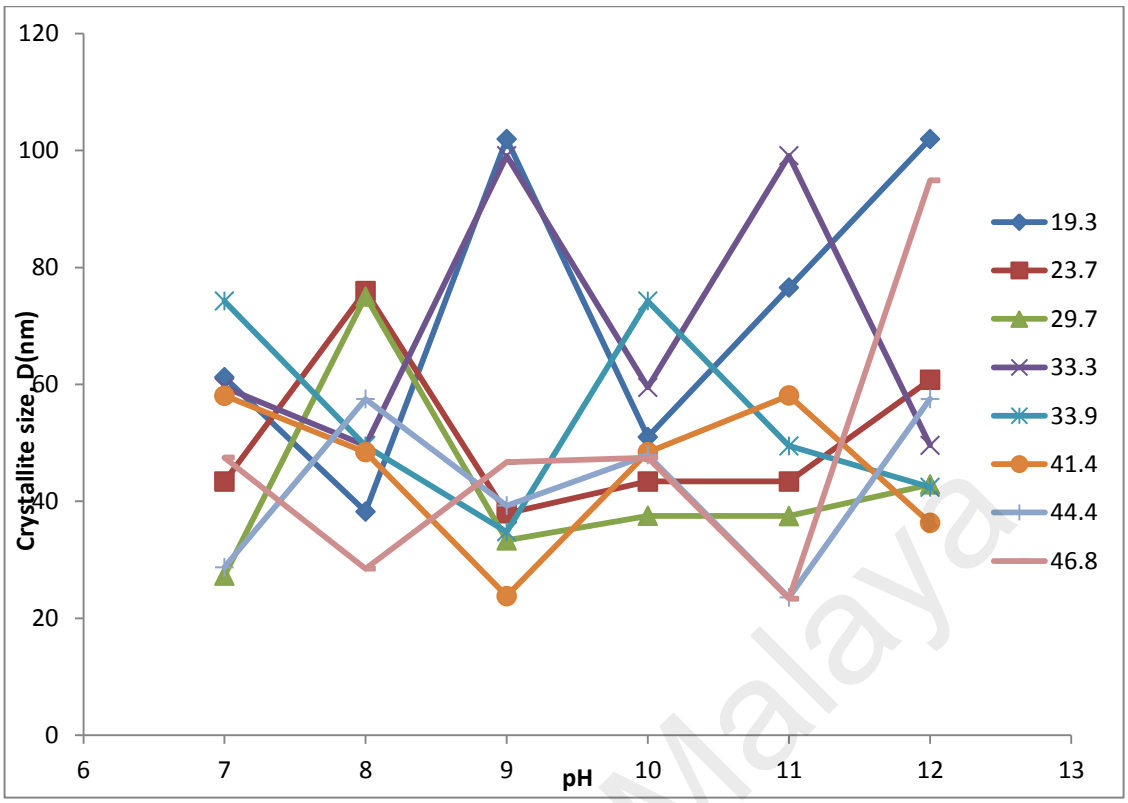

Figure 4.22: Particle size distribution for PPVA-$AlPO_4$ nanocomposites at different pH values (7-12)

Sample with pH 10 produced a homogeneous distribution of crystallite size and supported the thermal result where the maximum bonding of PPVA-$AlPO_4$ occurred. PPVA-$AlPO_4$ nanocomposites remained as crystalline in all pH values (7 – 12). The pH of the precipitation reflected the proportion of Al-OH to Al-PO_4 as observed in FTIR results (Figure 4.26) and may affect the particle size as observed in XRD peak intensity and FWHM. The details of XRD data and crystallite size are presented in Table 4.10.

Table 4.10: XRD data for 2θ value, d- spacing and FWHM for PPVA-$AlPO_4$ nanocomposite samples at different pH values (7 – 12)

pH 7			pH 8			pH 9			pH 10			pH 11			pH 12		
Pos. [°2Th.]	d-spacing [Å]	FWHM [°2Th.]	Pos. [°2Th.]	d-spacing [Å]	FWHM [°2Th.]	Pos. [°2Th.]	d-spacing [Å]	FWHM [°2Th.]	Pos. [°2Th.]	d-spacing [Å]	FWHM [°2Th.]	Pos. [°2Th.]	d-spacing [Å]	FWHM [°2Th.]	Pos. [°2Th.]	d-spacing [Å]	FWHM [°2Th.]
19.3159	4.5953	0.1279	19.2777	4.60434	0.2047	19.3621	4.58445	0.0768	19.2669	4.6069	0.1535	19.3011	4.5988	0.1023	19.2233	4.61725	0.0768
23.703	3.75379	0.1023	23.692	3.75551	0.1023	-	-	-	-	-	-	19.5838	4.53306	0.0768	-	-	-
23.9108	3.72163	0.1791	23.8456	3.73167	0.1023	23.7978	3.73904	0.2047	23.8395	3.7326	0.1791	23.8204	3.73555	0.1791	23.7379	3.74834	0.1279
24.1777	3.68115	0.1023	24.1183	3.69008	0.1023	24.1756	3.68146	0.0768	24.0996	3.6929	0.1279	24.0908	3.69423	0.1279	24.0614	3.69868	0.1023
29.7495	3.00318	0.2814	29.5643	3.01907	0.0936	-	-	-	-	-	-	-	-	-	-	-	-
-	-	-	29.711	3.00698	0.1023	29.6291	3.01511	0.2303	29.6909	3.00897	0.2047	29.7115	3.00694	0.2047	29.6119	3.01682	0.1791
32.5321	2.75011	0.156	-	-	-	32.5081	2.75208	0.0936	32.6094	2.74603	0.1535	32.4405	2.75995	0.1279	32.5763	2.74875	0.2047
32.6837	2.73997	0.1535	32.5985	2.74693	0.2047	32.6731	2.74083	0.1791	-	-	-	-	-	-	-	-	-
33.3424	2.68732	0.1279	33.3021	2.69049	0.1535	33.2773	2.69243	0.0768	33.3428	2.6873	0.1279	33.2249	2.69656	0.0768	33.2252	2.69654	0.1535
33.9987	2.63694	0.1023	33.9149	2.64326	0.1535	33.9965	2.63492	0.2184	33.9213	2.64278	0.1023	34.0562	2.63262	0.1535	34.0209	2.63526	0.1791
34.1804	2.62334	0.1023	34.1275	2.62728	0.1535	34.1638	2.62891	0.156	-	-	-	-	-	-	-	-	-
41.2918	2.18468	0.1248	41.396	2.18123	0.1535	41.4044	2.179	0.312	41.4163	2.1802	0.1535	41.4037	2.18084	0.1279	41.319	2.18511	0.2047
41.4869	2.17666	0.1279	-	-	-	-	-	-	-	-	-	41.9384	2.15248	0.0936	41.9861	2.15192	0.1535
42.0678	2.14793	0.1791	42.0383	2.14937	0.0768	42.0871	2.14522	0.2808	42.0886	2.14692	0.1279	42.0683	2.15146	0.0936	-	-	-
44.4395	2.03865	0.2558	44.4082	2.04002	0.1279	44.4342	2.0372	0.1872	44.385	2.04103	0.1535	44.4629	2.03595	0.312	44.3105	2.04429	0.1279
-	-	-	-	-	-	-	-	-	-	-	-	-	-	-	46.7421	1.94184	0.0936
46.8271	1.94012	0.1535	46.8265	1.94015	0.2558	46.8305	1.93839	0.156	46.838	1.9397	0.1535	46.8104	1.93917	0.312	46.8887	1.93772	0.0768

4.5.3 Field Emission Scanning Electron Microscopy (FESEM) analysis

Figure 4.23 shows the FESEM micrographs with 50k magnification for as prepared PPVA-$AlPO_4$ nanocomposites samples at different pH values. The homogeneous phase of nanoparticles was observed in samples of pH 8 and 10. Small phase layers together with spherical particles were observed for samples of pH 7 and 9. Meanwhile, the particle size becomes larger for sample of pH 11 due to non-spherical shape particles. The spherical particles are losing its shape after agglomeration, as the particles are joint together to form other geometrical shapes. This also occurred for sample of pH 12 due to the particle agglomeration. Other than that, the particle seems to melt away from reaction with excessive OH ions in the system.

Figures 4.24 and 4.25 shows the FESEM micrographs with higher magnification at 100k and 200k, respectively. All spherical particles observed in this micrograph are of nanometer size with the average size being less than 20 nm. Particles start to agglomerate at pH 9 to form a layered structure. However, the layer is vanished at pH 10 and homogeneous distribution of spherical particles is produced. A homogeneous precipitation of nucleation occurs quickly when the constituent species reaches critical super saturation. It can be concluded that sample at pH 10 reached the critical super saturation stage. Sample of pH 11 is observed with mixture of irregular and spherical shapes of nanoparticles. Menawhile, the melting of nanoparticles is observed at pH 12 sample. The formation of nanotube is also observed at this pH which is similar to what had been reported by Yang & Kau (2005). The effect of pH on PPVA-$AlPO_4$ nanocomposite samples show behaviors of crystal formation and disappearance. The aggregation of particles at a weak alkaline solution (pH 7 – 9) is influenced by H^+ ion. Critical super saturation is obtained at pH 8 and produced a homogeneous distribution of spherical nanoparticles. However, the OH^- anions reach its critical super saturation at

high alkaline region (pH 10). Beyond this pH 10, the shapes of particles are varied and its size became larger. At level of pH 13, the reaction to produce nanoparticles could not be performed, instead all the reactants were completely dissolved. Yang & Kau (2005) also reported the same observation on the synthesis of $AlPO_4$ nanoparticles at pH 13. Figure 4.21 shows two trends of particle size distribution as the pH value increases. The particle size of PPVA-$AlPO_4$ nanocomposite decreases from pH 7 to 8 and experienced sudden increase at pH 9. However the, particle size decreases again at pH 10 and higher pH. Homogeneous spherical nanoparticles are observed in samples of pH 8 and 10. This finding is in good agreement with the crystallite size from XRD patterns (Figure 4.22) that observed homogeneous distribution of particle size in the same pH. Samples that were prepared in pH 7, 9, 11 and 12 produced a wide distribution of nanoparticles and also possessed non-homogeneous distribution of particle size (Figure 4.22) due to the existence of heterogeneous phases of laminar layer, various geometrical shapes and melting behavior. Thus it is concluded that the particle size and morphologies of PPVA-$AlPO_4$ nanocomposites are dependent on pH values. Kawamura et al. (2007) earlier reported the same conclusion that different morphologies of aluminum phosphate depend on the pH and temperature. PPVA-$AlPO_4$ nanocomposites possessed strong crystallinity properties in the alkaline region. Jiang et al. (2013) observed an increase of crystallinity as pH decreased. Meanwhile Palacios et al. (2013) observed a reduction of the particle size as pH increases. The growth of phosphate particles was due to agglomeration and aggregation of small particles into nanoparticle size as observed in Figures 4.23, 4.24 and 4.25. Palacios et al. (2013) also reported a heterogeneous phase distribution of spherical nanoparticles and a pseudo hexagonal morphology that was related to taranakite structure. A laminar layer is observed at pH 9 that was formed from spherical nanoparticles which evolved to laminar particles. A nanotube is observed at higher pH 12 that may be formed from intermolecular H-bonding between PPVA

fractions with aluminum phosphate. A complete transformation of nanoparticle to nanotube did not occur as the final pH shows slight reduction and was still in strong alkaline. However, this is against the finding reported by Yang & Kau (2005) where the final pH is changed to neutral which shows a complete transformation of nanoparticle to nanotube. Synthesis of PPVA-AlPO4 nanocomposite was successfully formed at lower temperature. PPVA acted as the capping agent that cleaved the bonding between nitrates and accelerate the dissociation of Al^{3+} ions from the $AlNO_3$. The slow release of Al^{3+} ions from aluminum nitrate occurred at pH 7 which produced spherical nanoparticles. However, the particle size and morphology of the phase varies at increasing pH. Hence, the samples consist of spherical particles and laminar layers of PPVA-$AlPO_4$ nanocomposite.

Formation of $AlPO_4$ was discussed based on the pH values and concentration building unit in the synthesis mixture (Ganschow et al., 2001). The construction building units in PPVA-$AlPO_4$ nanocomposites are dependent on the Al-OH and Al-PO_4. The pH of the precipitation reflects the proportion of Al-OH to Al-PO_4 bonds and may affect the size of particles and the portion of the layer phase as observed in FESEM images (Figures 4.23 – 4.25). The ionization of phosphoric acid to dihydrogen phosphate ion, hydrogen phosphate ion and conjugate base PO_4^{3-} varies in an alkaline environment. Ionization of phosphoric acid to PO_4^{3-} is maximized above pH 7 (Yang & Kau, 2005). Nucleation of $AlPO_4$ is stopped after all available Al^{3+} and most free OH^- ions have reacted.

Sample with pH 10 produced a homogeneous distribution of particle size and supported the thermal finding with the occurrence of maximum bonding between PPVA and $AlPO_4$. The XRD analysis (Section 4.3.2) is also coherent with FESEM results where the homogeneous distribution of crystalline size occurred in the sample with pH 10. Therefore, the pH for the precipitation affected the portion of the morphology phase and particle size of PPVA-$AlPO_4$ nanocomposite.

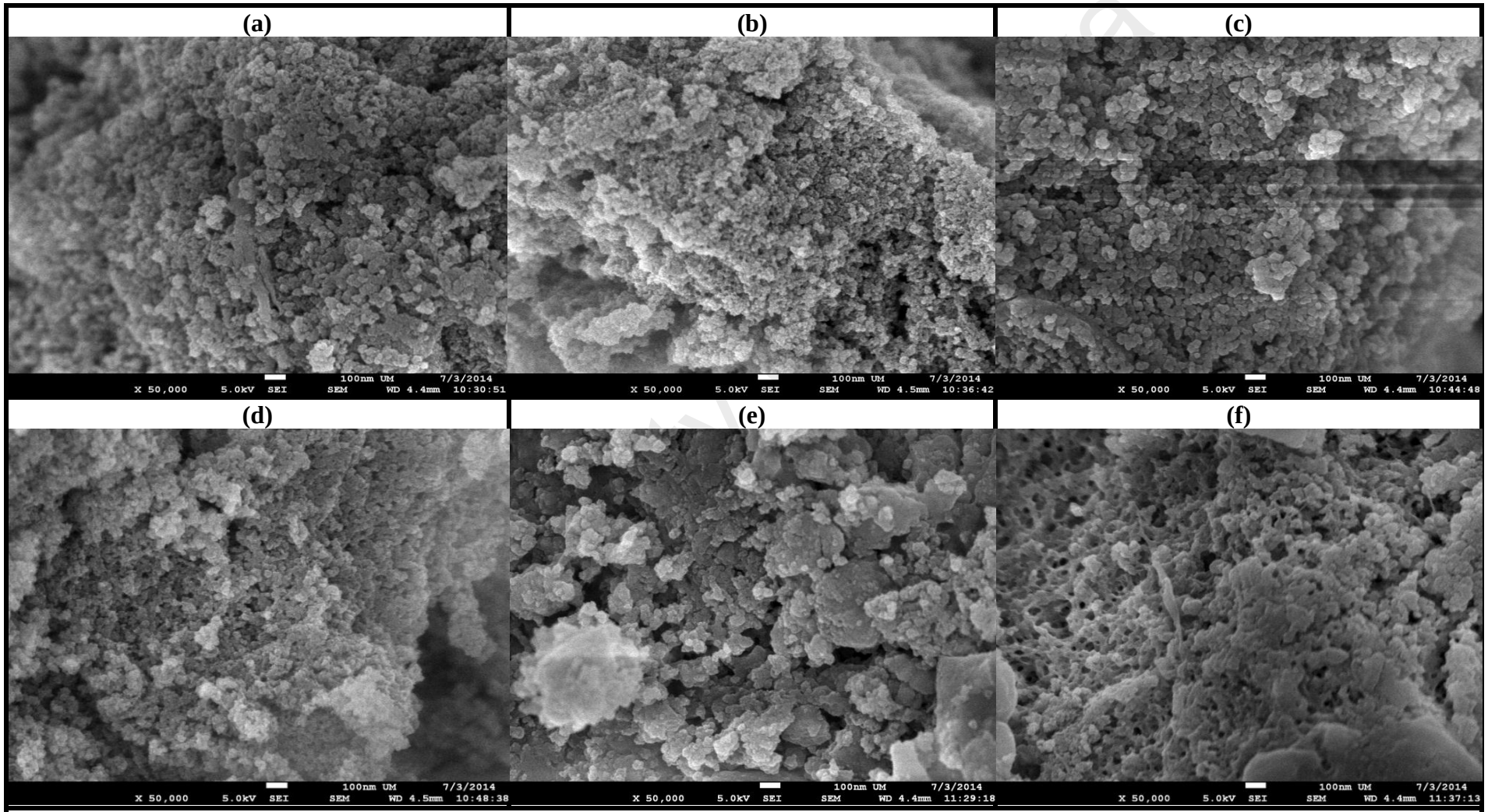

Figure 4.23: FESEM micrographs with 50k magnification of PPVA-$AlPO_4$ nanocomposite samples at different pH values (a) 7; (b) 8; (c) 9; (d) 10; (e) 11 and (f) 12

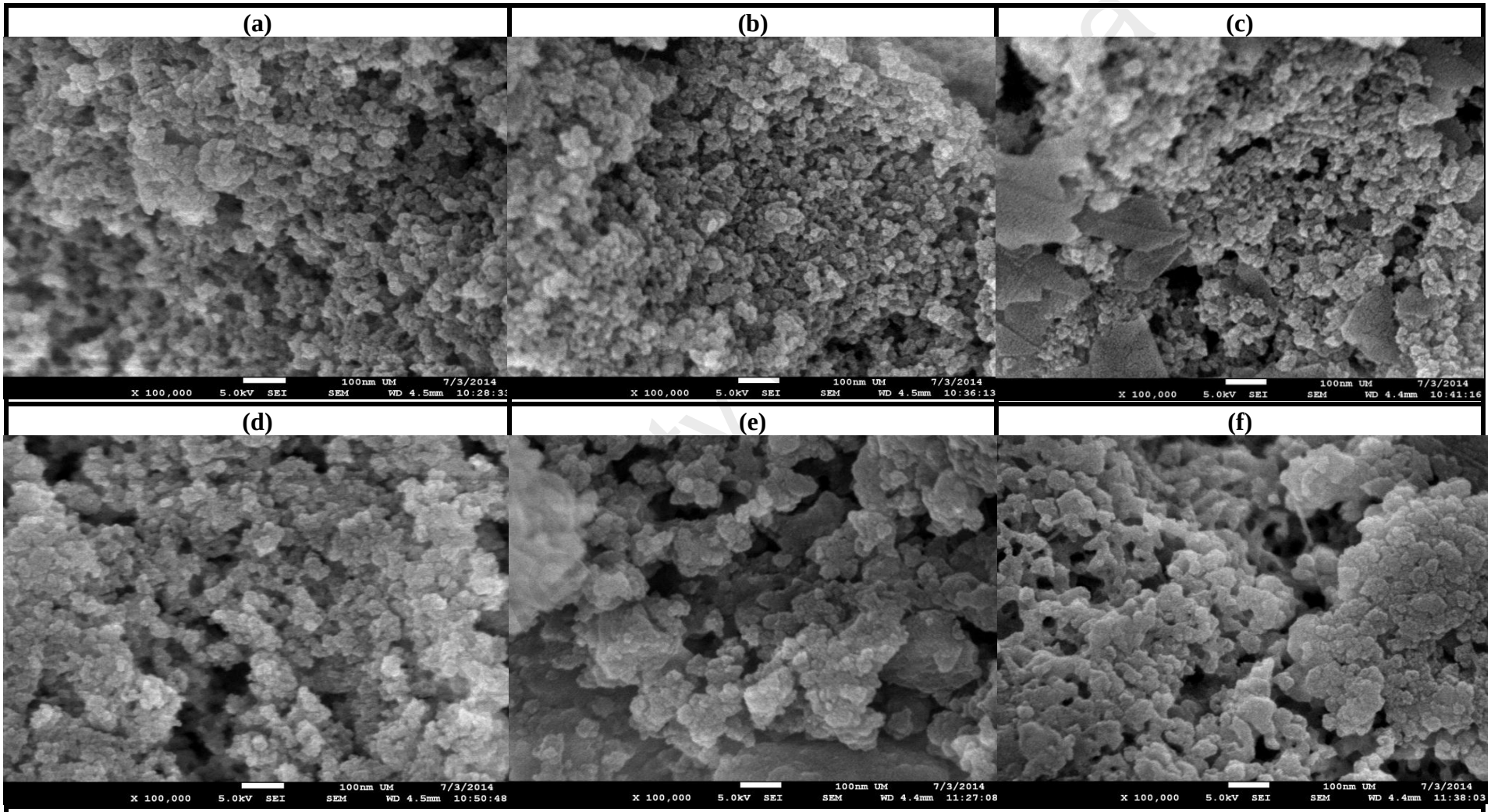

Figure 4.24: FESEM micrographs with 100k magnification of PPVA-$AlPO_4$ nanocomposite samples at different pH values (a) 7; (b) 8; (c) 9; (d) 10; (e) 11 and (f) 12

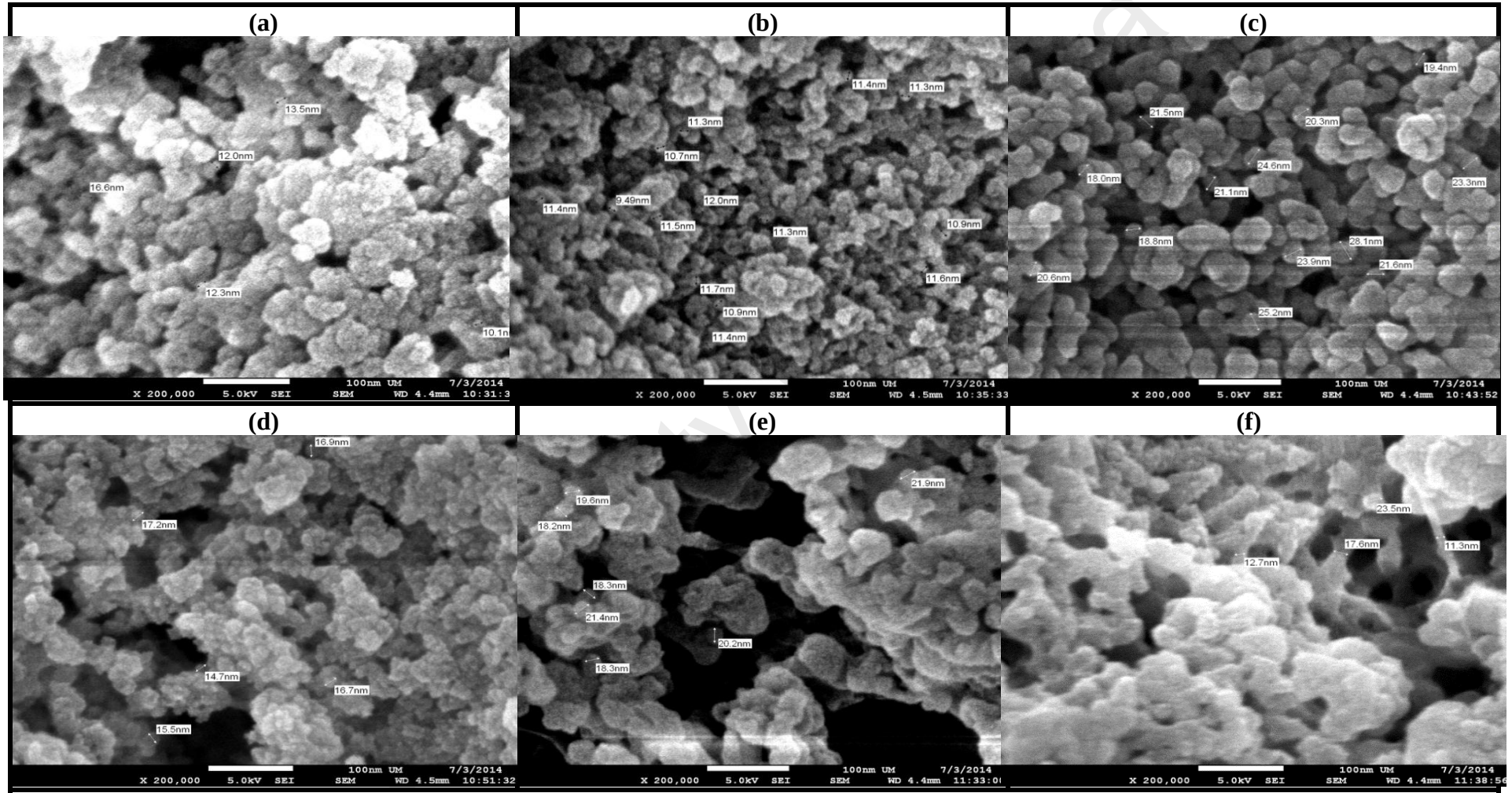

Figure 4.25: FESEM micrographs with 200k magnification of PPVA-$AlPO_4$ nanocomposite samples at different pH values (a) 7; (b) 8; (c) 9; (d) 10; (c) 11 and (f) 12

4.5.4 Fourier Transform Infrared (FTIR) Spectroscopy Analysis

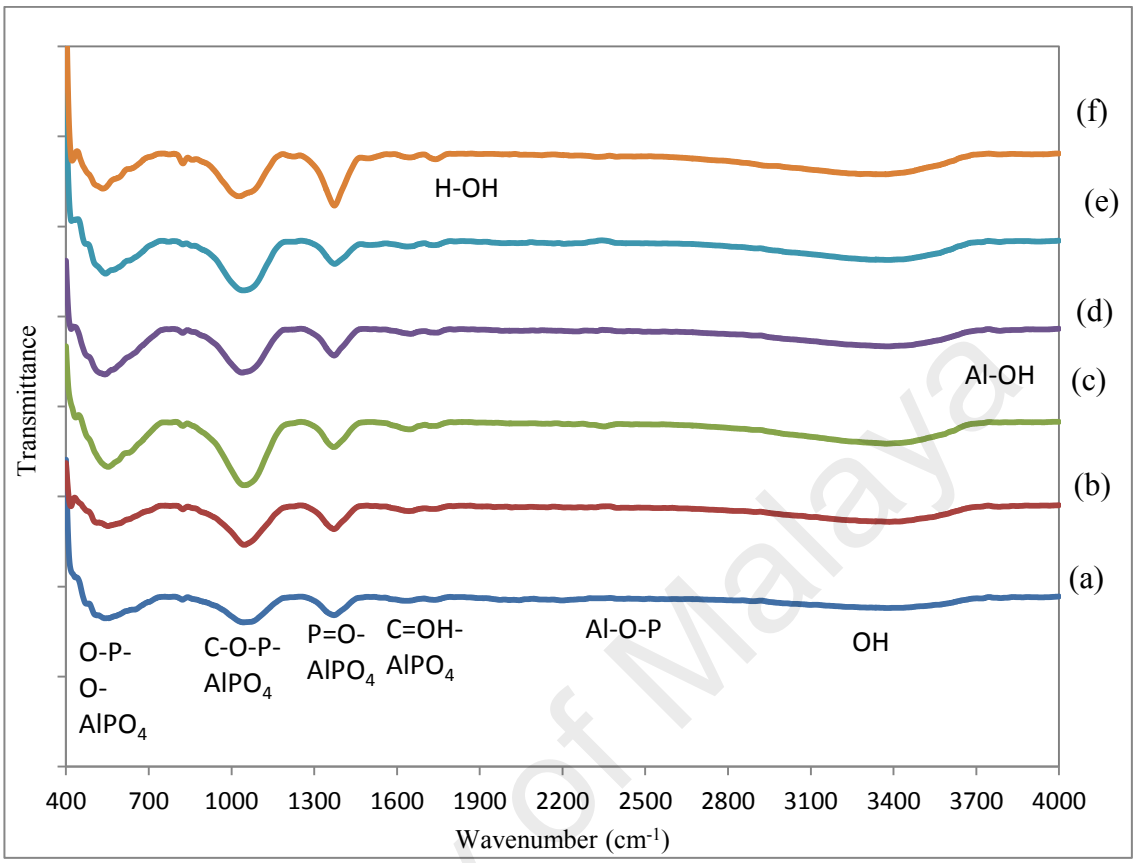

Figure 4.26: FTIR spectra for as prepared PPVA-$AlPO_4$ nanocomposite samples at different pH values (a) 7; (b) 8; (c) 9; (d) 10; (c) 11 and (f) 12

Figure 4.26 shows the FTIR spectra for as prepared PPVA-$AlPO_4$ nanocomposite samples at different pH values (7, 8, 9, 11, 11 and 12). Sample prepared at pH 10 shows the Al-OH peak at 3786 cm^{-1}. Meanwhile, samples prepared at pH 7, 9 and 11 shows the Al-O-P peaks at 2202, 2253 and 2206 cm^{-1}, respectively. The H-O-H plane bending vibration of water molecules is observed at lower wavenumber (1730 and 1740 cm^{-1}). All samples possessed peaks of OH (3371 – 3385 cm^{-1}), C-OH and mixture of H-O-H (1640 – 1649 cm^{-1}), P-O-$AlPO_4$ (1371 – 1374 cm^{-1}), C-O-P-$AlPO_4$ (1027 – 1047 cm^{-1}), HP-O-$AlPO_4$ (822 – 824 cm^{-1}) and O-P-O-$AlPO_4$ (533 – 553 cm^{-1}).

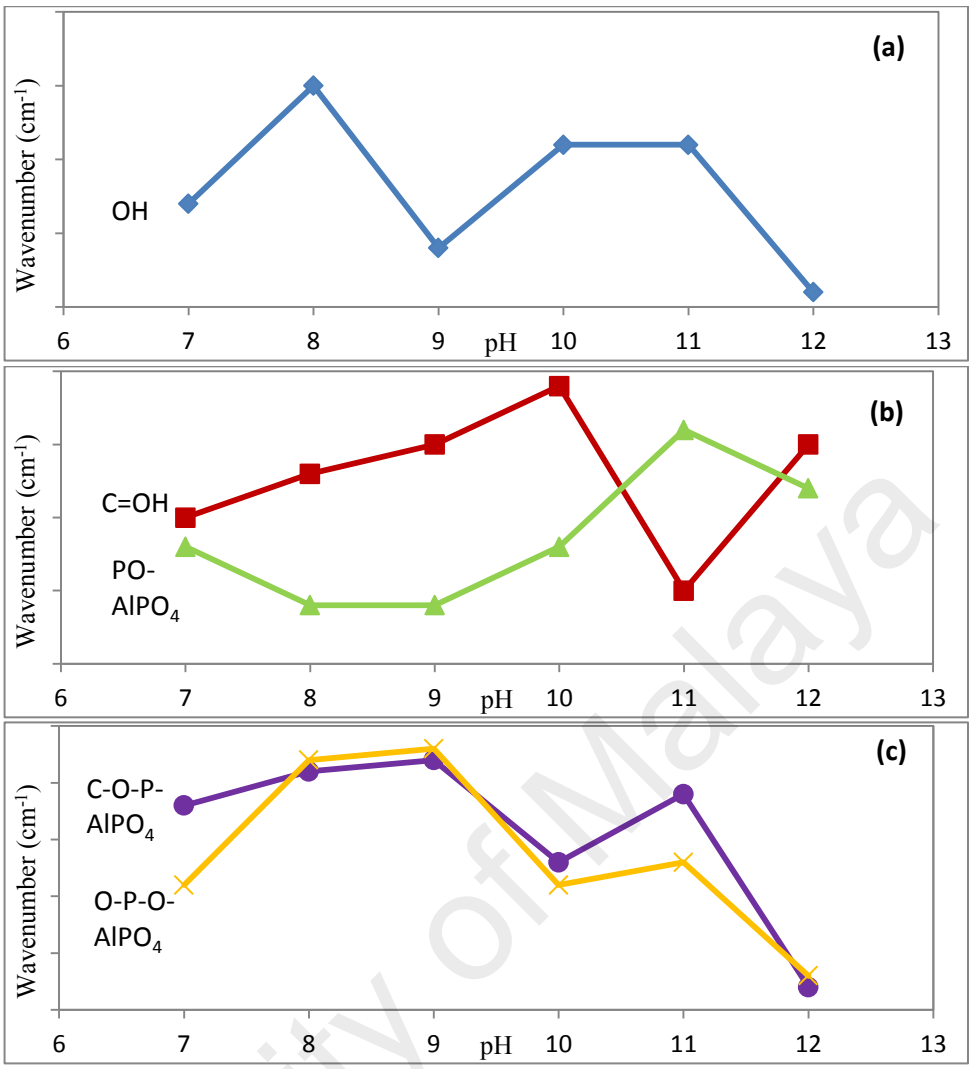

Figure 4.27: Selective FTIR bands of PPVA-$AlPO_4$ nanocomposite samples prepared at pH 7, 8, 9, 10, 11 and 12 (a) OH (3371-3385 cm^{-1}); (b) C=OH (1640-1649 cm^{-1}) and PO-$AlPO_4$ (1371-1374 cm^{-1}) and (c) C-O-P-$AlPO_4$ (1027-1047 cm^{-1}) and O-P-O-$AlPO_4$ (533-553 cm^{-1})

Figure 4.27 shows the pH effect in the selected five FTIR bands that exist in the nanocomposite samples. The corresponding OH, C-OH, P-O-$AlPO_4$ C-O-P-$AlPO_4$ and O-P-O-$AlPO_4$ bands are shifted to lower wavenumber as pH increases from weak to strong alkaline solution. The bands are shifted to higher wavenumber for samples of pH 7 to 9 and shifted to lower wavenumber in pH 10. At pH 11, the bands shifted to higher wavenumber and shifted back to lower wavenumber at pH 12 as shown in Figure 4.24 (a) and (c). Meanwhile Figure 4.24 (b) shows that the C=OH band is shifted to higher wavenumber from pH 7 to pH 10 and to pH 11 in PO-$AlPO_4$ band that is related to water and H bond. This water is decreased in pH 11 but increased in pH 12 due to

breaking of Al-O-P bond and crystal structure. The PO-$AlPO_4$ band reached maximum intensity in pH 12. The shifting of the band shows that the wavenumber increases as the protonation degree increases until pH 10 (Burrell et al., 1999) due to maximum interaction between polymer and aluminum. The normal mode of the vibrational spectra containing PO_4, HPO_4^{2-}, $H_2PO_4^{2-}$ and H_3PO_4 shows a decrease in the force for the P-O and P-OH bonds with the decreasing of the protonation degree. This is in accordance with the shifting to higher energy in the P-OH band as pH increases. This behavior is the experimental evidence for the increase of the phosphate character when the pH decreases (Palacios et al., 2013). Additionally, OH^- ion with O bond induced the bond to break and reform Al-O-P (Ma et al., 2008). Thus, it produced a variation in the shifting or wavenumber. The trend is almost similar to the XRD particle size analysis, due to the H^+ and OH^- ions which varies the Al-O-P and Al-OH bond in the PPVA-$AlPO_4$ nanocomposite samples. Thus, it affects the bond length and coordination number of nanoparticles. The development of crystal from particles agglomeration at pH 7 to 9 due to the influence of H^+ ion. However, the number of OH^+ ion influences the crystal structure and particle size at pH 10. Thus, it breaks the agglomeration into small particles and the second development of crystal begins from pH 10 to 11. However, the excess of OH^+ ions in the system obstructed the particles development. Further addition of OH^+ ion will completely vanish the Al-OH bond and crystal structure. The summary of FTIR peaks for various pH is presented in Table 4.11.

Table 4.11: Interpretation of PPVA-$AlPO_4$ nanocomposite FTIR spectra at various pH values (7, 8, 9, 10, 11, and 12)

		Band assignment and wavenumber (cm^{-1})									
Sample	pH	Al-OH	OH	Al–O–P	H-O-H	C-OH@ H-O-H	P-O-$AlPO_4$	C-O-P-$AlPO_4$	HP-O-$AlPO_4$	O-P-O-$AlPO_4$	O-P-O-$AlPO_4$
As prepared	7		3377	2202		1640	1372	1043	822	541	
	8		3385			1643	1371	1046	823	552	418
	9		3374	2253		1645	1371	1047	823	553	435
	10	3786	3381			1649	1372	1038	823	541	419
	11		3381	2206	1730	1635	1374	1044		543	420
	12		3371		1740	1645	1373	1027	824	533	422

4.5.5 UV visible (Uv-Vis) spectroscopy analysis

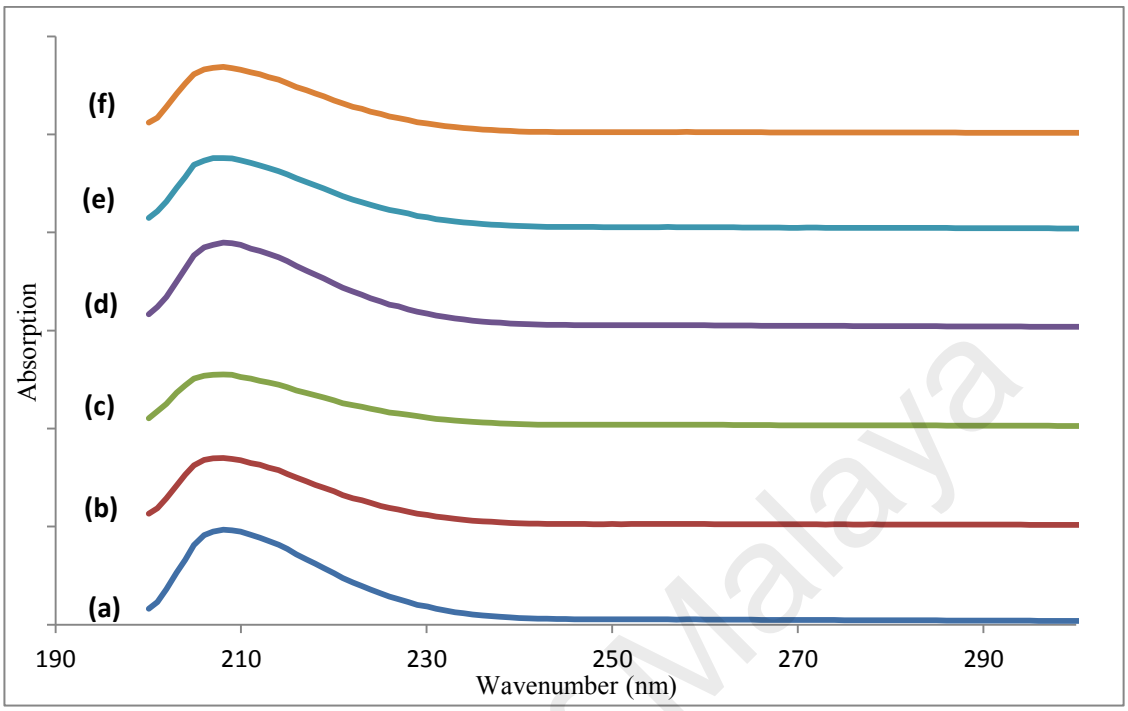

Figure 4.28: UV-vis spectra for PPVA-$AlPO_4$ nanocomposite samples at different pH values: (a) 7; (b) 8; (c) 9; (d) 10; (c) 11 and (f) 12

Figure 4.28 shows the uv-vis spectra for PPVA-$AlPO_4$ nanocomposite samples at various pH (7 – 12). The spectra demonstrates perfect curves at 208 nm for all pH values. The peak intensity for samples with pH 7 to 9 decreased following increased pH. However, the intensity suddenly increased at pH 10 but decreased again at pH 11 and 12.

The increase in peak intensity without peak shifting in the alkaline region (pH 7 to 12) is in contrast with the acidic region where a blue shift occurred at increasing pH as reported by An et al., (1996) for PPVA-Cu II system. The wavelength of absorption peak can be correlated with the type of bond in a given molecule, while peak intensity may relate to the microstructure development behavior in that a mixture of immiscible layers and particle size decreases as pH increases. This is due to the aggregation of globular primary nanoparticles from the reaction with H^+ and OH^- ions. The number of OH^- is higher at increasing pH and varies the particle shape and size. Al-OH is bonded

to Al-PO_4 at pH 10, thus reflecting the amount of amorphous and crystalline phases in the nanocomposite. Maximum peak intensity is found in sample with pH 10 where maximum bonding occurred between Al and PO_4 and produced homogeneous $AlPO_4$ nanoparticles in the system. The particles experience an aggregation at pH 11 and 12, then transforms to smaller particles and totally vanished at pH 13 as it becomes a clear solution. The formation of $AlPO_4$ is also affected by the pH values and concentration of the synthesis mixture (Ganschow et al., 2001).

4.6 Effect of crystallization time on PPVA-$AlPO_4$ optimum sample

4.6.1 Thermogravimetric (TGA) analysis

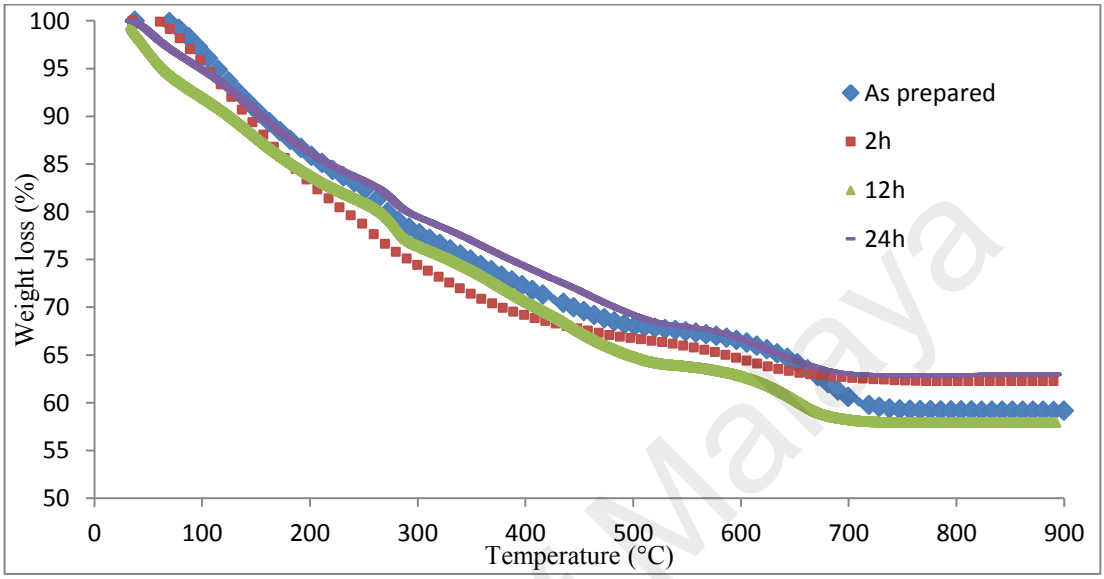

Figure 4.29: TGA traces for PPVA-$AlPO_4$ nanocomposite for samples as prepared and heat treated samples at 120°C for 2, 12 and 24 h

Figure 4.29 shows the TGA traces of PPVA-$AlPO_4$ samples at pH 10 for as prepared sample and heat treated samples at 120 °C for various crystallization times. Sample prepared at crystallization time of 2 and 24 hours produced maximum weight residue of 62 and 63 wt%, respectively. Meanwhile, the weight residue for as prepared sample and sample prepared at crystallization time of 12 hours are 59 and 58 wt%, respectively. A longer crystallization time produces higher weight residue due to more interaction between Al-O-P after the elimination of H and OH anions that affected the Al-O-P bond. The degradation stage was similar for all crystallization time and as prepared samples. Pramanik (2009) reported that the heat treated PPVA at 120 °C for 2 hours provided the maximum bonding between PVA and phosphate group. This result is in good agreement with Pramanik (2009) as the PPVA-$AlPO_4$ nanocomposite synthesized using a combination of refluxing, stirring, chemical precipitation and hydrothermal at

120 °C for 2 hours also produced maximum weight residue due to the maximum bonding between PPVA and $AlPO_4$.

4.6.1 X-Ray Diffraction (XRD) Analysis

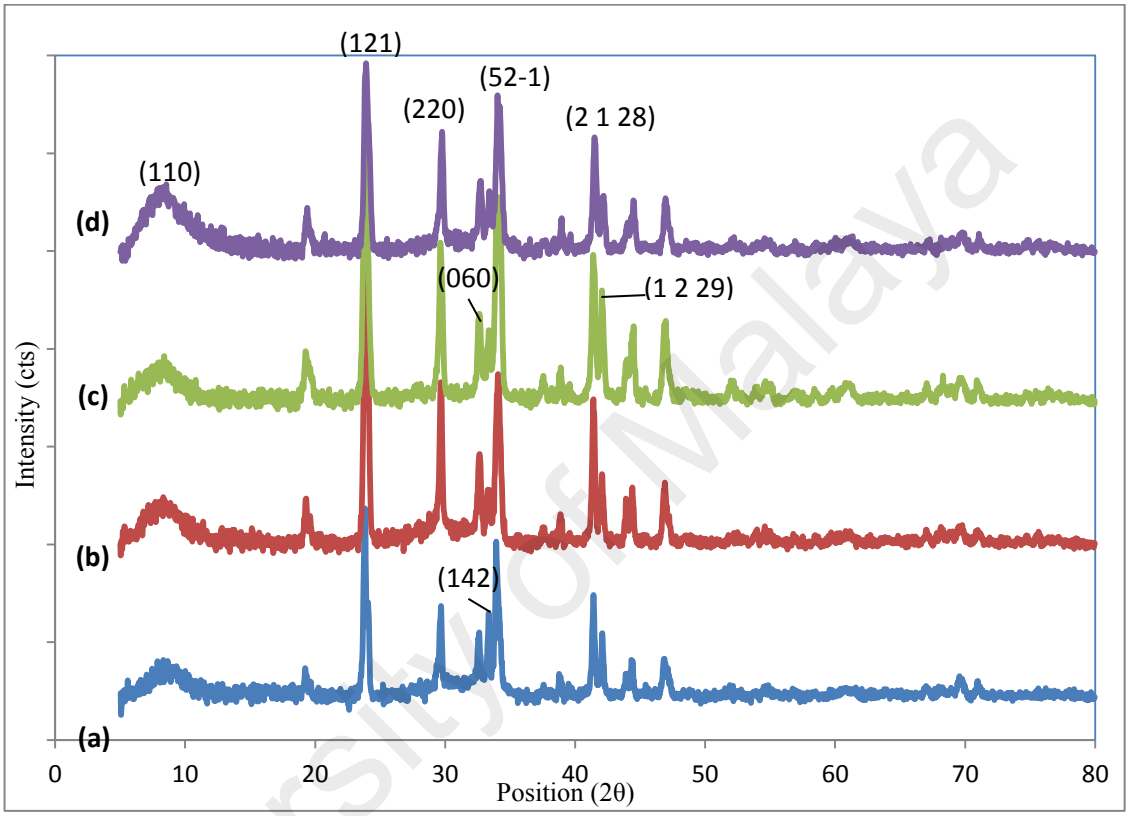

Figure 4.30: XRD patterns for PPVA-$AlPO_4$ nanocomposite samples for (a) as prepared and heat treated samples at 120°C for (b) 2 h; (c) 12 h and (d) 24 h

Figure 4.30 shows the XRD patterns for PPVA-$AlPO_4$ nanocomposite samples at pH 10 for as prepared and heat treated samples at 120 °C for various crystallization times. The XRD spectra at range of 5 – 12° (110), 23.84° (1 2 1) and 33.92° (5 2 -1) match the XRD pdf database 000-037-0189 of Potassium Aluminum Phosphate (K_2 Al_2 P_8 O_{28}) with a monoclinic crystal system. XRD peak at angle of 29.69° (220) match the XRD PDF database 000-036-1459 of Potassium Aluminum Phosphate (K Al P_2 O_7) with a monoclinic crystal system. Meanwhile 32.60° (0 6 0) and 33.34° (1 4 2) match the XRD PDF database of 98-007-4175 Aluminum Phosphate Hydrate (1/1/2.5) with hexagonal

crystal system. The XRD peak at 24.0996° (0 2 4), 41.4163° (2 1 28) and 42.0886° (1 2 29) also has the taranakite system that match the pdf reference code 01-089-0895 known as Potassium Aluminum Deuterium Phosphate Deuterate ($K_3Al_5(DPO_4)_6(PO_4)_2(D_2O)_{18}$) which has a rhombohedral crystal system. The (1 1 0) peak shows increase in intensity as crystallization time increases with maximum intensity being observed in sample with heat treated at 24 hours crystallization time. The peak also broadened as crystallization time increased due to interaction of PPVA and aluminum. The XRD peak at angle 19.27° originating from PVA and PPVA samples showed an increase in intensity from as prepared to 12 hours crystallization time samples due to interaction of PPVA with heat. The XRD peak of (121), (2 2 0), (0 6 0), (5 2 -1), (2 1 28) and (1 2 29) showed increase in intensity as crystallization time was increased to 12 hours. Then the intensity decreased as the crystallization time reached 24 hours. However, at peak of 33.34° and 37.5°, there was decrease in peak intensity as the crystallization time increased due to the Al(OH) peak that still occurred at lower temperature and slowly vanished at higher temperature or longer crystallization time.

Figure 4.31 shows the crystallite size distribution of as prepared sample and heat treated samples prepared at various crystallization times. The average crystallite size for as prepared samples is 53.26 nm and heat treated samples are 69.44 (2 hours), 67.92 (12 hours) and 57.72 nm (24 hours). The crystallite size increased as crystallization time increased to 2 hours, followed by a slight decrease at 12 hours and continued to decrease at 24 hours for most of the XRD peaks. The contrast finding is observed for peaks at angle of 32.6° and 41.4° which continued to decrease from 0 to 24 hours. However, peak at angle of 19.2° shows a fluctuating trend of the crystallite size. The dominant peak of the XRD pattern shows an increase in crystallite size until 12 hours then decrease at 24 hours.

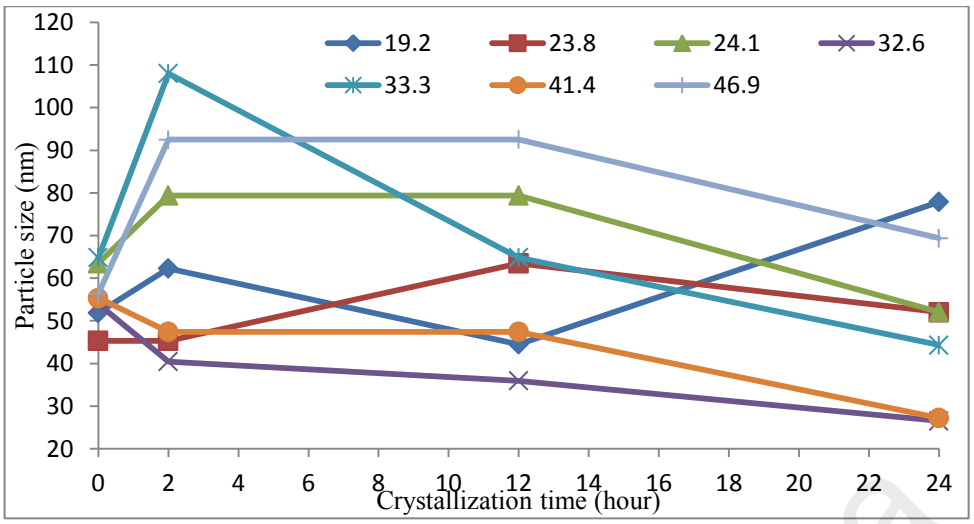

Figure 4.31: Particle size distribution for PPVA-$AlPO_4$ nanocomposite samples for as prepared sample and different crystallization time (2, 12 and 24 hours)

The variation in intensity and crystallite size of PPVA-$AlPO_4$ nanocomposite samples are due to the amount of water and OH^- and H^+ ions that influence the size and phase distribution of the various components in the system. Synthesis of PPVA-$AlPO_4$ nanocomposite in the alkaline region provides more OH^- ions in the reaction that can accelerate the crystallization of nanoparticles at lower temperature. Both H^+ or OH^- ions are expected to induce hydrolysis and condensation reactions. However, with a certain amount of water in autoclave, the induction time of crystallization will become much faster (Ma et al., 2008). Thus, the autoclaving process is suggested to produce a greater number of OH^- anion at the surface of aluminum that will increase the degree of substitution of phosphate anions (Ma et al. 2008). It is suggested that autoclaving at elevated temperature causes desorption of some phosphate from the surface of aluminum hydroxyphosphate. The decreased concentration of phosphate anions at the surface also accelerated the formation of double hydroxide bridges resulting in a more ordered structure with a lower surface area (Burrell et al., 1999). This suggests that the autoclave method promotes the synthesis kinetic by providing a sufficient amount of water that controls the crystallization process together with pH. The summary of XRD pattern, d-spacing, FWHM and calculated crystallite size is presented in Table 4.12.

Table 4.12: Summary of XRD data analysis of 2θ value, d- spacing, FWHM and crystallite size, D for PPVA-$AlPO_4$ nanocomposite at pH 10 with different crystallization time

pH 10-A				**pH 10-B**				**pH 10-C**				**pH 10-D**			
As prepared				**120 °C, 2hours**				**120 °C, 12hours**				**120 °C, 24hours**			
Pos. [°2Th.]	FWHM [°2Th.]	d-spacing [Å]	XRD crystal size, D (nm)	Pos. [°2Th.]	FWHM [°2Th.]	d-spacing [Å]	XRD crystal size, D (nm)	Pos. [°2Th.]	FWHM [°2Th.]	d-spacing [Å]	XRD crystal size, D (nm)	Pos. [°2Th.]	FWHM [°2Th.]	d-spacing [Å]	XRD crystal size, D (nm)
19.2669	0.1535	4.6069	51.90	19.2875	0.1279	4.6020	62.29	19.2746	0.1791	4.6050	44.48	19.4148	0.1023	4.57	77.87
23.8395	0.1791	3.7326	45.32	23.8538	0.1791	3.7303	45.32	23.7944	0.1279	3.7395	63.46	23.8202	0.156	3.73	52.03
-	-	-	-	-	-	-	-	-	-	-	-	23.9378	0.0936	3.72365	86.75
24.0996	0.1279	3.6929	63.50	24.1181	0.1023	3.6901	79.39	24.1019	0.1023	3.6925	79.39	24.2214	0.156	3.67157	52.07
29.6909	0.2047	3.0089	40.14	29.679	0.1791	3.0101	45.88	29.6363	0.1279	3.0143	64.24	-	-	-	-
-	-	-	-	-	-	-	-	29.7892	0.1023	2.9992	80.34	29.769	0.312	2.99877	26.34
32.6094	0.1535	2.7460	53.91	32.6842	0.2047	2.7399	40.43	32.6681	0.2303	2.7412	35.94	32.7229	0.312	2.73451	26.53
				33.2814	0.0936	2.6898	88.57	-	-	-	-	-	-	-	-
33.3428	0.1279	2.6873	64.83	33.3968	0.0768	2.6830	107.98	33.3345	0.1279	2.6879	64.82	33.3792	0.1872	2.68223	44.29
33.9213	0.1023	2.6427	81.17	-	-	-	-	33.924	0.0768	2.6425	108.13	-	-	-	-
				34.0873	0.1535	2.6302	54.12	34.0978	0.1023	2.6295	81.21	34.0287	0.156	2.6325	53.24
-	-	-	-	-	-	-	-	34.2736	0.1279	2.6164	64.99	34.2378	0.156	2.6169	53.27
41.4163	0.1535	2.1802	55.32	41.385	0.1791	2.1817	47.41	41.3785	0.1791	2.1821	47.40	41.5205	0.312	2.17317	27.22
42.0886	0.1279	2.1469	66.54	42.0666	0.1023	2.1479	83.19	42.0862	0.2047	2.1470	41.57	42.0811	0.156	2.14551	54.55
44.385	0.1535	2.0410	55.88	-	-	-	-	44.5017	0.0768	2.0359	111.75	44.5002	0.1248	2.03433	68.76
-	-	-	-	-	-	-	-	46.8284	0.1872	1.9384	46.24	-	-	-	-
46.838	0.1535	1.9397	56.39	46.9265	0.0936	1.9394	92.51	46.96	0.0936	1.9381	92.52	46.9293	0.1248	1.93453	69.38

4.6.2 Fourier Transform Infrared (FTIR) spectroscopy analysis

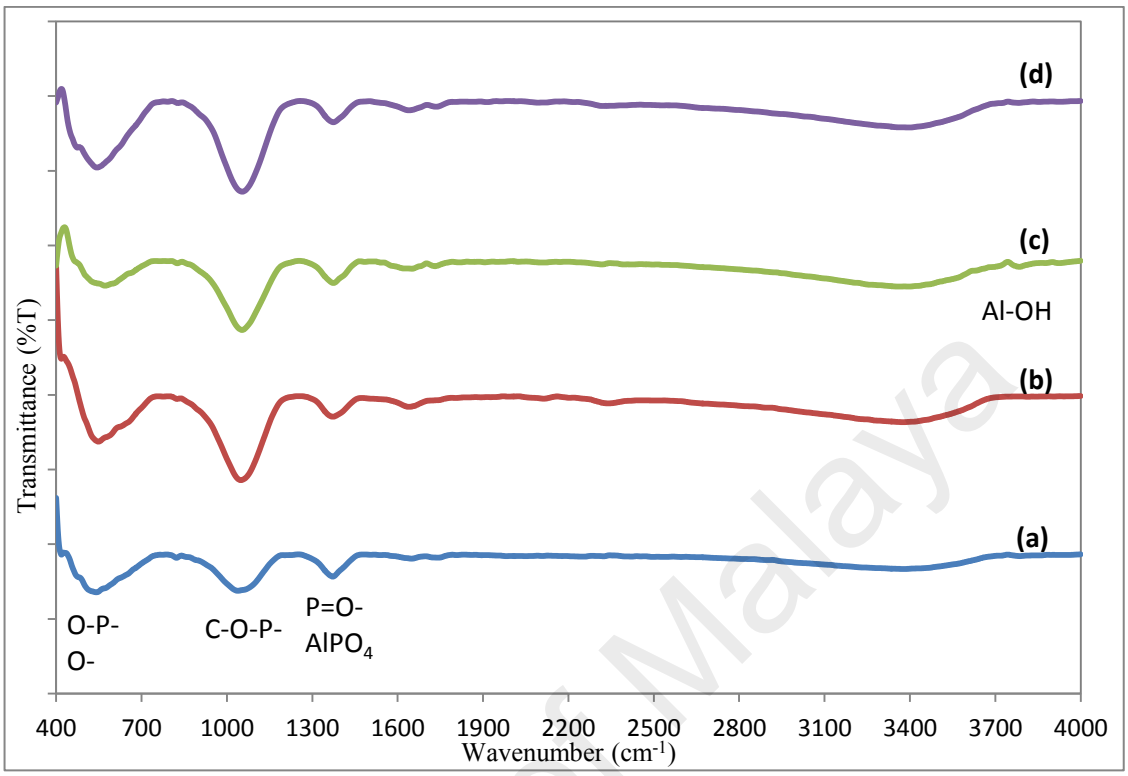

Figure 4.32: FTIR spectra for PPVA-$AlPO_4$ nanocomposite samples (a) as prepared and heat treated samples at 120 °C for (b) 2 h; (c) 12 h and (d) 24 h

Figure 4.32 shows the FTIR spectra for PPVA-$AlPO_4$ nanocomposites at pH 10 for as prepared and heat treated samples at 120 °C for various crystallization times. The Al-OH band was observed in as prepared and 12 hours samples due to the OH group. Samples prepared at lower crystallization time (2 hours) and at 12 hours show no Al-OH band. All samples produced OH peak (3371 – 3402 cm^{-1}), C-OH water bending (1615 – 1650 cm^{-1}), PO-$AlPO_4$ (1369 – 1376 cm^{-1}) and C-O-P-$AlPO_4$ (1030 – 1058 cm^{-1}) and O-P-O-$AlPO_4$ (541 – 593 cm^{-1}) regardless of crystallization time. Meanwhile, a few samples (2 hours crystallization time) showed the Al-O-P band in the region of 2349 – 2090 cm^{-1}. These samples show no water bending at range of 1730 – 1740 cm^{-1}. Figure 4.34 (a) and (b) shows the effect of crystallization time for the four FTIR bands. Both PO-$AlPO_4$ and C-O-P-$AlPO_4$ bands are shifted to higher wavenumber as the crystallization time increases. The OH band in Figure 4.34 (b) also had a similar trend.

However, O-P-O band is shifted to higher wavenumber until 12 hours of crystallization time. Beyond that, the wavenumber is shifted back to lower wavenumber. The shifted peak towards higher wavenumber shows that the OH band influences the PO-$AlPO_4$ and C-O-P-$AlPO_4$ bands. The amount of water increased for samples from 2 to 12 hours crystallization time. However at higher crystallization time of 24 hours, dehydration of sample took place and produced a peak which shifted back to the lower wavenumber. From the observation, sample prepared with 2 hours crystallization time produced more Al-O-P bond, less Al-OH and no water bending H-O-H at range of 1730 – 1740 cm^{-1}. The summary of the FTIR spectra bands for all crystallization and pH reaction is presented in Table 4.13.

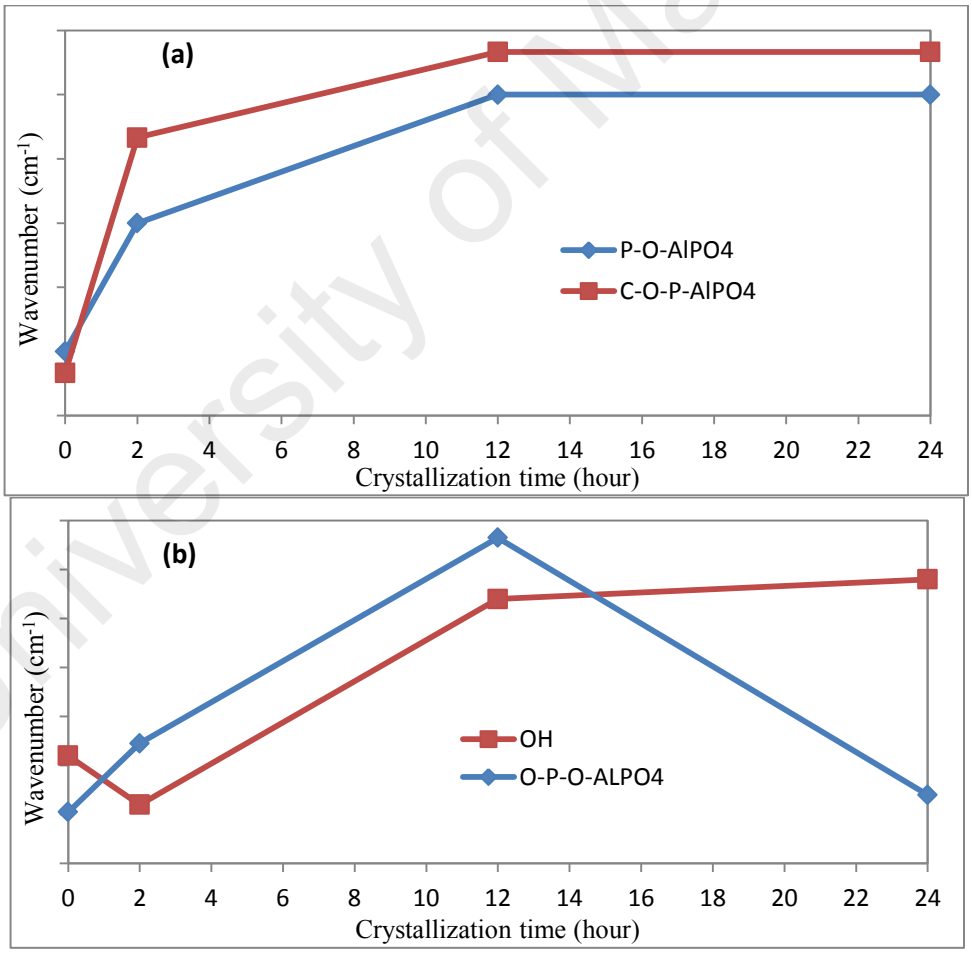

Figure 4.33: FTIR band of PPVA-$AlPO_4$ nanocomposite samples at pH 10 for as prepared and at various crystallization times in the range: (a) PO-$AlPO_4$ (1371 – 1374 cm^{-1}) and C-O-P-$AlPO_4$ (1027 – 1047 cm^{-1}) and (b) OH (3371 – 3385 cm^{-1}) and O-P-O-$AlPO_4$ (533 – 553 cm^{-1})

Table 4.13: Interpretation of PPVA-$AlPO_4$ nanocomposite FTIR spectra at various pH (7, 8, 9, 10, 11 and 12)

		Band assignment and wavenumber (cm^{-1})										
Sample	pH	Al-OH	OH	Al–O–P	Al–O–P	H-O-H	C-OH@ H-O-H	P-O-$AlPO_4$	C-O-P-$AlPO_4$	HP-O-$AlPO_4$	O-P-O-$AlPO_4$	O-P-O-$AlPO_4$
As prepared	pH 7-A		3377	2202			1640	1372	1043	822	541	
	pH 8-A		3385				1643	1371	1046	823	552	418
	pH 9-A		3374	2253			1645	1371	1047	823	553	435
	pH 10-A	3786	3381				1649	1372	1038	823	541	419
	pH 11-A		3381	2206		1730	1635	1374	1044		543	420
	pH 12-A		3371			1740	1645	1373	1027	824	533	422
120°C, 2h	pH 7-B		3374				1638	1369	1056		553	430
	pH 8-B		3378		2114		1640	1372	1050		546	415
	pH 9-B		3379	2341	2110		1640	1372	1048		545	419
	pH 10-B		3376	2340	2113		1640	1373	1049		549	418
	pH 11-B		3375				1644	1374	1049		546	
	pH 12-B		3379				1645	1374	1042		526	
120°C, 12h	pH 7-C	3786	3398	2349			1641	1369	1058		548	
	pH 8-C	3785	3389			1732	1653	1369	1055		560	408
	pH 9-C	3784	3399		2117		1644	1371	1056		550	
	pH 10-C	3785	3397			1732	1650	1374	1053	826	573	
	pH 11-C	3784	3368			1731	1647	1373	1052		562	
	pH 12-C	3784	3287			1732	1615	1370	1051	824		463, 409
120°C, 24h	pH 7-D		3395		2091		1641	1376	1057		552	
	pH 8-D		3404				1638	1375	1054		559	455
	pH 9-D		3402				1639	1375	1055		552	
	pH 10-D		3399			1735		1374	1053		543	
	pH 11-D		3375	2338	2090	1736	1643	1375	1048		558	
	pH 12-D	3787	3353		2164	1737		1372	1030	824	593	501,462

4.6.3 Field Emission Scanning Electron Microscopy (FESEM) Analysis

Figure 4.34 shows the FESEM images for PPVA-AlPO4 nanocomposite samples at pH 10 for as prepared and heat treated at 120 °C for various crystallization times. All samples contained spherical and layered structures. Spherical particles are observed in the as prepared samples as shown in Figure 4.34 (a). Layer structure formation is observed on the sample surface. The layer structure ratio increases and exists between the spherical particles as the crystallization time increases as shown in Figure 4.34 (c). No obvious change is observed in the particle size below 30 nm for all crystallization times. As the crystallization time increases, the ratio of component particulate and layer varies. The spherical particles are dominant at shorter crystallization time. However, at the longer crystallization time, the particles agglomerated to form layered structure. More layered structure is observed at 24 hours crystallization time compared to other samples. The spherical particle reduces as the crystal nucleation and growth accelerated at longer crystallization time. Yang et al., (2014) observed similar results whereby the crystallization time only influenced the aspect ratio and uniformity of particles.

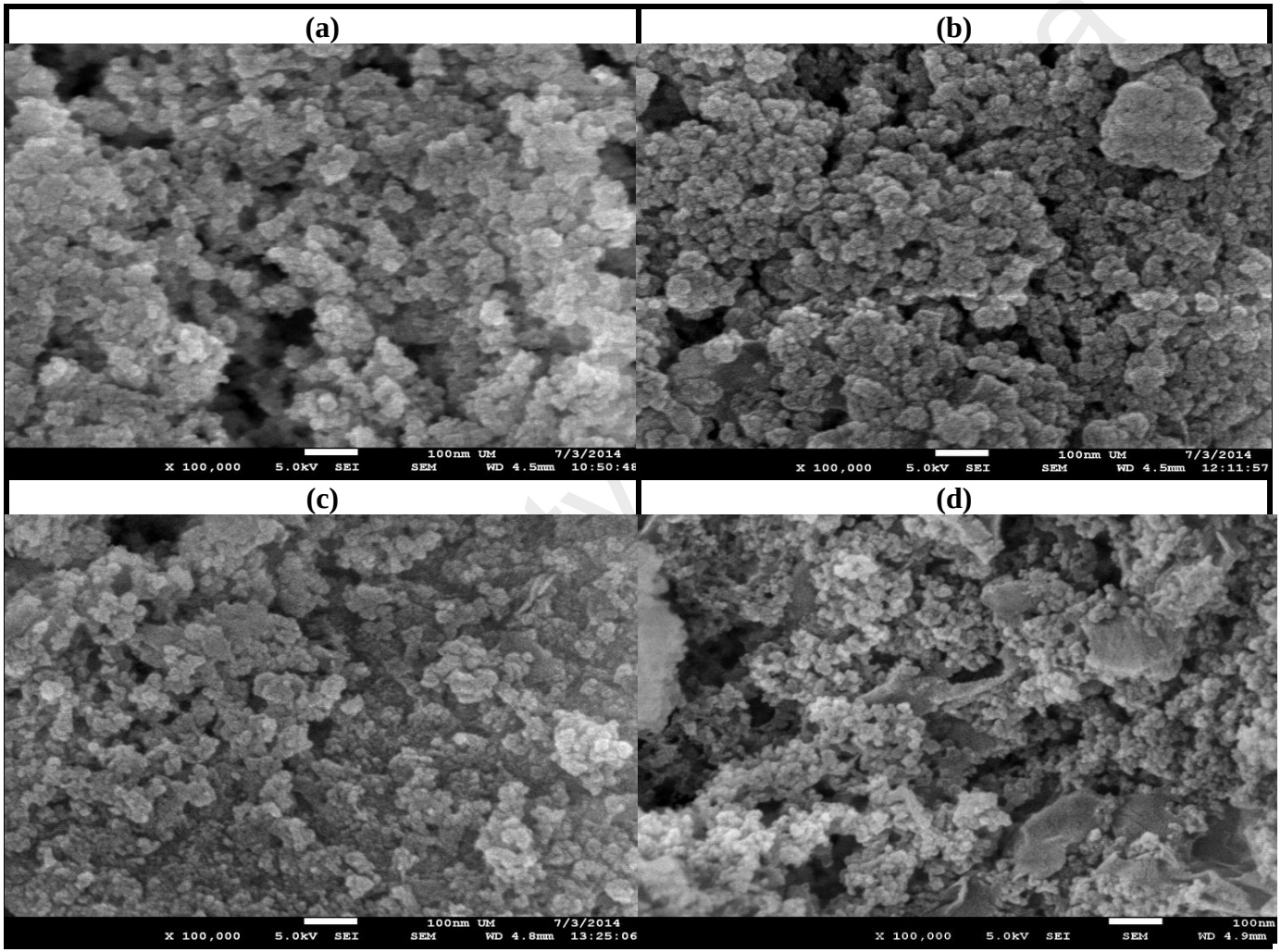

Figure 4.34: FESEM micrographs of PPVA-$AlPO_4$ nanocomposite samples for (a) as prepared and heat treated samples at 120°C for various crystallization time (b) 2 h; (c) 12 h and (d) 24 h

Figures 4.35 to 4.40 show the FESEM micrographs of PPVA-$AlPO_4$ nanocomposites at various crystallization times (2, 12 and 24 hours) and pH (7, 8, 9, 10, 11 and 12). Samples prepared at 2 hours crystallization time show spherical nanoparticles at pH 7, 8 and 9 as shown in Figures 4.35 and 4.36. Meanwhile, layered mixed with spherical and nanotube structures are observed at pH 10. However, more layers, nanotubes and heterogeneous structures are observed at pH 11 compared to spherical particles. Sample prepared at pH 12 shows spherical particles with less nanotube and bulk crystal of $AlPO_4$. The average particles size is less than 15 nm.

Figures 4.37 and 4.38 show the FESEM micrographs of PPVA-$AlPO_4$ nanocomposites prepared at 12 hours crystallization time. Sample prepared at pH 7 shows mainly spherical nanoparticles whereas samples prepared at pH 8 shows spherical particles with small ratio of flake layer. More structured layers of $AlPO_4$ are observed at pH 9 than at pH 8, which are immiscible between the spherical nanoparticles. Meanwhile, a bulky structure of heterogeneous shapes of $AlPO_4$ with distribution of spherical nanoparticles on the surface is observed at pH 10. The heterogeneous shape of $AlPO_4$ grew more and mixed with spherical particles and layered structures in the system at pH 11. Bulk structure with heterogeneous shape and without spherical nanoparticles is observed at pH 12. The average particle size for samples prepared at pH 7 – 11 is less than 10 nm.

Figures 4.39 and 4.40 show the FESEM micrographs of PPVA-$AlPO_4$ nanocomposite samples prepared at 24 hours crystallization time. Sample prepared at pH 7 shows spherical nanoparticles with flake layer structure. Meanwhile, samples prepared at pH 8 and 9 show homogeneous distribution of nanoparticles on the surface of PPVA-$AlPO_4$ nanocomposite. Spherical nanoparticles are distributed on the surface of layer structures as observed at pH 10. Also being observed is a small ratio of nanotube which co-exists with spherical and layered structures. Less spherical nanoparticles are observed at pH 11, where the nanoparticles embedded at the surface of the bulk $AlPO_4$ together with

aligning nanoparticles and formed and entangled link like hair. However, all the spherical nanoparticles slowly vanished and agglomerated to form flake layers and combined to produce bulk size $AlPO_4$. Sample prepared at shorter crystallization time of 2 hours shows homogeneous nanospherical particles at lower pH.

However, it produced a mixture of spherical and entangled aligned nanoparticles which formed a shape of similar to the nanotube at higher pH like 11. Yet, there is no study to confirm the occurrence of holes in the similar nanotube structure. The average particle size for samples prepared at pH 7, 8 and 9 is below than 13 nm. The size is slightly larger than 13 nm at pH 11. However, the size reduces to below than 11 nm at pH 12. Kawamura et al., (2007) reported that by controlling the pH and temperature, the number of H^+ and OH^- ions affecting the morphologies of PPVA-$AlPO_4$ nanocomposites can be controlled. Our observations suggest that at shorter crystallization time, the morphologies are affected by pH but not the size of particles. However, at longer crystallization time, it was observed that pH variation varied the geometrical structure and also the size of spherical particles. Palacios et al., (2013) also reported the similar observation of geometrical structure, nevertheless they observed an increase in particle size with increase of crystallization time.

Additionally, they also observed an agglomeration and heterogeneous morphology phase distribution as crystallization time increases. Yang & Kau (2005) reported that the dehydration and condensation of EO fraction used to synthesis $AlPO_4$ nanoparticle produced a chain shape. Thus the heat treatments do affect the morphologies of $AlPO_4$. Other than that, they elaborated that the phosphate ion condensation/polymerization leads to the formation of condensed phosphates, which can be linear, cyclic and or cross-linked/branched phosphates formed upon drying at higher temperature. This observation explained the occurrence of nanotube structures that appeared at pH 10 to 12 after autoclaving process. Burrell et al., (1999) reported that the various

morphologies occurred after autoclaving is due to the occurrence of double hydroxide bridges during autoclaving process. This double hydroxide bridge varies by the number of H^+ and OH^- ions present that may also contribute to the formation of nanotube structures.

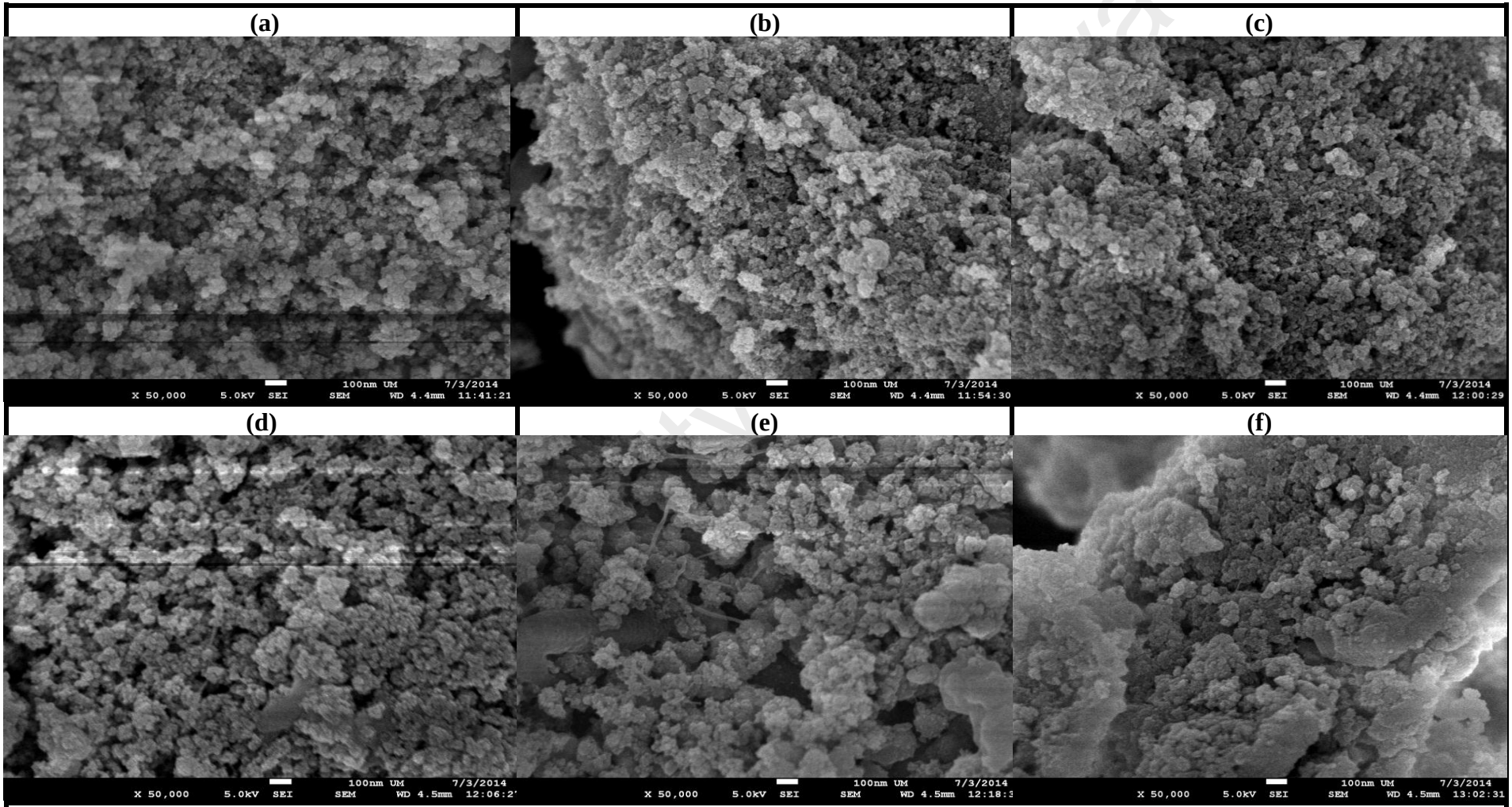

Figure 4.35: FESEM micrographs of PPVA-$AlPO_4$ nanocomposites prepared at 120 °C for 2 hours at different pH (a) 7; (b) 8; (c) 9; (d) 10; (e) 11 and (f) 12 at 50x magnification

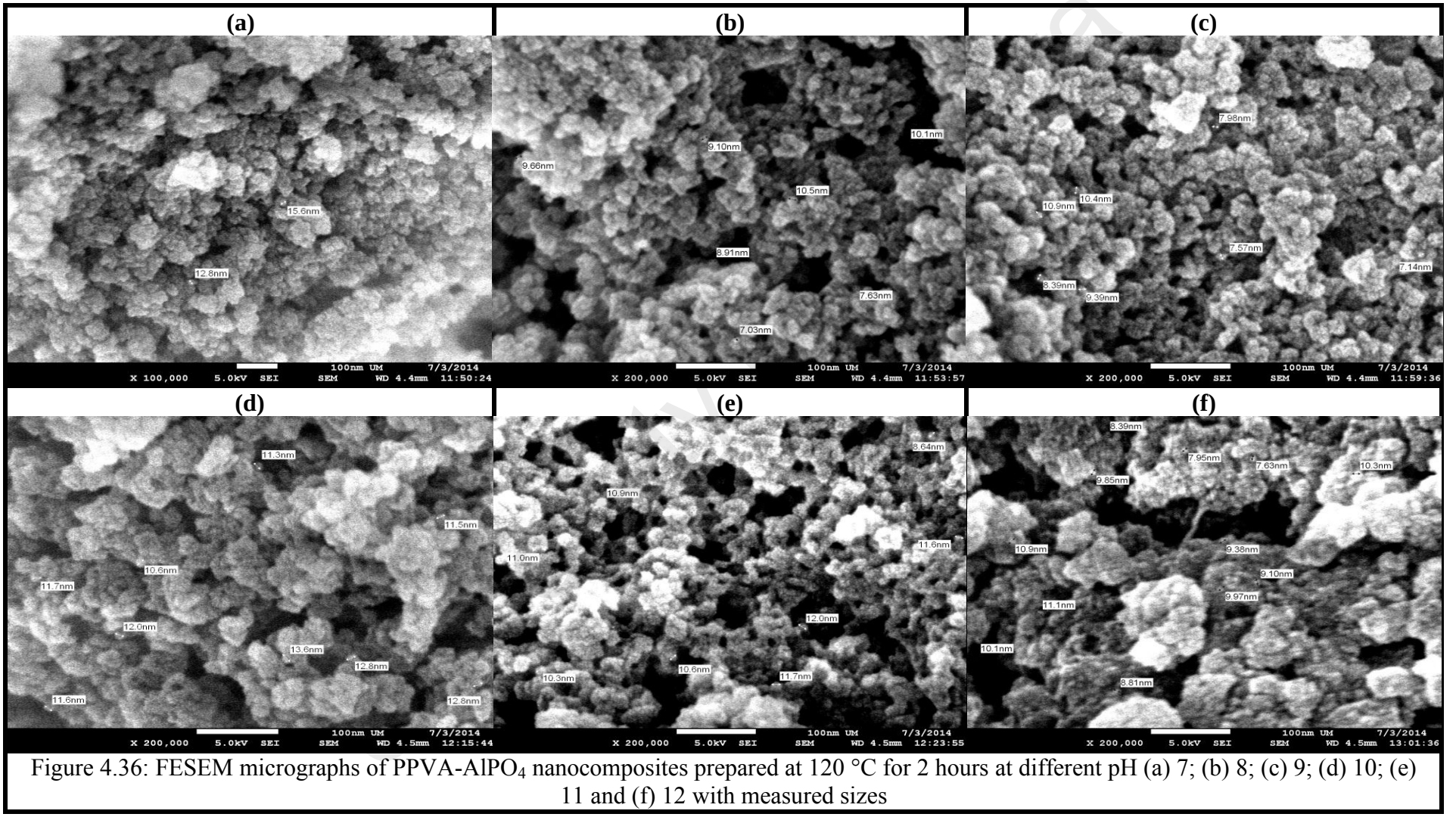

Figure 4.36: FESEM micrographs of PPVA-$AlPO_4$ nanocomposites prepared at 120 °C for 2 hours at different pH (a) 7; (b) 8; (c) 9; (d) 10; (e) 11 and (f) 12 with measured sizes

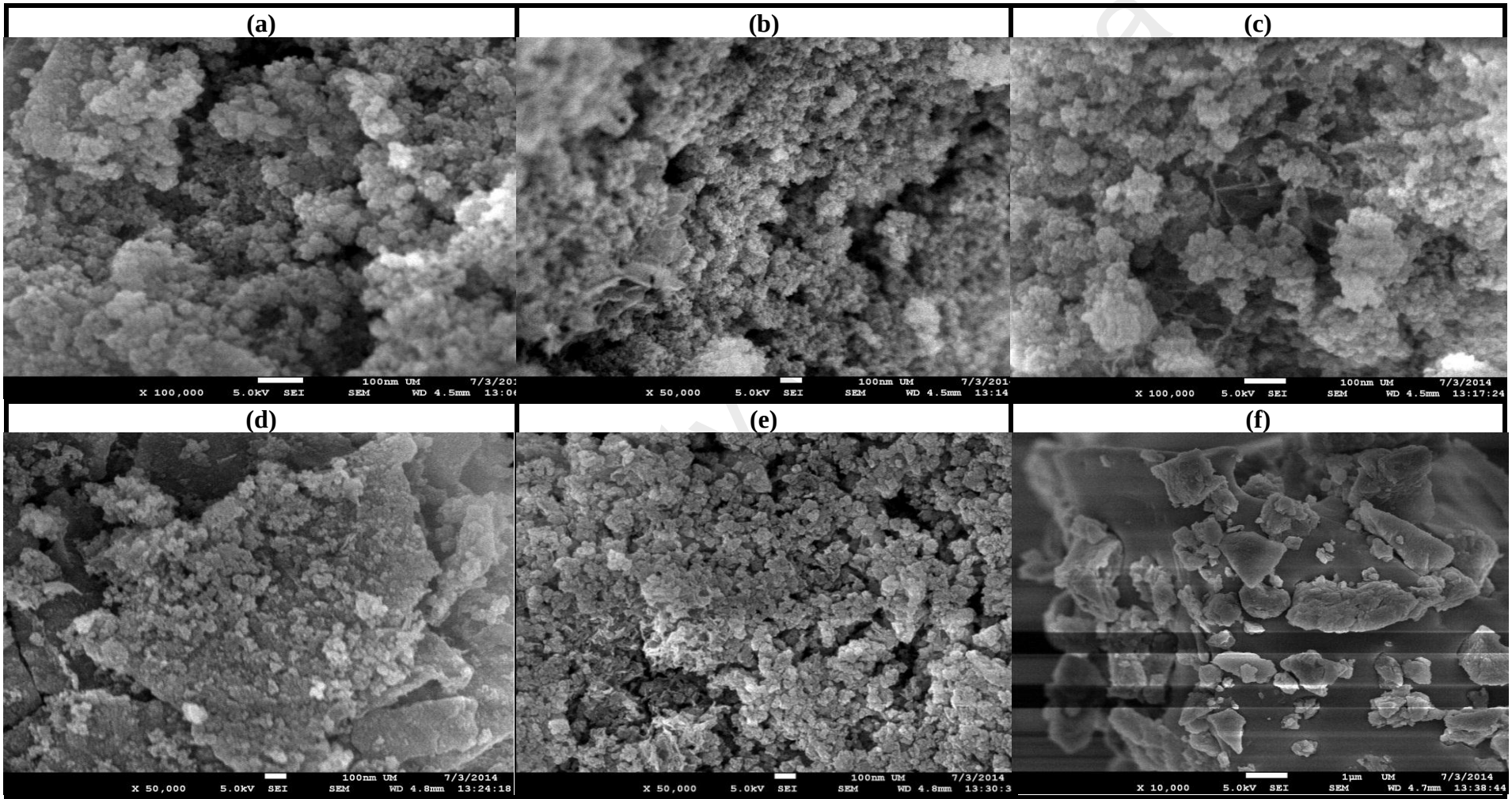

Figure 4.37: FESEM micrographs of PPVA-$AlPO_4$ nanocomposites prepared at 120 °C for 12 hours at different pH (a) 7; (b) 8; (c) 9; (d) 10; (e) 11 and (f) 12

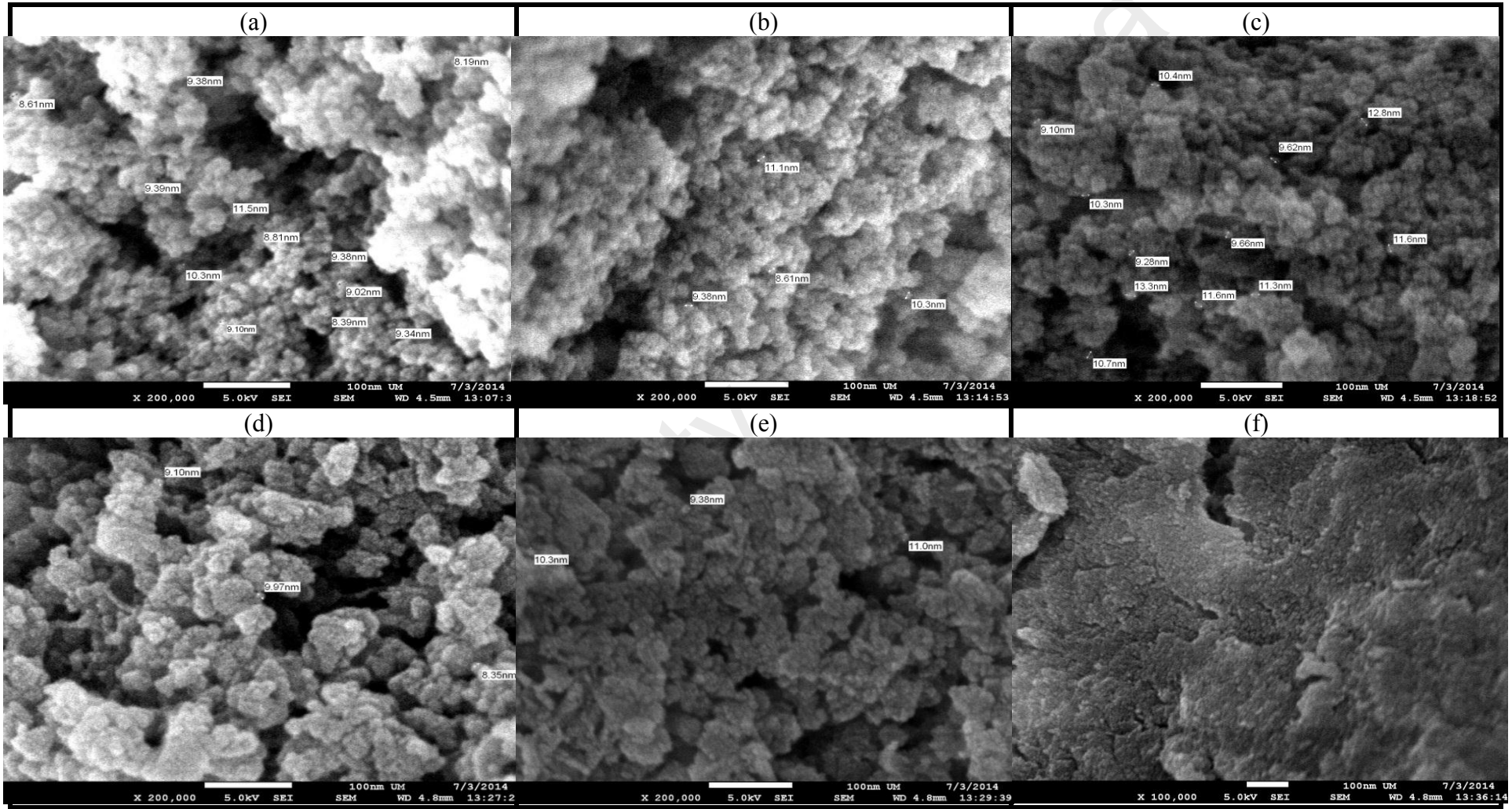

Figure 4.38: FESEM micrographs of PPVA-$AlPO_4$ nanocomposites prepared at 120 °C for 12 hours at different pH (a) 7; (b) 8; (c) 9; (d) 10; (e) 11 and (f) 12 with measured sizes

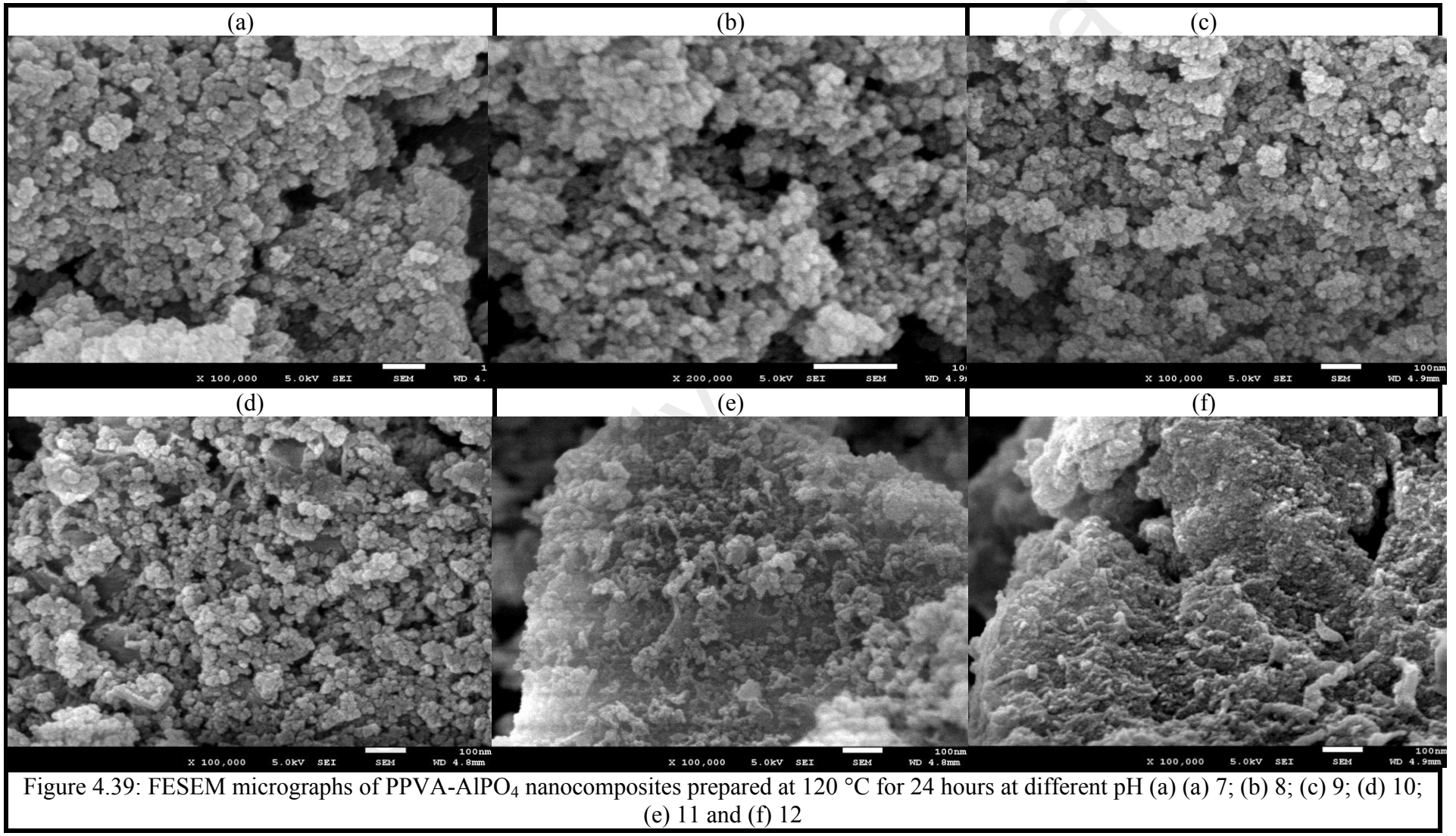

Figure 4.39: FESEM micrographs of PPVA-$AlPO_4$ nanocomposites prepared at 120 °C for 24 hours at different pH (a) (a) 7; (b) 8; (c) 9; (d) 10; (e) 11 and (f) 12

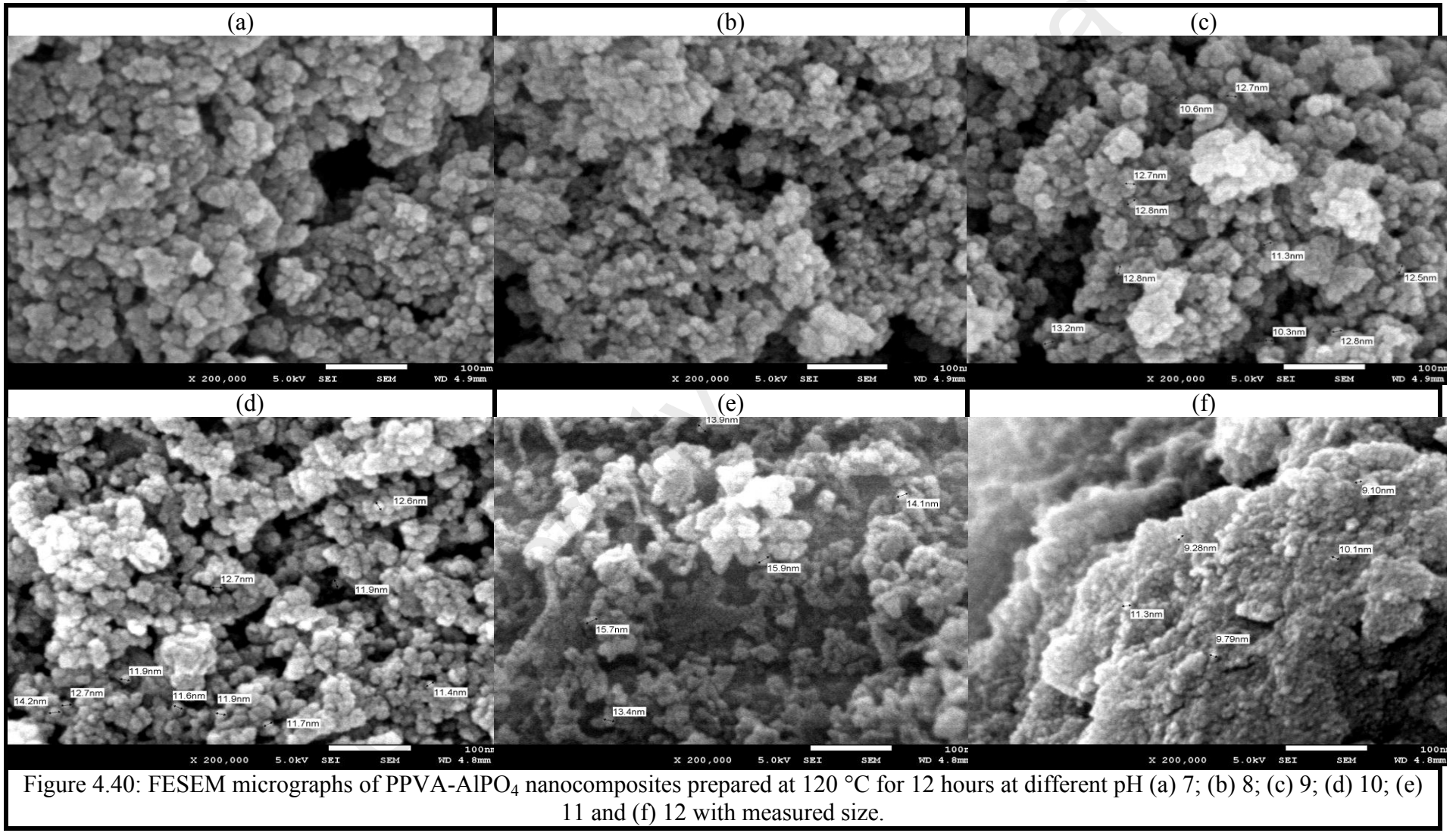

Figure 4.40: FESEM micrographs of PPVA-$AlPO_4$ nanocomposites prepared at 120 °C for 12 hours at different pH (a) 7; (b) 8; (c) 9; (d) 10; (e) 11 and (f) 12 with measured size.

4.7 Comparative studies on PVA, PPVA and PPVA-$AlPO_4$ nanocomposites at pH 10

4.7.1 Thermal Analysis (DSC, SDTA, TGA)

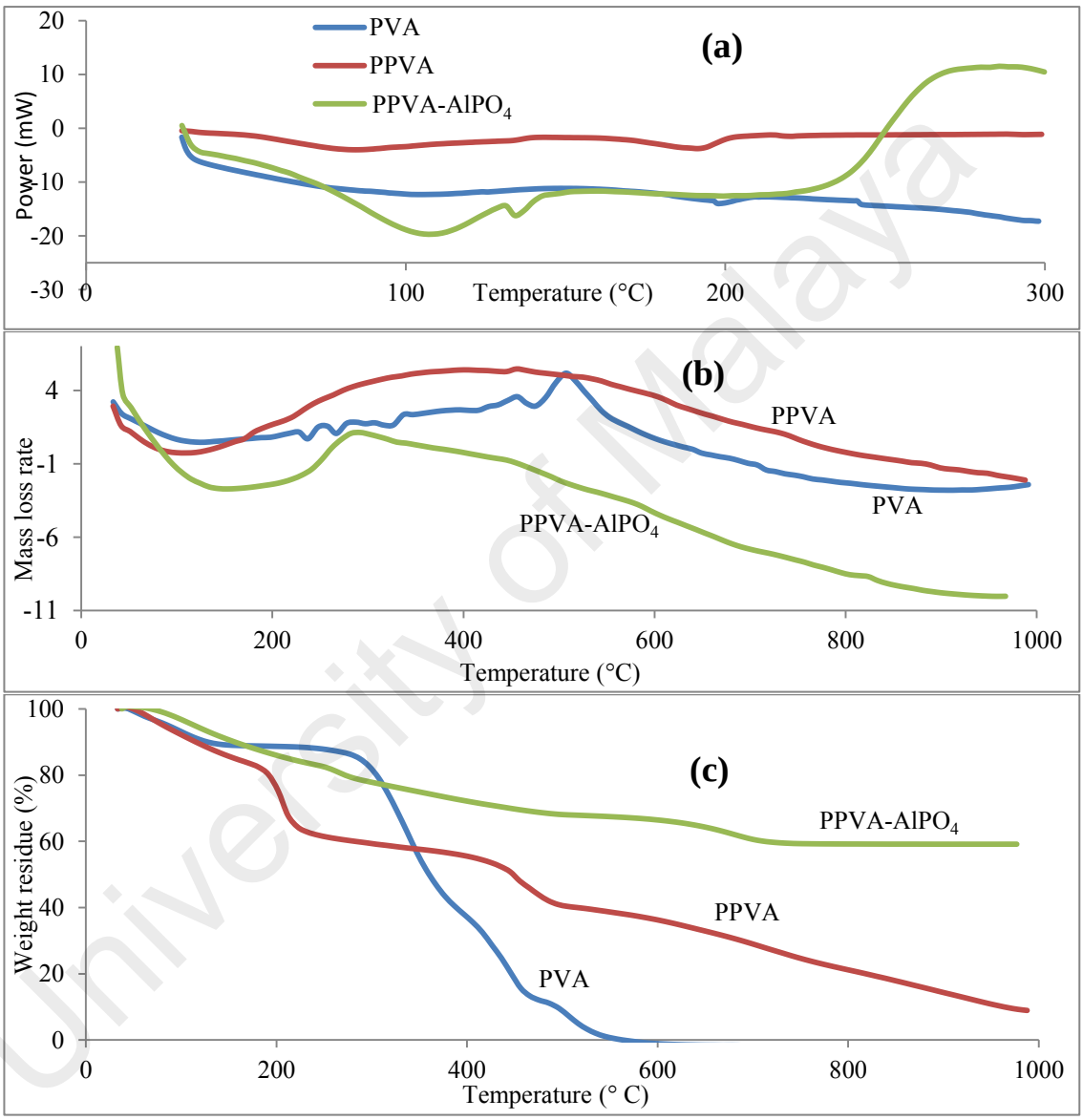

Figure 4.41: Thermal analysis patterns (a) DSC; (b) SDTA and (c) TGA for PVA, PPVA and PPVA-$AlPO_4$ samples

Figures 4.41 (a) and (b) show the DSC and SDTA patterns for PVA, PPVA and PPVA-$AlPO_4$ samples. An endothermic change is observed in DSC traces till 300 °C, while endothermic and exothermic changes are observed in SDTA traces until 1000 °C. Table

4.9 summarizes all the thermal results. PPVA-$AlPO_4$ optimum samples show a broad endothermic peak at the range of 30 – 250 °C. TGA results show the same at range of 0 - 280 °C. PPVA-$AlPO_4$ optimum sample released adsorbed and/or coordinated water with 21% weight loss. Moisture is eliminated at temperature below 100°C (Mekky & Nicholson, 2007). The elimination of water at temperature lower than 150°C is related to crystal water, whereas at temperature higher than 150°C it is related to water with coordination of the metal atom (Boonchom & Kongtaweelert, 2010; Bhagwat et al., 2003). Observation shows that PPVA has interaction with aluminum. The large endothermic peak within the range of 30 – 250°C may be due to elimination of water or dehydration produced by endothermic effect and phase transformation. Possible phase transformation occurs for $AlH_2(PO_4)_3$ + $AlH_3(PO_4)_2.H_2O$ at 105°C (Chen et al., 2003) and $AlPO_4 \cdot H_2O$-H_4 to $AlPO_4$+H_2O at 120°C (Boonchom et al. 2008). Meanwhile Druppel et al., (2007) reported that thermal stability at 200°C will limit the variscite and transform to more stable phases such as berlinite, augelite, trolleite and Al-metaphosphate [$Al(PO_3)_3$]. Most effective bonding occurred at 200°C in the form of $AlH_2(PO_4)_3$ and at 220°C in the form of $AlH_2(PO_4)_3$ and transformed it to the mixture of $AlH_2P_3O_{10}.2H_2O$ and $AlPO_4$ (trigonal system) (Chen et al., 2003). Spontaneous degradation of PPVA is also involved in this stage (285°C) and is associated with the exothermic peak as shown in SDTA pattern. Elimination of light organics occur at (270°C) (Mekky & Nicholson, 2007) and degradation of PPVA in PPVA-$AlPO_4$ composites started at 210°C until 346°C (Kalbasi & Izadi, 2013). Phase transformation of low temperature phosphor-berlinite to high temperature phosphor-tridymite may also occur with endothermic peak below 100 and 500°C. SDTA pattern shows that the 9 wt% of weight loss which occurred from 280 to 450°C involved the breakage of a carbon backbone at 455°C due to degradation of PPVA. A variation of $AlPO_4$ crystal system without dehydration started at 400 – 1000°C (Chen et al., 2003). 11 wt% weight

loss from 450 to 720°C and small endothermic peak at 680°C are due to decomposition of all organic materials and completion of a $AlPO_4$ crystallization (Mekky & Nicholson, 2007). Meanwhile, the 59 wt% weight loss which occurred from 720 to 1000°C is due to total decomposition of PPVA-$AlPO_4$ nanocomposite. Additional endothermic peak is observed without weight loss at 820°C due to phase transformation of amorphous $AlPO_4$ to crystalline α-cristobalite $AlPO_4$ (Campelo et al., 2003). The degradation of PPVA and PPVA-$AlPO_4$ samples begin at lower temperature compared to PVA. The first stage of degradation for PPVA and PPVA-$AlPO_4$ samples occur at a faster rate compared to PVA, whereas the second stage of degradation is a slower process. The amount of weight residue for PPVA-$AlPO_4$ sample (59 wt%) is higher compared to PPVA(10 wt%) and PVA (0 wt%). The higher weight residue is attributed from the higher crosslinking of di-phosphate and tri-phosphate as well as reactions with $AlPO_4$. The reaction of PPVA with $AlPO_4$ also results in an increase of the char formation which remains unoxidized in the waste at temperature higher than 700°C. As a result, the thermal stability of PPVA-$AlPO_4$ sample is improved compared to pure PVA and PPVA samples due to the interfacial bonding between $AlPO_4$ and PPVA. PPVA-$AlPO_4$ with $AlPO_4$ in the system catalyzes the char formation through promoting dehydrogenation of polymers at relatively lower temperature and finally improving the thermal stability of PPVA-$AlPO_4$ samples at higher temperature. Thus, enhancing the endurance of PPVA-$AlPO_4$ samples against thermal oxidation at high temperature due to the charring of polymers. The residue amount of PPVA-$AlPO_4$ sample is larger due to the residue of nanocomposites consisting of both char from the polymer matrix along with the $AlPO_4$ residue.

Table 4.14: Thermal properties of PVA, PPVA and PPVA-$AlPO_4$ optimum samples

Thermal properties	**PVA**		**PPVA**		**PPVA-$ALPO_4$**	
DSC	T (°C)		T (°C)		T (°C)	
T_g,	54		-		-	
1st peak	-		84 (broad endothermic peak)		30-250 (broad endothermic peak)	
2nd peak, T_m	195 (endo)		191(endo)		-	
SDTA	T (°C)		T (°C)		T (°C)	
1	30-200 (broad endothermic peak)		30-200 (broad endothermic peak)		30-250 (broad endothermic peak)	
2	250		-		285	
3	500 (exothermic peak)		450 (exothermic peak)		455 (exothermic peak)	
4	-		670		680	
					820 (exothermic peak)	
TGA	T (°C)	Weight residue (%)	T (°C)	Weight residue (%)	T (°C)	Weight residue (%)
1st stage	0 – 300	14	0-200	20	0-280	21
2nd stage	300-450	71	200-450	27	280-450	9
3rd stage	450-600	15	450-950	43	450-720	11
Final Weight residue	600-1000	0	950-1000	10	720-1000	59

4.7.1 X- Ray Diffraction (XRD) Analysis

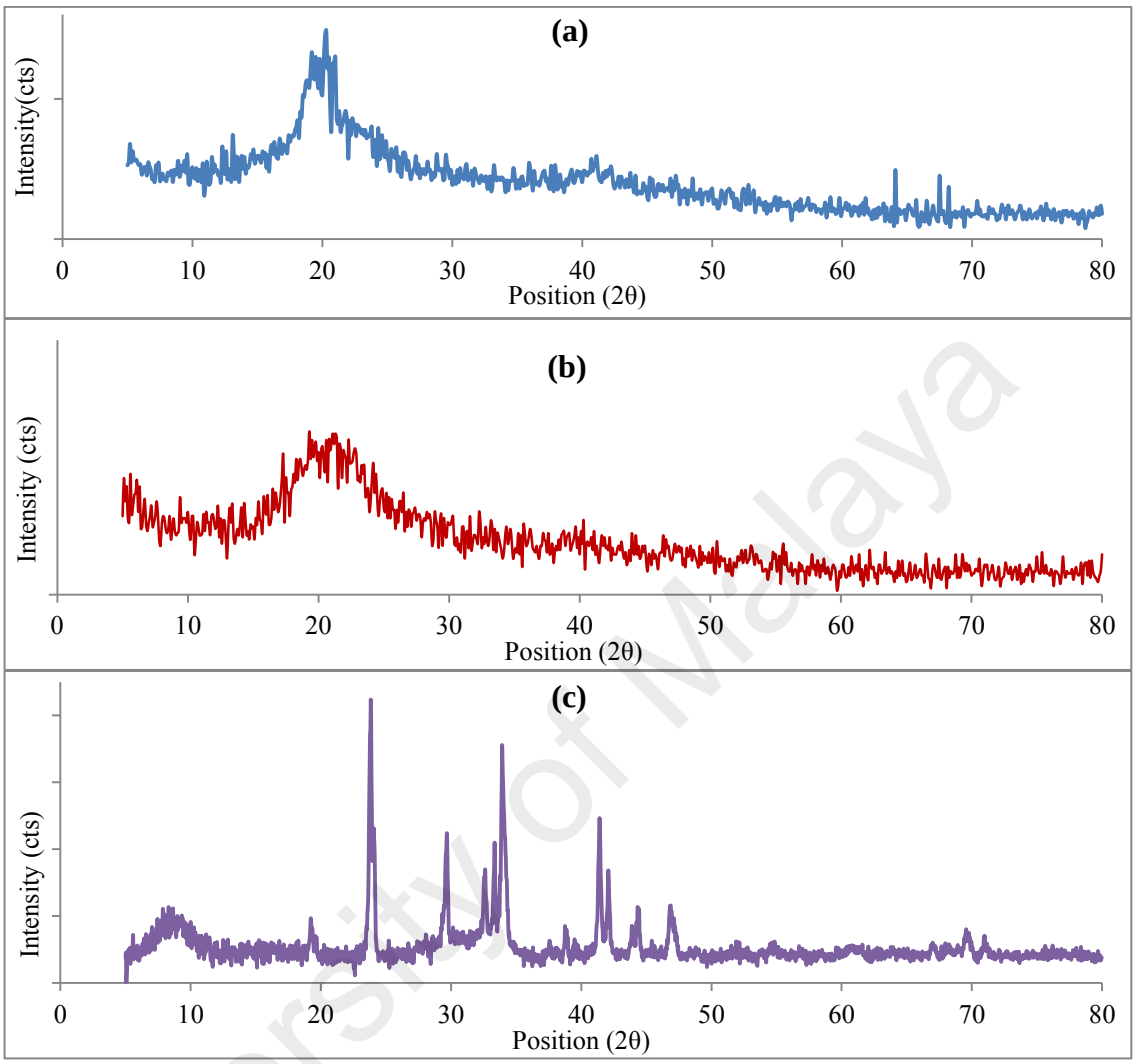

Figure 4.42: XRD patterns for (a) PVA; (b) PPVA and (c) PPVA-$AlPO_4$ optimum samples

Figure 4.42 shows the XRD patterns for PVA, PPVA and PPVA-$AlPO_4$ nanocomposite optimum samples. The XRD pattern for the PPVA-$AlPO_4$ samples (Figure 4.42 (c)) shows an amorphous phase at lower angle. However, the XRD pattern shows many several reflection peaks at higher angle which are indicative of a crystalline material. The peak for PPVA-$AlPO_4$ sample observed at angle of 19.27° originated from PVA and PPVA samples and shifted to lower angle. It became more intense and more crystalline due to interaction with the modified polymer. The left shift of the peak location corresponds to the decrease of basal spacing, which suggests that polymer

chains have encapsulated the $AlPO_4$ nanoparticles thus increasing its peak intensity. The peak broadening in XRD also decreased due to interaction of PPVA with aluminum. There are three peaks that match the XRD pdf database 000-037-0189 of Potassium Aluminum Phosphate (K_2 Al_2 P_8 O_{28}) with a monoclinic crystal system and lattice parameter of (a) is 16.5530, (b) is 12.3350 and (c) is 5.0910 Å. The peaks recorded are at the ranges of 5-12°, 23.84° and 33.92°. The peak of PPVA-$AlPO_4$ sample is broadened at lower angle (5-12°). However, in pdf database the peak recorded at 8.85° with crystal plane of (110) is observed as an intense peak. Therefore, the broadening of peak may be due to the interaction of PPVA and aluminum. The most intense peak for PPVA-$AlPO_4$ sample appeared at angle of 23.84° which matched with crystal plane of (121) and d-spacing of 3.730 Å. The third peak at angle of 33.92° has a crystal plane at (52-1). XRD PDF database 000-036-1459 of Potassium Aluminum Phosphate (K Al P_2 O_7) with a monoclinic crystal system and lattice parameter of (a) is 8.0461, (b) is 9.6570 and (c) is 7.3305 Å. XRD peak at 29.69° had a crystal system of (220). XRD PDF database of 98-007-4175 Aluminum Phosphate Hydrate (1/1/2.5) with hexagonal crystal system matched a number of XRD patterns for PPVA-$AlPO_4$ nanocomposite for peaks at 32.60° and 33.34° with lattice parameter of (060) and (142) separately. Also observed is a taranakite system that matched the pdf reference code 01-089-0895 with chemical formula $K_3Al_5(DPO_4)_6(PO_4)_2(D_2O)_{18}$ or known as Potassium Aluminum Deuterium Phosphate Deuterate with rhombohedral crystal system and lattice parameter of (a) is 8.6682, (b) is 8.6882 and (c) is 94.9800 Å. The crystal plane is (0 2 4), (2 1 28) and (1 2 29) referring to 24.0996, 41.4163 and 42.0886. The full width half maximum (FWHM) is used to calculate the crystallite size of PPVA-$AlPO_4$ sample. PPVA-$AlPO_4$ optimum sample consists of very small particulates that vary in component and shape. The spherical particle size of PPVA-$AlPO_4$ optimum sample was calculated using Debye-Scherrer‘s formula (Equation (4.1)) and layer of taranakite was calculated using the

Braggs law, $d=\lambda/2\sin\theta$ where, λ is X-ray wavelength (1.54056Å) and θ is the degree of the diffraction peak corresponding to the plane. XRD studies reveal that the PPVA-$AlPO_4$ optimum sample are nano-sized (48.59 nm) and crystalline. Meanwhile, the d spacing data for taranakite have average d-spacing of 0.26708 nm or 2.6708Å. The summary of all XRD data is presented in Table 4.10. Similar observation of diffraction peak of taranakite phase which appears at the 6° angle corresponds to the (600) phosphate plates stacking plane (Palacios et al., 2013). This suggested the occurrence of taranakite structure in the system coupled with spherical particulate at pH 6 with 480 min. Inorganic nanolayers at higher loading tend to agglomerate in polymer matrix due to the strong intermolecular interaction, which would retard the penetration of polymer chains into the interlayer (Jiang et al., 2013). All peaks, including the first diffraction peak is associated with the interlayer space. The broadening of peak is due to the existence of nanolayers within the nanoparticles. The nanolayers were covered with nanoparticles on their surface as a result of microstructure development from agglomeration of small particles to a bulk of accumulative nanoparticles and nanolayers.

Table 4.15: Summary of XRD data analysis and crystallite size for PVA, PPVA and PPVA-$AlPO_4$ optimum samples

PVA			PPVA			PPVA-$ALPO_4$			
Angle 2θ	**β (FWHM)**	**XRD crystallite size, D (nm)**	**Angle 2θ**	**β (FWHM)**	**XRD crystallite size, D (nm)**	**Angle 2θ**	**β (FWHM)**	**d-spacing (Å)**	**XRD crystallite size, D (nm)**
9.4			vanished			8.85 (1 1 0)	3.5	9.9792	2.27629
19.80 (100)	3.5	2.3081	21	7.5	1.0827	19.2669 (5 2 1)	0.1535	4.6069	52.4879
						23.8395 (1 2 1)	0.1791	3.7326	45.3286
						24.0996 (0 2 4)	0.1279	3.6929	63.5048
						29.6909 (2 2 0)	0.2047	3.0089	40.1447
						32.6094 (0 6 0)	0.1535	2.7460	53.9165
						33.3428 (1 4 2)	0.1279	2.6873	64.8310
						33.9213 (5 2 -1)	0.1023	2.6427	81.1784
40.7			vanished			41.4163 (2 1 28)	0.1535	2.3916	55.3227
						42.0886 (1 2 29)	0.1279	2.3199	66.5447
64, 67			vanished						

4.7.2 Fourier Transform Infrared (FTIR) Spectroscopy Analysis

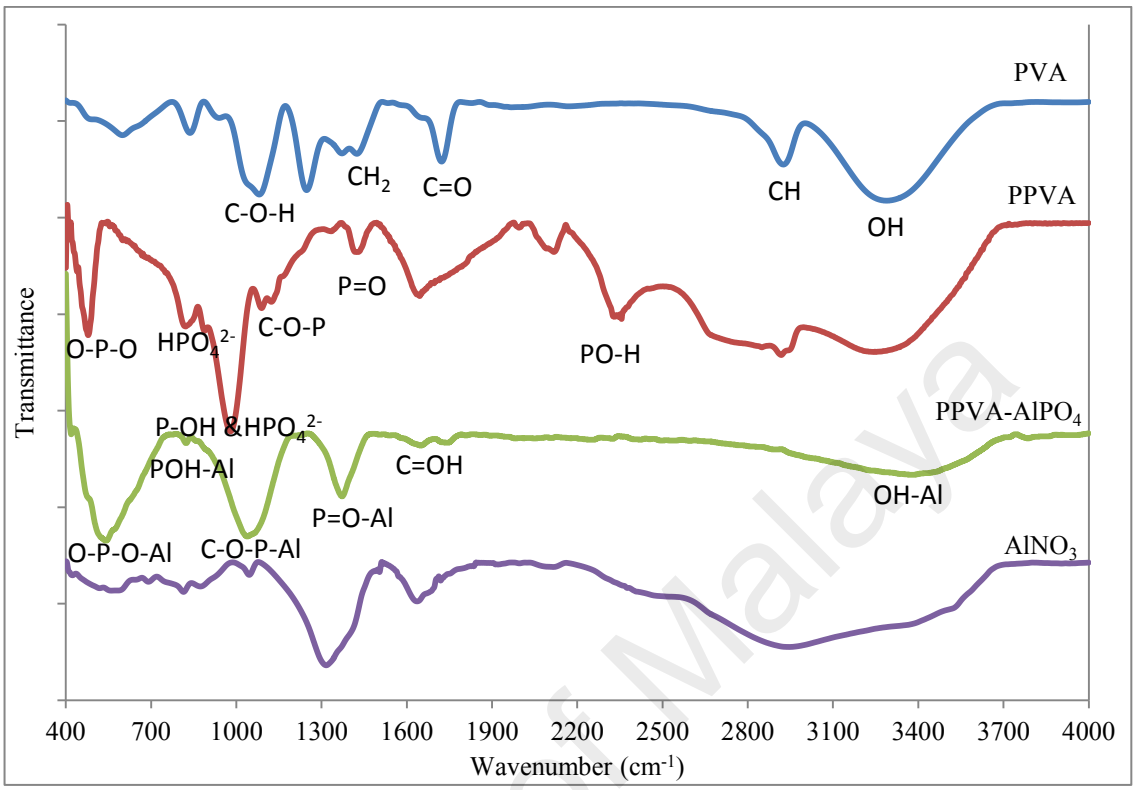

Figure 4.43: FTIR spectra of PVA, PPVA, PPVA-$AlPO_4$ optimum samples

Figure 4.43 shows the FTIR spectra of PVA, PPVA and PPVA-$AlPO_4$ optimum samples. Pure PVA spectrum shows FTIR bands of νO-H (3288 cm^{-1}), C-H (2925 cm^{-1}), C=O (1722 cm^{-1}), CH_2 (1423 and 1247 cm^{-1}), C-O-H (1080 cm^{-1}), C-C (836 cm^{-1}) and C-C (599 cm^{-1}). Meanwhile PPVA spectrum shows FTIR bands of νO-H (3252 cm^{-1}), C-H (2913 cm^{-1}), PO-H (2328 and 2117 cm^{-1}), C=C (1645 cm^{-1}), CH_2 (1417 cm^{-1}), P=O (1331 cm^{-1}), C-O-P(1086 cm^{-1}), overlapping of *ν*P-O(C) and *ν*HPO_4^{2-} (981 cm^{-1}), P-O groups which originated from $(H_2PO_4)^-$ and νHPO_4^{2-} (819 cm^{-1}) and O-P-O (477 cm^{-1}). The PPVA-$AlPO_4$ optimum sample exhibits different types of interaction starting with surface Al–OH (3786 cm^{-1}), O-H strength from H_2O (3381 cm^{-1}), water bending (1649 cm^{-1}), -CH_2- scissoring (1372 cm^{-1}), PO_4^{3-} stretching modes with C-O-P in PPVA with Aluminum in $AlPO_4$ (1038 cm^{-1}), mixture of C-OP and HPO_4^{3-} in PPVA react with $AlPO_4$ (821 cm^{-1}) and stretching mode PO_4^{3-} in $AlPO_4$ (541, 418 cm^{-1}). The peak

detections and comparisons for PVA, PPVA and PPVA-$AlPO_4$ optimum sample are listed in Table 4.16.

New peak for PPVA-$AlPO_4$ optimum sample shows decrease in intensity, broadening and shifting to higher wavenumber at 3791 cm^{-1}. This indicates the surface of Al–OH from the interaction of OH group with Aluminum (Kandori et al., 1998). Water peak is disturbed by both phosphate group and aluminum sources. OH group from PPVA is shifted to lower wavenumber at 3381 cm^{-1} due to the interaction with aluminum. Wang (2011) reported that this phenomenon is due to the occurrence of OH band in taranakite layer. The C-H peak observed in PPVA at 2913 cm^{-1} disappeared in the PPVA-$AlPO_4$ nanocomposite spectrum. The peak at 1649 cm^{-1} may have originated from the polymer referring to C=C and created a C-OH or H-O-H water bending due to interaction of phosphate group and aluminum. PPVA peak at 1331 cm^{-1} referring to P=O is shifted to higher wavenumber at 1372 cm^{-1} due to interaction with aluminum. Another important peak in PPVA at 1086 cm^{-1} (C-O-P) is shifted to lower wavenumber at 1047 cm^{-1} with PO_4^{3-} stretching modes to perform a C-O-P-$AlPO_4$ in PPVA-$AlPO_4$ nanocomposite. Peak at 821 cm^{-1} referring to the P-O bond is shifted at higher wavenumber of 819 cm^{-1}. This peak produces hydrogen bonding of P-O-H-$AlPO_4$ with aluminum. The last two important peaks for PPVA-AlPO4 nanocomposites observed at 541 and 418 cm^{-1} are referring to the stretching mode of PO_4^{3-} in $AlPO_4$ or O-P-O-$AlPO_4$ (Neuder et al., 2003a). The OH peak in PVA is shifted to a lower wavenumber in PPVA. However the peak is shifted to higher wavenumber than PVA in PPVA-$AlPO_4$ optimum sample. Other shifting peaks are observed as decreased in PPVA but increased in PPVA-$AlPO_4$ nanocomposite. However the value of PPVA-$AlPO_4$ optimum sample wavenumber is in between of PVA and PPVA. The C-O-H (1080 cm^{-1}) peak in PVA behaved differently, where it is shifted to higher wavenumber in PPVA (1086 cm^{-1}). However, in PPVA-$AlPO_4$ optimum sample it shifted to lower wavenumber than PVA (1038 cm^{-1}). The

phosphate group has given a remarkable change in OH peak and C-O-P peak due to the interaction of OH, phosphate and aluminum group. From observation, the interaction of PPVA with aluminum source basically comes from two different bonds that is a stronger P-O and weaker Al-O that later resulted in a broadening, shifting, vanishing and creation of new peaks. Nano-sized particles have different atomic arrangements from bulk crystal, thus affecting the bond length and coordination number. Crystal symmetry degraded in nano-sized particle will further result into shifting towards infra-red mode. In this case the FTIR modes are shifted to higher frequency mainly because of the nano particles obtained in the samples (Mathews Jose, 2010). The FTIR results for PVA, PPVA and PPVA-$AlPO_4$ nanocomposites are summarized in Table 4.16.

Table 4.16: Interpretation of FTIR spectra for PVA/PPVA and PPVA-$ALPO_4$ optimum sample

PVA		**PPVA**		**PPVA-$AlPO_4$**	
wavenumber (cm^{-1})	**Band assignments**	**wavenumber (cm^{-1})**	**Band assignments**	**wavenumber (cm^{-1})**	**Band assignments**
				3786	Al-OH
3288	OH	3252	OH	3381	O-H strength from H_2O
2925	C-H	2913	C-H		
		2328	PO-H		
		2117	PO-H		
1722	C=O	1645	C=C	1649	C=OH
1423, 1247	CH_2	1417	CH_2		
		1331	P=O	1372	O-P-O-$AlPO_4$
1080	C-O-H	1086	C-O-P	1038	PO_4^{3-} stretching modes in $AlPO_4$ @ C-O-P-$AlPO_4$
		981	C-O-P , P-O		
836	Sk (C-C)	819	P-O	823	P-O-$AlPO_4$
599	Sk			541	stretching mode PO_4^{3-} in $AlPO_4$ @ O-P-O-$AlPO_4$
		477	O-P-O	418	stretching mode PO_4^{3-} in $AlPO_4$ @ O-P-O-$AlPO_4$

4.7.3 Field Emission Scanning Electron Microscopy (FESEM) analysis for PPVA-$AlPO_4$ nanocomposite prepared at pH 10

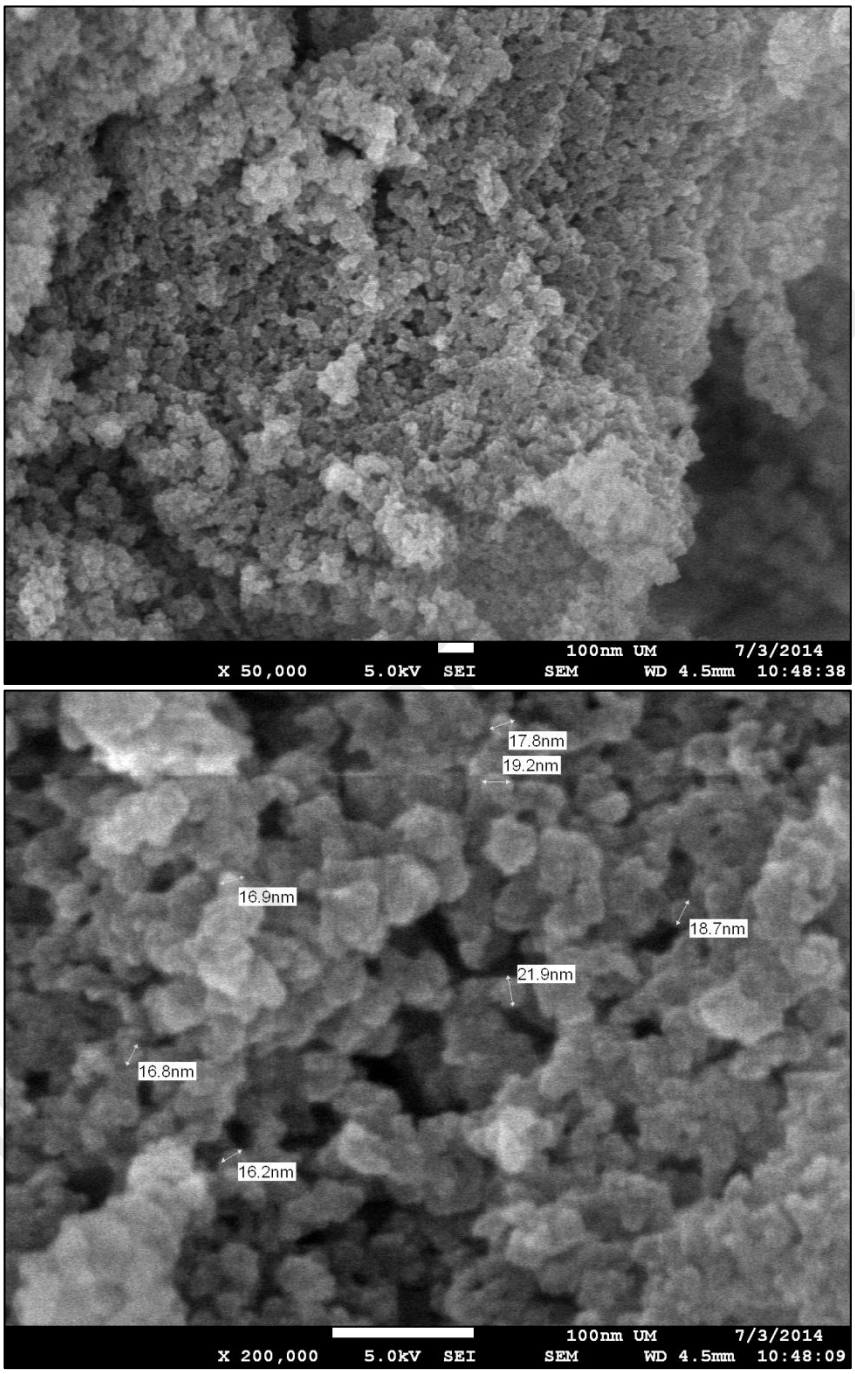

Figure 4.44: FESEM images of PPVA-$AlPO_4$ nanocomposite sample at pH 10 for different magnifications: (a) 50k; and (b) 200k

Figure 4.44 shows the FESEM morphology of PPVA-$AlPO_4$ sample at pH 10. Nanoparticle is homogeneously distributed with spherical shape and size less than 50

nm at the lower magnification of 50x. The presence of taranakite immiscible layer is also observed. At higher magnification (200x), the image shows agglomeration of $AlPO_4$ particles into various sizes (16 – 20 nm). This size is of different value from the calculated crystallite size through XRD. However, they are still in the nano region. There is no polymer phase observed in the system. The size of $AlPO_4$ nanoparticles is smaller and homogeneously distributed as compared to $AlPO_4$ nanoparticle obtained by Palacios et al. (2013) which was synthesized at pH 6 for 480 min. The homogeneous particle distribution with smaller size is due to the effectiveness of PPVA as encapsulate materials for better interfacial bonding through its pendant groups with aluminum phosphate. This is in good agreement with Pramanik et al. (2008) whom stated that PPVA provides an effective method for better dispersion of nanoparticles in the polymer matrix with a strong particle polymer interfacial bonding through its phosphate groups. The nuclei grow uniformly by diffusion of solutes from the solution to its surface until reaching the final shape. However, the uniform particles are also obtained after the occurrence of multiple nucleation. The observed nanoparticle is a result of microstructure development, where agglomeration of small particles accumulated and formed bigger particles. FESEM images show that $AlPO_4$ nanoparticles are developed from the agglomeration of very small particles. PPVA-$AlPO_4$ nanocomposite is also observed as containing immiscible layers and nanoparticles which is in good agreement with XRD pattern (Figure 4.21). From Ostwald ripening and Wuff construction theory, particles sized in the nanometer range and exhibiting irregular geometry will experience more stress and strain on the surface. However, for larger sized spherical particles, the stress and strain is less.

4.7.4 RAMAN Spectroscopy Analysis

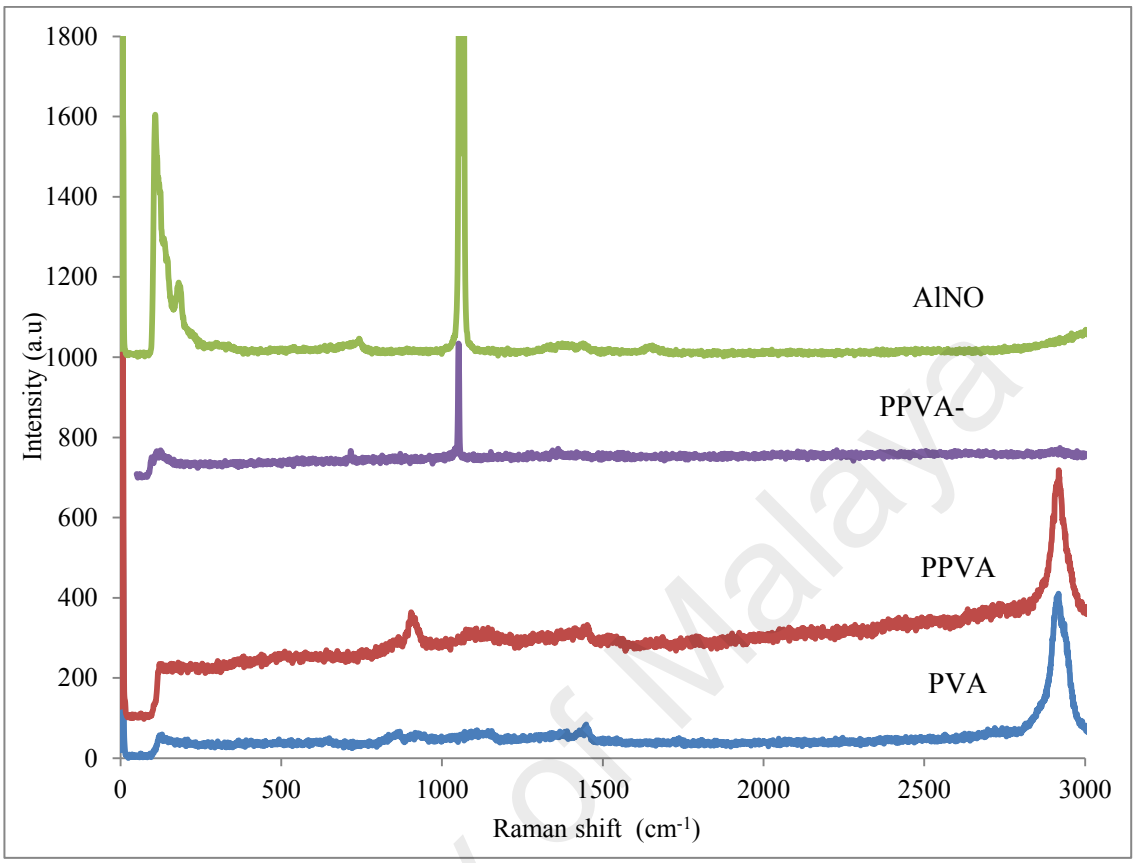

Figure 4.45: Raman spectra of PVA, PPVA and PPVA-$AlPO_4$ optimum samples

Figure 4.45 shows the Raman spectra for PVA, PPVA and PPVA-$AlPO_4$ optimum samples. Pure PVA is observed with intense band at 2900 cm^{-1} and weak bands of C-H vibration in CH_2 and O-H bending vibrations (1450 cm^{-1}), ester of oxygen C-O or C-O-H (1150 cm^{-1}) and C-C stretching band (850 cm^{-1}). Meanwhile PPVA is observed with a strong, intense peak of C-H and OH with PO, broad P $(OH)_2$ (1600 – 1300 cm^{-1}), broad C-O-P and P-O in PO_4^{3-} (1200 – 1100 cm^{-1}), P-OH in HPO_4^{2-} (901 cm^{-1}) and broad O-P-O (600 – 300 cm^{-1}). The addition of aluminum source to PPVA produces a Raman shift which is broad and less intense band, with a decrease in intensity at 2912 cm^{-1} in PPVA-$AlPO_4$ optimum sample as compared with the PPVA sample. The obvious decrease in intensity suggested that corresponding bonds have been distorted only for small micro-Raman active molecules that produced signals. The C-H and OH

with PO have interactions with aluminum in this band. Addition of Aluminum produces significant changes in the molecular bonding structure of PPVA at this band. New peak is observed with a weak band at 1344 cm^{-1} referring to CH-PO-Al interaction. Meanwhile, the PPVA-$AlPO_4$ optimum sample produced an intense peak at 1051 cm^{-1} referring to PO_3^{-4} vibrations (Boonchom et al., 2008). Band at 716 cm^{-1} is referring to aluminum sub-lattice vibration (Rokita et al., 2000) with reaction of P-O-P band (De Jager & Prinsloo, 2001) in PPVA. The smallest wavenumber for Raman shift was found at 124 cm^{-1} which originated from Aluminum source. This can be taken as a conclusion that there was interaction between PPVA and Aluminum. The strong bands in the FTIR spectra correspond to weak bands in the Raman and vice versa due to the electrical characteristics of the vibration. The OH bond or bond that is strongly polarized with a small change in its length such as that which occurred during vibration will have only a small additional effect of polarization. Vibrations involving polar bonds such as C-O and O-H are weak Raman scatters. C-O and O-H bonds carry their charges during the vibrational motion. However, the C-O bond was neutralised by C-O-P-Al bond at 1053 cm^{-1} which resulted in a large net dipole moment change and produced strong IR absorption band. Conversely, relatively neutral bonds such as C-C, C-H and C=C also suffer large changes in polarisability during a vibration, though this is less easy to visualize. Table 4.17 summarizes all the Raman results.

Table 4.17: Interpretation of PVA, PPVA and PPVA-$AlPO_4$ optimum samples of Raman spectra

PVA		**PPVA**		**PPVA-$AlPO_4$ optimum sample**	
wavenumber (cm^{-1})	**Band assignments**	**wavenumber (cm^{-1})**	**Band assignments**	**wavenumber (cm^{-1})**	**Band assignments**
2900	C-H and OH	2900	reaction between C-H and OH with PO	2900	Less intense peak. Decrease in intensity CH-PO-Al @ OH-Al
1450	C-H vibration in CH_2 and O-H bending vibration C-O-H	1600-1300	Broad $P(OH)_2$	1344	POH-Al
150		1100-1200	Broad C-O-P and P-O in PO_4^{3-}	1053	Mixture of C-O-P-$AlPO_4$ @ HPO-$AlPO_4$
850	C-C stretching vibration	901	P-OH in HPO_4^{2-}		
		300-600	Broad O-P-O	716	P-O-P - aluminum sub-lattice vibrations
				124	Origin from Al

4.7.5 UV Vis Spectroscopy Analysis

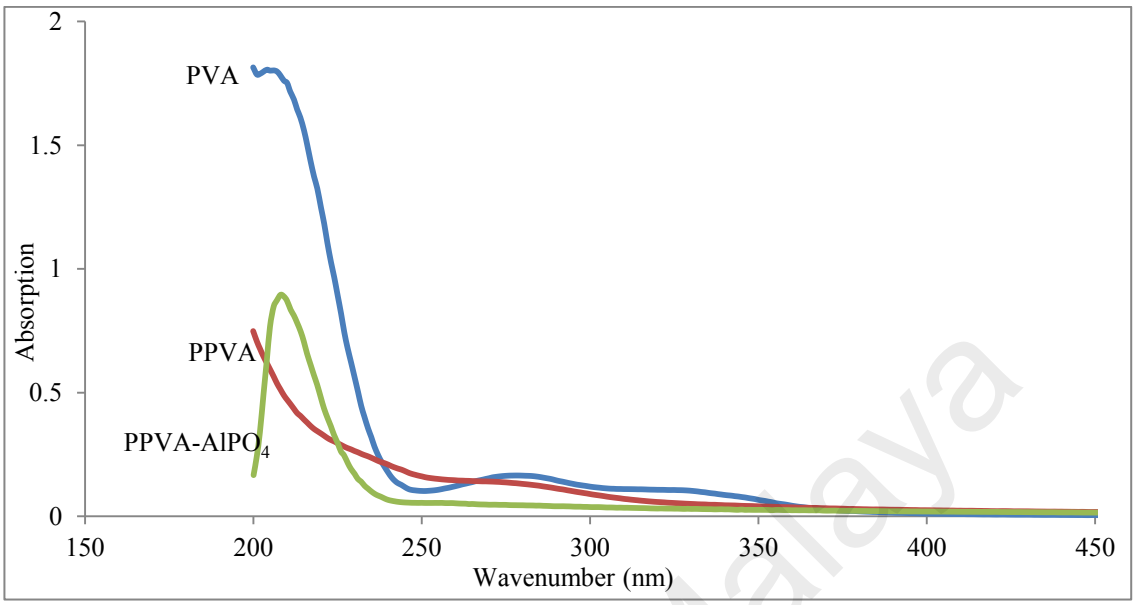

Figure 4.46: Absorption spectra of PVA, PPVA and PPVA-$AlPO_4$ optimum samples

Figure 4.46 shows the absorption spectra for PVA, PPVA and PPVA-$AlPO_4$ optimum samples. Pure PVA absorption band is observed at 204, 277 and 324 nm. Meanwhile, PPVA is observed with one absorption spectra at 274 nm. The absorption spectrum for PPVA-$AlPO_4$ optimum sample found a perfect peak at 208 nm. The absorption spectra for PPVA are shifted to lower wavenumber from 274 to 208 nm in PPVA-$AlPO_4$ nanocomposite due to interaction of PPVA with Aluminum group. Absorption spectra shows that the incorporation of aluminum and phosphate group produced a band at 210 nm indicating the presence of orthophosphate in $AlPO_4$, $ScPO_4$ and $GaPO_4$ (Trukhin et al., 2013). This is in good agreement with our findings. Figure 4.47 shows the optical band gap for PVA, PPVA and PPVA-$AlPO_4$ optimum samples and their values are presented in Table 4.18. The optical band gap for PPVA-$AlPO_4$ optimum sample was 5.55 eV which is lower than PPVA and higher than PVA. The optical band gap for PPVA-$AlPO_4$ nanocomposite is almost similar to the findings of Devamani (2012) for Aluminum Phosphate nanoparticle which is at 5.41 eV. The decrease in optical band as

compared to PPVA shows that the degree of disorder in films was improved with addition of aluminum in the nanocomposite. $AlPO_4$ has a structure with repetition of Al and P tetrahedrons. $AlPO_4$ observed a self-trapped exciton (STE) similar to silicon dioxide α-quartz. The UV visible band for STE is situated in the visible spectral range. The STE is related to Al-O bond rupture with creation of bond between non bridging oxygen and bonding oxygen on the opposite channel. However, in the PPVA-$AlPO_4$ optimum sample, the results suggest that the UV band is related to complex phosphate–oxygen ions.

Table 4.18: Optical parameters for pure PVA, PPVA and PPVA-$AlPO_4$ optimum samples

Samples	**Absorption peak, (nm)**	**Optical band gap, E_g (ev)**
Pure PVA	204, 277, 324	5.45
PPVA	274	5.75
PPVA-$AlPO_4$ nanocomposite	208	5.55

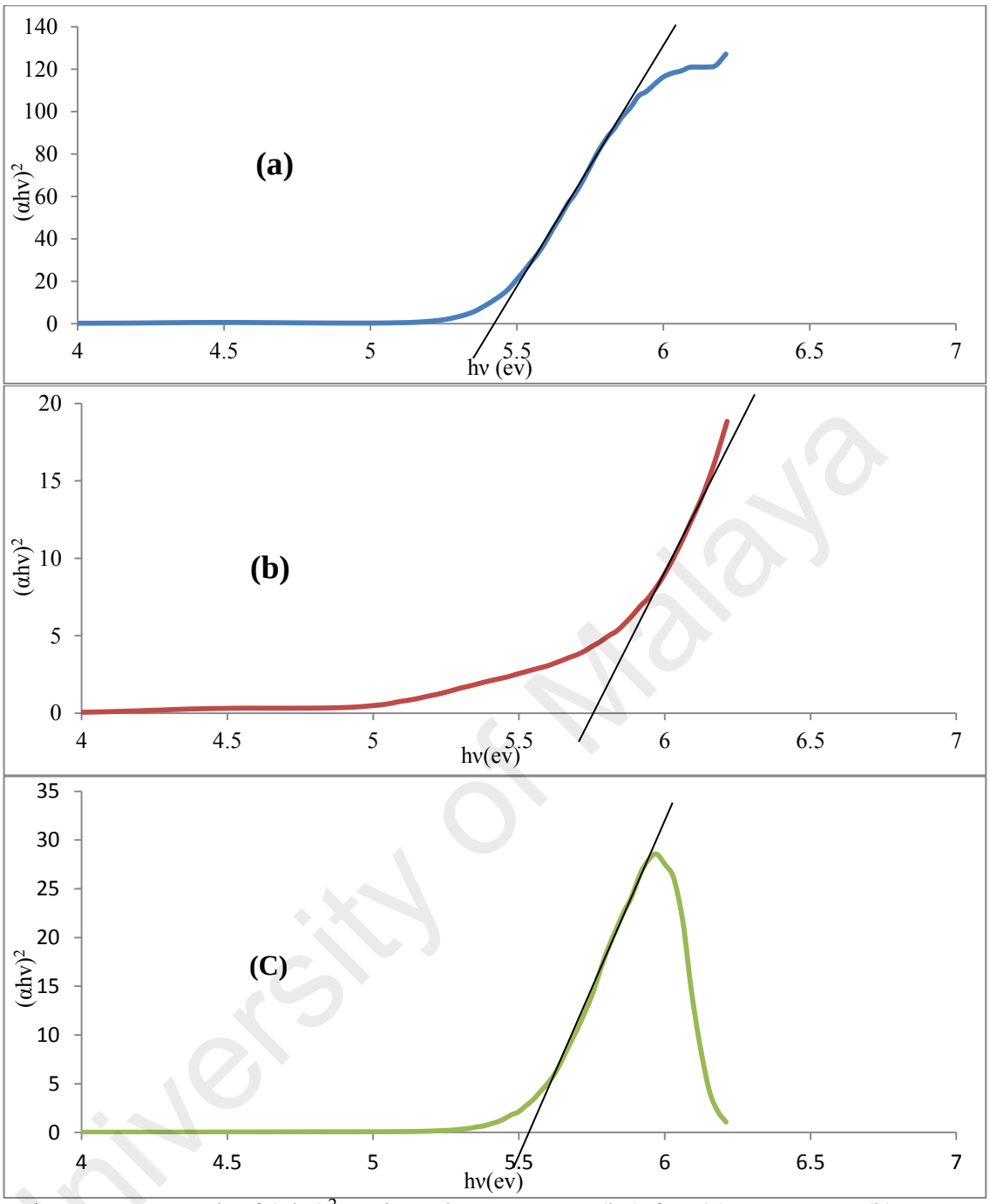

Figure 4.47: Graph of $(\alpha hv)^2$ against photon energy (hv) for: (a) pure PVA; (b) PPVA and (c) PPVA-$AlPO_4$ optimum sample

4.7.6 Photoluminescence (PL) Spectroscopy Analysis

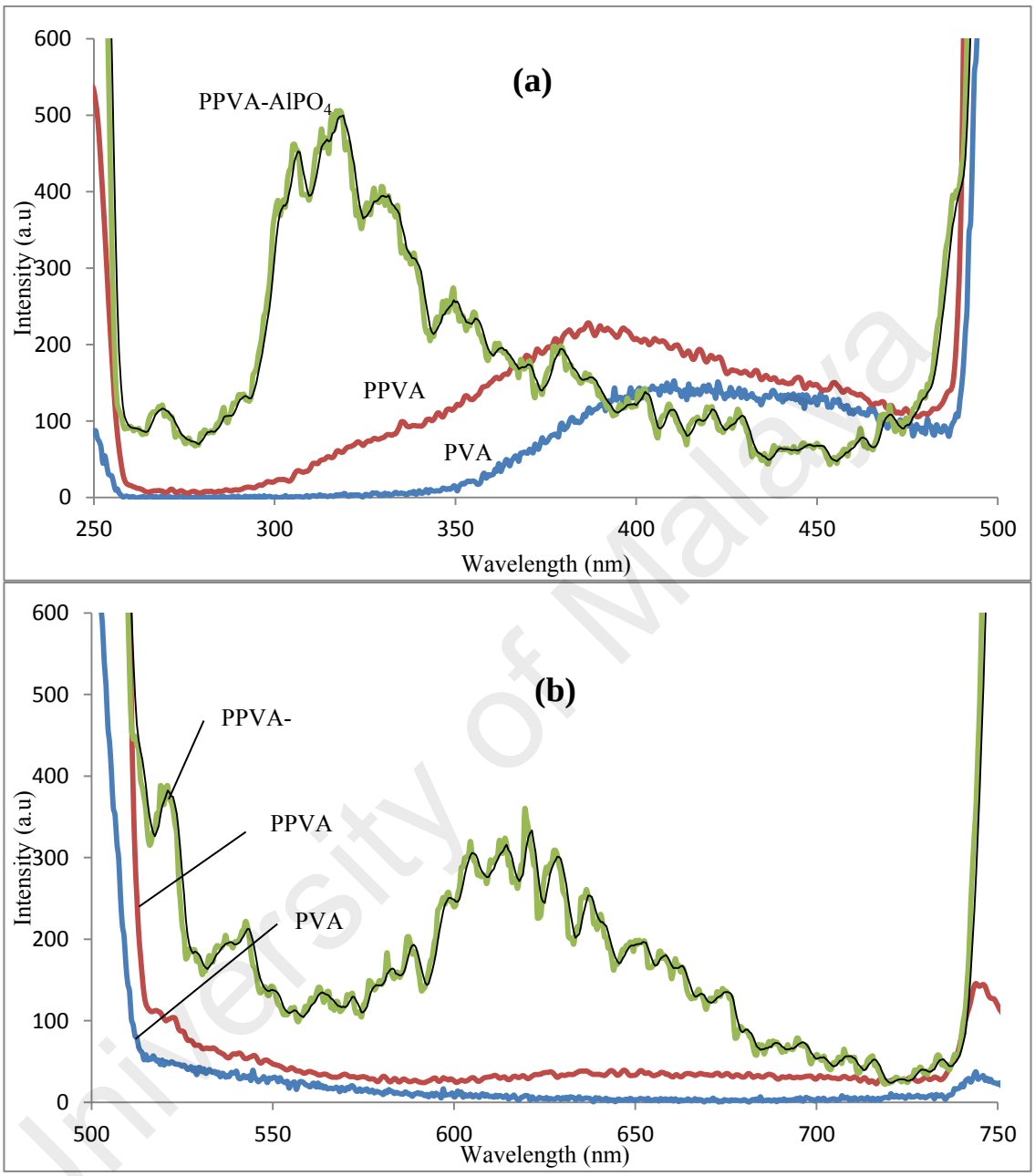

Figure 4.48: PL spectra of PVA, PPVA and PPVA-$AlPO_4$ optimum sample at excitation wavelength 250 nm in the range of (a) 250 – 500 nm and (b) 500 – 750 nm

Figure 4.48 shows the PL spectra for PVA, PPVA and PPVA-$AlPO_4$ optimum samples at excitation wavelength of 250 nm. The PL spectra of nanocomposites are shifted to lower wavelength after the addition of aluminum. The PPVA-$AlPO_4$ optimum sample produced a maximum peak in PL spectra at band of 318 nm, whereas two bands with

strong intensity at 521 and 620 nm arose due to the hydrogen related species. This finding was in good agreement with Yang et al., (2007) which reported that strong photoluminescence is observed at 533, 582, 649 and 688 nm in Al/SiO_2 nanocomposite. This finding concluded that a hydrogen bonding interaction has occurred in the composite system and is consistent with FTIR (Figure 4.43) and thermal analysis (Figure 4.41). Table 4.19 summarizes the PL data analysis.

Table 4.19: Photoluminescence data in various excitation wavelengths for all samples

Excitation wavelength λ_{exc} (nm)	Samples (mole ratio)	Band position (nm)	Intensity	Assignments
250	Pure PVA	412	70	s-PVA
	PPVA	396	230	i-PPVA
	PPVA-$AlPO_4$ nanocomposite	270	120	
		306,318, 330	460,500,400	
		350, 370	260,200	i- PPVA-$AlPO_4$
		403,410, 416, 421, 429	140,120,120,100	s- PPVA-$AlPO_4$
		462,470,	80, 100	i- PPVA-$AlPO_4$
		521, 543	380, 220	i- PPVA-$AlPO_4$
		563, 588	140,200	
		605, 614, 620, 628, 637	320, 320, 360, 300, 260	
		650,675, 698	200, 140,80	
		710,716	60,60	
300	Pure PVA	412	70	s-PVA
	PPVA	396	230	i-PPVA
	PPVA-$AlPO_4$ nanocomposite	No spectra		
350	Pure PVA	418, 440	148,148	s-PVA, a-PVA
	PPVA	421, 444	235,225	s-PPVA, a-PPVA
	PPVA-$AlPO_4$ nanocomposite	No spectra		
400	Pure PVA	462, 500	135,150	i-PVA
	PPVA	460, 485	125,115	i-PPVA
	PPVA-$AlPO_4$ nanocomposite	No spectra		

Chapter 5

CONCLUSION AND FUTURE RECOMMENDATIONS

This chapter describes the conclusion of the research and outlines future recommendations for further research.

5.1 Conclusion

Modification of PVA with phosphoric acid

The modification of PVA with phosphoric acid was successfully synthesized by solution casting technique. Weight loss begins at a lower temperature in PPVA compared to pure PVA. The highest weight residue is obtained in PPVA after thermal decomposition in air. This shows that the thermal stability of PPVA films is significantly higher than that for pure PVA, which proves a strong bonding between PPVA and aluminum phosphate. Moreover, the XRD pattern shows a significant broadening effect at angle of 20° and shifted to lower angle of 18 °, which proves the maximum bonding in PPVA ratio is 0.3. Besides, the FTIR spectra also reveal that the maximum bonding between PVA and PA occurs in the PPVA is 0.3 ratio. Raman shift had a similar trend with FTIR finding, however the OH, P $(OH)_2$ and C-O-P peaks were broaden as the phosphoric acid concentration increased. The effect of phosphoric acid concentration on the optical properties of PPVA complexes also revealed notable variations in peak intensity and position with an increase in mole ratio due to the interactions between PA ions and OH groups. The optical band gap of the PVA is slightly increases with the addition of PA due to the decrease in the formation of defects within the polymer matrix. It is observed that there are five distinct bands in the PL spectra at 391, 429, 442, 468, and 481 nm after excitation at five wavelengths (272, 300,

350, 400, and 500 nm) for PPVA films with a mole ratio of 0.3. The peak intensity varies nonlinearly with PA concentration, depending on the wavelength excitation. The five PL bands also are attributed to the $n \leftarrow \pi*$ transition of the free OH groups in s-, a-, and i-PPVA configurations. Other than that, the interactions between H_2O and PA modify bridging in the s-PPVA, which changes to a-PPVA configuration at higher PA concentrations. The lack of highly sensitive bridging makes the i-PPVA more sensitive to H-bonding with H_2O molecules. In general, the findings of this study are beneficial as they enhance the understanding on the modified PPVA properties such as, structural, thermal and optical properties, which will assist researchers in developing PPVA polymers for new applications.

Synthesis of PPVA-$AlPO_4$ nanocomposite

The effect of aluminum source in the $AlPO_4$ synthesis shown from XRD pattern proves that the crystalline structure can be obtained by using aluminum nitrate. Meanwhile, using aluminum hydroxide as aluminum source an amorphous phase is obtained, which needs further heat treatment to produce a crystalline phase. The thermal degradation of PPVA-$AlPO_4$ nanocomposite use of aluminum nitrate produces a higher weight residue compared to using aluminum hydroxide.

The XRD pattern of PPVA-$AlPO_4$ nanocomposite prepared at pH 10 shows that optimal bonding of aluminum and phosphate group occur at the range 1.3:3 or 0.4333.

The thermal properties of PPVA-$ALPO_4$ composite film exhibits enhancement compared to PPVA and PVA films. Weight loss begins at a lower temperature in PVA-$ALPO_4$, compared to PPVA and pure PVA. Meanwhile, the highest weight residue is obtained in PPVA-$AlPO_4$ nanocomposite after thermal decomposition in air, compared to PPVA and PVA. Thus, the thermal stability of PPVA-$AlPO_4$ films is significantly higher than that for pure PVA, which proves a strong bonding between PPVA and aluminum phosphate.

The XRD pattern shows a crystalline peak referring to multiple phase of $AlPO_4$, thus concluded the PPVA-AlPO4 nanocomposite was successfully synthesized. The XRD pattern matches the pdf database 000-037-0189 of Potassium Aluminum Phosphate (K_2 Al_2 P_8 O_{28}) with a monoclinic crystal system for (110)(121) and (52-1) crystal plane. Other XRD pdf database that match PPVA-AlPO4 nanocomposite XRD pattern are XRD PDF database 000-036-1459 of Potassium Aluminum Phosphate (K Al P_2 O_7) with a monoclinic crystal system for (220), PDF database of 98-007-4175 Aluminum Phosphate Hydrate (1/1/2.5) with hexagonal crystal system for (060) and (142), and the taranakite system match the pdf reference code 01-089-0895 with chemical formula $K_3Al_5(DPO_4)_6(PO_4)_2(D_2O)_{18}$, or known as Potassium Aluminum Deuterium Phosphate Deuterate with rhombohedral crystal system referring to (0 2 4), (2 1 28) and (1 2 29) crystal plane. The calculation of crystal size by assuming all spherical particles using Scherer equation confirmed that $AlPO_4$ is in nanosize. The FTIR results show the important bond of Al-OH and Al-PO_4 occurred in the PPVA-$AlPO_4$ nanocomposite. The RAMAN shift also supported FTIR result with the occurrence of $AlPO_4$ fingerprint peak at 1053 cm^{-1}, corresponding to phosphate group that shifted from PPVA with C-O-P-Al bond, proves the interaction between PPVA and aluminum phosphate.

In addition, the morphology of PPVA-$AlPO_4$ nanocomposite prepare at pH10 shows the presence of immiscible layer of taranakite with distribution of spherical nanoparticles on the surface. The spherical nanoparticle observed occurred due to agglomeration of very small particle of $AlPO_4$, measured size using FESEM also supported the XRD finding that composite is in nanosize with the average size of spherical nanoparticle below 50 nm. UV visible studies shows that PPVA-$AlPO_4$ nanocomposite produces a strong single peak at 208 nm. The optical band gap of PPVA-AlPO4 nanocomposite was in between pure PVA and PPVA with 5.5 eV. The photoluminescence spectra also shown the only absorption of PL peak, if PPVA-$AlPO_4$ nanocomposite had been excited

at wavelength of 250 nm. Besides that, the PPVA-$AlPO_4$ nanocomposite absorbance peak is shifted to lower wavelength as compared to PPVA and PVA, which confirms the interaction of PPVA and aluminum phosphate.

Effect of pH on the synthesis of PPVA-$AlPO_4$ nanocomposite

The effect of pH (7-12) for PPVA-$AlPO_4$ nanocomposite was studied for a sample without heat treatment, which produced maximum weight residue in sample pH 10. XRD analysis shows a change in peak intensity and calculated particle size, which produced two ranges of microstructure development of aggregation and agglomeration of small particle in the alkaline region from pH 7 to 9 and 10 to 12. The microstructural development was affected by the H and OH anion that varies with pH change. The FESEM micrograph observation supported the XRD finding as observed from approximately measured spherical particle size. In addition, the FESEM analysis observed a change in PPVA-$AlPO_4$ nanocomposite morphology ratio from spherical structure to layer structure. FESEM also observed the homogeneous distribution of particle size found in sample NAP10, which was prepared at reaction pH 10. Hence, the FTIR spectra shows the shifted of C-O-P-Al and O-P-O-Al to higher and lower wavenumber. Apart from that, the shift of the two bands are in similar trend as in XRD, where the shifted ones had two range from pH 7 to 9 and pH 10 to 12 that related to H and OH anion. The optical properties of PPVA-$AlPO_4$ nanocomposite observed in UV-Visible spectra shows no shifting in peak at 208 nm. However, the peak size change is increased and decreased in the same manner as observed by XRD and FTIR results. As a conclusion, the pH precipitation affected the portion of morphology phase and particle size of PPVA-$AlPO_4$ nanocomposite due the reaction of H and OH anion that varies as pH change.

Effect of crystallization time on the synthesis of PPVA-$AlPO_4$ nanocomposite

The effect of the crystallization time on PPVA-$AlPO_4$ nanocomposite analyzed from thermal analysis shows maximum weight residue at the crystallization time of 2 hours and 24 hours. The XRD, spherical particle size calculated shows that the average particle size is decreased as the crystallization time decreases. Moreover, the broad peak becoming more intense shows an increase in crystallinity of PPVA-$AlPO_4$ nanocomposite. This is seen in the FTIR analysis which shows intense C-O-P-Al and O-P-O-Al peak at both 2 and 12 hours of crystallization time due to the occurrence of more Al-PO_4, compared to Al-OH. At the 2 hour of crystallization time, there was no Al-OH peak at the water region, which suggested the best condition to produce PPVA-$AlPO_4$ nanocomposite However, the FESEM micrograph analysis observed various interesting morphology of PPVA-$AlPO_4$ nanocomposite, as the crystallization time increased. Sample prepared at the crystallization time of 2 and 24 hours shows a growth of nanotube at the high alkaline region. As conclusion to produce a better interaction of PPVA and aluminum phosphate with unique morphology, the best crystallization timing required would be 2 hours.

In the modification of PVA, the maximum bonding was obtained when PPVA ratio was 0.3. The synthesis of PPVA-$AlPO_4$ nanocomposite with aluminium nitrate produced crystalline phase and optimal bonding of aluminum and phosphate group occurred at the range 1.3:3 or 0.4333. Studies of the effect of pH on synthesis PPVA-$AlPO_4$ nanocomposite showed that pH 10 produced maximum bonding between PPVA and $AlPO_4$. Meanwhile, studies on the effect of crystallization time show that the crystallization time of 2 hours produced better bonding with more Al-PO_4 occurrence, compared to Al-OH. Moreover, the PPVA-$AlPO_4$ nanocomposite was successfully synthesized by in situ, with a nanosize particle and interaction of both PPVA and aluminium confirmed by thermal, structural, morphology and optical analysis

conducted. Thus in this study, all objectives have been successfully achieved and research finding have contributed to the knowledge of interaction between PPVA and aluminum phosphate.

5.2 Future recommendations

PPVA-$AlPO_4$ nanocomposites have interesting properties and can be explored for future recommendation as follows:

1. The study of morphology and size of PPVA-$AlPO_4$ nanoparticle using heat treatment by microwave.
2. The characterization of PPVA-$AlPO_4$ nanocomposite application as coating material for marine application.
3. The characterization of PPVA-$AlPO_4$ nanocomposite as new fire retardant materials in fiberglass boat industries.

REFERENCES

A. A. F. Sabirneeza, Subhashini, S. & Rajalakshmi, R., 2011. Water soluble conducting polymer composite of polyvinyl alcohol and leucine: an effective acid corrosion inhibitor for mild steel. *Mater. Corrosion*, 62(9999), pp.1–9.

Agrawal, S.L. & Awadhia, A., 2004. DSC and conductivity studies on PVA based proton conducting gel electrolytes. *Bulletin of Materials Science*, 27(6), pp.523–527.

Ahmad, F. & Sheha, E., 2013. Preparation and physical properties of $(PVA)_{0.7}(NaBr)_{0.3}(H_3PO_4)xM$ solid acid membrane for phosphoric acid—fuel cells,". *Journal of Advanced Research*, 4(2), pp.155–161.

Alaoui, L.M. et al., 2008. Phosphate of Aluminum as Corrosion Inhibitor for Steel in H_3PO_4. *Portugaliae Electrochimica Acta*, 26(4), pp.339–347.

Alexy, P. et al., 2002. "Poly(vinyl alcohol) stabilisation in thermoplastic processing,." *Polymer Degradation and Stability*, 78(3), pp.413–421.

Amorim da Costa, a. M. & Amado, a. M., 2001. Cation hydration in hydrogelic polyacrylamide-phosphoric acid network: A study by Raman spectroscopy. *Solid State Ionics*, 145, pp.79–84.

An, Y. et al., 1996. Complex formation of partially phosphorylated poly(vinyl alcohol), with metal ions in aqueous solution. *Polymer*, 37(14), pp.3097–3100.

An, Y. et al., 1995. Preparation and properties of highly phosphorylated poly(vinyl alcohol) hydrogels chemically crosslinked by glutaraldehyde. *Polymer*, 36(11), pp.2297–2301.

Banks, M., Ebdon, J.R. & Johnson, M., 1993. Influence of covalently bound phosphorus-containing groups on the flammability of poly (vinyl alcohol), poly(ethylene-co-vinyl alcohol) and low-density polyethylene. *Polymer*, 34, pp.4547–4556.

Bayer, E., Grathwohl, P.-A. & Geckeler, K., 1983. Poly(vinylalcohol) as polymeric support for metal chelating phosphorc acid and derivatives. *Die Angewandte Makromolekulare Chemie*, 113(Nr. 1803), pp.141–152.

Beppu, M.M., Emilia Celma De Oliveira Lima & Fernando Galembeck, 1996. Aluminum Phosphate Particles Containing Closed Pores : Preparation , Characterization , and Use as a White Pigment. *Journal of Colloid and Interface Science*, 178, pp.93–103.

Bhagwat, M., Satyanarayana, C.V. V & Ramaswamy, V., 2003. Synthesis and structural characterization of AlPO 4 -18 and Magnesium and Zinc substituted $AlPO_4$ -18. *Bulletin of the Catalyts Society*, 2, pp.60–67.

Bhajantri, R.F. et al., 2006. Microstructural studies on $BaCl_2$ doped poly(vinyl alcohol). *Polymer*, 47(10), pp.3591–3598.

Boonchom, B. et al., 2008. Synthesis of $AlPO_4$ and kinetics of thermal decomposition of $AlPO_4 \cdot H_2O$-H_4 precursor. *Journal of Thermal Analysis and Calorimetry*, 91(2), pp.511–516.

Boonchom, B. & Kongtaweelert, S., 2010. Study of kinetics and thermodynamics of the dehydration reaction of $AlPO_4 \cdot H_2O$. *Journal of Thermal Analysis and Calorimetry*, 99(2), pp.531–538.

Brock, S., 2005. *Material Safety Data Sheet Phosphoric Acid*,

Burrell, L. et al., 2001. Aluminium phosphate adjuvants prepared by precipitation at constant pH. Part II: physicochemical properties. *Vaccine*, 19, pp.282–287.

Burrell, L.S. et al., 1999. Stability of aluminium-containing adjuvants to autoclaving. *Vaccine*, 17(20-21), pp.2599–2603.

Callister, W.D., 2000. Composite and Polymer structure. In *Material Science and Engineering An Introduction.* pp. 446–561.

Campelo, J., Jaraba, M. & Luna, D., 2003. Effect of phosphate precursor and organic additives on the structural and catalytic properties of amorphous mesoporous $AlPO_4$ materials. *Chemistry of Materials*, 15(17), pp.3352–3364.

Chao, S. & Wrighton, M.S., 1987. Characterization of a solid-state polyaniline-based transistor: water vapor dependent characteristics of a device employing a poly(vinyl alcohol)/phosphoric acid solid-state electrolyte. *Journal of the American Chemical Society*, 109(22), pp.6627–6631.

Chen, D., He, L. & Shang, S., 2003. Study on aluminum phosphate binder and related Al2O3-SiC ceramic coating. *Materials Science and Engineering A384*, pp.29–35.

Chen, F. & Liu, P., 2011a. Conducting polyaniline nanoparticles encapsulated with polyacrylate via emulsifier-free seeded emulsion polymerization and their electroactive films. *Chemical Engineering Journal*, 168(2), pp.964–971.

Chen, F. & Liu, P., 2011b. High electrically conductive polyaniline/partially phosphorylated poly(vinyl alcohol) composite films via aqueous dispersions. *Macromolecular Research*, 19(9), pp.883–890.

Chen, F. & Liu, P., 2011c. Preparation of polyaniline/phosphorylated poly(vinyl alcohol) nanoparticles and their aqueous redispersion stability. *American Institute of Chemical Engineer Journal*, 57(3), pp.599–605.

Chen, H.-R. et al., 2002. Violet-blue photoluminescent properties of mesoporous zirconia modified with phosphoric acid. *Applied Physics Letters*, 81(15), p.2761.

Chen, X., Huang, R. & Pelton, R., 2005. The Reinforcement of Calcium Carbonate Filled Papers with Phosphorus-Containing Polymers. *Industrial & Engineering*

Chemistry Research, 44(7), pp.2078–2085.

Chung, D.D.L., 2003. Review Acid aluminum phosphate for the binding and coating of materials. *Journal of Materials Science*, 38, pp.2785–2791.

Cîntă Pînzaru, S. & Onac, B.P., 2009. Raman study of natural berlinite from a geological phosphate deposit. *Vibrational Spectroscopy*, 49(2), pp.97–100.

Datta, P., Chatterjee, J. & Dhara, S., 2012. Electrospun nanofibers of a phosphorylated polymer--a bioinspired approach for bone graft applications. *Colloids and surfaces. B, Biointerfaces*, 94, pp.177–83.

Daul, G.C., Reid, J.D. & Robert M. Reinhardt, 1954. Cation Exchange Materials from Cotton and Polyvinyl Phosphate. In *The fifth Southwest Regional Meeting, American Chemical Society*. pp. 1042– 1045.

Davis, E.A. & Mott, N.F., 1970. Conduction in non-crystalline systems. Conductivity, optical absorption and photoconductivity in amorphous semiconductors. *Philosophical Magazine*, 22, pp.903–922.

Devamani, R.H.P. & M., A., 2012. Synthesis and Characterization of Aluminium Phosphate Nanoparticles. *International Journal of Applied Science and Engineering Research*, 1(6), pp.769–775.

Druppel, K., Hosch, a. & Franz, G., 2007. The system Al_2O_3-P_2O_5-H_2O at temperatures below 200 °C: Experimental data on the stability of variscite and metavariscite $AlPO_4.2H_2O$. *American Mineralogist*, 92(10), pp.1695–1703.

Fernandes, D.M. et al., 2011. Preparation, characterization, and photoluminescence study of PVA/ZnO nanocomposite films. *Materials Chemistry and Physics*, 128(3), pp.371–376.

Ganschow, M. et al., 2001. Microwave-assisted preparation of uniform pure and dye-loaded $AlPO_4$-5 crystals with different morphologies for use as microlaser systems. *Journal of Materials Chemistry*, 11, pp.1823–1827.

Gong, K.-C. & Shou-Cai, H., 1989. Electrical properties of poly(vinyl alcohol) complexed with phosphoric acid. *Material Research Society*, 135, pp.377–381.

Gregora, I. & Magneron, N., 2003. Raman study of $AlPO_4$ (berlinite) at the α–β transition. *Journal of Physics-Condensed Matter*, 15, pp.4487–4501.

Guo, Z. et al., 2005. Synthesis and Structure of Large $AlPO_4$ -5 Crystals. , pp.29–33.

Gupta, P.N., 2008. Thermal properties and electrochromic behaviour of PVA complexed electrolytes using PEG as plasticizer. *Indian Journal of Pure & Applied Physics*, 46(September 2008), pp.657–659.

Gupta, P.N. & Singh, K.P., 1996. SOLID of H , PO , based PVA complex system. , 88, pp.319–323.

Gutiérrez-Mora, F. et al., 2006. High-temperature deformation of amorphous $AlPO_4$-

based nano-composites. *Journal of the European Ceramic Society*, 26(7), pp.1179–1183.

Helen, M., Viswanathan, B. & Murthy, S.S., 2007. Synthesis and characterization of composite membranes based on ??-zirconium phosphate and silicotungstic acid. *Journal of Membrane Science*, 292, pp.98–105.

Hema, M. et al., 2010. Laser Raman and ac impedance spectroscopic studies of PVA: NH_4NO_3 polymer electrolyte. *Spectrochimica Acta - Part A: Molecular and Biomolecular Spectroscopy*, 75, pp.474–478.

Hirofusa Shirai et al., 1996. Metal complexes of partially phosphorylated poly(vinyl alcohol)-Function and applications. *Macromol. Symp.*, 222(105), pp.217–222.

Holland, B.J. & Hay, J.N., 2002. The thermal degradation of poly(vinyl acetate) measured by thermal analysis-Fourier transform infrared spectroscopy. *Polymer*, 43(8), pp.2207– 2211.

Hu, Y. et al., 1995. Thermochemical Study of the Relative Stability of Dense and Microporous Aluminophosphate Frameworks. *Chemistry of Materials*, 7(10), pp.1816–1823.

Inagaki, N., Tomiha, K. & Katsuura, K., 1973. Studies on the thermal degradation of phosphorus containing polyrners : T . Thermal degradation of phosphorylated poly (vinyl alcohol). *Polymer*, 15, pp.1–4.

Iribarren, A., López-Marzo, A. & Lemmetyinen, H., 2009. Absorption in polyvinyl alcohol phosphoric acids films under different processing conditions. Kinetic study. *Revista Cubana de Quimica*, 21, pp.3–9.

Jabbar, W.A., Habubi, N.F. & Chiad, S.S., 2010. Optical characterization of silver doped poly (vinyl alcohol) films. *Journal of the Arkansas Academy of Science*, 64, pp.101–105.

De Jager, H.J. & Prinsloo, L.C., 2001. The dehydration of phosphates monitored by DSC/TGA and in situ Raman spectroscopy. *Thermochimica Acta*, 376, pp.187–196.

Jiang, F.Y. et al., 2006. Synthesis of $AlPO_4$-5 crystals using TBAOH as template. *Microporous and Mesoporous Materials*, 92(1-3), pp.129–133.

Jiang, F.Y. et al., 2005. Synthesis of large optically clear $AlPO_4$-5 single crystals. *Journal of Crystal Growth*, 283(1-2), pp.108–114.

Jiang, S. et al., 2013. 2D Lamellar Aluminophosphate Nanolayers for Enhancing Flame Retardancy and Mechanical Properties of Polymers. *Industrial & Engineering Chemistry Research*, 52(47), pp.16766–16773.

Jiang, X. et al., 2014. Synthesis and characterization of Polyaniline/Partially Phosphorylated Poly(vinyl alcohol) Nanoparticles. *Chinese Journal of Polymer Science*, 32(1), pp.35–42.

Jin, Y., Diniz da Costa, J.C. & Lu, G.Q., 2007. Proton conductive composite membrane of phosphosilicate and polyvinyl alcohol. *Solid State Ionics*, 178, pp.937–942.

Joseph, P. & Tretsiakova-mcnally, S., 2011. Reactive modification of some chain- and step-growth polymer with phosphorus-containing compounds: effects on flame retardance - a review. *Polymer Advance Technologies*, 22, pp.395–406.

Kalbasi, R.J. & Izadi, E., 2013. Hydrothermal synthesis of pure AlPO4-5 without fluoride medium: synthesis, characterization and application as a support. *Journal of Porous Materials*, 20, pp.547–556.

Kandori, K. et al., 1996. Control of size and adsorptive properties of spherical aluminum phosphate particles. *Journal of Colloid and Interface Science*, 430, pp.425–430.

Kandori, K. et al., 1998. Synthesis of Mesoporous Spherical Aluminum Phosphate Particles Using Metal Ions. *Journal of Colloid and Interface Science*, 202(2), pp.369–376.

Kawamura, K., Shibuya, K. & Okuwaki, A., 2007. Morphology of aluminum phosphate by the Al-EDTA mediated particle formation in aqueous solutions at high temperatures. *Materials Research Bulletin*, 42(2), pp.256–264.

Khanna, P.K. et al., 2005. Synthesis and optical properties of CdS/PVA nanocomposites. *Materials Chemistry and Physics*, 94(2-3), pp.454–459.

Kimura, T., 2005. Surfactant-templated mesoporous aluminophosphate-based materials and the recent progress. *Microporous and Mesoporous Materials*, 77(2-3), pp.97–107.

Kirk Othmer, 1983. Thyroid and antithyroid preparation to vinyl polymer. *Encyclopedia of Chemical Technology.*, pp.848–864.

Kushwaha, K. et al., 2012. Synthesis and photoluminescence of CdSe/PVA nanocomposites. *Journal of Physics: Conference Series*, 365, pp.1–3.

L. Laventis et al., 1990. Characterization of a ―Solid-State" Microelectrochemical Diode. *Chemistry of Materials*.

Lazareva, T.. et al., 1999. Structural Applied Field-Induced Metastability of the Compositions Based on Polyvinyl Alcohol, Orthophosphoric Acid, and Variable-Valence Metals. *International Journal of Modern Physics B*, 13(14), pp.1956–1965.

Lazareva, T.G., Yakovleva, O.V. & Shinkareva, E. V., 2002. Rheological and electrical characteristics of polyvinyl alcohol composites with phosphoric acid. *Russian Journal of Applied Chemistry*, 75(6), pp.965–968.

Lee, J.-G. et al., 2004. Effect of $AlPO_4$-Nanoparticle Coating Concentration on High-Cutoff-Voltage Electrochemical Performances in $LiCoO_2$. *Journal of The Electrochemical Society*, 151(6), p.A801.

Lee, K., Jeong, S. & Cho, J., 2013. Roles of surface chemistry on safety and electrochemistry in lithium ion batteries. *Accounts of chemical research*, 46(5), pp.1161–1170.

Leute, M., 2007. Macromolecules with Phosphorus Functionalities. *Deposit.Ddb.De*.

Li, L., Xu, L. & Wang, Y., 2003. Novel proton conducting composite membranes for direct methanol fuel cell. *Materials Letters*, 57(8), pp.1406–1410.

Liu, J. et al., 2010. A novel approach to prepare hybrid $AlPO_4$/nano-carbon (graphite-like) ($AlPO_4$/NCG) material from layer-structured $AlPO_4$/Benzylamine. *Materials Letters*, 64(8), pp.905–907.

Ma, H. et al., 2008. Effect of water on the ionothermal synthesis of molecular sieves. *Journal of the American Chemical Society*, 130(26), pp.8120–1.

Maruyama, K. et al., 1985. Assignment of conjugat double bond systems produced in heated PVA film by absorption and excitation spectra. *Bulletin Chemical Society Japan*, 58, pp.2923–2928.

Mathews Jose, 2010. *Studies on the properties of certain nanocrystalline metal phosphates - Chapter 3 FTIR, Thermal and NMR studies*. Mahatma Gandhi University. Available at: http://hdl.handle.net/10603/516.

Mekky, W. & Nicholson, P.S., 2007. Nano-aluminum-phosphate via a polymerized organic–inorganic complex route. *Journal of Materials Processing Technology*, 190(1-3), pp.393–396.

Mercedes P. Castañeda, 2003. *Electronic Paper Power Supply*,

Mitra, S. et al., 2011. Novel fluorescent matrix embedded carbon quantum dots for the production of stable gold and silver hydrosols. *Journal of Materials Chemistry*, 21(44), pp.17638–17641.

Mohapatra, S. et al., 2006. Synthesis and characterization of ultrafine poly (vinylalcohol phosphate) coated magnetite nanoparticles. *Journal of Nanoscience and Nanotechnology*, 6(3), pp.823–829.

Monteiro, V.A. do R. et al., 1999. Aluminum Polyphosphate Nanoparticles: Preparation, Particle Size Determination, and Microchemistry. *Journal of colloid and interface science*, 217(2), pp.237–248.

Narayanan, T.S.N.S., 2005. Surface pretreatment by phosphate conversion coatings - A review. *Reviews on Advanced Materials Science*, 9, pp.130–177.

Neuder, H. et al., 2003. Molecular design of in situ phosphatizing coatings (ISPCs) for aerospace primers. *Progress in Organic Coatings,*, 47(3- 4), pp.225–232.

Nourmohammadi, A. et al., 2012. Photoluminescence emission of nanoporous anodic aluminum oxide films prepared in phosphoric acid. *Nanoscale research letters*, 7(1), p.689.

Oh, Y. et al., 2008. Nanoscale Control of Cathode Materials for the Enhanced Cycle-Life Performances. *Electronic Materials Letters*, 4(1), pp.9–12.

Palacios, E. et al., 2013. Influence of the pH and ageing time on the acid aluminum phosphate synthesized by precipitation. *CrystEngComm*, 15(17), p.3359.

Peng, F. et al., 2014. Synthesis and properties of hemicelluloses-based semi-IPN hydrogels. *International journal of biological macromolecules*, 65(21), pp.564–72.

Prajapati, G.K. & Gupta, P.N., 2009. Study of ionic conductivity, dielectric characteristics and capacitance measurement of γ -irradiated conducting polymeric electrolytes. *Phase Transitions*, 82(1), pp.1–9.

Prajapati, G.K., Roshan, R. & Gupta, P.N., 2010. Effect of plasticizer on ionic transport and dielectric properties of PVA–H_3PO_4 proton conducting polymeric electrolytes. *Journal of Physics and Chemistry of Solids*, 71(12), pp.1717–1723.

Pramanik, N. et al., 2008. Synthesis of hydroxyapatite/poly(vinyl alcohol phosphate) nanocomposite and its characterization. *Polymer Composites*, 29(4), pp.429–436.

Pramanik, P., 2009. Some simple chemistry for exotic polymers. *Proceedings of the 17th International conference composite/nano engineering (ICCE '09),World Journal of Engineering, Honolulu, Hawaii, USA, 2009.*, 6, pp.1–2.

Pritchad, J.G., 1970. *Poly (vinyl alcohol) basic properties and uses.*, Macdonal Technical & Scientific.

Prosanov, I.Y., 2011. Raman Spectroscopy of PVA with metal compounds thermal decomposition. *Physics of the Solid State*, 53(4), pp.883–886.

Prosanov, I.Y. & Matvienko, a. a., 2010. Study of PVA thermal destruction by means of IR and Raman spectroscopy. *Physics of the Solid State*, 52(10), pp.2203–2206.

Rajeswari, N. et al., 2013. Structural, vibrational, thermal, and electrical properties of PVA/PVP biodegradable polymer blend electrolyte with CH_3COONH_4. *Ionics*, 19, pp.1105–1113.

Rajkumar, M., Sundaram, N.M. & Rajendran, V., 2010. In-situ preparation of hydroxyapatite nanorod embedded poly (vinyl alcohol) composite and its characterization. *International Journal of Engineering Science*, 2(6), pp.2437–2444.

Ram, S. & Mandal, T.K., 2004. Photoluminescence in small isotactic, atactic and syndiotactic PVA polymer molecules in water. *Chemical Physics*, 303(1-2), pp.121–128.

Rao, N.R., 1967. *Ultraviolet and Visible Spectroscopy: Chemical Applications*, Butterworth, London, UK.

Rivas, B.L., 2004. Metal Ion Binding Capability of the Water-Soluble Poly(Vinyl Phosphonic Acid) for Mono-, Di-, and Trivalent Cations. *Journal of Applied*

Polymer Science, 92, pp.2917–2922.

Rives, S. et al., 2013. Diffusion of CH_4 , CO_2 , and Their Mixtures in $AlPO_4$-5 Investigated by QENS Experiments and MD Simulations. *Journal of Physical Chemistry*, 117, pp.13530–13539.

Rokita, M., Handke, M. & Mozgawa, W., 2000. The $AlPO_4$ polymorphs structure in the light of Raman and IR spectroscopy studies. *Journal of Molecular Structure*, 555, pp.351–356.

Rosseto, R., Dos Santos, A. C.M.A. & Galembeck, F., 2006. Hydrous non-crystalline phosphates: Structure, function and a new white pigment. *Journal of the Brazilian Chemical Society*, 17(8), pp.1465–1472.

Sambasivan, S., 2000. Alcohol-Based Precursor Solutions for Producing Metal Phosphate Materials and Coatings. , pp.0–2.

Selvasekarapandian, S. et al., 2010. Characterization of PVA-NH_4NO_3 polymer electrolyte and its application in rechargeable proton battery. *Journal of the Physical Society of Japan*, 79(3), pp.163–168.

Sergio I. Sanchez, 2007. *The role of phosphorus in fire retardant polymers*,

Shadak Alee, K., Kuladeep, R. & Narayana Rao, D., 2013. In-situ investigation of the formation of silver nanoparticles in polyvinyl alcohol through micro-Raman spectroscopy. *Optics Communications*, 293, pp.69–74.

Singh, K.P. & Gupta, P.N., 1998. Study of dielectric relaxation in polymer electrolytes. *European Polymer Journal*, 34(7), pp.1023–1029.

Somani, P., Amalnerkar, D.P. & Radhakrishnan, S., 2000. Effect of moisture (in solid polymer electrolyte) on the photosensitivity of conducting polypyrrole sensitized by prussian blue in solid-state photocells. *Synthetic Metals*, 110, pp.181–187.

Somani, P.R. et al., 2001. Charge transfer complex-forming dyes incorporated in solid polymer electrolyte for optical humidity sensing. *Sensors and Actuators B: Chemical*, 80(2), pp.141–148.

Somani, P.R. et al., 2001. Novel dye+solid polymer electrolyte material for optical humidity sensing. *Organic Electronics*, 2(2), pp.83–88.

Somani, P.R. et al., 2003. Thermal degradation properties of solid polymer electrolyte (poly(vinyl alcohol)+phosphoric acid)/methylene blue composites. *Polymer Degradation and Stability*, 79(1), pp.77–83.

Suzuki, M. et al., 2000. Ionic conduction in partially phosphorylated poly(vinyl alcohol) as polymer electrolytes. *Polymer*, 41(12), pp.4531–4536.

Suzuki, M. et al., 1999. Proton conduction in new polymer hydrogel films consisting of crosslinking partially phosphorylated poly(vinyl alcohol)s. *Phys. Chem. Chem. Phys*, 1, pp.2749–2753.

Szumera, M., 2015. Molybdenum modified phosphate glasses studied by 31P MAS NMR and Raman spectroscopy. *Spectrochimica Acta part A: Molecular and Biomolecular Spectroscopy*, 137, pp.111–115.

Thanganathan, U., Parrondo, J. & Rambabu, B., 2011. Nanocomposite hybrid membranes containing polyvinyl alcohol or poly(tetramethylene oxide) for fuel cell applications. *Journal of Applied Electrochemistry*, 41(5), pp.617–622.

Tripathi, J. et al., 2013. Degradation study on structural and optical properties of annealed Rhodamine B doped poly(vinyl) alcohol films. *Polymer Degradation and Stability*, 98(1), pp.12–21.

Tripathi, J. et al., 2012. Influence of Rhodamine (B) doping on vibrational, morphological and absorption properties of poly(vinyl) alcohol. *Journal of Physics and Chemistry of Solids*, 73(8), pp.1026–1033.

Trukhin, A.N. et al., 2013. Ultraviolet luminescence of $ScPO_4$, $AlPO_4$ and $GaPO_4$ crystals. *Journal of physics. Condensed matter : an Institute of Physics journal*, 25(38), p.385502.

Umoren, S.A. et al., 2006. Effect of halide ions on the corrosion inhibition of aluminium in alkaline medium using polyvinyl alcohol. *J. Appl. Polymer Science*, 103, pp.2810–2816.

Vargas, M.., Vargas, R.. & Mellander, B.-E., 2000. More studies on the PVAl+H_3PO_2+H_2O proton conductor gels. *Electrochimica Acta*, 45, pp.1399–1403.

Vargas, R. a. et al., 2001. More thermal studies on the PVOH/H_3PO_2/H_2O solid proton conductor gels. *Electrochimica Acta*, 46, pp.1699–1702.

Vargas, R. a., Garc a, a. & Vargas, M. a., 1998. Phase behavior of complexes of PVA and acid salts. *Electrochimica Acta*, 43, pp.1271–1274.

Venkateswaran, C.S., 1936. The Raman spectra of ortho-phosphoric acid and some phosphates. *Proceedings of the Indian Academy of Sciences - Section A*, 3(1), pp.25–30.

Wan, Y. et al., 1999. Synthetic studies on stoichiometric reaction gels of AlPO4-5. *Green Chemistry*, 1(June), pp.169–171.

Wang, D.L. et al., 2007. A novel intumescent flame-retardant system containing metal chelates for polyvinyl alcohol. *Polymer Degradation and Stability*, 92, pp.1555–1564.

Wang, N., 2011. *Flame Retardancy of Polymer Nanocomposites based on Layered Aluminum Phosphate and Computational Study of Intercalation of Amines into α-Zirconium Phosphate and Adsorption of a Model Organic Pollutant*.

Wang, Y. & Sherwooda, P.M.A., 2003. Interfacial interactions of polyer coating with oxide free phosphate films on metal surfaces. *J. Vac. Sci. Technol. A*, 21(4),

pp.1120–1125.

Xu, R. et al., 2006. Epitaxial growth of highly-oriented $AlPO_4$-5 molecular sieve films for microlaser systems. *Journal of Materials Chemistry*, 16(22), p.2200.

Yang, C.-S. & Kau, K.-Y., 2005. Synthesis of Morphology Processable α-$AlPO_4$ Nanoparticles , Nanowires and Multi-strand Nano-ropes. *Journal of the Chinese Chemical Society*, 52, pp.477–487.

Yang, H., Yao, X. & Huang, D., 2007. Sol–gel synthesis and photoluminescence of AlP nanocrystals embedded in silica glasses. *Optical Materials*, 29(7), pp.747–752.

Yang, W. et al., 2014. Synthesis and crystal morphology control of AlPO4-5 molecular sieves by microwave irradiation. *Solid State Sciences*, 29, pp.41–47.

Yu, Q. & Carlsen, P., 2008. Synthesis of Polynucleotide Analogs Containing a Polyvinyl Alcohol Backbone. *Molecules*, 13(3), pp.701–715.

Yuan, L. et al., 2011. Supporting Information Flexible Solid-State Supercapacitors Based on Carbon Nanoparticles / MnO 2 Nanorods Hybrid Structure. *Science And Technology*, (Xx), pp.1–8.

Yue, Z., Economy, J. & Mangun, C.L., 2003. Preparation of fibrous porous materials by chemical activation 2. H_3PO_4 activation of polymer coated fibers. *Carbon*, 41, pp.1809–1817.

Zhan, F. et al., 2004. Preparation of superabsorbent polymer with slow-release phosphate fertilizer. *Journal of Applied Polymer Science*, 92(5), pp.3417–3421.

Zurbriggen, R., 2001. Investigation of the segregation behavior of different mortar constituents with TGA/SDTA. *UserCom 2001*.

LIST OF PAPERS PUBLISHED FROM THIS WORK

1. Asmalina Mohamed Saat and Mohd Rafie Johan, "The Surface Structure and Thermal Properties of Novel Polymer Composite Films Based on Partially Phosphorylated Poly(vinyl alcohol) with Aluminum Phosphate," The Scientific World Journal, vol. 2014, Article ID 439839, 2014.

2. A. M. Saat, N. A. Latiff, S. Yaakup and M. R. Johan. "Synthesis and characterisation of composite partially phosphorylated polyvinyl alcohol–aluminium phosphate as protective coating." *Materials Research Innovations* 2014; 18(S6).

3. Asmalina Mohamed Saat and Mohd Rafie Johan, "Effect of Phosphoric Acid Concentration on the Optical Properties of Partially Phosphorylated PVA Complexes," International Journal of Polymer Science, vol. 2014, Article ID 495875, 2014.

LIST OF CONFERENCES

1. 2nd International Conference on the Science & Engineering of Materials (ICoSEM 2015), Kuala Lumpur. "Effect of aluminum source in the synthesis of PPVA-$AlPO_4$ nanocomposite." Paper presenter. (Nov 2015)

2. 1st International Conference on the Science & Engineering of Materials (ICoSEM 2013), Kuala Lumpur. "Synthesis and characterisation of composite partially phosphorylated polyvinyl alcohol–aluminium phosphate as protective coating." Paper presenter. (Nov 2013)

3. 3rd International Conference on Multifunctional, Hybrid & Nanomaterials. Sorrento, Italy. "Synthesis and characterisation of composite polyvinyl phosphate–aluminium phosphate (PVAPO-$AlPO_4$) as protective coating." Poster presenter. (Mac 2013)

APPENDIX

APPENDIX A: FRONT PAGE OF ACCEPTED PAPER

Hindawi Publishing Corporation
The Scientific World Journal
Volume 2014, Article ID 439839, 7 pages
http://dx.doi.org/10.1155/2014/439839

Research Article

The Surface Structure and Thermal Properties of Novel Polymer Composite Films Based on Partially Phosphorylated Poly(vinyl alcohol) with Aluminum Phosphate

Asmalina Mohamed Saat[1,2] and Mohd Rafie Johan[2]

[1] *Universiti Kuala Lumpur, Malaysian Institute of Marine Engineering Technology, 32200 Lumut, Perak, Malaysia*
[2] *Nanomaterials Engineering Research Group, Advanced Materials Research Laboratory, Department of Mechanical, Faculty Engineering, Universiti Malaya, 50603 Kuala Lumpur, Malaysia*

Correspondence should be addressed to Asmalina Mohamed Saat; asmalina@unikl.edu.my

Received 19 March 2014; Accepted 12 August 2014; Published 20 November 2014

Academic Editor: Levent Ballice

Partially phosphorylated polyvinyl alcohol (PPVA) with aluminum phosphate ($ALPO_4$) composites was synthesized by solution casting technique to produce $(PPVA)_{100-y}-(ALPO_4)_y$ ($y = 0, 1$, and 2). The surface structure and thermal properties of the films were characterized using Fourier transform infrared (FTIR) spectroscopy and thermogravimetric analysis (TGA). The results showed that the films have higher thermal stability with strong bonding between PPVA and $ALPO_4$.

1. Introduction

The development of new polymer-inorganic composite materials has garnered much interest over the years due to their unique microstructures and physical and chemical properties, which are markedly different from other materials. Polyvinyl alcohol (PVA) is one of the most important polymeric materials in the industry as it is environmentally friendly and of low cost. PVA is a hydrophilic polymer which is frequently used as a matrix for a variety of inorganic particles. PVA provides a convenient route to prepare composites whereby the inorganic particles are dispersed to a high degree of uniformity and fineness. The addition of polyacids to water-soluble PVA produces hydrogen bonded complexes. In the case of strong phosphoric acids (PA), the reaction of PVA may produce partial reactions to cyclic phosphate esters [1]. The remaining replaceable hydrogen of the cyclic phosphate groups is ionized in water and the esterified polymer behaves as a polyelectrolyte. Furthermore, there is physical rubbery after esterification [2]. The phosphorylation of PVA with phosphoric acid (PA) in producing partially phosphorylated poly(vinyl alcohol) (PPVA) has attracted considerable interest in the applications such as fire-retardant materials [3–8], electrolyte [2, 9–12], membranes [13–15], metal chelating [16–18], paper making [19], sensors [20–23], synthetic bones/teeth [17, 24], and nanoparticle/nanocomposite [25–28].

PPVA increases the amorphous structure of the polymer by decreasing its glass transition temperature (T_g) and melting temperature (T_m) [29]. PPVA complexes possess favourable properties such as good film forming, ion exchange, conductivity, chemical resistance, and flammability. Aluminum phosphate ($ALPO_4$) is used industrially as a high temperature dehydrating agent. In addition, $ALPO_4$ also serves as a fluxing agent, binder, and catalyst in organic synthesis. $ALPO_4$ exhibits a rich structural diversity in both dense and crystalline microporous series framework.

In this paper, the synthesis of PPVA-$ALPO_4$ composite films is described and their surface structures are examined. The thermal decomposition behaviour of PPVA-$ALPO_4$ composites films is also investigated and compared with the decomposition characteristics of pure PVA.

Synthesis and characterisation of composite partially phosphorylated polyvinyl alcohol–aluminium phosphate as protective coating

A. M. Saat*[1,2], N. A. Latiff[1], S. Yaakup[1] and M. R. Johan[2]

Partially phosphorylated polyvinyl alcohol–aluminium phosphate was synthesised through continuous stirring and condensation at 80°C. The compositions of the resulting phosphorylated polyvinyl alcohol–aluminium phosphate samples were varied, by adjusting the ion ratio and concentration of complex forming additives in the electrolyte solution. The as-synthesised phosphorylated polyvinyl alcohol–aluminium phosphate was then subjected to various chemical, thermal and structural characterisations. Fourier transform infrared studies show the bonding between phosphorylated polyvinyl alcohol and $ALPO_4$ at phosphate containing group. Differential scanning calorimetric studies show that T_g, T_m and degree of crystallinity increase as $ALPO_4$ filler was added to the system. Electrochemical impedance spectroscopy analysis shows good promising new inhibitor material for mild steel immersed in NaCl medium.

Keywords: Protective coating, Composite, Phosphate, Interfacial bonding, Thermal stability

Introduction

The developments in new polymer-inorganic composite materials with polyacid promise a wide application. Polyvinyl alcohol (PVA) modified with phosphoric acid (PA) is used as fire retardant materials,[1] electrolyte,[2] membrane,[3] metal chelating,[4] paper making,[5] sensor,[6] synthetic bone,[7] nanoparticles/nanocomposite[8] and anticorrosion coating.[9] Polyvinyl alcohol has been reported as corrosion inhibitor for mild steel in 0.5 M H_2SO_4 with 30% of maximum efficiency.[10] Polymer composite PVA-L-serine-coated mild steel is also reported giving 95% efficiency of 0.6% by weight.[11] Phosphorylated polyvinyl alcohol (PPVA) combined with PANI forms a nanoparticle coating, giving two mechanisms of protection: passive layer of Fe_2O_3 and iron-phosphate secondary complex.[9] Meanwhile, aluminium phosphate ($ALPO_4$) is used as a new approach in organic coating. $ALPO_4$ explores an inhibition of corrosion of steel in 0.33 M H_3PO_4 and improves 84% efficiency at 10^{-2} M of $ALPO_4$.[12] The purpose of this study is to enhance the adhesive between coating material (PPVA–$ALPO_4$) and mild steel. In this work, a polymer composite made of PPVA–$ALPO_4$ was synthesised and its inhibition effect on the corrosion behaviour of mild steel in 3.5% NaCl was investigated.

[1]Universiti Kuala Lumpur, Malaysian Institute of Marine Engineering Technology, Lumut, Perak
[2]Nanomaterials Engineering Research Group, Advanced Materials Research Laboratory, Department of Mechanical Engineering, Universiti Malaya, Kuala Lumpur, Malaysia

*Corresponding author, email asmalina@unikl.edu.my

Methodology

Partially phosphorylated polyvinyl alcohol was obtained from a mixture of PVA (6.6 g), phosphoric acid (PA) (0.10–0.5 M) and deionised water (25 mL). Meanwhile, the refluxing process was conducted at 80°C with continuous stirring. Composite was prepared by adding $ALPO_4$ filler (1 and 2 wt-%) to PPVA with continuous stirring for 1 hour and then coated to mild steel (MS) by brush technique. Metals underwent the process of grinding, blasting and etching before coated with coating materials. Coated and uncoated samples were immersed in 3.5% of NaCl for 40 days. The chemical properties were analysed using a Perkin-Elmer System 2000 FTIR scan at 4 cm^{-1} resolution in the range 4000 to 400 cm^{-1}. The thermal properties were recorded using Mettler Toledo thermogravimetric analysis/SDTA851 from 25 to 1000°C and using Perkin-Elmer DSC-7 at 20–350°C in air with heating rate of 10°C min^{-1}. Degree of crystallinity was calculated from the melting endothermic area, where ΔH is the enthalpy of fusion from DSC thermograms and ΔH_o is the enthalpy of fusion for 100% crystalline PVA (ΔH_o = 138.6 J g^{-1}).[13] Corrosion was measured using electrochemical impedance spectroscopy (EIS) for MS specimens (5 cm × 4 cm × 1 mm) of equal composition. The tri-electrode system of EIS was used with working electrode,

DOI 10.1179/1432891714Z.000000000974

Hindawi Publishing Corporation
International Journal of Polymer Science
Volume 2014, Article ID 495875, 8 pages
http://dx.doi.org/10.1155/2014/495875

Research Article

Effect of Phosphoric Acid Concentration on the Optical Properties of Partially Phosphorylated PVA Complexes

Asmalina Mohamed Saat[1,2] and Mohd Rafie Johan[2]

[1] *Malaysian Institute of Marine Engineering Technology, Universiti Kuala Lumpur, 32200 Lumut, Perak, Malaysia*
[2] *Nanomaterials Engineering Research Group, Advanced Materials Research Laboratory, Department of Mechanical Engineering, Faculty of Engineering, Universiti Malaya, 50603 Kuala Lumpur, Malaysia*

Correspondence should be addressed to Asmalina Mohamed Saat; asmalina@unikl.edu.my

Received 10 July 2014; Revised 23 October 2014; Accepted 25 October 2014; Published 18 November 2014

Academic Editor: Yulin Deng

Partially phosphorylated polyvinyl alcohol (PPVA) films were prepared at five mole ratios of phosphoric acid (PA) using solution casting technique. The optical properties of the PPVA films were examined using UV-visible (UV) and photoluminescence (PL) spectroscopy. The UV absorption spectra reveal that the absorption peaks are blue-shifted with an increase in PA concentration added to the pure PVA. The PL spectra show the presence of peaks which are characteristic of isotactic (389–398, 460–462 nm), syndiotactic (418–420 nm), and atactic (440–446 nm) configurations of the PPVA. The results also show the peak of O–P–O bonding at a wavelength range of 481–489 nm.

1. Introduction

Polyvinyl alcohols (PVA) have garnered much interest over the years due to their vast range of applications. PVA is a material where its physicochemical properties are dependent on the degree of polymerization, hydrolysis, and distribution of its hydroxyl groups (OH). Partially phosphorylated PVA (PPVA) is produced by reacting PVA with a very strong phosphoric acid (PA) [1]. The use of PPVA is commonplace in the industry due to its array of favorable properties such as excellent film forming [2], conductivity [3], ion exchange [4], chemical resistance [5], and flammability [6]. Variations of the PA concentration will result in a color change in the complexes from transparent to brown [7]. However, it is found that only a few studies have studied the reaction between PVA and PA, with emphasis on the optical properties of the product [8]. The UV-visible spectra of a PVA/H_3PO_4/CV system in [9] show that the absorption peaks can be mainly ascribed to CV and the complexes of PVA/H_3PO_4 are said to have very weak absorption peaks. Two intense characteristic absorption peaks of phosphotungstic acid are observed at 199.3 and 270.1 nm for PWA/PVA composite membranes, which proves the interactions among PWA, PVA, and phosphate groups [10]. The UV-visible spectra of a Cu II-PPVA system recorded at 20–300 nm and 550–800 nm show the presence of two absorption bands at 253 and 780 nm for a pH of 2.5–3. The system becomes blue-shifted when the pH level is increased to 7, in which the absorption peak shifts to a lower wavelength at 218 nm [4]. In [8], annealing of PPVA at 70°C for 20 h produces an absorption peak at 350 nm. The peak intensity increases and becomes more visible with an increase in PA concentration. The absorption band of PVA/H_3PO_4 and methylene blue is observed at 425, 605, 675, and 750 nm. The appearance of peak at 605–750 nm is due to methylene blue whereas the peak at 425 nm is due to the presence of PVA/H_3PO_4 [7].

The photoluminescence (PL) spectra for PPVA films exhibit broad emission bands which correspond to $n \leftarrow \pi^*$ electronic transition of the OH groups characteristic of three distinctive polymer configurations (isotactic, syndiotactic, and atactic) in the aqueous solution. Such broad emissions may also be due to oxygen vacancies and the presence of impurities [11]. Basically, tacticity is used to describe the way pendent groups on a polymer chain are arranged on